THE UNIVERSITY
of EDINBURGH

Erosion, Vegetation and the Evolution of Hillslopes in Upland Landscapes

THE UNIVERSITY
of EDINBURGH

David T. Milodowski B.A. M.Sci. (Hons)

Ph.D. Atmospheric and Environmental Sciences

University of Edinburgh - 2016

Thesis submitted for the degree of Doctor of Philosophy

University of Edinburgh

2016

Contents

Abstract

The geomorphic and geochemical characteristics of landscapes impose a physical template on the establishment and development of ecosystems. Conversely, vegetation is a key geomorphic agent, actively involved both soil production and sediment transport. The evolution of hillslopes and the ecosystems that populate them, are thus intimately coupled; their co-dependence potentially has a profound impact on the way in which landscapes respond to environmental change. This thesis explores how rates of erosion, integrated over millennia, impact on the structural characteristics of the mixed conifer forest that presently mantles this landscape, the development of the underlying soils and emergence of bedrock. The focus for this investigation is the Feather River Region in the northern Sierra Nevada in California, a landscape characterised by a striking geomorphic gradient accompanied by spatial variations in erosion rate spanning over an order of magnitude, from 20 mm ka^{-1} to over 250 mm ka^{-1}. Using LiDAR data to quantify forest structure, I demonstrate that increasing rates of erosion drive a reduction in canopy height and aboveground biomass. Subsequently, I exploit a novel method to map rock exposure, based on a metric of topographic roughness, to show that as erosion rates increase and soil thickness consequently decreases, the degree of bedrock exposed on hillsides increases. Importantly, this soil-bedrock transition is gradual, with rapidly eroding hillslopes frequently possessing a mosaic of bedrock outcrop and intermittent soil mantle. Both the ecological and geomorphic trends are shown to be impacted by the underlying bedrock, which provides an additional source of heterogeneity in the evolution of the

Feather River landscape. The negative correlation between AGB and erosion rate has potential implications for soil production. Using a simple hillslope model I show that if this decrease in AGB is associated with a drop in biotic soil production, then feedbacks between soil thickness and biotic soil production are capable of generating a complex response to geomorphic forcing, such that hillslopes possess multiple stable states: for intermediate rates of erosion, equilibrium hillslopes may be either soil mantled or bedrock. Hillslope evolution in these simulations is path dependent; once exposed at the surface, significant patches of bedrock exposure may persist over a wide range of incision rates.

Lay Summary

Life and landscape are intimately linked. The geomorphic characteristics of hillslopes. The characteristics of hillslopes, such as gradient, soil thickness and rock outcrop, provide a physical template on which ecosystems develop. Conversely, vegetation itself is an active geomorphic agent that drives the production of soil and affects the efficiency with which this material is transported across hillslopes. In this thesis, I investigate how the rate of erosion, integrated over timescales of thousands of years, controls the physical and ecological characteristics of hillslopes in upland landscapes, and explore how both vegetation and underlying geology affect the way that hillslopes respond to changes in erosion rate.

The focus of the study is the Feather River landscape, located in the northern Sierra Nevada Mountains of California. Long term rates of erosion in this landscape vary spatially by an order of magnitude, from 20 mm ka^{-1} to over 250 mm ka^{-1}. This setting therefore provides an excellent natural laboratory in which to explore these linkages. The site was subject to a Light Detection And Ranging (LiDAR) survey in 2008. This provides a high resolution point cloud dataset, from which it is possible to extract detailed information on the structure of the forest canopy and the morphology of the ground surface.

I exploit this dataset to map out changes in canopy height and aboveground biomass across the landscape. I show that as erosion rates increase, aboveground biomass decreases. I hypothesise that this is caused by a reduction in the amount of moisture

that can be stored in hillslopes eroding more rapidly, because of a reduction in the thickness of soils and underlying saprolite.

Following this, I develop and validate a novel method to map rock exposure from high resolution digital elevation models. I then use this method to explore how the abundance of rock exposure on hillslopes increases with erosion rate in two landscapes – the Feather River landscape mentioned previously, and a second site in Idaho. I show that as erosion rates increase, there is a gradual, patchy transition from gentle, soil mantled hillslopes, to steep, rapidly eroding hillslopes that exhibit a mosaic of bedrock outcrop and soil.

Finally, I explore the geomorphic and ecological response of hillslopes to changing erosion rates in more detail. Specifically I look at how the relationships between erosion rate and both aboveground biomass and rock exposure are affected by the underlying rock type, and consider how the coupling of these ecological and geomorphic changes may feedback to impact on the evolution if this landscape. I show that rock type imposes a significant control on both the transition from soil mantled to bedrock hillslopes and forest structure. I hypothesise that there is a positive feedback between soil production and vegetation: a reduction in forest biomass would drive a reduction in the rate at which plants produce soil from underlying bedrock; a reduction in soil thickness would result in a reduction in forest biomass. Incorporating this coupling into a numerical model, I demonstrate that illustrate that feedbacks between soil thickness and biotic soil production are capable of generating a complex response to geomorphic forcing, including the persistence of bare bedrock hillslopes across a range of erosion rates once a significant exposure has been generated.

Acknowledgements

And now comes the hardest part…

First and foremost, my eternal thanks go to Simon Mudd. Your passion and depth of knowledge have been an inspiration over the course of the project. Thank you for your unending enthusiasm, support and patience, for countless thought-provoking conversations and for a summer of distraction digging up weeds in the allotment (geomorphology in action!). Thanks also to Ed Mitchard for welcoming me into the brave new world of Ecology; your expertise have made a huge difference to the development of this aspect of my research. I'd also like to make a particular acknowledgement to Simon's team of hackers: Martin Hurst, Stuart Grieve and Fiona Clubb. When Simon first floated the idea of developing some topographic analysis software, I think the initial development timescale was around the order of six months; three and a half years later and we are still working on it, having each written and re-written tens of thousands of lines of computer code in the process. Seeing the fruits of this labour now finally being put to good use is immensely satisfying. Thank you all for the many hours spent discussing anything and everything from the vagaries of channel head locations to the best ways of stemming a memory leak. My thanks also go to the other members of LSD, but particularly to Ed Baynes, Mikael Attal, Hugh Sinclair, Lizzie Dingle, John Higson, Marie-Alice Harel and Rachel Walcott, discussions with whom have provided hugely valuable insights over the past few years. Thanks to everyone else (with a particular mention to Andrew Tedstone) who has

inhabited the hallowed walls of Lower Lewis and made it such a fun environment in which to work.

A number of other people have made hugely significant contributions to my project. I'd like to thank Dan Hobley for agreeing to help out on that ill-fated field excursion to Lebec and the Transverse Ranges, and maintaining my sanity over the course of the trip (Fiona and Louis Kinnear deserve some credit here too!) – thanks also for managing to get the car out of Red Rock Canyon, as I'm not sure what we'd have done otherwise. I am indebted to Manny Gabet for time spent together in the field, and for several forthright and stimulating discussions that have been immensely valuable in developing my research. I am also hugely grateful to Niels Hovius, Dimitri Lague, Rob Parker, TC Hales and Anthony Newton for many illuminating discussions during the course of this work. Thanks to Kate Meyer for welcoming me to Stanford on two visits, and to Claire Kouba and Valerie Rowen for the invitation to join you on a very productive week of field work at the Feather River site. Also, I'd like to thank to Bodo Bookhagen for hosting me for two very enjoyable weeks at UCSB.

My family, particularly my Mum and Dad, have been hugely supportive throughout the entire project, and I am hugely grateful for everything you have done. Finally, I wish to thank Rosa Sharp. Your continued love and support, demonstrated in so many different ways throughout the past four years (and beyond), and your enduring faith in my abilities, far outlasting my own, have been an endless source of strength and encouragement; without you I would probably have never finished this.

Sorry to anyone else that I have missed.

Declaration

This thesis has been composed by myself and represents my own work. Chapters three to five have been presented as research papers that have either been published (Chapters 3-4) or are due to be submitted for review (Chapter 5); the co-authors for this work have been acknowledged appropriately. I personally led the research reported in all three chapters, conducted the analysis, wrote the text and produced the figures. Dr Simon Mudd contributed to all aspects of this project, from the research design, to its execution and interpretation. Discussions with Dr Edward Mitchard throughout this project have been provided an invaluable source of knowledge on Ecology and Remote Sensing, and he contributed towards the parts of the research design cognate to these disciplines and to the subsequent interpretation. Although I was responsible for the preparation of the manuscripts, both S. M. and E. M. participated in their subsequent refinement and editing, prior to submission and during the review process.

The software that underpins this analysis forms part of a broader project, led by S. M., to develop an open source, object-orientated topographic analysis package: LSDTopoTools (https://lsdtopotools.github.io/). This has been a collaborative endeavour shared between S. M., myself, Stuart Grieve, Fiona Clubb, Dr Martin Hurst and Declan Valters. Most of the code used in the analysis presented was written by myself, including all the point cloud processing, and the analysis of canopy structure, hillslope isolation, rock exposure and landscape morphology. The development of the underlying framework, however, was shared amongst the aforementioned

collaborators. In particular, S. M. developed the object-orientated code structure and wrote the flow routing algorithms, and facilitated other aspects of algorithm design; F. C. wrote the DrEICH channel extraction algorithm; S. G. contributed towards the extraction of ridgelines and hilltops, and also the development of a basin statistics module.

Signed:  Date: 17/05/2016

Chapter 1. Introduction

1.1 Overview

The morphology of mountain landscapes represents the cumulative impact of geomorphic processes, integrated over thousands to millions of years [e.g. *Gilbert*, 1877; *Ahnert*, 1970; *Molnar and England*, 1990; *Willett et al.*, 2001; *Whipple*, 2004; *Allen*, 2008; *Anderson and Anderson*, 2010; *Whittaker*, 2012]. These processes act to erode, redistribute and deposit sediment in response to climatic and tectonic forcing and in so doing, sculpt hillslopes and channels, shaping the environments in which ecosystems become established and develop. The flora and fauna that constitute these ecosystems are also active geomorphic agents in themselves. Vegetation plays a direct role in the weathering of bedrock to produce soil [e.g. *Heimsath et al.*, 2001; *Amundson et al.*, 2007, 2015; *Bonneville et al.*, 2009; *Taylor et al.*, 2009; *Wilkinson et al.*, 2009; *Gabet and Mudd*, 2010; *Roering et al.*, 2010], and in the subsequent transport of this material across hillslopes [e.g. *Wainwright et al.*, 2000; *Roering et al.*, 2002, 2003; *Gabet et al.*, 2003; *Vanacker et al.*, 2007; *Gallaway et al.*, 2009; *Hales et al.*, 2009; *Hughes et al.*, 2009; *Phillips*, 2009; *Walther et al.*, 2009]. Landscapes are thus coupled eco-geomorphic systems in which life and landscape are intimately and inextricably linked. However, this complexity is typically poorly captured in existing models of landscape evolution, limited by a lack of observations of eco-geomorphic coupling in real landscapes. Quantifying the interrelationships between ecosystems and surface/near-surface processes therefore represents a key challenge for Earth scientists

in order to improve our ability to forecast how landscapes respond to change [e.g. *Murray et al.*, 2008; *Reinhardt et al.*, 2010; *Brantley et al.*, 2011; *Osterkamp et al.*, 2012; *Stoffel et al.*, 2013; *Amundson et al.*, 2015].

One way to address this knowledge gap is to exploit "natural experiments" in landscape evolution that illuminate key aspects of landscape dynamics, and can be used to test and develop landscape evolution models [*Tucker*, 2009]. Several recent studies have started to utilise such an approach with a specific emphasis on understanding the linkages between biota and geomorphic and pedogenic processes across environmental gradients [e.g. *Porder et al.*, 2005a; *Istanbulluoglu et al.*, 2008; *Vitousek et al.*, 2009; *Roering et al.*, 2010; *Deligne et al.*, 2013; *Detto et al.*, 2013; *Pelletier et al.*, 2013; *McGuire et al.*, 2014]. In many cases these studies have been facilitated by analysis of airborne Light Detection and Ranging (LiDAR) data, the advent of which has revolutionised the fields of both geomorphology and ecology as a consequence of its ability to yield high resolution information on canopy structure [e.g. *Lefsky et al.*, 1999a, 2002; *Means et al.*, 2000; *Popescu and Wynne*, 2004] and the morphology of the Earth's surface [e.g. *Slatton et al.*, 2007; *Passalacqua et al.*, 2010a, 2015; *Roering et al.*, 2010; *Hurst et al.*, 2012] at the landscape scale.

In this thesis I utilise LiDAR data to explore in detail the ecological and geomorphological complexity of the evolution of the Feather River catchment in the northern Sierra Nevada of California. The Feather River landscape provides an excellent natural experiment in landscape evolution because erosion rates, which strongly influence topography and geomorphic processes, vary over an order of magnitude [*Riebe et al.*, 2000; *Hurst et al.*, 2012]. Consequently, it has been the focus

of a growing body of research into how erosion rates control the geomorphic evolution of landscapes and the concurrent development of soils and saprolite on hillslopes [*Yoo et al.*, 2011; *Hurst*, 2012; *Hurst et al.*, 2012, 2013b; *Attal et al.*, 2015; *Gabet et al.*, 2015]. This thesis adds to this existing body of work in three research chapters, the scientific content of which have either been accepted or are to be submitted to scientific journals, and which can be read as standalone, autonomous papers: (i) Chapter 3 investigates how changes in fluvial incision rates propagate into the biosphere, providing the first empirical relationship between erosion rates and aboveground biomass; (ii) Chapter 4 introduces a novel technique for mapping rock exposure in eroding landscapes from high resolution topographic data and investigates the transition from soil-mantled to bedrock hillslopes associated with increasing erosion rates; (iii) Chapter 5 builds upon Chapters 3 and 4, exploring in more detail how lithology and ecology couple to modulate the landscape response to changing rates of fluvial incision. Together these chapters explore the control that long term landscape evolution places on ecosystem development and hillslope characteristics, and the role biology and lithology play in modulating the hillslope response to geomorphic forcing.

The remainder of this chapter is dedicated to providing the rationale and background to the project. It includes a review of the relevant geomorphological and ecological literature (Section 1.3), in addition to a review of the use of LiDAR data and its applications to investigating both geomorphic and ecological systems (Section 1.4). The following chapter (Chapter 2) provides an overview of the study site, placing it in its regional geologic, climatic, ecologic and geomorphic context.

1.2 Rationale and Motivation

Landscapes are sculpted by erosion and sediment transport processes [*Gilbert*, 1877, 1909; *Penck*, 1905; *Hack*, 1960; *Culling*, 1965; *Bagnold*, 1977]. In so doing, fresh bedrock is advected towards the surface where it is exposed to climatic and biotic weathering processes, driving the formation of saprolite and soils [*Gaillardet et al.*, 1999; *West et al.*, 2005; *Amundson et al.*, 2007; *Mudd et al.*, 2013]. The resultant porous surface provides a hospitable substrate on which ecosystems can become established. In turn, biota actively modify their host environment, actively driving the breakdown of bedrock and subsequent transport of this material [*Paton*, 1995; *Gabet*, 2000; *Gabet et al.*, 2003; *Yoo et al.*, 2005; *Gabet and Mudd*, 2010; *Roering et al.*, 2010; *Chadwick et al.*, 2013]). The evolution of the Earth's surface and near surface, from the depths of the groundwater zone to the uppermost limit of the canopy, is thus modulated by the complex interplay between chemical, physical and biological processes [*Amundson et al.*, 2007; *Brantley et al.*, 2011; *Chorover et al.*, 2011]. Untangling these linkages is fundamental to understanding how both geomorphic and ecological systems respond to changes in climate, tectonic uplift and anthropogenic disturbance.

Within upland landscapes, hillslopes account for the majority of the topographic surface area, providing the site for the establishment of life and the primary source of sediment to the fluvial network. The geomorphic and geochemical properties of hillslopes impose a physical template on the development of ecosystems, impacting on the availability of moisture [e.g. *Urban et al.*, 2000; *Wilcox et al.*, 2003; *Phillips and Marion*, 2004; *Graham et al.*, 2010; *Detto et al.*, 2013; *Hahm et al.*, 2014a],

nutrients [*Vitousek et al.*, 2003, 2009; *Porder et al.*, 2005a, 2007, 2015; *Kellner et al.*, 2011; *Hilton et al.*, 2013; *Brocard et al.*, 2015; *Taylor et al.*, 2015] and disturbance frequency [e.g. *Guariguata*, 1990; *Hilton et al.*, 2011; *Dislich and Huth*, 2012; *Sass et al.*, 2012; *Stoffel et al.*, 2013]. Many landscapes exhibit striking geomorphic gradients, driven by spatial variations in erosion rate, lithology and active geomorphic process. Such geomorphic gradients are likely to be an important source of variance in the properties of ecosystems, yet relatively few studies have explicitly addressed their ecological impact.

From a process geomorphology perspective, erosion rates place fundamental constraints on the characteristics of hillslopes. The rate of erosion of a hillslope is typically controlled by the rate of fluvial incision at its base [*Culling*, 1965; *Roering et al.*, 1999; *Mudd and Furbish*, 2007a], which to a large extent dictates its gradient and relief [*Gilbert*, 1909; *Culling*, 1963, 1965; *Roering et al.*, 1999; *Binnie et al.*, 2007] and the rate and style of sediment transport [*Hovius et al.*, 2000; *Roering et al.*, 2001a]. Furthermore, by limiting the residence time to which bedrock is exposed to weathering processes [*Gaillardet et al.*, 1999; *West et al.*, 2005; *Ferrier and Kirchner*, 2008; *Gabet and Mudd*, 2009; *Hilley et al.*, 2010; *Mudd and Yoo*, 2010a], erosion rates place strong controls on the characteristics of the soil and underlying saprolite [*Heimsath et al.*, 1997, 2001, 2012; *Pelletier and Rasmussen*, 2009b; *Dosseto et al.*, 2011; *Dixon et al.*, 2012; *Rempe and Dietrich*, 2014], which in turn has potentially important impacts on the availability of both moisture [*Meyer et al.*, 2007; *Graham et al.*, 2010] and nutrients [*Vitousek et al.*, 2003; *Porder et al.*, 2007, 2015; *Hilton et al.*, 2013; *Brocard et al.*, 2015]. The rate of erosion is thus a fundamental characteristic that not only

underpins the physical and chemical properties of landscapes, but also directly links their geomorphic evolution with that of the biosphere. Despite this, the relationship between erosion rate and the ecological characteristics of forests has received very little attention.

The research presented in this thesis aims to address this knowledge gap by investigating the linkages between long term (10^4-10^6 years) erosion rate, soil production and forest ecosystems in the Northern Sierra Nevada. Specifically I aim to test the following set of hypotheses:

- ***H1*** Rapidly eroding hillslopes support forests with smaller canopies and lower aboveground biomass compared to hillslopes eroding at slower rates.
- ***H2*** As erosion rates increase and soil thickness consequently decreases, the degree of bedrock exposed on hillsides increases. At the landscape scale, this soil-bedrock transition is gradual and patchy, rather than abrupt.
- ***H3*** The expression of the above relationships, if present, in the Sierra Nevada landscape is modulated by lithology.
- ***H4*** Biotic soil production in forested landscapes helps maintain a soil mantle on rapidly eroding hillslopes.

H1 explores the potential bottom-up control that gradients in erosion rate impose on the structural characteristics and carbon storage of forests hosted within the landscape. Gradients in erosion rate are widespread, both in tectonically active [*Whittaker et al.*, 2007b; *Hurst et al.*, 2013a] and quiescent [*Prince et al.*, 2011; *Willett et al.*, 2014]

settings, therefore represent a potentially important, yet underappreciated, source of variance in forest ecosystems.

H2 addresses one of the fundamental transitions in the evolution of landscapes – the boundary between soil mantled hillslopes and bedrock hillslopes. These geomorphic domains are sculpted by different ensembles of erosion and sediment transport processes; constraining whether the transition between the two is gradual or abrupt is important in understanding the interactions between processes of soil production and sediment transport [*Heimsath et al.*, 1997, 2012; *Pelletier and Rasmussen*, 2009b; *Gabet and Mudd*, 2010]. However, the nature of the soil-bedrock transition has a number of broader implications: maintaining soil in rapidly eroding landscapes is a prerequisite for the maintenance of complex forest ecosystems [*Graham et al.*, 2010], and also facilitates rapid rates of chemical weathering in these environments, thus impacting on the efficacy of feedbacks between erosion, mountain building and global climate [*Larsen et al.*, 2014a].

H3 builds on the above hypotheses to investigate the extent to which varying lithology introduces heterogeneity in both the geomorphic and ecological the evolution of hillslopes responding to changes in environmental boundary conditions.

H4 considers the linkages between ecological and geomorphic systems, specifically looking at how the feedbacks between biotic soil production, soil thickness and erosion rate on hillslopes, and how this coupling contributes towards complexity in the dynamics of the hillslope system.

Together these hypotheses combine to address a significant knowledge gap at the interface of the fields of Geomorphology and Ecology. Testing these hypotheses, in the absence of time-series data spanning the timescales of landscape development, requires the quantification of both landscape and ecological characteristics that can be used to make inferences about their coupled evolution. Within any given setting, the topography will be subject to a suite of different geomorphic processes, each potentially leaving a distinctive signature in the morphology of the affected topography [*Stock and Dietrich*, 2003; *Roering et al.*, 2007, 2010; *DiBiase et al.*, 2010, 2012; *Passalacqua et al.*, 2010a; *Hurst et al.*, 2012; *Kirby and Whipple*, 2012; *Booth et al.*, 2013]. Landscapes are thus an encrypted record of their formative processes. If topographic form can be quantitatively linked to process, topographic analysis can be used to directly test landscape evolution models [e.g. *Whittaker et al.*, 2007a; *Roering*, 2008; *Pelletier et al.*, 2011; *Hurst et al.*, 2012], predict variations in rates and processes of erosion [e.g. *Ahnert*, 1970; *Snyder et al.*, 2000; *Kirby and Whipple*, 2001; *Roering et al.*, 2007; *Cyr et al.*, 2010; *DiBiase et al.*, 2010; *Hurst et al.*, 2012], and ultimately make quantitative empirical observations constraining the dynamics of landscape systems.

1.3 Hillslope Geomorphology and Eco-geomorphic Coupling

This review section is split into three parts. As this thesis is relevant to both geomorphologists and ecologists, this review is necessarily broad in order to be accessible to researchers from both fields. Section 1.3.1 comprises a general review of hillslope geomorphology, linking together processes of weathering, soil production and sediment transport on hillslopes. It thus provides the basic context that underlies both the more detailed discussion of the interplay between hillslope geomorphology and ecology that follows, and some of the process-based topographic analysis described in Section 1.4 [*Ahnert*, 1970; *Roering et al.*, 2007; *Hurst et al.*, 2012]. This review continues with a discussion of how the geomorphic setting impacts on ecosystems, before concluding with an overview of the role of vegetation in soil production and sediment transport and the coupling of geomorphic and ecological systems. I note here that in order to maintain its relevance to the subsequent research chapters this review is limited to processes operating in non-glaciated environments. Furthermore, while sections 1.3.2 and 1.3.3 are intended to give an overview into the links between life and landscape, they are not exhaustive in their scope. Site-specific details concerning the geomorphic and ecological characteristics of the Feather River site, which forms the target of this thesis, can be found in Chapter 2.

1.3.1 Hillslopes

Any quantitative description of hillslope erosion must be founded on the principal of conservation of mass. This forms the basis for the derivation of geomorphic transport functions to describe sediment fluxes and provides a process-based framework on which to base the following review. Geomorphic transport functions are mathematical

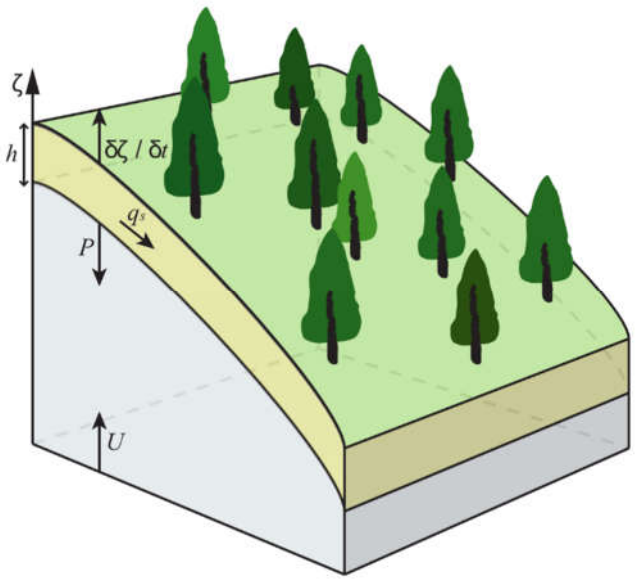

Figure 1.1 A characteristic hillslope system

erosion models, derived from physical principals, parameterising geomorphic processes and form the basis for a quantitative understanding of surface processes [*Dietrich et al.*, 2003; *Tucker and Hancock*, 2010]. Typically, they represent a compromise between theory based purely on physics, which is too complex to apply quantitatively in real landscapes, and simple 'rules' based approaches which are not directly related to physical mechanisms and may not capture the important physics of the processes.

Erosion rates on hillslopes are ultimately paced by rates of incision in the adjacent river channel, as this sets the base level for the hillslope [e.g. *Gilbert*, 1877, 1909; *Culling*, 1965; *Carson and Kirkby*, 1972; *Koons*, 1989; *Rosenbloom and Anderson*, 1994; *Arrowsmith et al.*, 1996; *Roering et al.*, 1999; *Mudd and Furbish*, 2005, 2007a]. For the hillslope system presented in Figure 1.1, assuming for simplicity that the

density of the soil and parent material are equal, the conservation of mass necessitates that the rate of change of elevation, ζ, is dictated by the relative competition between the erosion rate, *E*, the soil production rate, *P*, and the rate of change of soil thickness, $\partial h/\partial t$:

$$\frac{\partial \zeta}{\partial t} = E - P + \frac{\partial h}{\partial t} \tag{1.1}$$

For the purposes of understanding the physical erosion of hillslopes, one can consider the soil layer as being defined by the physically disturbed zone, PDZ, which is directly involved in active sediment transport and on hillslopes characterises mobile colluvium [*Yoo and Mudd*, 2008]. Bedrock is considered to incorporate both unaltered rock, and a chemically altered zone, CAZ, which is immobile, and is broadly synonymous with saprolite. This distinction between PDZ and CAZ is satisfactory for understanding eroding landscapes as physical erosion fluxes are typically several orders of magnitude higher than chemical weathering fluxes [*Gaillardet et al.*, 1999; *West et al.*, 2005], in which case chemical weathering is expected to have a minimal impact on hillslope morphology [*Mudd and Furbish*, 2004].

In soil mantled landscapes, the divergence of sediment transport is linked to the storage and production of sediment:

$$-\nabla q_s = \frac{\partial h}{\partial t} - P \tag{1.2}$$

The sediment flux, q_s, is described by a geomorphic transport function. Broadly speaking, sediment transport processes can be divided into diffusive processes, in

which the individual transport events are small relative to the length of the hillslope, and advective processes, involving mass movements that may traverse several 10s to 100s of metres of hillslope in a single event.

Combining equations 1.1 and 1.2, the rate of change of surface elevation of a hillslope can be described by:

$$\frac{\partial \zeta}{\partial t} = E - \nabla q_s \tag{1.3}$$

Within this framework there are three possible conditions for eroding landscapes [*Dietrich et al.*, 2003]:

(i) Transport limited; soil mantled landscapes in which the rate of sediment removal is controlled by the transport capacity of the system, and equation 1.3 is always applicable.

(ii) Weathering limited; erosion rates are sufficient to expose bedrock, and the rate of erosion is controlled by the production of regolith.

(iii) Detachment limited; Transport capacity is greater than the erosion rate, and thus the rate of erosion is a function of this difference. Erosion occurs by flows, with the thinning and removal of sediment sufficient so that the bedrock is actively subject to wear.

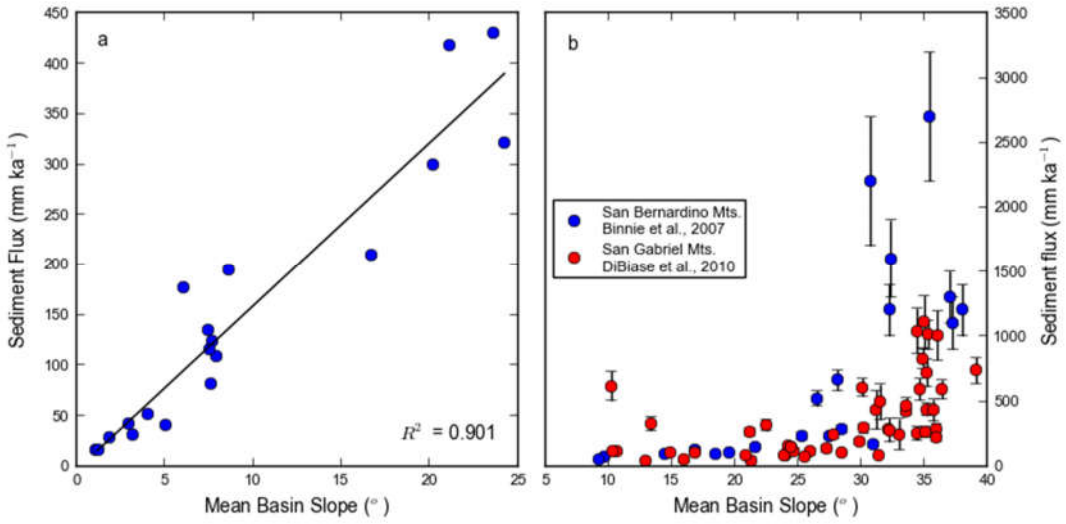

Figure 1.2 Functional relationships between mean basin slope and sediment flux: (a) linear correspondence between mean basin slope and sediment flux for a suite of large catchments [redrawn from *Ahnert*, 1970]; (b) compilation of mean basin slope and corresponding catchment-wide erosion rate estimate based on concentrations of cosmogenic ^{10}Be in fluvial sediments from the San Bernardino [*Binnie et al.*, 2007] and San Gabriel Mountains [*DiBiase et al.*, 2010].

Sediment Transport

In his seminal paper on the Geology of the Henry Mountains, Gilbert [1877] postulated that the efficacy of erosion processes is controlled at least in part by the topographic gradient. This qualitative statement underlies much of the quantitative theoretical developments that have followed. From a hillslope perspective, Gilbert [1909] demonstrated that the smooth, parabolic morphology that is ubiquitous to soil-mantled hillslopes is a direct manifestation of this gradual, slope-dependent sediment transport, providing a theoretical explanation to Davis' earlier observations [*Davis*, 1892]. Culling [1960, 1963, 1965] expanded on this to provide an elegant mathematical underpinning for this theory, demonstrating that if sediment transport is assumed to be

linearly dependent on slope, then it can be described using a simple equation for linear diffusion:

$$q_s = -\kappa \nabla \zeta \quad (1.4),$$

where κ is the hillslope sediment transport coefficient, also referred to as hillslope diffusivity. κ defines the efficiency of sediment transport across the hillslope; it incorporates the effects of soil characteristics, such as grain size distribution of the soil, moisture content, and the disturbance mechanisms that drive the mobilisation of sediment.

Support for this simple formulation of hillslope sediment flux arose from early quantitative studies, notably by Ahnert [1970], that suggested sediment exported by rivers obeyed a linear relationship with the mean hillslope gradient within their host catchments (Figure 1.2.a). However, more recent studies – aided by the emergence of digital elevation models [e.g. *Burbank et al.*, 1996; *Montgomery and Brandon*, 2002] and contemporaneous development of methods to quantify absolute erosion rates using cosmogenic radionuclides [e.g. *Lal*, 1991; *Granger et al.*, 1996; *Kirchner et al.*, 2001] – demonstrate that in high relief landscapes the relationship between hillslope sediment flux and hillslope gradient is actually strongly non-linear, with hillslope gradients becoming insensitive to rates of erosion and the linear diffusion flux drastically under-predicting actual sediment fluxes [*Howard*, 1994; *Burbank et al.*, 1996; *Roering et al.*, 1999, 2001a; *Gabet*, 2000; *Montgomery and Brandon*, 2002; *Binnie et al.*, 2007, 2010; *Roering*, 2008; *Ouimet et al.*, 2009; *DiBiase et al.*, 2010; *Hurst et al.*, 2012; *Larsen and Montgomery*, 2012; *Larsen et al.*, 2014b] (Figure 1.2.b).

Many sediment transport processes that are active on hillslopes act through the disturbance of grains in mobile soil; this includes sediment transport through rain-splash [*Furbish et al.*, 2007; *Dunne et al.*, 2010], tree throw [*Gabet et al.*, 2003; *Gallaway et al.*, 2009; *Martin et al.*, 2013], dry ravel [*Roering et al.*, 2001a; *Gabet*, 2003; *Gabet and Mendoza*, 2012], bioturbation [*Gabet*, 2000; *Roering et al.*, 2002; *Yoo et al.*, 2005] and freeze/thaw and wetting/drying cycles [*Carson and Kirkby*, 1972]. Considering creep as a cumulative impact of a series of isotropic disturbance events in which sediment transport is governed by the balance between gravitational forces, which act to resist upslope and promote downslope movement, and frictional forces, which act to resist movement in all directions, Roering et al. [1999] derived a non-linear diffusive sediment flux model, in which sediment flux rapidly approach infinity as topographic gradients steepen towards a critical slope, S_c [see also *Andrews and Bucknam*, 1987] (Figure 1.3):

$$q_s = \frac{\kappa \nabla \zeta}{1 - \left({}^{|\nabla \zeta|}/_{S_c} \right)^2} \tag{1.5}$$

The above non-linear diffusion model is able to reproduce several of the salient features found in real and experimental soil-mantled landscapes [*Howard*, 1994; *Roering et al.*, 1999, 2001a, 2001b, 2007; *Yoo et al.*, 2005; *Roering*, 2008; *Pelletier et al.*, 2011; *Hurst et al.*, 2012, 2013a; *Marshall and Roering*, 2014]. At low erosion rates, the non-linear flux described in equation

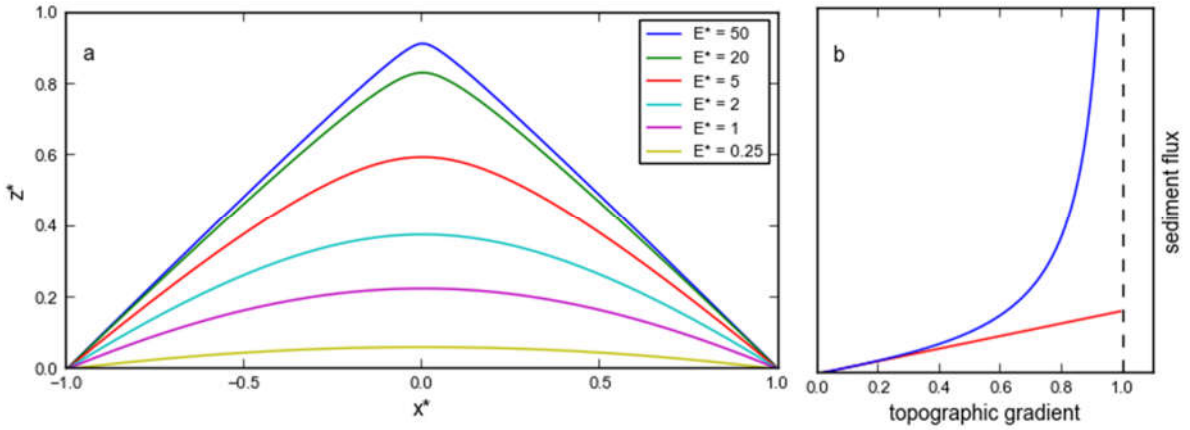

Figure 1.3(a): Steady state topographic profiles for hillslopes eroding according to the non-linear sediment flux model (Equation 1.5), plotted in non-dimensional space (see Section 1.4.2); (b) a comparison of the gradient dependence of the linear (Equation 1.4) and non-linear sediment flux models of hillslope sediment transport.

1.5 is well approximated by the linear flux described in equation 1.4; the resultant low-relief hillslopes exhibit the broad, convex-up profiles that are characteristic of low relief landscapes [e.g. *Gilbert*, 1909; *Carson and Kirkby*, 1972; *McKean et al.*, 1993]. At high erosion rates, hillslopes become increasingly planar, with curvature focused at the ridge crest (Figure 1.3), generating steep, planar hillslopes that are characteristic of non-glaciated, soil-mantled mountain ranges, such as the Oregon Coast Range [*Roering et al.*, 1999; *Roering*, 2008; *Marshall and Roering*, 2014] and northern Sierra Nevada [*Hurst et al.*, 2012, 2013b]. An alternative form of the non-linear flux law has been proposed, in which the hillslope sediment flux is also dependent on soil depth, based on the role of biotic sediment transport [*Roering*, 2008]:

$$q_s = \frac{\kappa^* \nabla \zeta}{1 - \left({}^{|\nabla \zeta|}/_{S_c} \right)^2} \qquad (1.6a),$$

Where the hillslope sediment transport coefficient, κ^*, is dependent on soil depth. Based on an hypothesised exponential decrease in disturbance events with depth, Roering [2008] suggested that the depth dependence could be approximated as:

$$\kappa^* = 1 - e^{-\beta h \cos\theta} \quad (1.6b),$$

where the exponent β determines the rate of decay of disturbance with depth, and $h\cos\theta$ defines the slope-normal soil thickness. Coupled topographic analysis and modelling studies provide support for this model [*Roering*, 2008; *Pelletier et al.*, 2011], although the standard non-linear sediment flux model given in Equation 1.5 is still considered to provide a reasonable approximation [*Roering*, 2008; *Hurst*, 2012; *Hurst et al.*, 2012].

A key limitation when interpreting landscape evolution through the perspective of the geomorphic transport functions described above, is that within a given setting, they effectively represent the aggregated effects of multiple processes that are potentially active on any given hillslope. In addition to the aforementioned diffusion-like processes in which sediment is mobilised and translated through a series of local disturbances, advective processes, such as overland flow, may also be important, or even dominant, contributors to sediment transport on hillslopes [*Dunne and Aubry*, 1985; *Dunne*, 1991; *Wainwright et al.*, 2000; *Dunne et al.*, 2016]. Overland flow may be particularly prevalent in landscapes with limited canopy cover and is capable of generating similar convex hillslopes to diffusion-like processes, particularly if paired with the locally diffusive impact of rain splash, which is typically concomitant with overland flow generation during heavy rainfall [*Dunne*, 1991; *Dunne et al.*, 2016].

Considering that different processes may be differentially sensitive to environmental change, the aggregated response of the ensemble of sediment transport processes may potentially exhibit pronounced nonlinearities and threshold behaviour that cannot readily be reconciled into a simplified geomorphic transport framework [e.g. *Marshall et al.*, 2015]. This issue is likely to be particularly prevalent in landscapes with large gradients in environmental conditions such as climate, vegetation or base level. Some efforts have been made to quantify the absolute contribution of specific sediment transport processes to the overall sediment budget [e.g. *Dunne and Aubry*, 1985; *Dunne*, 1991; *Gabet et al.*, 2003; *Yoo et al.*, 2005; *Gallaway et al.*, 2009; *Dunne et al.*, 2010, 2016; *Constantine et al.*, 2012; *Martin et al.*, 2013]. A comprehensive parameterisation of these processes, informing an assessment of their relative roles and sensitivity to change is, however, hugely challenging given the discrete nature of sediment transport processes and the timescales over which they operate.

Furthermore, while diffusive models such as Equations 1.5 and 1.6 are able to produce topography that compares well with soil mantled hillslopes observed in nature, they do not capture the full dynamics of hillslope sediment transport. As hillslope erosion rates increase, the sediment flux becomes dominated increasingly by landslides [e.g. *Burbank et al.*, 1996; *Hovius et al.*, 1997, 2000; *Roering et al.*, 2001a; *Binnie et al.*, 2007; *Larsen and Montgomery*, 2012]. Landslides contribute the overwhelming majority of sediment to the fluvial network in active mountain belts, where most hillslopes are close to the threshold for failure due to rapid rates of fluvial incision [*Hovius et al.*, 1997, 2000; *Larsen and Montgomery*, 2012]. Sediment transport on landslide dominated hillslopes is strongly stochastic, driving temporally variable

sediment fluxes to the channel network [*Benda and Dunne*, 1997; *Hicks et al.*, 2000; *Hovius et al.*, 2000; *Roering et al.*, 2001a], which in turn can play an important role in the wider evolution landscapes [*Densmore et al.*, 1998]. Yet while the non-linear diffusion models (Equations 1.5 & 1.6) capture the time-integrated flux of sediment derived through landslides [*Roering et al.*, 2001a], by treating sediment transport as a continuum process it fails to capture the inherent temporal variability.

Another critical limitation of diffusive sediment transport models is that they assume that sediment transport distances are small, relative to the length of the hillslope. This locality assumption breaks down because hillslope sediment transport occurs in discrete events, some of which will be local, but some may drive cascades of sediment that propagate significant distances across hillslopes and may even traverse the entire hillslope [*Furbish et al.*, 2009; *Furbish and Haff*, 2010; *Tucker and Bradley*, 2010; *Gabet and Mendoza*, 2012]. Moreover, the effect of nonlocality increases as rates of erosion increase, because longer transport paths are promoted by steeper gradients [*Tucker and Bradley*, 2010; *Gabet and Mendoza*, 2012; *Furbish and Roering*, 2013; *DiBiase et al.*, 2014a]. Non-local models permit more varied topographic evolutions of hillslopes, particularly toe-slopes, which have large potential upslope contributing areas [*Furbish and Roering*, 2013], and this may ultimately permit a more detailed assessment of the coupling of hillslopes and channels. Development, and particularly validation, of nonlocal models of sediment transport represents the present frontier of geomorphic process modelling on hillslopes [*Foufoula-Georgiou et al.*, 2010; *Furbish and Haff*, 2010; *Tucker and Bradley*, 2010; *Furbish and Roering*, 2013]. Nevertheless, the ability of local non-linear models, particularly Equation 1.5, to

capture many aspects of the relationship between topography and erosion rate makes them useful tools for exploring landscape dynamics through topographic analysis [*Roering et al.*, 2007; *Hurst*, 2012; *Hurst et al.*, 2012, 2013a, 2013b; *Marshall and Roering*, 2014].

The above discussion considers the attributes of hillslope morphology in equilibrium with a given set of boundary conditions. However environmental forcing is typically variable in time: on timescales of ~100 ka, climate and sea level fluctuate to the rhythm of glacial-interglacial cycles, while there have been even greater changes (such as the transition from hothouse conditions in the Eocene to icehouse conditions in the Oligocene) over longer timescales [*Zachos et al.*, 2001]; the locus and magnitude of tectonic deformation grows, decays and shifts during the evolution of mountain ranges in many tectonic systems [*Goldsworthy and Jackson*, 2001; *Hilley and Arrowsmith*, 2008; *Whittaker et al.*, 2008; *Kirby and Whipple*, 2012]; drainage networks shift and reorganise, even in tectonically quiescent regions [*Prince et al.*, 2011; *Willett et al.*, 2014; *Giletycz et al.*, 2015]. Landscapes thus frequently exist in a state of transience. Transient landscapes are useful, as the dynamics of the cohort of active surface processes are typically more clearly expressed in the transient adjustment of landforms to changes in environmental boundary conditions [e.g. *Dunne*, 1991; *Whipple and Tucker*, 2002; *Almond et al.*, 2007; *Mudd and Furbish*, 2007a; *Whittaker et al.*, 2007b; *Attal et al.*, 2008, 2011; *Hurst et al.*, 2013a].

For a hillslope, transience may be triggered either by bottom-up forcing, driven by a change in the rate of fluvial incision at the base of the hillslope [*Mudd and Furbish*, 2007a; *Gallen et al.*, 2011; *Hurst et al.*, 2012, 2013a], or top-down forcing, such as a

change in climate driving changes in precipitation [*Fernandes and Dietrich*, 1997] or vegetation [*Roering et al.*, 2004; *Hughes et al.*, 2009; *Dosseto et al.*, 2010]. On bedrock hillslopes, transient adjustment is likely to be driven by changes in the frequency of landslide events [*Larsen and Montgomery*, 2012], thus response times will likely be determined to a large extent by the strength of the bedrock [*Moore et al.*, 2009; *Larsen et al.*, 2010]. On soil-mantled hillslopes, changes in boundary conditions are transmitted diffusively; in the case of a top-down forcing, the entire hillslope will respond simultaneously; conversely in the case of a bottom-up forcing, the change will migrate upslope gradually [*Mudd and Furbish*, 2007a; *Hurst et al.*, 2012, 2013a]. Mudd and Furbish derived an analytical solution for the response time, τ, of a hillslope of length L_H, in which sediment transport obeys the linear diffusion model (Equation 1.4):

$$\tau = {4{L_H}^2}\Big/{\pi^2\kappa} \tag{1.7}$$

For the nonlinear case (Equation 1.5), the response time is shorter, and decreases nonlinearly as hillslope gradients increase [*Roering et al.*, 2001b, 2007]. The response time is also dictated by L_H (positively related) and κ (inversely related). L_H may vary according to the relative competition between hillslope and channel processes [*Tucker and Bras*, 1998; *Perron et al.*, 2009]. κ is controlled by the material properties of soil including thickness, grain size distribution, and root reinforcement which may directly influence the efficiency of sediment transport, and the mechanism by which sediment is transported [*Furbish et al.*, 2009]; κ may thus vary as a function of lithology [*McKean et al.*, 1993; *Hurst et al.*, 2013b], climate [*Hanks*, 2000; *Owen et al.*, 2011;

Chadwick et al., 2013] and vegetation [*Roering et al.*, 2002; *Gabet et al.*, 2003; *Gallaway et al.*, 2009; *Hughes et al.*, 2009; *Constantine et al.*, 2012; *Martin et al.*, 2013].

Soil Production

The presence of a soil mantle is a characteristic that is common to many hillslopes across a wide range of tectonic and climatic settings (Figure 1.4). The thickness of this soil mantle is dictated by the balance of local soil production and erosion (Equation 1.2) [*Heimsath et al.*, 1997; *Vanwalleghem et al.*, 2013a]. Within any landscape, soil thicknesses can vary significantly due to the role of a range of local factors. Convergent parts of the topography, such as hollows, accumulate material due to colluvial transport from upslope hillslopes in addition to soils produced *in situ* [*Dietrich and Dunne*, 1978; *Reneau and Dietrich*, 1991; *Dietrich et al.*, 1995], and thus tend to possess greater soil thicknesses than divergent sites, such as ridgelines [*Heimsath et al.*, 1999; *Tesfa et al.*, 2009; *Crouvi et al.*, 2013; *Gabet et al.*, 2015]. Variations in the mineralogy, texture and fracture distribution of bedrock can drive differences in both the pervasiveness of weathering and the ease with which intact bedrock can be physically broken down into mobile regolith [e.g. *Pye*, 1986; *Godard et al.*, 2001; *White et al.*, 2001; *Migoń*, 2006; *Buss et al.*, 2008; *Nicótina et al.*, 2011; *Bazilevskaya et al.*, 2013; *Goodfellow et al.*, 2014b]. Furthermore, many soil production processes, for example tree throw, bioturbation and frost cracking, occur as discrete events in space and time, and thus drive rates of bedrock lowering that are spatially heterogeneous, at least at short timescales [*Heimsath et al.*, 2001; *Yoo et al.*, 2005; *Gabet and Mudd*, 2010; *Roering et al.*, 2010].

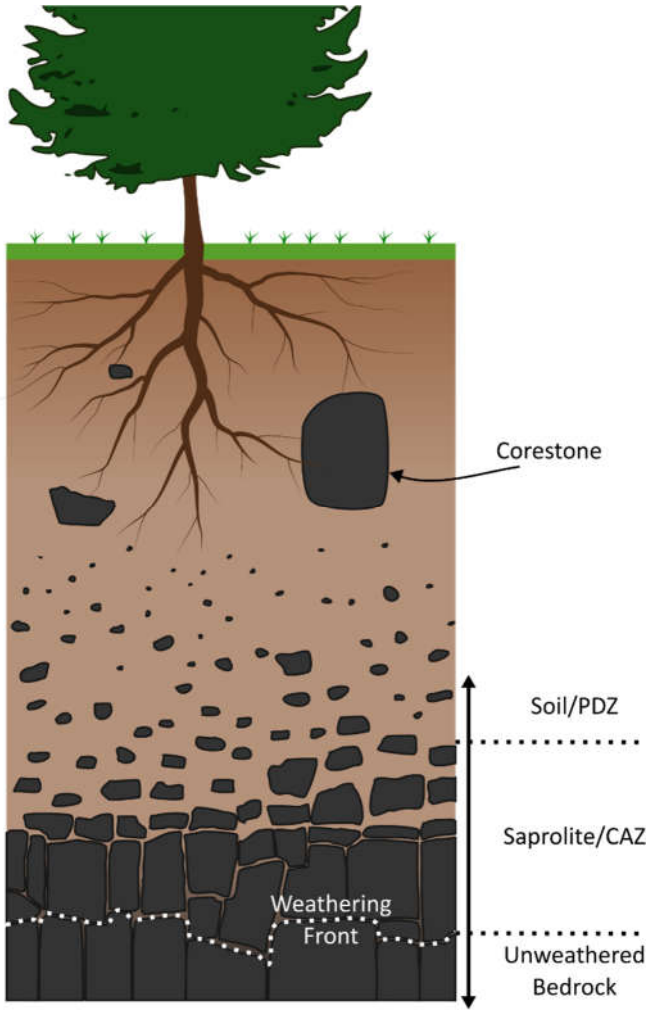

Figure 1.4 A schematic soil profile, illustrating the transition from un-weathered bedrock to saprolite and ultimately soil.

Observations of cosmogenic nuclide concentration profiles from soil pits in many locations indicate that rates of soil production decrease exponentially with increasing soil depth [e.g. *Heimsath et al.*, 1997, 1999, 2001, 2012; *Small et al.*, 1999; *Anderson et al.*, 2002; *Dixon et al.*, 2009a; *Larsen et al.*, 2014a]. This matches the expectations of theoretical models in which the rate of lowering of the interface between the PDZ and CAZ is proportional to the frequency of disturbance; for example, the impact of bioturbation should decrease as soil depths increase [*Rosenbloom and Anderson*,

1994; *Dietrich et al.*, 1995; *Heimsath et al.*, 1997; *Anderson et al.*, 2002; *Pelletier and Rasmussen*, 2009b]. Two competing models exist concerning the exact form of the soil production function, *P* (Figure 1.5). The first is the simple exponential production function [*Carson and Kirkby*, 1972; *Montgomery and Dietrich*, 1994; *Dietrich et al.*, 1995; *Heimsath et al.*, 1997, 1999], in which the soil production rate, *P*, is at a maximum, P_0, when rock is exposed at the surface and decreases exponentially with soil depth, *h*:

$$P = P_0 e^{-\gamma h} \quad (1.8),$$

where γ is a constant that describes how quickly soil production attenuates with depth Heimsath et al., [1997] were the first to find empirical support for such a soil production function.

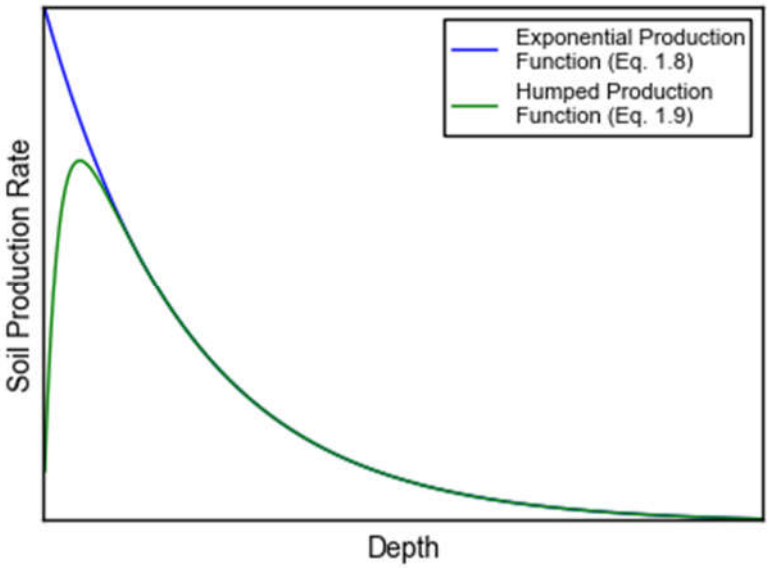

Figure 1.5 Functional relationship between soil production rate and soil depth for two common soil production functions

The second is a humped soil production function [*Gilbert*, 1877; *Carson and Kirkby*, 1972; *Cox*, 1980; *Furbish and Fagherazzi*, 2001; *Anderson*, 2002; *Wilkinson et al.*, 2005; *Strudley et al.*, 2006b; *Heimsath et al.*, 2009; *Pelletier and Rasmussen*, 2009b; *Gabet and Mudd*, 2010], in which the production rate initially increases as soil depth increases towards some optimum depth, then decreasing under thick soils as the frequency at which the bedrock-soil interface is disturbed is reduced, e.g.:

$$P = P_0(e^{-\gamma_1 h} - ke^{-\gamma_2 h}) \quad (1.9)$$

[*Strudley et al.*, 2006a, 2006b], where γ_1 and γ_1 are decay constants and k scales the production rate of a bare bedrock surface relative P_0. Note that this is just one of many possible equations to describe a humped production function.

The humped production function, first postulated by Gilbert [1877], is intuitively appealing; soil retains moisture, thus prolongs the timescale of water-rock interaction, promoting weathering [*Wahrhaftig*, 1965; *Godard et al.*, 2001; *Gabet et al.*, 2006, 2015; *Goodfellow et al.*, 2011]. In addition, vegetation requires at least high porosity to become established [*Graham et al.*, 2010]; moreover, soil provides a hospitable substrate necessary for most biological agents of soil production [*Gilbert*, 1877; *Wilkinson et al.*, 2005, 2009; *Yoo et al.*, 2005; *Meyer et al.*, 2007; *Bonneville et al.*, 2009; *Taylor et al.*, 2009; *Gabet and Mudd*, 2010]. Furthermore, even a casual observer in many landscapes could not fail to notice the juxtaposition of bedrock outcrops and soil mantled hillslopes, and the persistence of bedrock cliffs and tors in arid and semi-arid environments, implying that under a range of conditions both a

finite soil thickness and bare bedrock must be simultaneously stable hillslope configurations [*Anderson*, 2002; *Migoń*, 2006; *Strudley et al.*, 2006a, 2006b; *Pelletier and Rasmussen*, 2009b].

Initial doubts over the suitability of the humped production function were grounded on the fact that it was apparently unstable. Modelling hillslope erosion as a continuous, diffusive process, Carson and Kirkby [1972] found that a positive feedback between bedrock erosion and soil cover resulted in thin soils being inherently stable. Consequently, they concluded that a temporary increase in erosion rates would drive runaway soil erosion, leaving a bare bedrock surface. However, this apparent instability arises as a consequence of the inadequate representation of hillslope transport and soil production processes, most of which occur as discrete, stochastic events [*Heimsath et al.*, 2001; *Yoo et al.*, 2005; *Strudley et al.*, 2006b; *Roering et al.*, 2010; *Sweeney et al.*, 2012]. Using an event-based numerical model for bedrock erosion by tree throw, Gabet and Mudd [2010] demonstrated not only that the humped soil production function is reproduced by this stochastic process, but also that such a production function produces stable soils of variable thickness that can persist even at high erosion rates, producing rugged mixed soil-bedrock terrain. In addition, Strudley et al. [2006a, 2006b] demonstrated that for a landscape subject to erosion by discrete overland flow events (i.e. storms), the erosion-weathering feedback associated with decreasing soil production efficiency under thin soils may be responsible for the formation of tors that are common in arid, granitic environments [*Wahrhaftig*, 1965; *Oberlander*, 1972]. Moreover, stochastic models of soil production are also more consistent with the widespread observation that the boundary between the PDZ and

CAZ typically exhibits significant relief [*Heimsath et al.*, 2001; *Gabet and Mudd*, 2010; *Roering et al.*, 2010].

When local erosion rates exceed the maximum rate of soil production rock is exposed at the surface [*Heimsath et al.*, 1997, 2012]. The transition from soil-mantled to bedrock hillslopes also marks a shift from the transport limited endmember condition, characterised by a continuous mantle of mobile soil, to hillslopes that are either weathering limited or detachment limited. It thus represents a fundamental change in the dynamics of both sediment transport and hillslope hydrology [*Dietrich et al.*, 2003; *Binnie et al.*, 2007]; it also demarcates a limiting transition for the establishment of vegetation [*Heimsath et al.*, 1997; *Graham et al.*, 2010; *Hahm et al.*, 2014a]. Constraining the nature of the soil-bedrock transition remains significant challenge in understanding the links between erosion rate, soil production and weathering [e.g. *Heimsath et al.*, 2012; *Larsen et al.*, 2014a]. In the San Gabriel Mountains of southern California, there is a clear, albeit gradual, transition from soil mantled hillslopes at low erosion rates to steep, rocky hillslopes in response to greater rates of fluvial incision, with peak soil production rates calculated to be 0.37 mm yr^{1} [*DiBiase et al.*, 2012; *Heimsath et al.*, 2012]. In contrast, in the Southern Alps of New Zealand, maximum observed soil production rates are an order of magnitude higher and hillslopes below the tree line retain a soil mantle at erosion rates that reach in excess of 10 mm yr^{-1} [*Larsen et al.*, 2014a]. Larsen et al. [2014a] posited that this persistence of soil at high erosion rates was due to the ability of vegetation to rapidly produce soil from the heavily fractured bedrock following periodic landslide events that dominate the hillslope sediment flux in the region [*Hovius et al.*, 1997]. This appears to be

supported by observations from a small tributary catchment of the Feather River, where the hillslopes exhibited limited changes in soil thickness despite a large gradient in erosion rates, [*Yoo et al.*, 2011]. The functional relationship between the limits of soil production and erosion is likely to be complex, with the emergence of bedrock exposure on hillslopes in eroding landscapes modulated by vegetation, climate and lithology [*Gabet and Mudd*, 2010; *Heimsath et al.*, 2012; *Larsen et al.*, 2014a; *Stark and Passalacqua*, 2014; *Amundson et al.*, 2015].

Weathering

So far this review has considered the production of physically mobile soil from intact rock, and the mechanisms by which this material is subsequently transported across hillslopes and into the channel network. However, the dynamics of weathering in the CAZ may also be significant in both the geomorphic and geochemical evolution of hillslopes [*Godard et al.*, 2001; *Migoń*, 2006; *Dixon et al.*, 2009b] and the establishment of vegetation [*Graham et al.*, 2010; *Hahm et al.*, 2014a], particularly in regions like the Sierra Nevada where the soil is relatively thin and weathered saprolite provides crucial additional water storage [*Jones and Graham*, 1993; *Rose et al.*, 2003; *Holbrook et al.*, 2014].

The CAZ is separated from unaltered bedrock by a reaction front; this defines the lower limit of chemical weathering [*Lebedeva et al.*, 2007]. The nature of this weathering front can be highly variable; in some locations it can be sharp, in others broader and diffuse, and its depth can vary significantly at both local and landscape scales [*Ruxton V and Berry*, 1959; *Godard et al.*, 2001; *Migoń*, 2006; *Befus et al.*, 2011; *Bazilevskaya*

et al., 2013; *Goodfellow et al.*, 2014a] . Comparisons of rates of physical erosion and chemical weathering, estimated both through catchment-wide fluxes [*Gaillardet et al.*, 1999; *West et al.*, 2005] and degree of chemical depletion of soils and saprolite [*Riebe et al.*, 2004; *Dixon et al.*, 2009b; *Rasmussen et al.*, 2011b; *Larsen et al.*, 2014a], indicate that at very slow erosion rates, weathering rates are limited by the supply of fresh minerals into the weathering zone (supply-limitation), whereas in actively eroding landscapes there is abundant fresh mineralogy, thus the kinetics of the chemical reactions that drive weathering become increasingly dominant (kinetic-limitation). This relationship has been captured in theoretical studies coupling physical and chemical denudation [*Gabet*, 2007; *Lebedeva et al.*, 2007; *Ferrier and Kirchner*, 2008; *Gabet and Mudd*, 2009]. Of particular importance in controlling the rate of weathering in the kinetically limited regime is the flux of water through the linked pore space networks permeating the bedrock [*Maher*, 2010, 2011; *Bazilevskaya et al.*, 2013].

Chemical weathering is driven by (i) hydrolysis, where the infiltrating water reacts with primary mineralogy to form clay minerals; (ii) hydration, where water is absorbed into crystal lattice, often causing lattice expansion and consequent breakdown of the mineral structure. Different minerals are variably susceptible to these processes: biotite is particularly prone to hydration [*Wahrhaftig*, 1965; *Isherwood and Street*, 1976; *Buss et al.*, 2008]; plagioclase feldspar and mafic minerals are particularly susceptible to hydrolysis, whereas potassium feldspar, muscovite and quartz are more resistant, quartz especially so [*Goldich*, 1938; *Flageollet*, 1977; *Godard et al.*, 2001; *White et al.*, 2001]. Lithological variations thus place a major control on the rate of

weathering, and thus ultimately saprolite thickness [*Heckman and Rasmussen*, 2011; *Dosseto et al.*, 2012].

Weathering reactions are promoted by prolonged contact with water [*Gabet et al.*, 2006]; weathering is typically more pervasive proximal to fractures and joints that provide conduits through which water can penetrate more deeply into bedrock [*Ruxton V and Berry*, 1959; *Godard et al.*, 2001; *Migoń*, 2006; *Buss et al.*, 2008; *Goodfellow et al.*, 2011, 2014a]. Critically, weathering rates are tightly coupled to the fluid residence times and thus flow rates; at very low flow rates, pore fluids will tend towards equilibrium with their host matrix retarding the weathering rate [*Maher*, 2010; *Lebedeva and Brantley*, 2013], whereas an active through-flux of water drives continued disequilibrium and thus enhanced weathering rates [*Maher*, 2010, 2011]. This is broadly in agreement with the observation that weathering extent typically decreases downslope [*Yoo et al.*, 2007]. Groundwater fluxes in hillslopes are promoted by fluvial incision and relief generation, as this produces a lateral head gradient draining toward the channel [*Rempe and Dietrich*, 2014]. Coupling a groundwater flow model to a nonlinear hillslope sediment flux model (Equation 1.5), Rempe and Dietrich [2014] demonstrated that at the hillslope scale, saprolite thickness should increase towards the ridge crest; in their model domain saprolite thickness initially increases with erosion rate, as the higher relief promotes the flux of meteoric fluids through the weathering zone, then decreases as hillslope gradients approach their limit of stability, thus limiting further development of physical relief [*Roering et al.*, 1999].

The texture of the bedrock is also vitally important; in crystalline bedrock fluid is typically transported through interconnected micro-pores and along grain boundaries, thus weathering is promoted by coarse, granular fabrics which generally have higher hydraulic conductivity than their fine grained counterparts [*Godard et al.*, 2001; *Migoń*, 2006; *Bazilevskaya et al.*, 2013], micro-fractures and mineral cleavage [*Pye*, 1986; *Buss et al.*, 2008]. This has been illustrated by a Bazilevskaya et al. [2013], who found weathering profiles were 20 times thicker on a granitic ridgeline compared to a neighbouring diabase ridgeline, despite the fact that from a reaction kinetics perspective the converse would be expected, due to the coarser texture of the granitic bedrock permitting a greater degree of connectivity within the porosity network. The interplay between bedrock properties – mineralogy, texture, structure – and chemical weathering is particularly important in the evolution of landscapes underlain by crystalline plutonic rocks [*Godard et al.*, 2001; *Migoń*, 2006]. Differences in crystal size distribution and jointing patterns are manifest in the structure, relief and soil thickness of their host landscape, with tor formation favoured in coarse grained granites and low densities of high angle cooling joints [*Goodfellow et al.*, 2014a; *Migoń and Vieira*, 2014]. Many of these characteristics relate to the formation, emplacement and cooling histories of the pluton, thus linking the geomorphic dynamics of these landscapes to petrogenesis [*Goodfellow et al.*, 2014a].

The role of saprolite and saprolite weathering in the scheme of broader landscape evolution is still relatively unexplored [*Dixon et al.*, 2009b]. Dixon et al. [2009b] found that saprolite weathering in the Sierra Nevada was at least in part climatically controlled, and that physical erosion and saprolite weathering were closely coupled.

They suggested that extensive saprolite weathering may promote more rapid rates of erosion by progressively weakening the substrate, although based on the previous discussion the direction of causality is arguably not uniquely defined. Moreover, in granite landscapes, slowly eroding, low relief topography is often underlain by thick weathered saprolite. Typically, granitoid rocks will readily disaggregate into a sandy grus under prolonged exposure to moisture [*Wahrhaftig*, 1965; *Thomas*, 1974; *Isherwood and Street*, 1976; *Migoń and Lidmar-Bergström*, 2001; *Migoń*, 2006]; formation of grussic saprolite may in fact be distinctive to weathering of granitoid lithologies [*Migoń*, 2006]. One distinctive feature of this weathering product is that the grain size distribution is overwhelmed by fine sand and silt calibre sediment [*Migoń*, 2006; *Attal et al.*, 2015]. As a result, rivers draining these deeply weathered regions will have a dearth of coarse bedload, thus potentially limiting the efficacy of fluvial incision and restricting the ability of rivers to respond to changes in base level [*Sklar and Dietrich*, 2001, 2004; *DiBiase et al.*, 2014b; *Gabet*, 2014; *Attal et al.*, 2015].

1.3.2 Geomorphic controls on ecosystems

Terrestrial ecosystems are heavily dependent on the presence of a hospitable substrate from which plants can derive the nutrients and moisture required to support their growth and function [e.g. *Graham et al.*, 2010; *Vitousek et al.*, 2010]. The patchwork of soil and rock outcrop that is common to many upland landscapes imposes its own spatial structure on that of the forest that it supports [*Gabet and Mudd*, 2010; *Sheffer et al.*, 2013]. Furthermore, variations in slope and aspect drive microclimatic variations that mediate evapotranspiration and moisture stress [*Stephenson*, 1990; *Urban et al.*, 2000; *Franklin*, 2003]. The physical template on which these ecosystems

develop in fundamentally dictated by the geomorphic setting, from the morphology of hillslopes, to the thickness and degree of weathering of the soil and saprolite, and the frequency at which ecosystems are disturbed by mass wasting processes such as landslides. Geomorphic gradients will thus drive ecological gradients, with the consequent transitions contributing to landscape-level biodiversity [*Hack and Goodlett*, 1960; *Smith et al.*, 1997]. In the following section I highlight three different mechanisms – moisture, nutrient availability and disturbance frequency – through which geomorphic processes may directly impact on the biosphere.

Moisture Limitation

Access to moisture is a prerequisite for the establishment of virtually all vegetation. A characteristic common to many landscapes is that ridgelines, which are dispersive, are relatively dry, whereas valley bottoms and hollows, which are convergent, are in general wetter; this is reflected in changing species composition in a range of forest settings [*Hack and Goodlett*, 1960; *Urban et al.*, 2000; *Hwang et al.*, 2009; *Chase et al.*, 2012; *Detto et al.*, 2013]. In seasonally dry forests, such as those that mantle the slopes of the Californian Sierra, the presence of a significant subsurface water store is crucial to moderate drought stress and maintain productivity through the growing season [*Royce and Barbour*, 2001; *Rose et al.*, 2003; *Witty et al.*, 2003; *Bales et al.*, 2011; *Colgan et al.*, 2012b; *Goulden et al.*, 2012; *Tague and Peng*, 2013; *Holbrook et al.*, 2014]. Climatic limitation on evapotranspiration and productivity is reflected in the macro-scale vertical zonation of forest ecosystems across the Sierra Nevada, with xeric woodlands and scrub in the lowlands giving rise to more mesic species as elevations increase and drought stress is reduced by the combination of lower

temperatures and greater precipitation [*Stephenson*, 1990, 1998; *Barbour and Billings*, 2000; *Urban et al.*, 2000]. Variations in hillslope aspect drive altitudinal shifts in ecotones, contributing towards spatial variability in forest communities [*Stephenson*, 1990; *Urban et al.*, 2000].

In granite terrain, weathered saprolite has an available water capacity of ~12%, while the capacity of soil is ~20% [*Jones and Graham*, 1993; *Graham et al.*, 2010]. In contrast, soil thickness in the Sierra Nevada is typically only 1-2 m in thickness [*Meyer et al.*, 2007; *Graham et al.*, 2010; *Yoo et al.*, 2011; *Gabet et al.*, 2015], compared to deeply weathered saprolite that is often an order of magnitude thicker. Within the first few years of their lifecycle, the root networks of trees growing in these settings penetrate into bedrock [*Witty et al.*, 2003], exploiting structural and crystallographic micro-fractures [*Jones and Graham*, 1993; *Zwieniecki and Newton*, 1995]; mycorrhizal hyphae permeate the rock fabric, enabling plants to access water stored within the confines of the weathered rocks porosity [*Egerton-Warburton et al.*, 2003; *Bornyasz et al.*, 2005]. The importance of the saprolite moisture store, after exhausting soil moisture, is directly implicated by coupled observations of soil moisture and evapotranspiration [*Bales et al.*, 2011; *Goulden et al.*, 2012]. Gradients in soil and saprolite thickness must therefore also result in gradients in moisture storage, productivity and drought stress [*Graham et al.*, 2010]. Given that soil and saprolite characteristics are fundamentally controlled by erosion rate, the dynamics of erosion should directly feed into the biosphere in moisture limited environments, although this coupling has not been explored previously. Finally, it is important to note that while the emphasis here is on forests in seasonally dry climates, soil and saprolite water

storage capacity has been implicated in explaining the vulnerability of trees to droughts even in normally very wet regions [*Slik et al.*, 2002].

Nutrient Limitation

The role of nutrient supply represents a second key linkage between the ecosystems and landscape evolution. For most ecosystems, key nutrients such as potassium, K, calcium, Ca and particularly phosphorous, P, are derived from weathering bedrock [*Walker and Syers*, 1976; *Vitousek et al.*, 2010; *Mage and Porder*, 2013; *Porder and Ramachandran*, 2013], while nitrogen primarily accumulates in soils through a combination of atmospheric deposition and biological fixation [*Amundson et al.*, 2003]. Ecosystem productivity is strongly dependent on the coupled availability of N and P [*Elser et al.*, 2007]. Variations in landscape characteristics that modify either P or N availability may thus impose a limit on biological productivity. Soil P concentrations are strongly regulated by bedrock composition [*Mage and Porder*, 2013; *Porder and Ramachandran*, 2013; *Hahm et al.*, 2014a]. For example, in the Californian Sierra Nevada, the compositional variations of the plutons that constitute the Sierra Nevada Batholith exhibit significant variations in P (and other cations) [*Hahm et al.*, 2014a]; plutons with exceptionally low P concentrations are not able to support any vegetation, giving rise to the formation of the distinctive "balds" that outcrop along the length of the range.

The dependence of productivity on nutrient availability underpins one of the paradigms of ecosystem ecology: productivity tends to decrease with soil age, as a result of the gradual exhaustion of P [*Walker and Syers*, 1976]. This effect has been

observed in variations in forest structure, productivity and nutrient status across chronosequences in a range of settings [*Vitousek et al.*, 2009; *Eger et al.*, 2011; *Kellner et al.*, 2011]. In landscapes that have been geomorphologically stable for thousands of years, erosion rejuvenates the bedrock-derived nutrient supply, promoting productivity [*Vitousek et al.*, 2003; *Porder et al.*, 2005a, 2005b]. In eroding landscapes, the effective soil age is determined by the rate of soil turnover, which controls the flux of fresh minerals into the critical zone [*Porder et al.*, 2007; *Mudd and Yoo*, 2010a; *Hilton et al.*, 2012]; this is itself inversely related to the erosion rate. Porder et al. [2007] demonstrated that in very slowly eroding landscapes, particularly in warm, humid climates that promote extensive weathering, ecosystems are likely to be P-limited; as erosion rates increase, the advection of fresh P-bearing minerals into the weathering zone reduces the extent of P-limitation, and ecosystems become N-limited, as there is less time for N accumulation to balance the increased P influx [*Amundson et al.*, 2003]; at very high rates of erosion, as observed in rapidly uplifting mountain ranges, P-limitation may be induced again, because there is not sufficient time for the P to become bio-available [*Porder et al.*, 2007]. Moving across the topographic transition from the base of the Andes (active erosion) into the Amazon Basin (active deposition), Asner et al. [2015] observed this expected transition in the canopy chemistry, which showed a marked change from relative P enrichment to relative N enrichment (P depletion), illustrating the role of the geomorphic template on nutrient status. In the Puerto Rico uplands, a transient increase in erosion rate, triggered by the passage of a tectonically induced incision wave, have been demonstrated to increase the availability of nutrients in the soil, alongside enhanced

fluvial solute fluxes [*Brocard et al.*, 2015; *Porder et al.*, 2015]. Conversely, Hilton et al. [2013] found that N-limitation could be induced as a consequence of landslides in steep, rapidly eroding landscapes, due to the export of organic material from the hillslopes and into the river system, restricting landscape N concentrations.

Forest Disturbance

Hillslope geomorphology additionally imposes an underlying control on the natural disturbance regime of forests, in particular the susceptibility to landslides [*Guariguata*, 1990; *Montgomery and Dietrich*, 1994; *Dietrich et al.*, 1995; *Roering et al.*, 2001a]. Landslides play an important role in the ecology of forests established on steep hillslopes [*Guariguata*, 1990; *Dislich and Huth*, 2012; *Stoffel et al.*, 2013; *Asner et al.*, 2014], and drive the erosion of soil and organic material (including aboveground biomass) [*Hilton et al.*, 2011, 2012, 2013]. Through the creation of clearings, landslides locally reset the forest succession sequence; the resultant canopy gaps typically receive much greater levels of insolation than penetrates undisturbed canopy, encouraging the establishment of light-demanding pioneer species [*Guariguata*, 1990]. Landslides therefore promote heterogeneity in both the structural characteristics of forests and biodiversity of species. Furthermore, by promoting forest turnover landslides may actually promote long term productivity, suppressing ecosystem retrogression [*Hilton et al.*, 2011]. The legacy of landslides may persist for many decades, even centuries, both in terms of recovery of the structure and composition [*Guariguata*, 1990; *Dislich and Huth*, 2012], and the overall levels of biomass of the forest community [*Dislich and Huth*, 2012]; ultimately the nature of

the speed and success of forest regeneration following disturbance is itself likely to be determined in part by the hospitality of the soils and bedrock [*Sass et al.*, 2012].

1.3.3 Vegetation as an active geomorphic agent

While the geomorphic setting imposes a physical template on the development of ecosystems, vegetation is itself an active geomorphic agent. Ruminating on the influence of rainfall and plants, Gilbert suggested:

> *"the general effect of vegetation is to retard erosion; and since the direct effect of rainfall is the acceleration of erosion, it results that its direct and indirect tendencies are in the opposite directions"* [*Gilbert*, 1877].

This effect was echoed by Langbein and Schumm's [1958] classic study of sediment yields exported from river catchments across climate zones within the USA; river sediment yields were found to increase with decreasing vegetation, resulting in higher fluxes in semi-arid catchments compared to more humid catchments. However, the emerging picture of the links between vegetation and geomorphic processes is significantly more complex and interconnected; vegetation is intimately involved in actively modifying the landscape through the production and transport of soils, and modulating the efficiency with which other geomorphic processes erode and transport sediment [e.g. *Hack*, 1960; *Thornes*, 1983, 1985; *Dietrich and Perron*, 2006; *Phillips*, 2009; *McGuire et al.*, 2014; *Stark and Passalacqua*, 2014; *Amundson et al.*, 2015]. Perhaps the most significant ways through which vegetation impacts on the geomorphic evolution of landscapes are: (i) stabilisation of soil through root reinforcement, impacting on shallow landslides [*Schmidt et al.*, 2001; *Gray and*

Barker, 2004] and reducing the efficacy of surface run-off by promoting infiltration and reducing flow velocity by obstructing flow [*Wainwright et al.*, 2000; *Istanbulluoglu and Bras*, 2005]; (ii) production of soil, both through the direct breakdown of bedrock [e.g. *Gabet and Mudd*, 2010; *Roering et al.*, 2010], and through the promotion of chemical weathering [*Taylor et al.*, 2009; *Brantley et al.*, 2011]; (iii) driving sediment transport through tree throw, and more gradual displacement by root network [*Norman et al.*, 1995; *Gabet et al.*, 2003; *Gallaway et al.*, 2009].

Resistance to Erosion

As surmised by Gilbert [1877], the root network of vegetation plays a major role in mechanically reinforcing shallow soils, and thus reducing susceptibility to landslides [*Terwilliger and Waldron*, 1991; *Schmidt et al.*, 2001; *Roering et al.*, 2003; *Gray and Barker*, 2004], and erosion via overland flow [*Dunne*, 1991; *Wainwright et al.*, 2000; *Istanbulluoglu and Bras*, 2005, 2006; *Ludwig et al.*, 2005; *Gutierrez-Jurado et al.*, 2007; *Saco et al.*, 2007; *Gutiérrez-Jurado et al.*, 2013]. The latter effect is compounded by the fact that vegetation increases interception, and increases the roughness of surface flow pathways, promoting infiltration and reducing the quantity and velocity of overland flow [*Wainwright et al.*, 2000; *Gutierrez-Jurado et al.*, 2007]. This stabilisation effect has been well documented in many studies of landscapes that have experienced significant increases in landslides frequency and overall sediment flux following forest disturbance following clear cutting or fires [e.g. *Benda and Dunne*, 1997; *Montgomery et al.*, 2000; *Moody and Martin*, 2001; *Schmidt et al.*, 2001; *Roering and Gerber*, 2005; *Rengers et al.*, 2016], and conversely stabilisation of hillslopes after afforestation or vegetation recovery [e.g. *Benda and Dunne*, 1997;

Vanacker et al., 2007], while the link between forest disturbance and sediment flux has been identified as a key driver of the stochasticity of hillslope sediment fluxes [*Dunne*, 1991; *Benda and Dunne*, 1997; *Iida*, 1999]. Considering shallow landslides within the context of the non-linear flux framework (Equation 1.5), Roering and Gerber [2005] calculated that the transient elevated sediment fluxes derived from post-fire shallow landslides in the Oregon Coast Range could be attributed to a reduction in S_c from 1.27 to 1.03 as a result of reduced root reinforcement.

The degree of root reinforcement is controlled by root tensile strength which itself varies with root thickness and density distribution of the root network, tree species present, and topographic position [*Montgomery et al.*, 2000; *Schmidt et al.*, 2001; *Roering et al.*, 2003; *Reubens et al.*, 2007; *Cohen et al.*, 2009; *Hales et al.*, 2009; *Schwarz et al.*, 2010]. The magnitude of root reinforcement within soils on vegetated hillslopes is dependent on the laterally aggregated properties of the root network, for which the behaviour under tensile stress is analogous to that of a bundle of fibres with varying diameters and mechanical properties [*Cohen et al.*, 2009, 2011; *Schwarz et al.*, 2010]. As the tensile stress within the soil increases, roots fail progressively; typically, fine roots break prior to thicker roots and thus their aggregated effect with respect to maximum root reinforcement is both sub-additive and strongly dependent on the distribution of root diameters present within the soil [*Cohen et al.*, 2011; *Schwarz et al.*, 2011]. Root reinforcement tends to be greatest proximal to trees, or where there is significant overlap of rooting systems of neighbouring trees [*Schwarz et al.*, 2012].

Moreover, mature, natural forest provide greater degrees of root reinforcement (25.6–94.3 kPa) than plantation forests (6.8–23.2 kPa), whereas root reinforcement in non-forested areas does not usually exceed <10 kPa [the figures quoted are based on observations of root reinforcement in the American Pacific Northwest; *Schmidt et al.*, 2001]. Root reinforcement also tends to be greater on drier micro-topographic sites (e.g. ridges) than in persistently moist sites (e.g. hollows), due to a reduction in the cellulose content of the roots [*Hales et al.*, 2009]. Incorporation of spatially variable root reinforcement, based on canopy properties, demonstrably improves estimates of slope stability in shallow landslide models [*Hwang et al.*, 2015].

Soil Production

In addition to retaining a soil mantle, vegetation actively drives the breakdown of bedrock to form soil *in situ*. In shallow soils, the root network of many tree and shrub species will penetrate pervasively both macro- and micro-fractures in the underlying saprolite and bedrock [*Jones and Graham*, 1993]. The high axial (1.45 MPa) and radial (0.91 MPa) pressures exerted by roots on the host rock [*Bennie*, 1991] are sufficiently high to propagate and widen existing fractures in the bedrock. Blocks of bedrock are often ripped up in the root wad of toppled trees [*Wilkinson et al.*, 2009; *Gabet and Mudd*, 2010]; this process is likely to be at least partly responsible for the local relief at the boundary between the PDZ and CAZ [*Heimsath et al.*, 2001; *Gabet and Mudd*, 2010; *Roering et al.*, 2010]. In addition to the physical break up of intact bedrock, the accumulation and subsequent oxidation of organic material at the soil-bedrock interface and within fractures and pore space reduces the pH of the proximal groundwater facilitating chemical weathering [*Berner et al.*, 2003; *Bonneville et al.*,

2009; *Taylor et al.*, 2009; *Brantley et al.*, 2011; *Rasmussen et al.*, 2011b]. Recent efforts to model chemical weathering from a more holistic perspective of the critical zone as the flow of Earth Energy and Mass Transfer (EEMT) that incorporates the influence of both climate and vegetation have yielded closer agreement with present day weathering fluxes [*Rasmussen and Tabor*, 2007; *Pelletier and Rasmussen*, 2009b; *Chorover et al.*, 2011].

The pedalogical role of vegetation has wider impacts on the evolution of landscapes. The efficiency with which vegetation breaks down bedrock, enables soil production to keep pace with more rapid rates of erosion in steep terrain [*Gabet and Mudd*, 2010; *Yoo et al.*, 2011; *Larsen et al.*, 2014a], particularly where the bedrock itself is sufficiently porous or fractured to provide an initial foothold after soil is stripped by landslides. Soil transported within the root wad during tree throw may also help to spread a veneer of soil over neighbouring exposed bedrock, in so doing expanding the extent of the soil mantle and providing more sites for vegetation and other biota to become established and drive further soil production [*Phillips and Marion*, 2004; *Osterkamp et al.*, 2006; *Gabet and Mudd*, 2010]. In localities where lithology is limited in its ability to support vegetation, such as through diagenetic controls on rock hardness [*Marshall and Roering*, 2014], or compositional controls on nutrient availability [*Hahm et al.*, 2014a], the absence of biotic soil production has been suggested to contribute to a reduction in bedrock lowering rates, generating relief. Compiling erosion rate estimates from studies of cosmogenic nuclide concentrations in the Sierra Nevada, Hahm et al. [2014a] noted a systematic drop in erosion rates where vegetation was absent, indicating that the impact of vegetation (or lack of) is

significant at geomorphological timescales. Likewise, in northern Chile, the transition to hyper-arid conditions (<10mm MAP) in the Atacama Desert is marked by a reduction in the rate of bedrock erosion by several orders of magnitude, associated with a shift from weathered soil-mantled hillslopes dominated by bioturbation to barren hillslopes with patchy/non-existent soils with weathering limited bedrock erosion driven by salt-mediated processes [*Owen et al.*, 2011; *Amundson et al.*, 2012].

Active Sediment Transport

While commonly associated with hillslope stabilisation and resistance to erosion, vegetation – particularly trees – plays an important role in transporting sediment across hillslopes. Diffusive sediment transport in forested terrain is particularly efficient [*Roering et al.*, 2004; *Hughes et al.*, 2009; *Hales et al.*, 2012]. Sediment transport via vegetation occurs due to small, grain-scale disturbances caused by the growth and propagation of the root network, and, more significantly, in discreet tree-throw events, in which larger volumes of sediment are transported in the root wad of the toppled tree [*Norman et al.*, 1995; *Gabet et al.*, 2003]; in forests where trees fall through snapping of the trunk rather than topple at the root wad, infilling of the stump hole left following the decomposition of the base may also be significant [*Phillips and Marion*, 2006]. A number of attempts have been made to quantify the degree to which tree throw specifically contributes to hillslope sediment transport [*Roering et al.*, 2002; *Gabet et al.*, 2003; *Gallaway et al.*, 2009; *Walther et al.*, 2009; *Constantine et al.*, 2012; *Martin et al.*, 2013], with order of magnitude estimates varying between 10^{-4} – 10^{-3} m^3 m^{-1} yr^{-1}, increasing with topographic slope.

Vegetation changes are increasingly being recognised as critical mediators in the geomorphic response of hillslopes to changing climate [*Roering et al.*, 2002; *Hughes et al.*, 2009; *Dosseto et al.*, 2010; *McGuire et al.*, 2014; *Stark and Passalacqua*, 2014]. On the low gradient (<30°) hillslopes of the Charwell Basin, New Zealand, changes in ecosystem composition from a patchwork of grassland and scrub to forest across the Pleistocene-Holocene transition are associated with more vigorous bioturbation and soil mixing [*Roering et al.*, 2002], and an increase in the colluvial sediment flux into the fluvial network [*Hughes et al.*, 2009]. Likewise, asymmetry of cinder cones in California and Arizona has been attributed to the higher rates of colluvial transport by vegetation integrated over the Quaternary period [*McGuire et al.*, 2014].

1.3.4 Conclusions

Life and landscape are intimately and inextricably linked. The physical and chemical characteristics of landscapes place fundamental constraints on the nature of ecosystems, modulating biogeochemical cycles and impacting on the availability of both moisture and nutrients. Geomorphic gradients are therefore likely to be an important, albeit unexplored, source of variance in ecosystem structure and may impact the dynamics of forest succession. Likewise, vegetation actively modifies the geomorphic evolution of landscapes, driving the production of soil, stabilising this soil on hillslopes, while also contributing to its transport. Vegetation is therefore likely to be a key intermediary modulating the landscape response to changes in climate or tectonics, while the geomorphic setting will simultaneously mediate the resilience of ecosystems to these same changes. Similarly, climate may modulate the sensitivity of ecosystems to geomorphic changes, in addition to the primary mechanism through

which this influence is felt. Nevertheless, despite the importance of the coupling of ecological and geomorphic systems, its impact on long term landscape evolution remains poorly constrained.

In most, if not all, commonly used geomorphic transport functions and soil production functions, the role of biology is bound up inside a series of numerical constants; there is no functional inclusion of biotic processes. Notable exceptions include inclusion of tree throw to understand aspects of soil production [*Gabet and Mudd*, 2010] and sediment transport [*Gabet et al.*, 2003; *Gallaway et al.*, 2009; *Constantine et al.*, 2012; *Martin et al.*, 2013], coupling of soil production, landslides and storm frequency [*D'Odorico and Fagherazzi*, 2003; *Stark and Passalacqua*, 2014; *Hwang et al.*, 2015], and combining climatic and biotic controls on chemical weathering through EEMT [*Rasmussen and Tabor*, 2007; *Rasmussen et al.*, 2011a, 2015; *Pelletier et al.*, 2013]. However, even in these cases, the predictive capacity of landscape evolution models is severely hindered by a dearth of empirical observations at the landscape scale that link life and landscape. These are a prerequisite to developing functional relationships between ecological systems and geomorphic processes, while in many cases computational requirements dictate that specific processes need to be up-scaled to be computationally tractable at the landscape scale. While this knowledge gap has begun to be addressed from both sides of the interdisciplinary divide, it is evident that there is a pressing need for many more studies that examine in detail the coevolution of vegetation, topography and erosion in a range of geomorphic and climatic settings.

1.4 LiDAR – a Mine of Ecological and Geomorphic Information

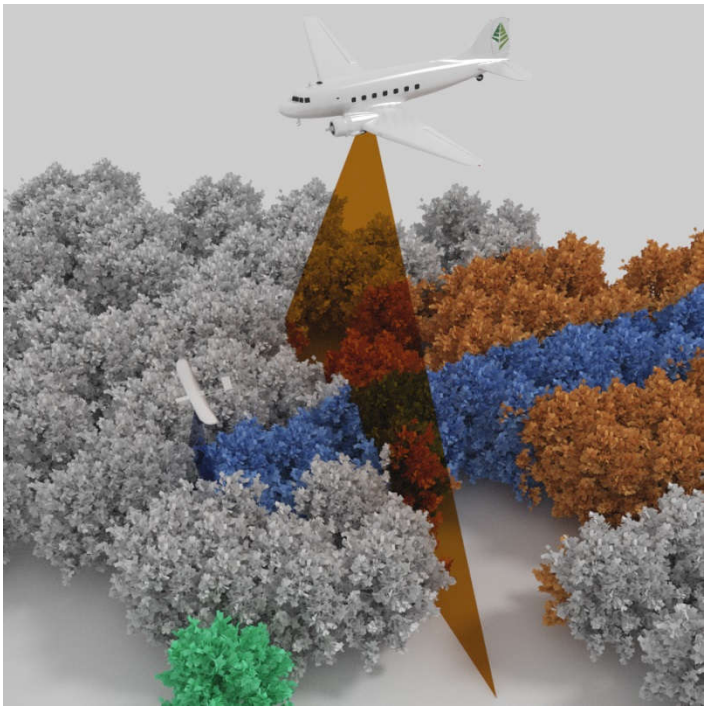

Figure 1.6 An illustration of three LiDAR survey methods: terrestrial LiDAR scanning (green), Airborne Laser Swath Mapping (ALSM) using manned planes (red) and UAVs (blue) [Image courtesy of Carbomap Ltd.; http://www.carbomap.com/]

1.4.1 An Introduction to LiDAR

The emergence of LiDAR over the past two decades has driven a revolution in the study of both the ecological and geomorphological characteristics of landscapes, by providing a rich level of high resolution detail regarding both canopy structure [*Lefsky et al.*, 1999a, 1999b, 2002; *Means et al.*, 2000; *Drake et al.*, 2003; *Lim et al.*, 2003; *Coops et al.*, 2007; *Næsset et al.*, 2011; *Asner et al.*, 2012, 2014] and the topography of the ground surface [*Slatton et al.*, 2007; *Glennie et al.*, 2013; *Roering et al.*, 2013; *Tarolli*, 2014; *Passalacqua et al.*, 2015].

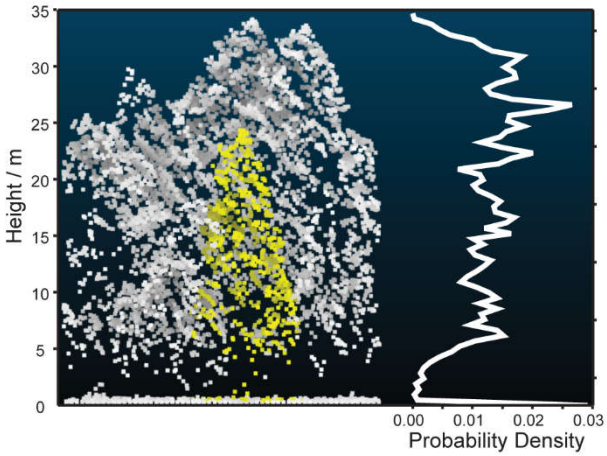

Figure 1.7 A sample from a LiDAR point cloud in extracted from a mixed conifer forest in the Californian Sierra Nevada, alongside a profile illustrating the vertical distribution of returns from the canopy. Note that the density of the point cloud is sufficiently high to segment individual trees, as indicated by the conifer in the foreground (coloured yellow).

At its essence, LiDAR comprises surveys conducted using laser range finding technology, in which pulses of laser light with a precisely defined waveform are fired at the survey target; on hitting a surface obstructing the trajectory of the ray-path, usually either the ground surface or vegetation, these incident pulses of light are partially or completely reflected; these reflected waveforms are subsequently detected by the LiDAR scanner. Typically, LiDAR surveys are conducted on either airborne or terrestrial platforms (Figure 1.6). In Airborne Laser Swath Mapping (ALSM), the LiDAR apparatus is fixed to a plane and then scanning proceeds by mapping a series of overlapping swaths across the landscape. In this manner, survey coverage can span large spatial scales. The resultant survey product usually consists of a three dimensional point cloud, each point representing a peak in the returning reflected waveform (Figure 1.7): point cloud densities of state-of-the-art airborne surveys regularly exceed several points per m^2 [e.g. *Means et al.*, 2000; *Lefsky et al.*, 2002;

Asner et al., 2012], with resolution of the ground surface at less than 1 m [*Slatton et al.*, 2007; *Glennie et al.*, 2013], and a high degree of accuracy and precision; typical horizontal and vertical errors are 10 – 20 cm and 5 - 10 cm respectively [*Shrestha et al.*, 2007]. The development of full waveform LiDAR products has the potential to yield yet greater degrees of detail on the bio-physical characteristics of vegetation, including species, and on the underlying substrate [e.g. *Mallet and Bretar*, 2009]. Terrestrial platforms provide higher resolution still, frequently at the centimetre scale [e.g. *Heritage and Hetherington*, 2007; *Brodu and Lague*, 2012], but at the expense of being spatially limited. The increasing accessibility of Unmanned Aerial Vehicles (UAVs) to the research community may provide potential to marry the benefits of these two approaches [e.g. *Lin et al.*, 2011].

LiDAR point clouds yield an exceptional level of detail regarding both canopy structure and the morphology of the topographic surface. In this section, I review the applications of LiDAR to document both the geomorphological and ecological characteristics of landscapes, providing the foundation on which my methodology is subsequently developed. An entire field of research exists on the pre-processing and classification of LiDAR data [see *Shrestha et al.*, 2007; *Slatton et al.*, 2007; *Glennie et al.*, 2013; among many others] however, as the LiDAR data used in this project had already been subject to this process, it is not considered further in this review.

1.4.2 Extraction of Geomorphic Information from LiDAR-derived Digital Elevation Models (DEMs)

In the absence of time-series data spanning the timescales of landscape development, addressing the long-term evolution of topography requires the quantification of both landscape and ecological characteristics that can be used to make inferences about their coupled evolution. Within any given setting, the topography will be subject to a suite of different geomorphic processes, each potentially leaving a distinctive signature in the morphology of the affected topography [*Stock and Dietrich*, 2003; *Roering et al.*, 2007, 2010; *DiBiase et al.*, 2010, 2012; *Passalacqua et al.*, 2010a; *Hurst et al.*, 2012; *Kirby and Whipple*, 2012; *Booth et al.*, 2013]. Landscapes are thus an encrypted record of their formative processes. Developing an understanding of how the dynamics of landscape evolution are encoded into this topographic record represents a challenge with huge potential: if topographic form can be quantitatively linked to process, topographic analysis can be used to directly test landscape evolution models [e.g. *Whittaker et al.*, 2007a; *Roering*, 2008; *Pelletier et al.*, 2011; *Hurst et al.*, 2012], predict variations in rates of erosion [e.g. *Ahnert*, 1970; *Snyder et al.*, 2000; *Kirby and Whipple*, 2001; *Roering et al.*, 2007; *Cyr et al.*, 2010; *DiBiase et al.*, 2010; *Hurst et al.*, 2012], and potentially recover past histories of uplift and subsidence [e.g. *Wobus et al.*, 2006; *Pritchard et al.*, 2009; *Roberts and White*, 2010; *Hurst et al.*, 2013a; *Perron and Royden*, 2013; *Fox et al.*, 2014, 2015; *Goren et al.*, 2014].

A Brief History of Topographic Analysis

The morphology of the Earth's surface represents the cumulative effects of constructive processes, such as tectonic uplift and faulting, which build topography,

and sediment production and transport, acting through a suite of climate- and gravity-driven geomorphic processes, which sculpt the landscape and generate relief. The premise of topographic analysis is that specific morphological features encode information regarding aspects of these formative processes, which can then be isolated and interrogated to characterise landscape attributes [e.g. *Dietrich et al.*, 2003]. Early pioneers of topographic analysis relied heavily on painstaking analysis of topographic contour maps to link topographic form to geomorphic process [e.g. *Hack*, 1960; *Ahnert*, 1970; *Carson and Kirkby*, 1972; *Dietrich and Dunne*, 1978]. In his seminal study on erosion rates, Ahnert [1970] compiled a dataset of large drainage basins and demonstrated that the sediment flux at the basin outlets obeyed a broadly linear relationship with the average topographic gradient within those catchments (Figure 1.2.a), in agreement with the expectations from simple diffusive models of hillslope erosion [*Gilbert*, 1909; *Culling*, 1965; *Carson and Kirkby*, 1972]. Ahnert's study was particularly influential because it highlighted the potential to derive quantitative information on rates of geomorphic change from the topographic structure of landscapes.

The increasing prevalence of Digital Elevation Models (DEMs) within geomorphological research greatly increased the ability of researchers to address research questions concerning the development of landscapes and dynamics of geomorphic processes with a quantitative foundation at scales not previously possible. In a range of settings, the characteristics of mountain range topography could be connected to the competition between rates of uplift and erosion [e.g. *Fielding et al.*, 1994; *Burbank et al.*, 1996; *Snyder et al.*, 2000; *Kirby and Whipple*, 2001; *Montgomery*

and Brandon, 2002], and to variations in climate [*Montgomery et al.*, 2001]. From a process perspective, DEMs also facilitated investigations concerning the routing of water and sediment through landscapes [e.g. *Tarboton et al.*, 1991; *Dietrich et al.*, 1993; *Montgomery and Dietrich*, 1994]. These early studies relied on DEMs derived primarily from digitised contour maps [e.g. *Fielding et al.*, 1994], and the resolution, accuracy and availability of these datasets varied significantly depending on location.

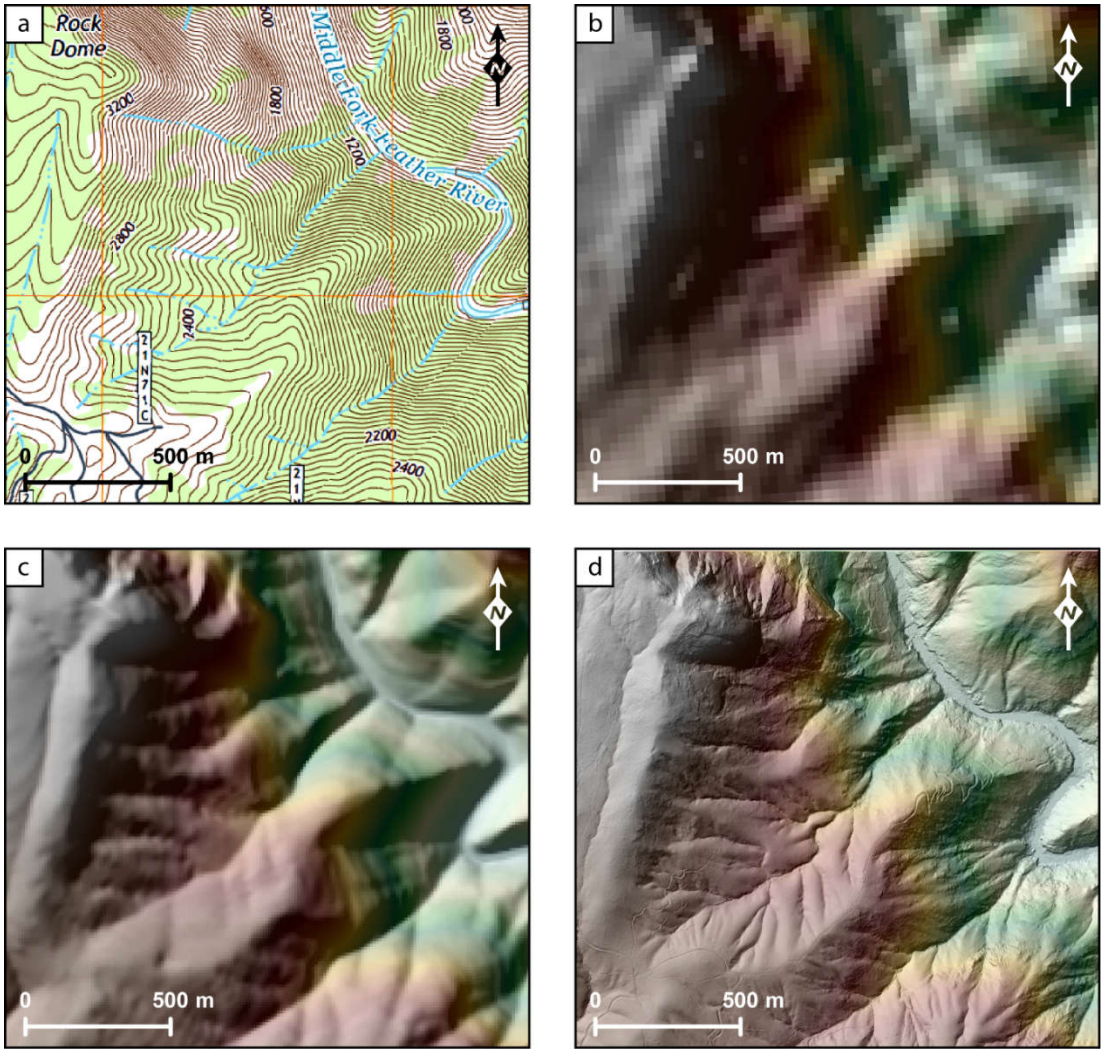

Figure 1.8 A comparison of different topographic datasets covering Bald Rock Basin, a tributary catchment of the Feather River, CA. (a) USTOPO topographic map; (b) 90 m resolution SRTM data; (c) 10m NED data; (d) 1 m LiDAR data.

The arrival of the "space-age" at the turn of the millennium, with the launch of NASA's Shuttle Radar Topography Mission [SRTM; *Rabus et al.*, 2003; *Farr et al.*, 2007] and Advanced Spaceborne Thermal Emission and Reflection Radiometer [ASTER; *Yamaguchi et al.*, 1998; *San and Suzen*, 2005] platforms, provided DEMs with near-global coverage and a horizontal resolution of 90 m and 30 m respectively, although the most recent version of SRTM now also has a resolution of 30 m. Concurrently, the USGS National Elevation Dataset, a DEM derived from USGS topographic maps, was released, providing 10 m horizontal resolution for the conterminous USA [*Gesch et al.*, 2002]. Whilst these datasets have raised the feasibility of topographic analysis applications worldwide at a resolution that was sufficient to examine the generation and structure of relief [*Wobus et al.*, 2006; *Miller et al.*, 2007; *Ouimet et al.*, 2009; *DiBiase et al.*, 2010; *Kirby and Whipple*, 2012], even 10 m resolution is still too coarse to analyse topography at the length-scales at which many specific geomorphic processes operate [e.g. *Stark and Stark*, 2001; *Passalacqua et al.*, 2010b; *DiBiase et al.*, 2012; *Hurst et al.*, 2012; *Fisher et al.*, 2013] (Figure 1.8). It is therefore unsurprising that the emergence of LiDAR, with horizontal resolutions surpassing 1 m, has driven such remarkable development in our understanding of process geomorphology and its relationship with topography.

Identification of geomorphic process domains

The structure of topographic relief is controlled by different geomorphic processes operating at different spatial scales [*Perron et al.*, 2008a, 2008b, 2009]. At length-scales of tens to thousands of km, topography is controlled by tectonic and mantle processes, which dictate the long wavelength patterns of uplift and subsidence that

provide the impetus for geomorphic processes to do erode and transport sediment [e.g. *Koons*, 1989; *Montgomery et al.*, 2001; *Roberts and White*, 2010; *Faure Walker et al.*, 2012; *Kirby and Whipple*, 2012; *Braun et al.*, 2013, 2014]. Within mountain belts, topographic relief is scaled by that of the fluvial network [*Burbank et al.*, 1996; *Ouimet et al.*, 2009; *DiBiase et al.*, 2010], and at wavelengths greater than ~100 m, topography is dominated by the spacing of ridges and valleys [*Perron et al.*, 2008a, 2008b, 2009]. On hillslopes, processes of erosion and sediment transport operate at length-scales that range from millimetres [e.g. rain splash: *Furbish et al.*, 2007; *Dunne et al.*, 2010], to metres [e.g. tree throw: *Norman et al.*, 1995; *Gabet et al.*, 2003; and bioturbation: *Yoo et al.*, 2005], to tens and hundreds of metres [e.g. landslides: *Montgomery and Dietrich*, 1994; *Hovius et al.*, 1997; *Ekström and Stark*, 2013]. As LiDAR data permits the quantification of topographic form at resolutions exceeding 1 m, this raises the prospect of being able to accurately delineate specific process domains, based on the characteristic "signature" that these processes engrave into the topography [*Tarolli and Dalla Fontana*, 2009; *Passalacqua et al.*, 2015]. As this thesis primarily deals with the hillslope domain, the review here is restricted to the isolation of the hillslope domain and the characterisation of hillslope form and active processes.

Perhaps the most fundamental process domain transition is that which separates the hillslope and channel domains, as this transition sets many aspects of landscape scale, such as hillslope length and drainage density [*Montgomery and Dietrich*, 1992; *Tucker and Bras*, 1998; *Perron et al.*, 2008b, 2009]. The problem of how best to characterise this process domain transition has long vexed geomorphologists and hydrologists [*Montgomery and Dietrich*, 1988]. The metre scale resolution provided by LiDAR

has enabled significant advances on the automated extraction of channel networks (and therefore also the isolation of hillslopes), due to the fact that the morphology of hillslopes is now characterised by hundreds of pixels along their lengths, rather than tens of pixels, at best, permitted by coarser datasets [*Slatton et al.*, 2007]. Several methods have been proposed with which to map the extent of the channel network; these can broadly be split into two families: geometric- [*Lashermes et al.*, 2007; *Passalacqua et al.*, 2010a, 2010b; *Pirotti and Tarolli*, 2010; *Sofia et al.*, 2011; *Pelletier*, 2013] and process-based [*DiBiase et al.*, 2012; *Clubb et al.*, 2014] methods. The former group, geometric-based methods, are based on the premise that hillslopes are divergent features in the landscape, while channels are convergent; the *channel* network can therefore be delineated using a positive curvature threshold, which may be derived from the statistical properties of the landscape [*Lashermes et al.*, 2007; *Passalacqua et al.*, 2010a]. Process-based methods look for the portions of the landscape for which the relief structure is controlled by specific geomorphic processes; fluvial profiles tend to exhibit systematic scaling of slope with upstream catchment area [*Hack*, 1957; *Whipple and Tucker*, 1999; *Perron and Royden*, 2013] , and the upstream extent of the *fluvial* network may be defined by the locations in the topography at which this scaling relationship breaks down [*Montgomery and Dietrich*, 1988, 1992; *Whipple and Tucker*, 1999; *Clubb et al.*, 2014].

In many soil-mantled landscapes, the transition from hillslope to channel processes is consistent with the changing competition between diffusive hillslope processes and advective fluvial processes [*Perron et al.*, 2009]. However, it is important to note that in steep landscapes, the evolution of headwater catchments and colluvial hollows may

be dominated by shallow landslides and debris flows [*Reneau and Dietrich*, 1991; *Stock et al.*, 2005], which adds a layer of complexity to this domain transition [*Stock and Dietrich*, 2003; *Tarolli and Dalla Fontana*, 2009; *DiBiase et al.*, 2012]. In these settings, the *channel* and *fluvial* networks are not necessarily directly equivalent; the method with which the channel network is defined will depend in part on the research question being addressed; indeed, it may be necessary to utilise *both* methods in some cases.

On hillslopes, processes of erosion and sediment transport operate at distinct length-scales. The relief structure of hillslopes thus provides a potential record of the dominant formative processes. Spectral analyses of high resolution topography provide a particularly good illustration of this: in landscapes where tree throw is prevalent, such as the Oregon Coast Ranges, roughness is concatenated into wavelengths below 7.5 m [*Roering et al.*, 2010; *Marshall and Roering*, 2014]; in contrast, active deep-seated landslides generate significant roughness at ~ 11–50 m [*McKean and Roering*, 2004; *Booth et al.*, 2009, 2013]. Further to spectral methods, other roughness metrics have commonly been used to characterise topography, facilitating the identification of specific process domains [*McKean and Roering*, 2004; *Tarolli and Dalla Fontana*, 2009; *Tarolli et al.*, 2010; *Lin et al.*, 2013; *Whelley et al.*, 2014].

Another potential source of topographic roughness at the hillslope scale is the emergence of bedrock. The transition from soil-mantled to bedrock topography drives a fundamental change in the nature of hillslope erosion [*Dietrich et al.*, 2003; *Binnie et al.*, 2007]; DiBiase et al. [2012] exploited LiDAR data in the San Gabriel Mountains

to map bedrock using the Rock Exposure Index (REI), which is based on the locations where the local topographic gradient exceeded a limit gradient beyond which soil is unstable. Within this setting, this method has been successfully utilised to explore the links between fire and sediment flux [*DiBiase and Lamb*, 2013]. While undoubtedly a useful development, particularly given the ease of implementation, the REI is limited in that in many landscapes, rock exposure may occur in low gradient settings, particularly in areas with thin, unstable regolith [*Anderson*, 2002; *Strudley et al.*, 2006a, 2006b; *Pelletier and Rasmussen*, 2009b], where bedrock heterogeneity drives variations in weathering rate [*Goodfellow et al.*, 2014a; *Migoń and Vieira*, 2014], and along ridgelines [*Gabet et al.*, 2015]. While not rendering it useless, a key limitation of the REI is that as it is solely predicated on local slope, it is not appropriate for testing hypotheses governing the emergence of bedrock that are not directly controlled by changing hillslope gradient. Complementary methods to map the occurrence of bedrock are thus required to explore the soil-bedrock transition in more detail.

Finally, it is pertinent to conclude this section with a brief discussion of filters at this point. Topographic data is inherently noisy. Some of this noise arises during data collection and processing: registration errors in original survey, classification errors, interpolation of sparse point cloud to a regular grid; some is geomorphic noise: e.g. bedrock outcrop on hillslopes, tree throw pits, boulders proximal to channels etc.. In many feature extraction processes, their success requires some degree of filtering is required; this is particularly the case for channel extraction, due to the sensitivity of curvature measurements to noise in the DEM [*Pirotti and Tarolli*, 2010]. Early work on channel extraction from LiDAR utilised a Gaussian filter to smooth the topography

[*Lashermes et al.*, 2007]; more recently, non-linear filters have been preferred due to their potential for improved feature preservation, notably the Perona-Malik filter [*Perona and Malik*, 1990; *Catté et al.*, 1992; *Passalacqua et al.*, 2010a, 2010b], Wiener filter [*Wiener*, 1949; *Pelletier*, 2013], and non-local means filter [*Buades et al.*, 2004; *Hurst et al.*, 2013a]. Alternatively, polynomial surface fitting [*Evans*, 1980] has been widely utilised to extract geometric derivatives of topography such as slope and curvature, with the size of the surface fitting window determining the degree of smoothing [*Tarolli et al.*, 2010; *Hurst et al.*, 2012; *Sofia et al.*, 2013]. There has been significant debate as to which filter is most appropriate [see for example the discussion within: *Clubb et al.*, 2015; *Passalacqua and Foufoula-Georgiou*, 2015]. However, it is not immediately apparent how the "noise" removed by each filter actually relates to the characteristics of the physical landscape under investigation, nor is this trivial to test in the field. Ultimately it is usually a case of finding the filter that works best for the particular landscape and research question.

Functional relationships between hillslope form and erosion rate

A second frontier of topographic analysis is to exploit the form of landscapes to reveal rates of change [e.g. *Kirby and Whipple*, 2001, 2012; *Ouimet et al.*, 2009; *DiBiase et al.*, 2010; *Hurst et al.*, 2012; *Whittaker*, 2012; *Perron and Royden*, 2013]. Rates of erosion are of particular interest due to the fact that to a large extent they dictate many aspects of topographic form, critical zone architecture and the nature of sediment transport (see section 1.3). While considerable attention has been given to estimating incision rates (and incision histories) from river profiles [*Kirby and Whipple*, 2001, 2012; *Ouimet et al.*, 2009; *Pritchard et al.*, 2009; *DiBiase et al.*, 2010; *Roberts and*

White, 2010; *Perron and Royden*, 2013; *Royden and Perron*, 2013; *Goren et al.*, 2014; *Mudd et al.*, 2014; *Fox et al.*, 2015], the form of soil mantled hillslopes also represents a potentially fruitful archive [*Roering et al.*, 2007; *Hurst*, 2012; *Hurst et al.*, 2012, 2013a, 2013b; *Wood*, 2013; *Marshall and Roering*, 2014]; it is the latter that is the focus of this section.

At low gradients the non-linear diffusion law (Equation 1.5) is approximated by the linear diffusion law (Equation 1.4; Figure 1.3), and erosion rates are proportional to topographic curvature. Hurst et al. [2012, 2013a, 2013b] exploited this relationship, using hilltop curvature, C_{HT}, as a direct measure of the spatial distribution of erosion rates across soil mantled landscapes:

$$E = -\frac{\rho_s}{\rho_r}\kappa C_{HT} \quad (1.10).$$

ρ_s and ρ_r represent the soil and bedrock densities respectively. The extent to which Equation 1.10 can be used as a quantitative indicator of erosion rate may depend on the variability of the PDZ: if the efficiency of sediment transport is depth-dependent [*Heimsath et al.*, 2005; *Roering*, 2008; *Pelletier et al.*, 2011], then the relationship between curvature and erosion rate will be modulated by soil depth. Reductions in soil depth are an expected consequence of increased rates of erosion [*Carson and Kirkby*, 1972; *Heimsath et al.*, 1997], while local topography also exerts an influence on the variability of soil thickness, due to feedbacks between moisture availability, vegetation and weathering [*Gabet et al.*, 2015]. Variations in lithology may also modulate this relationship, again likely due to its influence on soil characteristics [*Hurst et al.*, 2013b]. Hurst et al. [2012] averaged curvature over ridgeline segments

in order to reduce the variance in erosion rate estimates; encouragingly, their comparison of catchment-wide erosion rates derived from cosmogenic radionuclide concentrations in river sediments and catchment-averaged hilltop curvature yield a strong linear correlation ($R^2 = 0.83$), fuelling optimism that this approach can produce meaningful results.

In addition to quantifying erosion rates, hillslope form, obtained through LiDAR surveys, can be exploited to test the validity of geomorphic transport models, and look for topographic signatures of transience. Roering et al. [2007] provide a non-dimensional framework for analysing the relationships between denudation and topography using dimensionless parameters for relief and erosion rate that are readily extracted from DEMs. They define dimensionless relief, $R^* = R/(S_c L_H)$, and dimensionless erosion rate $E^* = E/E_R$ where L_H defines the hillslope length and E_R is a reference erosion rate defined by:

$$E_R = \frac{\kappa S_c}{2L_H(\rho_s/\rho_r)} \tag{1.11}.$$

Combining equations 1.10 and 1.11 gives a new parameterisation for E^*:

$$E^* = \frac{-2C_{HT}L_H}{S_c} \tag{1.12}.$$

Similarly, R^*, can be recast for the non-linear sediment flux model (Equation 1.5) using mean slope as:

$$R^* = \frac{\overline{S}}{S_c} = \frac{1}{E^*}\left[\sqrt{1+(E^*)^2} - \ln\left(\frac{1}{2}\left(1+\sqrt{1+(E^*)^2}\right)\right) - 1\right] \tag{1.13}.$$

The equilibrium form of a hillslope governed by Equation 1.5 is characterised by a systematic relationship between E^* and R^*, described by Equation 1.13 (Figure1.9). Since L_H, C_{HT} and S_c are readily obtained from high resolution DEMs, this framework permits direct comparisons between the systematics of denudation and topography for landscapes subject to distinct rates of erosion, while also providing a method to test the applicability of different geomorphic transport functions. Working in the Feather River region of the Sierra Nevada, Hurst et al. [2012] demonstrated that the covariation of relief, hillslope length and ridgetop curvature (E^* vs. R^*) correspond well with the expectations of steady state hillslopes predicted by the non-linear flux law posited by Roering et al. [1999, 2007].

This non-dimensional framework can also be utilised to explore hillslope transience, as highlighted by Hurst et al. [2013a], who investigated the evolution of Dragon's Back Ridge, California, to a pulsed uplift field generated by a compressive bend on the San Andreas Fault [*Hilley and Arrowsmith*, 2008]. Elevated uplift rates drive an upstream propagating wave of

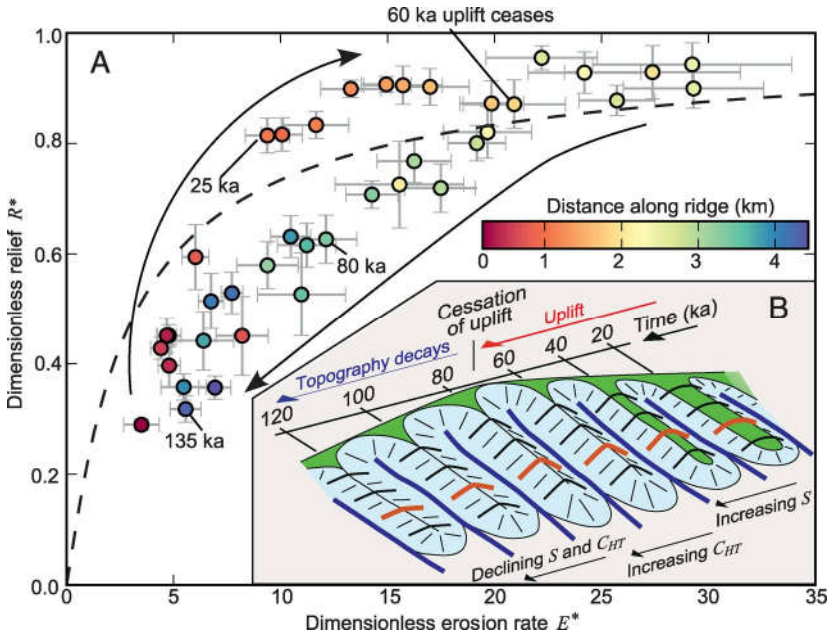

Figure 1.9 The transient evolution of a hillslopes along Dragon's Back Ridge, California, in E*-R* space. The dashed line indicates the steady state relationship predicted by Equation 1.13. Hillslopes that are adjusting to increased rates of incision at their base, associated with the base level fall due to tectonic uplift plot above this line – relief is generated before the signal propagates up to the hilltop. Hillslopes relaxing post-uplift, i.e. decaying topography, fall below the steady state line. Redrawn from Hurst et al. [2013a].

incision; in response to greater incision at their, hillslopes steepen, but it takes time for this signal to propagate to the ridgetop. "Growing" landscapes, adjusting to a recent increase in base level fall, should thus lie above the expected steady state line within E^*-R^* space [*Hurst et al.*, 2013a]; in contrast, hillslopes responding to a drop in the rate of incision at their base should plot just below this steady state line, particularly if the fluvial transport capacity drops to the extent that the river switches from incision to deposition. Hillslopes therefore exhibit striking hysteresis (Figure 1.9) when subject to a pulse of uplift, which is well captured in the topography of Dragon's Back Ridge [*Hurst et al.*, 2013a].

1.4.3 Analysis of vegetation

Quantification of canopy structure and aboveground biomass

The power of LiDAR in exploring ecosystem properties lies in the fact that it provides direct observations of the three-dimensional structural characteristics of forests, such as canopy height [*Nelson et al.*, 1984; *Lefsky et al.*, 1999a; *Means et al.*, 2000; *Khosravipour et al.*, 2014] and gap distributions [*Koukoulas and Blackburn*, 2004; *Asner et al.*, 2013]. Laser pulses are reflected back to the sensor from leaves and branches, and in so doing characterise the vertical stratification of material within the canopy; pulses that penetrate through to be reflected from the ground surface provide a means with which to accurately determine the absolute height above ground of these returns. By constraining the physical dimensions of the canopy, LiDAR can be readily exploited to map the distribution of aboveground biomass (AGB) within landscapes, due to the allometric scaling of biomass with tree size [*Lefsky et al.*, 1999b; *Means et al.*, 2000; *Asner et al.*, 2012]; LiDAR surveys have been successfully employed for this purpose in a range of biomes, from tropical rainforests to boreal forests [e.g. *Lefsky et al.*, 1999b, 2002; *Means et al.*, 2000; *Drake et al.*, 2003; *Lim et al.*, 2003; *Næsset and Gobakken*, 2008; *Næsset et al.*, 2011; *Asner et al.*, 2012; *Sankey et al.*, 2013; *Asner and Mascaro*, 2014; *Taylor et al.*, 2015]. Additionally, these observations can be made at a level of detail that is sufficient, in many cases, to capture the crown of individual trees [*Chen et al.*, 2006; *Brandtberg*, 2007; *Popescu*, 2007; *Li et al.*, 2012; *Jakubowski et al.*, 2013; *Khosravipour et al.*, 2014] (Figure 1.7).

Prior to the emergence of LiDAR, obtaining such direct observations of the architectural attributes of the canopy necessitated laborious field measurements. As a consequence of the heterogeneity exhibited in many forests, many inventory plots are required to accurately characterise forest biomass stocks in this manner [*Keller et al.*, 2001; *Chave et al.*, 2003]; furthermore, labour-intensive large plot sizes (~1 Ha) are demanded as plot biomass is non-normally distributed at small plot sizes [*Chave et al.*, 2003]. While other remote sensed technologies besides LiDAR – such as satellite-based methods exploiting optical imagery, such as those provided by Landsat [*Skole and Tucker*, 1993; *Goward and Williams*, 1997; *Foody et al.*, 2003; *Hansen et al.*, 2013] and radar [*Waring et al.*, 1995; *Kasischke et al.*, 1997; *Mitchard et al.*, 2009] – also provide a solution to the scale problem, readily collecting data covering large spatial scales; however, the footprint of these methods typically spans the order of tens of metres. As a result they are not able to resolve canopy structure at the scale of individual trees, while uncertainty increases significantly in regions where there is significant topographic relief.

The underlying premise of most estimates of tree biomass is that biomass scales systematically with tree size, such that there exist functional allometric relationships between biomass and the physical aspects of tree form, such as height and trunk diameter [e.g. *Chave et al.*, 2005]. Allometric models are typically constructed via harvesting of individual trees at different stages in their growth, with trunk diameter, then tree height accounting for the most variance in biomass between samples [e.g. *Chave et al.*, 2005; *Návar*, 2009; *Halpern and Means*, 2011]. Due to the labour intensity involved, often the samples upon which allometric models are limited in

terms of size, particularly in the case of large trees. As a result of heteroscedasticity, uncertainties at the plot level are dominated by the largest trees [*Chave et al.*, 2003]. Furthermore, in most cases there are no site-specific – and frequently no species-specific – models, thus necessitating the use of regional-national levels allometric models based on species groups [*Jenkins et al.*, 2003]. The application of these allometric models to estimate tree biomass in different species or regions presents a major source of uncertainty, with potential for systematic bias [*Jenkins et al.*, 2003; *Chave et al.*, 2004; *Yanai et al.*, 2010].

In the case of LiDAR-based AGB mapping, the vast majority of AGB-scaling relationships are calibrated through regression against *estimates* derived from field inventory plots [e.g. *Lefsky et al.*, 1999b; *Asner et al.*, 2012; *Zhao et al.*, 2012], rather than against *measured* AGB from harvested, stand-level plots that provide a direct quantification of the AGB that is "perceived" by the LiDAR sensor [*Colgan et al.*, 2012a]. Uncertainty in LiDAR-derived biomass is therefore fundamentally dependent on the errors inherent to the plot inventory collection, and particularly on the quality and uncertainty of the allometric models used to estimate biomass [*Clark and Kellner*, 2012]. Different sets of allometric equations can lead to significant differences in the plot-based AGB [*Zhao et al.*, 2012; *Chen*, 2015]; Zhao et al. [2012] found a reduction in the variance of ~10% between plot-based and LiDAR-based AGB estimates within a Sierra Nevadan conifer forest when utilising regional allometric equations that incorporated tree height [*Waddell et al.*, 2005], rather than national-level models that accounted for trunk diameter alone [*Jenkins et al.*, 2003, 2004].

Additional sources of error in the calibration of LIDAR metrics arise as a consequence of the discordance between the AGB estimated within the plot, and that observed by the LIDAR, specifically: (i) GPS positional error, both in the location of the inventory plot and the geo-referencing of the LIDAR point cloud [*Asner*, 2009; *Frazer et al.*, 2011]; (ii) temporal differences between LiDAR and field surveys; (iii) a mismatch between trees identified within the field plots (stem localised) and the corresponding LiDAR point cloud (crown-delimited), which in turn leads to differential inclusion of overlapping canopy and may account for 50% of the overall uncertainty [*Mascaro et al.*, 2011]. In general, errors of type (i) and type (iii) decrease as the inventory size used in the calibration process increases [*Frazer et al.*, 2011; *Mascaro et al.*, 2011]. Propagating errors through the calibration process using a Monte Carlo approach, Gonzalez et al. [2010], calculated that uncertainties in biomass quantification at the plot level can be as much as 25% for forests in Northern California, but when integrated over the extent of their field site (>50 km^2), uncertainties fall below <1%.

1.4.4 Conclusions

Topographic data derived from LiDAR surveys can be used to identify active hillslope processes and quantify the rate at which they are eroding. Variations in canopy height, mapped from the LiDAR point cloud, can be used to extract a rich level of detail on canopy structure, providing high fidelity maps of biomass with significantly lower uncertainty bounds. Moreover, of the few studies that have started to bridge the link between the physical template imposed by landscapes and the ecosystems established upon them, airborne surveys have played a pivotal role [*Roering et al.*, 2010; *Kellner et al.*, 2011; *Colgan et al.*, 2012b; *Deligne et al.*, 2013; *Detto et al.*, 2013; *Pelletier et*

al., 2013; *McGuire et al.*, 2014; *Asner et al.*, 2015; *Gabet et al.*, 2015; *Taylor et al.*, 2015]. The ability to quantify both topographic form and canopy structure across scales of several tens of kilometres at the metre-scale resolution required to quantify hillslope form and processes, makes LiDAR an immensely valuable tool with which to integrate analyses of landscape ecology and geomorphology.

1.5 Thesis Outline

The thesis comprises six chapters, each of which can be read instead as standalone papers. This broad introduction (Chapter 1) and following overview of the primary study site (Chapter 2) provide the context for the three subsequent research chapters (Chapters 3-5). Of these, Chapters 3 investigates how erosion rate modulates the characteristics of the Sierra Nevada mixed conifer forest; Chapter 4 introduces a novel method to map rock exposure on hillslopes, while Chapters 5 explores the ecological and geomorphic response of hillslopes to the fluvial incision history of the Middle Fork Feather River. A more detailed breakdown of the research chapters is given below. Finally, in Chapter 6 I assimilate these branches into an overall synthesis, before drawing the thesis to a close with my final conclusions.

Chapter 3 Erosion rates as a potential bottom-up control on forest structural characteristics

In chapter 3 I explore how the gradient in erosion rates exhibited by the Feather River landscape impacts on the biosphere. By utilising LiDAR data to characterise both the covariation of erosion rate with aboveground biomass, I illustrate that rates of erosion place a major control on the characteristics of the mixed conifer forest in this region.

Chapter 4 Surface roughness as a topographic signature of the emergence of bedrock in eroding landscapes

In this chapter I introduce a new method with which to locate areas of hillslope on which rock emerges at the surface, based on a measure of surface roughness. I then validate this method in two test sites with variable degrees of bedrock exposure, before

utilising it in a tributary catchment of the Feather River, in addition to an additional transient landscape in Idaho, to explore the nature of the transition from soil mantled to bedrock hillslopes as fluvial incision rates at their base is increased.

Chapter 5 Lithology, vegetation and sources of complexity in the coupled geomorphic and ecological response of hillslopes to incision

Chapter 5 builds on the previous research chapters, exploring the variability exhibited in both the ecological and geomorphic characteristics of hillslopes. Building on previous work by Hurst et al. [2012, 2013b] and the research presented here in Chapters 3 and 4, I illustrate the degree of heterogeneity exhibited within the hillslope response to differing rates of fluvial incision. This includes differences in both the transition from soil-bedrock hillslopes, and in the characteristics of the mixed conifer forest that mantles them. Combined, this heterogeneity appears to drive differential evolution trajectories in response to comparable geomorphic forcing. Moreover, heterogeneity appears to be strongly linked to geology, reflecting both inter- and intra-lithological differences. These results strongly suggest that the evolution of landscapes underlain by mixed bedrock, particularly hard, crystalline basement rock, is modulated by the complex interplay between lithology, soil production and vegetation. Furthermore, I use a simple numerical model for the evolution of a hillslope that explicitly incorporates the coupling of vegetation and soil production to illustrate that the soil-bedrock transition is modulated by eco-geomorphic feedbacks.

Chapter 2. Study Site: Feather River, Californian Sierra Nevada

A review of the geological, ecological and geomorphological setting

2.1 Introduction

This chapter provides a brief summary of long term evolution of the Sierra Nevada Mountains in the western United States, focusing on the Northern Sierra Nevada, in addition to summarising the geomorphology and ecology of this region. A full review of these topics is comfortably beyond the scope of this thesis, but it is hoped that the material covered is sufficient to provide a foundation of knowledge of the broader setting within which the subsequent observations are nested. For further detail, I warmly encourage the reader to explore the references within; in particular, Gabet [2014] provides a detailed review of the geomorphic evolution of the Sierra Nevada mountains that is particularly pertinent to later chapters of this thesis; Decelles [2004] provides a thorough overview of the tectonic genesis of the range, while an extensive characterisation of the structure, lithology and petrology within the field site was undertaken by Hietanen [1951, 1976] and Compton [1955].

2.2 Regional Setting: Sierra Nevada Mountains, Western USA

The Sierra Nevada Mountains form the montane spine along the eastern flank of the State of California. From Fredonyer Pass, the northern-most limit of the Feather River catchment and boundary with the southern Cascade Mountains, the range stretches continuously over ~650 km to the Tehachapi Pass and Mojave Desert in the south

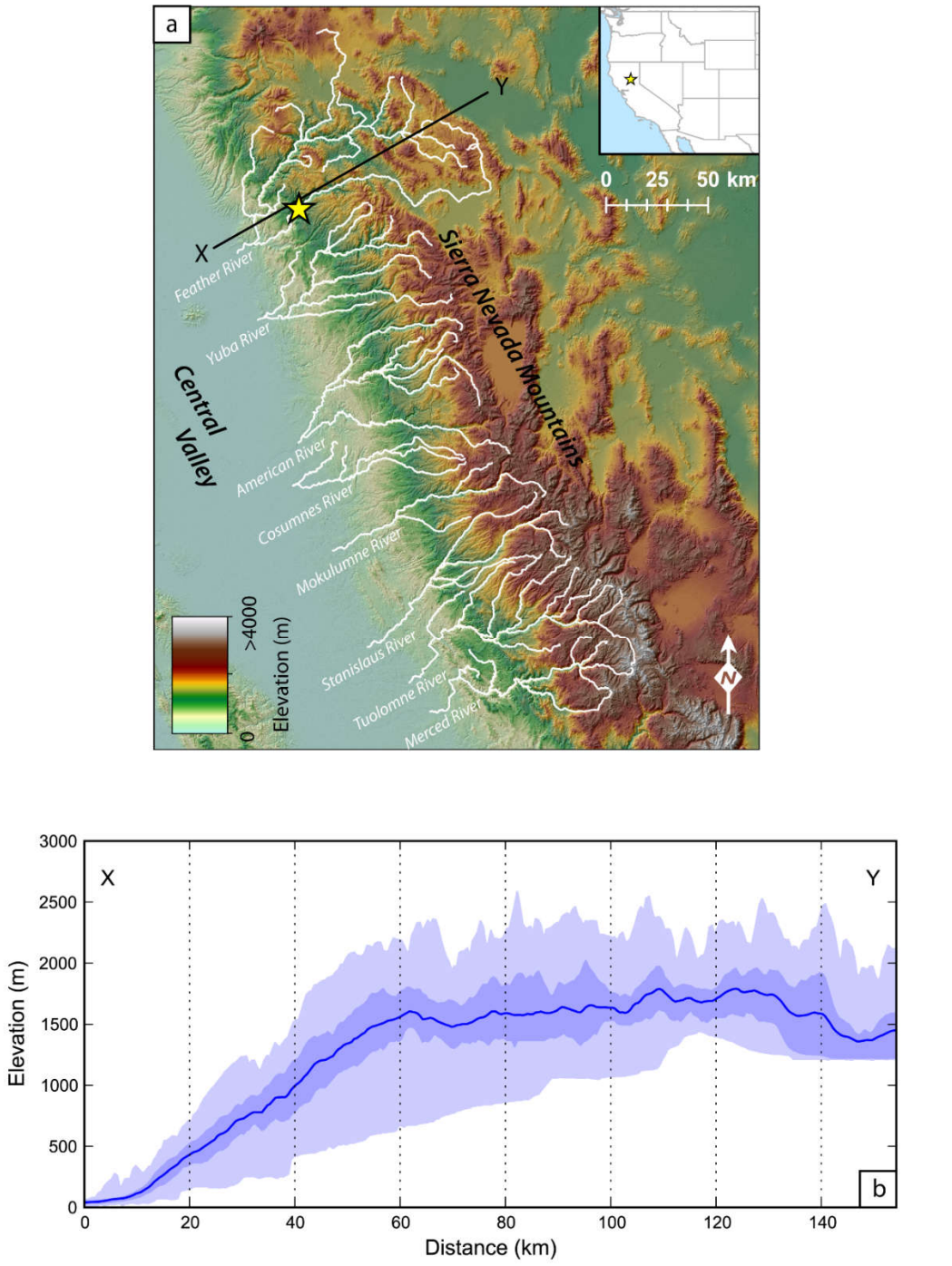

Figure 2.1 (a) Topographic map covering the Northern Sierra Nevada Mountains, based on 30 m SRTM. The location of the study site is indicated by the yellow star; (b) topographic profile for a 100 km wide swath taken along the transect X-Y, displaying the mean elevation along the transect, bounded by the interquartile range (darker blue region) and full range (light blue region) of elevations.

(*Figure 2.1*). The range is distinctly asymmetric, rising steeply from the range-bounding faults in the East to elevations exceeding 3000 m at the range crest, before descending more gradually westwards towards the Central Valley.

The long term evolution of this mountain range fits into the broader evolution of the North American Cordillera, a broad swath of mountainous terrain that runs ~6000 km along the convergent western margin of the North American plate. Active orogenesis in the Sierra Nevada occurred from the Late Jurassic to the Paleocene, driven by convergence and subduction at the arc-trench system established at the western margin of the North American Plate, punctuated by the tectonic accretion of a succession of island arcs and inter-arc basin terranes [*DeCelles*, 2004; *Dickinson*, 2004]. Voluminous arc magmatism above the Cascadia subduction zone during the Jurassic and Cretaceous emplaced a suite of batholithic granitoid plutons, which now form the core of the Sierra Nevada mountain range [*Ducea*, 2001; *Cecil et al.*, 2012].

Exhumation rates, determined through thermo-chronometric dating of apatite and zircon grains, peaked towards the end of the Cretaceous and into the early Cenozoic [*House et al.*, 1998, 2001; *Cecil et al.*, 2006]. High topography in the Sierra Nevada throughout the Cenozoic is indicated by paleo-botanical observations from lacustrine deposits [*Wolfe et al.*, 1998], and paleo-climatic studies, based on oxygen and deuterium isotopes, which suggest the persistence of an orographic rainfall gradient [*Poage and Chamberlain*, 2001; *Horton et al.*, 2004; *Mulch et al.*, 2006, 2008; *Cassel et al.*, 2009, 2014; *Hren et al.*, 2010; *Chamberlain et al.*, 2012]. Throughout this period, the Sierra Nevada landscape was subject to alternating periods of erosion and deposition of fluvial sediments and volcanogenic deposits [*Busby and Putirka*, 2009;

Cassel et al., 2009, 2012; *Chamberlain et al.*, 2012; *Gabet*, 2014], concurrent with major changes in global climate [*Zachos et al.*, 2001]. To the east, contemporaneous crustal extension through the Miocene, driven by crustal collapse of the previously high elevation Nevadaplano, generated the neighbouring Basin and Range Province [*DeCelles*, 2004; *Busby and Putirka*, 2009; *Cassel et al.*, 2014], the western-most extent of which is marked by the range-bounding normal faults at the eastern margin of the Sierra Nevada. Moving into the Holocene, estimates of incision rates from cosmogenic nuclides, which average over millennial timescales, indicate a relatively recent pulse of fluvial incision in the precipitous canyons that have been carved along the length of the range [*Riebe et al.*, 2000; *Stock et al.*, 2004; *Hurst et al.*, 2012]. Moreover, the drainage system has undergone a complex history of incision, aggradation, disruption and reorganisation since the emergence of the Sierra Nevada range [*Cassel and Graham*, 2011; *Gabet*, 2014].

Ecologically, at the macro-scale, the Sierra Nevada are characterised by a vertical stratification of ecosystems, moving from oak and chaparral woodland in the lowlands, through mixed conifer forests that typically mantle the Sierran foothills, to alpine coniferous forests that occupy the high Sierra [*Barbour and Billings*, 2000]. The distribution of the ecotones that bound these forest types are primarily constrained by elevation-controlled changes in climate [*Stephenson*, 1990, 1998; *Urban et al.*, 2000]. At low elevations, close to the Central Valley, productivity and actual evapotranspiration is limited by moisture availability through the dry summer months, hence the dominance of xeric woodland communities; as drought stress decreases with increasing elevation through the foothills, coniferous species become increasingly

prevalent. Ultimately, low winter temperatures become an increasingly dominant factor limiting productivity in the high Sierra Nevada mountains [*Stephenson*, 1990; *Urban et al.*, 2000; *Goulden et al.*, 2012].

Focusing on the mid-elevations of the Sierra Nevada, the mixed conifer forests that dominate the mid-elevations of the Sierra range are typically established on thin soils (<2 m), underlain by often extensively weathered saprolite [*Hubbert et al.*, 2001; *Meyer et al.*, 2007; *Graham et al.*, 2010; *Yoo et al.*, 2011; *Gabet et al.*, 2015]. As the growing season is characterised by long periods of little to no precipitation, these forests are strongly dependent on the moisture stored within the substrate [*Rose et al.*, 2003; *Witty et al.*, 2003; *Graham et al.*, 2010; *Bales et al.*, 2011; *Goulden et al.*, 2012]. Weathered granitic saprolite has an available water capacity of ~12%, which, whilst lower than that of soil (~20%), makes it a vital water store that continues to supply vegetation with moisture through the dry season long after the soil moisture has been exhausted [*Rose et al.*, 2003; *Witty et al.*, 2003; *Graham et al.*, 2010; *Bales et al.*, 2011]. Within the first few years of growth, the root networks of pine, oak and chaparral species penetrate into bedrock to exploit this resource [*Witty et al.*, 2003], with extensive propagation of rooting systems through both macro and micro fractures within the bedrock [*Jones and Graham*, 1993]. Mycorrhizal hyphae facilitate the extraction of moisture and nutrients from the bedrock, linking the roots to moisture and nutrients with the water stored within the pore space in the saprolite matrix [*Egerton-Warburton et al.*, 2003; *Witty et al.*, 2003; *Bornyasz et al.*, 2005]. The dependence of this forest ecosystem on the characteristics of the substrate potentially renders it particularly sensitive to the history of erosion and weathering on hillslopes

on their combined impact on development of saprolite and soils [*Meyer et al.*, 2007; *Graham et al.*, 2010].

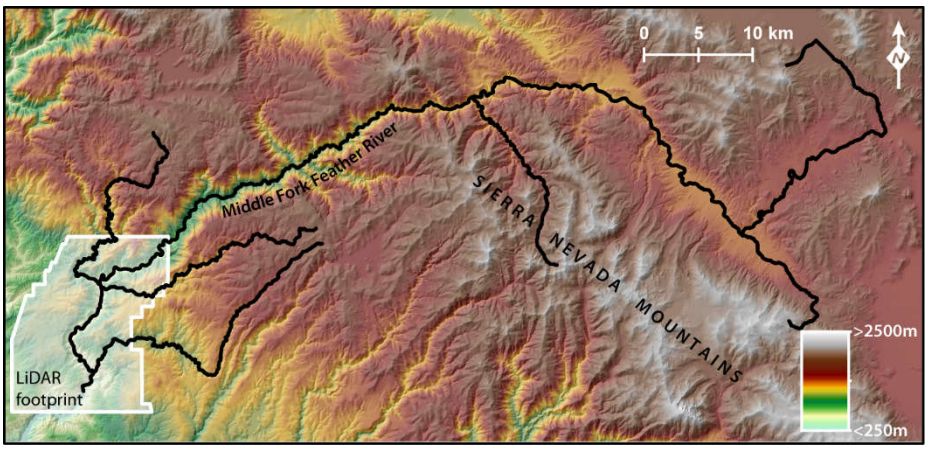

Figure 2.2 The Middle Fork Feather River; the extent of the LiDAR survey is indicated

2.3 Middle Fork Feather River, Northern Sierra Nevada

The Feather River is the most northerly of the principal transverse rivers draining the western flank of the Sierra Nevada (*Figure 2.1*). It comprises four tributary forks, the North Fork, Middle Fork, South Fork and West Branch, which amalgamate into Lake Oroville Reservoir, from which it flows southwards, into California's Central Valley where it ultimately flows into the Sacramento River. The field site that forms the primary focus of this study lies within the boundaries of the Plumas National Forest, located along the lower reaches of the Middle Fork Feather River (*Figure 2.2*), the main stem of which stretches over 160 km from its headwaters in the Sierra Valley, draining a catchment area covering ~2750 km^2. The site is bounded by the extent of an airborne Light Detection And Ranging (LiDAR) survey spanning ~208 km^2, undertaken in September 2008 by the National Center for

Airborne Laser Mapping (NCALM; http://ncalm.cive.uh.edu/; data available from http://www.opentopography.org/).

2.3.1 Geology

Detailed geologic mapping of the Feather River region was undertaken during the latter half of the 20th Century [*Hietanen*, 1951, 1976; *Compton*, 1955; *Day et al.*, 1985; *Saucedo and Wagner*, 1992]. The bedrock geology is characterised by a cluster of plutons that have been intruded into an assemblage of metamorphic Slate Creek Complex [*Hietanen*, 1976; *Saucedo and Wagner*, 1992] (*Figure 2.3*). The Slate Creek Complex is a suite of ophiolite-derived, greenschist to epidote-amphibolite facies, metamorphosed sedimentary, igneous and ultramafic rocks, dated at ~200-170 Ma and representing the remnants of an island arc and inter-arc basin. Intrusion of the plutonic rocks occurred at ~160 Ma [*Edelman et al.*, 1989; *Saleeby et al.*, 1989; *Day and Bickford*, 2004], during a period of extensive Jurassic arc magmatism across the Sierra Nevada that was responsible for the genesis of the Sierra Nevada Batholith [*Ducea*, 2001]. Within the extent of the field area, there are three primary plutons: (i) Cascade Pluton, the oldest of the three plutons, comprising a coarse-grained, flow-banded unit that grades from quartz-diorite to tonalite towards the core of the pluton [*Hietanen*, 1976]; (ii) Merrimac Pluton, which is similar in characteristics and composition to the Cascade Pluton [*Hietanen*, 1951]; (iii) Bald Rock Pluton, a predominately trondhjemite pluton, grading into tonalite at the margins, that is variably foliated to massive [*Compton*, 1955; *Hietanen*, 1976]. A tongue of trondhjemite extends northwards from Bald Rock Pluton, cross-cutting the older Cascade Pluton (*Figure 2.3*). The plutonic rocks typically exhibit high angle jointing (>50°), although regions

of the Bald Rock Pluton in particular are massive, with a very low fracture density. The emplacement of these plutonic units deformed the overlying bedrock structure such that the regional, broadly range-parallel, trend of the bedding and foliation planes has been distorted to wrap concomitantly around the pluton boundaries [*Hietanen*, 1951, 1976; *Compton*, 1955].

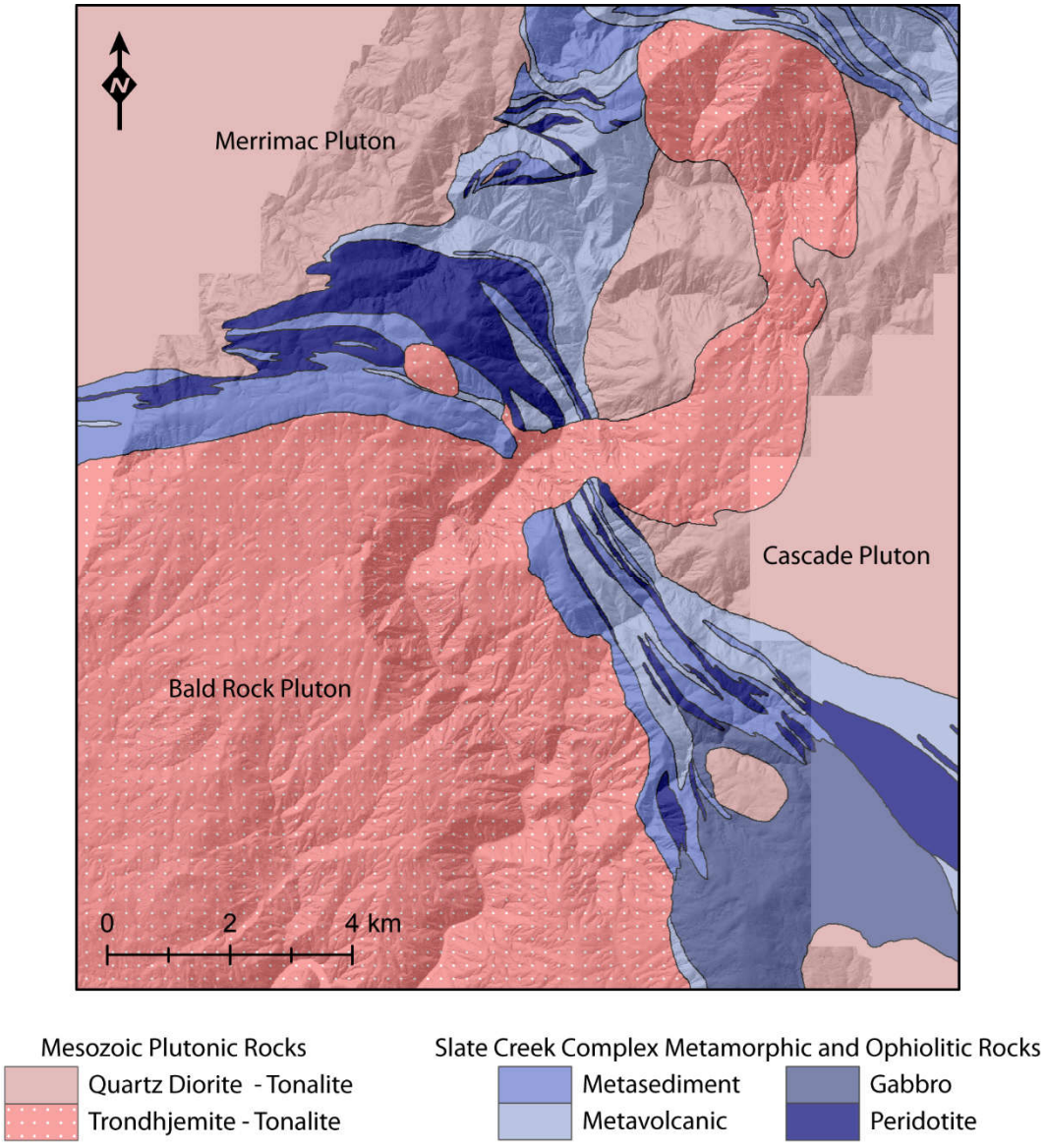

Figure 2.3 Bedrock geology of the study site; redrawn and adapted from existing geological maps by Hietanen (1976) and Saucedo and Wagner (1992)

2.3.2 Climatology

The Sierra Nevada climate is strongly seasonal: within the study site, typical maximum (minimum) monthly temperatures range from 9(-1) ^{0}C in the depths of winter to 30(12) ^{0}C at the height of summer; precipitation totals ~1750 mm annually, but of this more than 90% falls between the October and April (*Figure 2.4*) [PRISM Climate Group, Oregon State University; www.prism.oregonstate.edu/], often during intense storms. Extended dry periods are commonly observed through the summer months and forest fires are relatively common occurrences [*Stephens and Collins*, 2004]; a significant portion of the site was affected by the Canyon Complex Fires of June-July 2008, which occurred prior to the LiDAR survey and in some areas caused severe and extensive damage to the canopy.

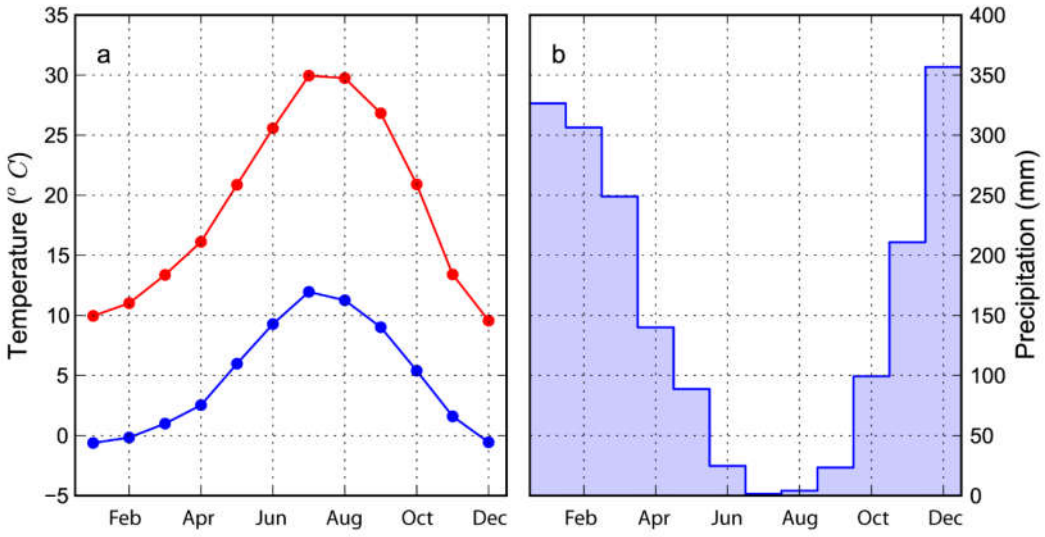

Figure 2.4 Climate data for field site: (a) maximum and minimum monthly temperatures; (b) precipitation (based on 30-year climate normals; PRISM Climate Group, Oregon State University; www.prism.oregonstate.edu/)

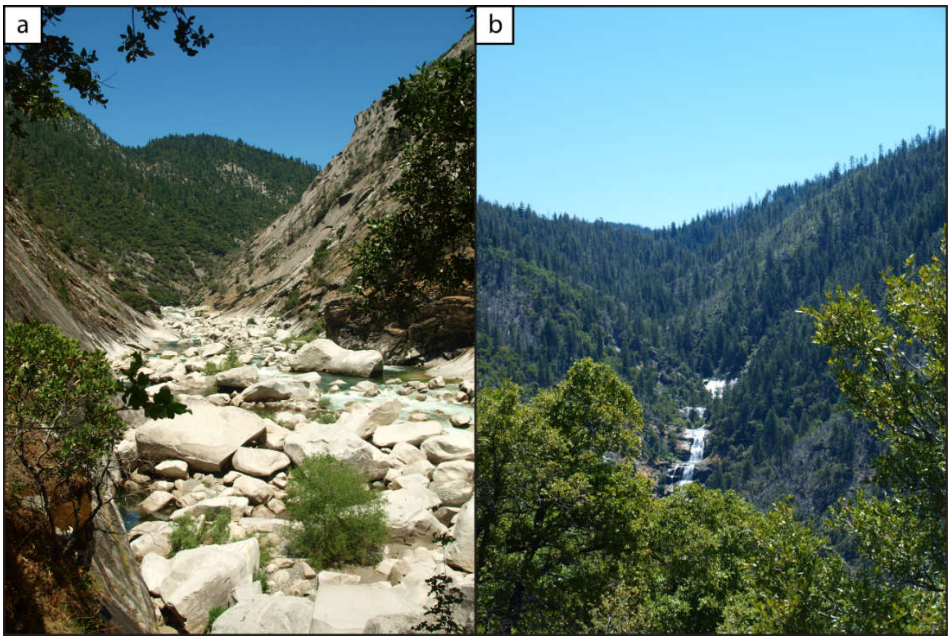

Figure 2.5 The Northern Sierra Nevada landscape: (a) Feather River Canyon; (b) Cascade Falls. Note the transition from steep, rapidly eroding topography below the waterfall, to more gradual, convex hillslopes upstream.

2.3.3 Geomorphology and Geochemistry

Like many of the principal channel systems across the Northern Sierra Nevada, the Middle Fork Feather River and its principal tributaries have carved a deep, precipitous canyon ~600 m into the relatively low-relief surrounding landscape (Figure 2.5). Tributaries draining into the main stem possess prominent, steepened knickzones that frequently host spectacular waterfalls marking the upstream limit of the propagation of this canyon incision; notable examples include Feather Falls on the Fall River, and Cascade Falls on Cascade Creek. While the age of the Feather River canyon is presently poorly constrained, stratigraphic relationships indicate that the canyons occupied by the Yuba and American Rivers immediately to the south have been occupied since Eocene time [*Cassel and Graham*, 2011; *Gabet*, 2014]; it is likely that the Feather River canyon is comparable in age to these neighbouring systems.

In more recent times, the Feather River has undergone a period of enhanced incision: erosion rates, integrated over millennial timescales, reach over 250 mm ka^{-1} along the inner canyon that bounds the trunk channel and primary tributaries, in comparison to the plateau-like low relief topography, that is eroding at a more sedate 20 – 40 mm ka^{-1} [*Riebe et al.*, 2000; *Hurst et al.*, 2012]. The presence of a landscape that exhibits such strong a degree of disequilibrium, with the juxtaposition of contrasting topography that is subject to erosion rates that vary over an order of magnitude, has motivated a growing body of research exploring the transient evolution of landscapes, and the control that erosion rates place on their physical and chemical characteristics

[*Riebe et al.*, 2000, 2001b; *Yoo et al.*, 2011; *Hurst et al.*, 2012, 2013b; *Attal et al.*, 2015; *Gabet et al.*, 2015].

Across the erosion rate gradient, the characteristics of hillslopes change markedly. Rapidly eroding topography is characterised by steep, planar hillslopes rising up to acute ridges, with curvature focused at the ridge crest [*Hurst et al.*, 2012, 2013b] (Figure 2.5). Hillslopes here comprise a rugged mosaic of bedrock outcrop, intermittent soil cover and scree cones, with steeper hillslopes affected by bedrock landslides [*Attal et al.*, 2015] (Figure 2.6). Where present, soils may reach ~0.5 m, and have experienced little chemical weathering, with minimal-absent B horizons and relatively low levels of chemical alteration in the underlying saprolite [*Yoo et al.*, 2011; *Attal et al.*, 2015; *Gabet et al.*, 2015] (Figure 2.6 b). The grain size distribution of sampled soil pits reflects this immaturity: they are typically dominated by sand and rock fragments [*Attal et al.*, 2015] and possessing very low clay fractions [*Yoo et al.*,

2011; *Attal et al.*, 2015; *Gabet et al.*, 2015]; very coarse rock fragments and boulders dominate landslide deposits [*Attal et al.*, 2015] (Figure 2.6 c and d).

Figure 2.6 Landscapes and processes proximal to the rapidly eroding inner canyon of the Middle Fork Feather River. Expansive bedrock outcrops are common (a, d), but much of the landscape remains soil mantled, supporting fairly continuous canopy cover (b, e, f). Panel (b) illustrates the nature of the thin, weakly developed soil, overlying fractured bedrock that exhibits limited chemical weathering. Mass wasting processes (c, d) are significant hillslope mechanisms of erosion are sediment transport on these steepened hillslopes, and contribute significant amounts of coarse rock clasts and boulders to the channel network [*Attal et al.*, 2015]. Photos marked with a '*' were kindly made available by Mikael Attal.

Figure 2.7 Landscapes and processes in the slowly eroding, low relief parts of the Feather River landscape. Hillslopes are typically broad with low gradients and possess a continuous soil mantle, with rock exposure typically limited to small outcrops and corestones (g). Hillslope sediment transport is dominated by diffusion like processes, such as bioturbation (i) tree throw (j, k). Figures marked with a '*' were kindly made available by Mikael Attal.

As erosion rates decrease and hillslope gradients relax, the soil mantle becomes more continuous, with rock exposure generally limited to isolated outcrops and corestones (Figure 2.7). Soil thickness range between 0.5 and 1.5 m [*Yoo et al.*, 2011; *Gabet et al.*, 2015]. Longer soil residence times are accompanied by a greater extent of weathering, with a much greater abundance of clay, and a reduction in coarse, weakly weathered rock fragments [*Yoo et al.*, 2011; *Attal et al.*, 2015; *Gabet et al.*, 2015], while the underlying saprolite also exhibits a greater degree of chemical depletion [*Yoo et al.*, 2011]. Quantitative observations regarding the relative contribution of specific sediment transport processes are lacking, however field observations suggest that hillslope sediment transport in the more slowly eroding portions of the landscape is likely dominated by localised diffusion-like processes, such as tree throw and soil creep, the former of which has been suggested to play an important role in the physical production of soil and in buffering soil thickness against changes in erosion rate [*Yoo et al.*, 2011]. The dominance of diffusion-like processes over overland flow, which may also generate convex hillslopes [*Dunne*, 1991; *Dunne et al.*, 2016], is further suggested by the observations that (i) hillslopes exhibit near full canopy closure; and (ii) colluvium fills much of the lower order valley network, with evidence for transport by overland flow not observed until a significant distance downslope from the onset of convergent hollow topography, and sometimes below second order valley junctions [*Clubb et al.*, 2014]. In steeper parts of the low-relief topography, colluvial hollow gradients may still be sufficient to feed shallow landslides and debris flows in places [*Attal et al.*, 2015].

Moreover, the changes in the morphology of soil mantled hillslopes across the erosion rate gradient are consistent with the expectations based on the non-linear diffusion model for sediment transport [*Roering et al.*, 1999, 2007; *Hurst et al.*, 2012]. The transition towards increasingly planar hillslopes leads to a decoupling of hillslope gradients from channel incision rates (mean basin slope accounts for only 69% of the variance in erosion rate calculated from cosmogenic ^{10}Be), whereas hilltop curvature appears to remain sensitive across the range of erosion rates observed (catchment-average hilltop curvature accounts for 83% of variance in erosion rate) [*Hurst et al.*, 2012]. Based on the calibration of hilltop curvature against catchment-wide erosion rates, Hurst et al. [2012, 2013b] calculated values of the hillslope sediment transport coefficient (D) of 8.8 ± 3.3 m^2 ka^{-1} for hillslopes underlain by granitoid bedrock and 4.8 ± 1.8 m^2 ka^{-1} for hillslopes underlain by schist of the Slate Creek Formation. Corresponding response times for these soil mantled hillslopes have been calculated to be on the order of $10^4 – 10^7$ years, depending on the erosion rate and length of the hillslope [*Hurst et al.*, 2012, 2013b], which is rapid relative to the response times of fluvial systems [e.g. *Whipple and Tucker*, 1999; *Snyder et al.*, 2000; *Whittaker et al.*, 2008; *Whittaker and Boulton*, 2012]. Soil mantled hillslopes should therefore be sensitive to changing incision rates [*Hurst et al.*, 2012, 2013b]. Response times of bedrock hillslopes may be much greater, depending on the strength of the underlying bedrock and susceptibility to mass wasting processes such as landslides [*Molnar et al.*, 2007; *Moore et al.*, 2009; *Clarke and Burbank*, 2010], thus diminishing sensitivity to fluctuations in fluvial incision. Understanding the dynamics of soil production and the

Figure 2.8 A selection of photographs of the mixed conifer forest in the field site

transition from soil-bedrock hillslopes at the landscape scale therefore represents an important challenge still to be addressed in this landscape.

2.3.4 Ecology

Situated within the elevation range 225 – 1500 m, the Feather River landscape lies within the elevation band occupied by mixed conifer forest (Figure 2.8). The forest within the field site comprises a heterogeneous mixture of: (i) coniferous stands, predominately inhabited by a variable mixture of *Pseudotsuga menziesii* (Douglas Fir), *Pinus ponderosa* (Ponderosa Pine), *Calocedrus decurrens* (Incense Cedar) and *Pinus lambertiana* (Sugar Pine); (ii) patches of oak woodland, dominated by *Quercus kelloggii* (California Black Oak) and *Quercus chrysolepis* (Canyon Live Oak); (iii) *Arctostaphylos* (Manzanita) chaparral groves. Aside from anthropogenic clearances, becoming increasingly prevalent outside the boundary of the Plumas National Forest limits, and fire damage, hillslopes support a near continuous forest canopy. A

significant exception here is a suite of low relief "balds" – distinctive, spatially extensive bedrock surfaces with very low fracture densities that are present in the topography underlain by the Bald Rock Pluton. Similar features elsewhere in the Sierra Nevada have been shown to correlate with bedrock that contains exceptionally low levels of phosphorous [*Hahm et al.*, 2014a].

Despite the dependence of the mixed conifer ecosystem on substrate characteristics, the ecological implications of the geomorphic gradient remain largely unconstrained. Qualitative field observations suggest that forest community is sensitive to the erosion rate gradient [*Gabet et al.*, 2015]. In slowly eroding parts of the landscape, soil mantled hillslopes support a forest that predominately comprises coniferous species (Douglas Fir, Incense Cedar, Ponderosa and Sugar Pines). As erosion rates increase and soils are more weakly developed, the canopy opens up and more drought-tolerant species – oaks and xeric chaparral shrubs – become increasingly important components in the forest composition. Quantifying changes in forest structure across the erosion rate gradient represents an important first step in understanding the linkages between the mixed conifer forest ecosystem and the evolution of its host landscape and forms the target of the following chapter. Furthermore, given the important geomorphic role played by vegetation in the formation and transport of soils, these changes may also feedback to modify the geomorphic response of hillslopes to these changes, as is explored later in the thesis.

Chapter 3. Erosion Rates as a Potential Bottom-up Control of Forest Structural Characteristics in the Sierra Nevada Mountains

Published in Ecology: D.T. Milodowski, S.M. Mudd, and E.T.A. Mitchard (2015a), Ecology, 96(1), 31–38, doi:10.1890/14-0649.1

Abstract

The physical characteristics of landscapes place fundamental constraints on vegetation growth and ecosystem function. In actively eroding landscapes, many of these characteristics are controlled by long-term erosion rates: increased erosion rates generate steeper topography and reduce the depth and extent of weathering, limiting moisture storage capacity and impacting on nutrient availability. Despite the potentially important bottom-up control that erosion rates place on substrate characteristics, the relationship between the two is largely unexplored. I investigate spatial variations in aboveground biomass (AGB) across a structurally diverse mixed coniferous/deciduous forest with an order of magnitude erosion rate gradient in the northern Californian Sierra Nevada, using high resolution LiDAR data and field plots. Mean basin slope, a proxy for erosion rate, accounts for 32% of variance in AGB within my field area ($p < 0.001$), considerably outweighing the effects of mean annual precipitation, temperature and bedrock lithology. This highlights erosion rates as a potentially important, but hitherto unappreciated, control on AGB and forest structure.

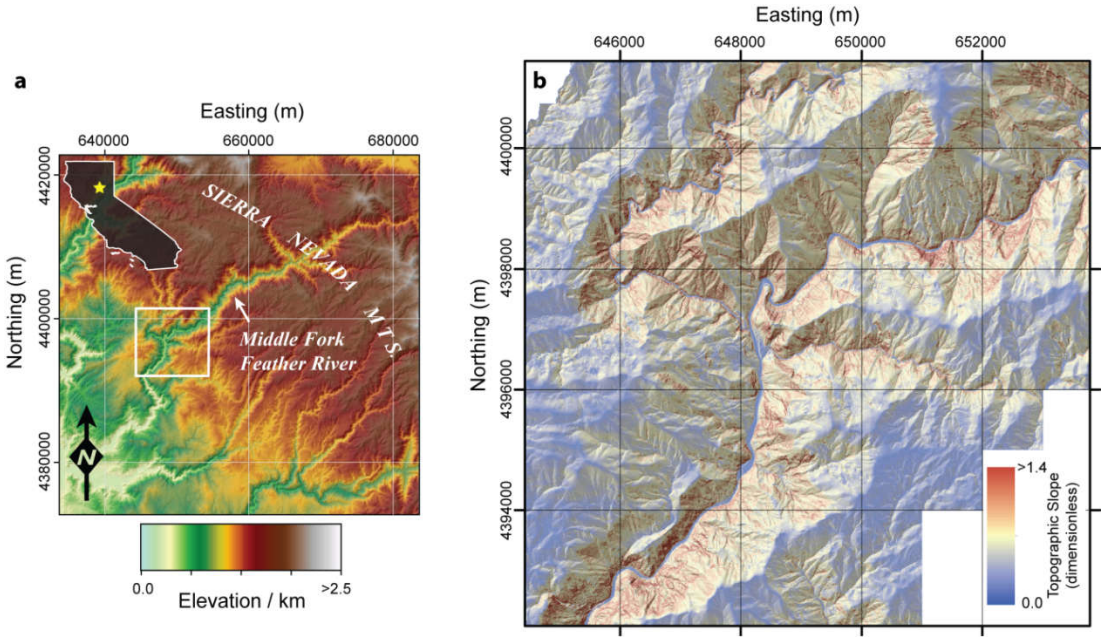

Figure 3.1 (a) Location map; the site is located in the Northern Californian Sierra Nevada (inset, star). The extent of the study area is indicated by the white box. (b) A map of topographic gradient across the study site. Elevated incision along the trunk channel of the Feather River and principal tributaries has driven a steepening of hillslope gradients. Topographic knickpoints record the propagation of this incision upstream. The coordinate system for both maps is UTM Zone 10N.

3.1 Introduction

Geomorphic processes act to generate, erode and redistribute sediment, sculpting the landscape and creating the physical template on which ecosystems develop [*Urban et al.*, 2000; *Chase et al.*, 2012; *Detto et al.*, 2013]. In addition, vegetation is an important geomorphic agent, playing a direct role in soil production and modifying the efficacy of erosion and sediment transport [*Gabet et al.*, 2003; *Gabet and Mudd*, 2010; *Roering et al.*, 2010]. Life and landscape are thus intimately linked; their coevolution connected by the interplay between erosion and sediment transport, chemical weathering, hydrology, ecology and biology.

It is widely documented that elevation-dependent variations in precipitation and temperature place important controls on ecosystem development and functioning in

mountain environments. In the Californian Sierra Nevada these "top-down" controls are manifest in the macro-scale altitudinal zonation of ecosystems, primary productivity and evapotranspiration [*Stephenson*, 1998; *Bales et al.*, 2011; *Goulden et al.*, 2012]. In contrast, "bottom-up" controls imposed by the geomorphic evolution of landscapes have received significantly less attention, yet the balance between uplift and geomorphic processes determines the distribution of elevations in a landscape. In addition, geomorphic processes play a key role in determining the thickness, chemistry and texture of soils, the substrate upon which ecosystems develop [*Kirkby*, 1985; *Heimsath et al.*, 1997, 2012; *Dixon et al.*, 2012; *Vanwalleghem et al.*, 2013b].

In actively eroding landscapes, rates of erosion are typically paced by fluvial incision, which sets the lower base-level of adjacent hillslopes [*Gilbert*, 1909; *Roering et al.*, 1999]. In response to increased fluvial incision, hillslopes steepen, raising the rate at which sediment is transmitted across hillslopes into the channel network. On steeper hillslopes, gravitational forces begin to overcome resisting forces and sediment transport increases rapidly, limiting further development of hillslope relief [*Roering et al.*, 1999, 2001a]. Erosion rates not only control the distribution of elevation and topographic gradient across a landscape, they also can control soil texture and chemistry by modulating soil residence time. Minerals in rapidly eroding landscapes spend less time in the soil than minerals in slowly eroding landscapes, thus limiting their exposure to weathering and reducing the potential for clay formation [*Mudd and Yoo*, 2010b]. There is a strong feedback between erosion rate and residence time because not only do minerals move through rapidly eroding soils more quickly, in addition rapidly eroding soils are thinner than slowly eroding soils [*Heimsath et al.*,

1997]. Thus, erosion rates are directly tied to both moisture storage capacity [*Graham et al.*, 2010] and the bio-availability of key nutrients [*Vitousek et al.*, 2003; *Porder et al.*, 2007; *Hilton et al.*, 2013]. Given that the establishment of forest communities is fundamentally dependent on the presence of a hospitable substrate from which vegetation can extract moisture and nutrients, long-term erosion rates may place important controls on forest characteristics; however, the relationship between forest structure, AGB and erosion rate is largely unexplored.

In this chapter, I use airborne Light Detection And Ranging (LiDAR) data to investigate spatial variations of AGB in a mixed conifer forest in the Sierra Nevada, California. Rates of erosion in this landscape vary spatially by an order of magnitude, providing a natural laboratory for investigating the role of changing erosion rates on land surface dynamics. This has motivated a significant body of geomorphological and geochemical research at the site [*Riebe et al.*, 2000, 2001a; *Yoo et al.*, 2011; *Hurst et al.*, 2012, 2013c], providing a rich knowledge base from which to explore landscape-scale controls on ecosystem properties.

3.2 Study site

Located in the north-western Sierra Nevada Mountains, California, the field site comprises 83 km^2 of mixed conifer forest (dominated by *Pseudotsuga menziesii*, *Pinus ponderosa*, *Calocedrus decurrens*, *Pinus lambertiana* and *Quercus kelloggii*), predominately within the boundaries of the Plumas National Forest (Figure 3.1a). The modern climate is strongly seasonal; maximum (minimum) monthly temperatures range from 9(-1)^{0}C to 30(12)^{0}C and annual precipitation is ~1750 mm, with >90% falling between October and April, (http://www.prismclimate.org), much of this as

snow. Summer moisture balances represent important limitations in ecosystem productivity under seasonally dry climates [*Hubbert et al.*, 2001; *Witty et al.*, 2003]; periodic dry season fires are an important additional factor in driving ecosystem turnover, the most recent of which was the 2008 Scotch fire, which affected a significant area on the eastern side of the field site.

Draining from the high Sierras, the Middle Fork Feather River incises into bedrock comprising granite and granodiorite plutons as well as metamorphosed volcanic and sedimentary rocks [*Saucedo and Wagner*, 1992]. The landscape is composed of incised gorges near the Middle Fork Feather River and its larger tributaries, dissecting a lower relief plateau (Figure 1b). Erosion rates calculated from ^{10}Be concentrations in detrital river silts show an order of magnitude difference in erosion rates across the landscape, from 20-40 mm ka^{-1} on the plateau surface, to >250 mm ka^{-1} in the high-relief topography adjacent to the actively incising channels [*Riebe et al.*, 2000; *Hurst et al.*, 2012].

3.3 Methods

Airborne LiDAR acquisition (September 2008) and processing were carried out by the National Center for Airborne Laser Mapping (http://www.ncalm.org), giving a point cloud with an average point density of 9.8 pts.m^2, which was interpolated to a 1 m-resolution Digital Elevation Model (DEM) of the ground surface. LiDAR can be readily used to quantify the spatial distribution of AGB by exploiting the natural allometric scaling of stem AGB with tree size [e.g. *Lefsky et al.*, 1999b]. I mapped the mean return height (MRH), which combines information on both canopy height and canopy cover, for all returns within a moving 10 m-radius window (Figure 3.2a).

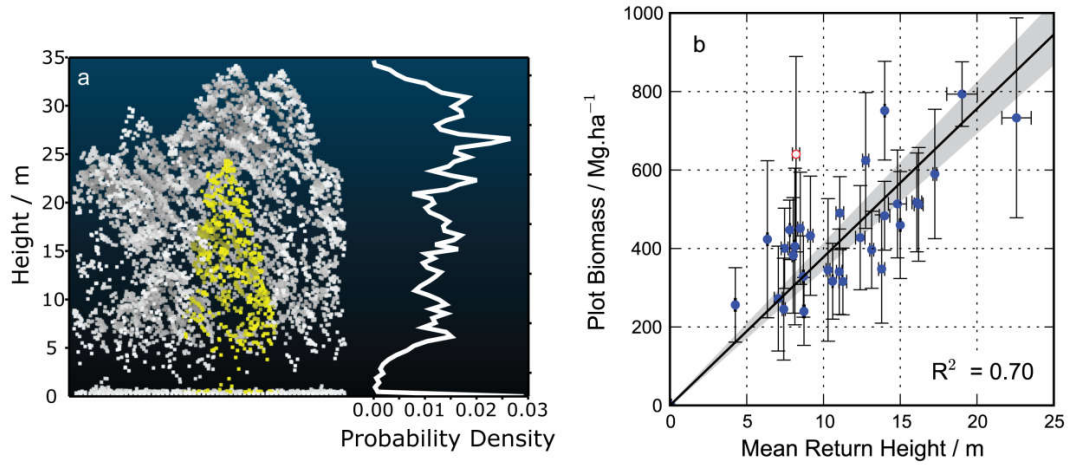

Figure 3.2 (a). A view of the LiDAR point cloud extracted for one of the field inventory plots and corrected for topography, so that the point elevations reflect height above ground, alongside the corresponding LiDAR return profile. (b) Plot-based biomass estimates for 31 (0.031ha) field inventory plots, and MRH of the corresponding return profile. The black line indicates the SMA-fitted trend, forced through the origin; the grey region indicates the 95% confidence interval. The hollow data point indicates an outlier, which was excluded from the regression.

Simple canopy metrics like this have been shown to be excellent predictors of AGB [*Asner et al.*, 2012].

In order to calibrate the AGB estimates, I undertook 31 tree inventory plots during the summers of 2012 and 2013, each with a 10 m radius. For each plot I recorded the species and diameter at breast height (1.3 m), DBH, for all trees with DBH >10 cm. AGB estimates for the field plots were obtained using previously published allometric equations relating DBH to AGB [Table S1; *Jenkins et al.*, 2003; *Návar*, 2009; *Halpern and Means*, 2011]. Since there are significant sources of uncertainty in both LiDAR-derived metrics [*Mascaro et al.*, 2011] and plot-based biomass estimates [*Chave et al.*, 2004], I used Standardized Major Axis (SMA) regression to fit a linear model to the data [*Warton et al.*, 2006] (Figure 3.2b). The regression is fixed through the origin, justified because a plot with no return heights above ground level will have zero AGB.

I employ a simple linear model, as the calibration data do not support the use of a more complex parameterisation. Uncertainties in both field plot-based biomass and LiDAR-derived canopy metrics were estimated using a Monte Carlo framework [*Gonzalez et al.*, 2010; *Yanai et al.*, 2010], but these uncertainty estimates are not used to weight the regression, due to the fact that they are poorly constrained, and errors in the allometric relationships are likely to have significant bias. One outlier is excluded from the regression analysis (marked as a hollow symbol in Figure 3.2b), as the plot biomass was skewed by the presence of one very large tree (*Quercus decurrens*, DBH > 1 m).

In order to explore the relationship between erosion rate and AGB I compare aggregated characteristics of second order drainage basins (defined by Strahler stream order; Appendix), where the channel network is defined using the method outlined by Clubb et al. [2014]. Basins with catchments smaller than 20,000 m^2 are excluded from my analysis. I use mean basin slope as a proxy for locally averaged erosion rate: all else being equal, higher erosion rates will generate steeper topography [*Ahnert*, 1970]. The functional relationship between mean basin slope and erosion rate is non-linear [*Montgomery and Brandon*, 2002]: mean basin slopes become increasingly insensitive to erosion rates as hillslope gradients steepen towards the threshold of stability and gravitational forces begin to overcome resisting forces, limiting the further development of relief [*Roering et al.*, 1999]. Nevertheless, a comparison of mean basin slope and cosmogenic radionuclide derived erosion rates in the Feather River region by Hurst et al. [2012] indicates that mean basin slope remains a sensitive metric

across the range of erosion rates observed here, and is therefore sufficient to illustrate the erosion gradient in my analysis.

Climate also poses a significant influence on forest characteristics in the Sierra Nevada [*Stephenson*, 1998; *Urban et al.*, 2000; *Franklin*, 2003]. It is therefore important to take into account local climate gradients within the field site. To achieve this I utilise 800 m resolution maps of Mean Annual Precipitation, MAP, and Mean Annual Temperature, MAT, from the PRISM Climate Group at Oregon State University [http://www.prismclimate.org; see also *Daly et al.*, 2008]. In order to take into account variations in microclimate generated by topography, I downscale these maps following the method described by Chorover et al. [2011]. Soil characteristics can also influence plant community composition and growth; to account for soil parent material, I divided the catchments into two principal bedrock lithologies (granodiorite and meta-volcanic/peridotite). I then used a General Linear Model (GLM) framework to explore the relative importance of erosion rate (mean basin slope), climate and bedrock lithology in driving the observed distribution of AGB.

The region was affected by the Scotch Fire in 2008, six months prior to the LiDAR acquisition. In order to test for bias in the results due to the influence of the recent fire, I repeated the analysis using USFS burn intensity maps (http://www.fs.usda.gov/, accessed 14/11/2013) to exclude parts of the forest that suffered significant damage to the structurally dominant vegetation [moderate/high intensity; *Miller and Thode*, 2007]. A full description of my methods is given in the supplementary information at the end of this chapter (Section 3.7). A data table summarising the forest inventory plots are included in a second appendix (Section 3.8).

Table 3.1The results from nine different GLM analyses exploring the controls on the variation of mean AGB for all 2nd order drainage basins within the study region.

	Model	Nº. Basins	Adj. R^2	F-statistic	p-value
1	AGB ~ MBS†	374	0.34	194.6	$<2.2\times10^{-16}$
2	AGB ~ MBS*MAP*MAT†	374	0.47	47.68	$<2.2\times10^{-16}$
3	AGB ~ MBS	287	0.32	137.2	$<2.2\times10^{-16}$
4	AGB ~ MAP	287	0.04	12.8	0.0004
5	AGB ~ MAT	287	0.12	40.4	8.1×10^{-10}
6	AGB ~ MBS*MAP	287	0.39	60.6	$<2.2\times10^{-16}$
7	AGB ~ MBS*MAT	287	0.35	51.9	$<2.2\times10^{-16}$
8	AGB ~ MAP*MAT	287	0.18	22.3	5.5×10^{-16}
9	AGB ~ MBS*MAP*MAT	287	0.44	32.9	$<2.2\times10^{-16}$

Notes: †**full dataset; for all other models, the analysis excluded areas that suffered moderate-severe canopy disturbance during the 2008 Scotch fire, and completely excludes basins for which the affected area accounted for >50% of the total catchment area. Abbreviations: MBS = mean basin slope; MAP = mean annual precipitation; MAT = mean annual temperature. A tabulation of all the GLM models explored is given in Table S3.2, alongside a comprehensive breakdown of the respective parameter sets in Table S3.3.**

3.4 Results

A comparison of the LiDAR-derived AGB estimates against the field plot AGB estimates yields an R^2 value of 0.70 and a Root Mean Squared Error (RMSE) of 103.3 Mg ha^{-1} (Figure 3.2b). Comparing the distribution of AGB produced by extending the analysis across the study region (Figure 3.3a) against the distribution of slopes (Figure 3.1b), some important features stand out: (i) a general trend of high biomass on the plateau and lower AGB on steeper, more rapidly eroding topography; (ii) the presence of weak aspect-driven variations in AGB; (iii) the AGB distribution on the plateau is

disrupted by a series of low AGB patches, often with sharp, quasi-geometric boundaries, where there has been recent active logging. The latter is likely to add significant scatter to basin-averaged AGB for low gradient basins draining the plateau.

The results from the GLM analysis (Table 3.1; Supplementary Tables 3.2, 3.3) reveal that mean basin slope, temperature and precipitation can together explain 44% of the variance in AGB observed in this landscape ($F_{x,y}$ – 32.9, $p<0.001$, $n=287$). A comparison of single variable regressions indicates that of these variables, mean basin slope produces the strongest correlation with AGB at the scale of second order basins, accounting for 73% of this explanatory power (Figures 3.3b-e). Accounting for bedrock lithology typically explains a further 2% of the variance in a given model: granodiorite basins tend to have lower biomass than their meta-volcanic counterparts. A comprehensive tabulation of the GLM results is provided in Appendix (Supplementary Tables 3.2, 3.3). Adding extra terms into the GLM analysis generated incremental improvements to model fit, with no unexpected deviations in model behaviour. Importantly, the trends between mean basin slope and AGB are sufficiently

Figure 3.3 (across page) A map showing the distribution of aboveground biomass, estimated using the calibrated LiDAR-metric. Areal extent is identical to Figure 3.2 (b). Regions with no data indicate regions that suffered moderate-severe burn severity (as defined by Miller and Thode [2007]) in the 2008 Scotch Fire. Logged areas on the plateau are visible as uniformly low biomass patches, often with sharp boundaries. The coordinate system is UTM Zone 10N. (b) Estimated AGB plotted against mean basin slope for all 2nd order basins with catchment areas >20,000m^2. (c-e) AGB plotted against (c) mean basin slope, (d) MAP and (e) MAT for those same basins, but filtered to exclude areas which suffered moderate-high severity burn damage in 2008. Basins for which more than 50% of the area was affected were also removed. Note that including the burned areas does not affect the overall trends.

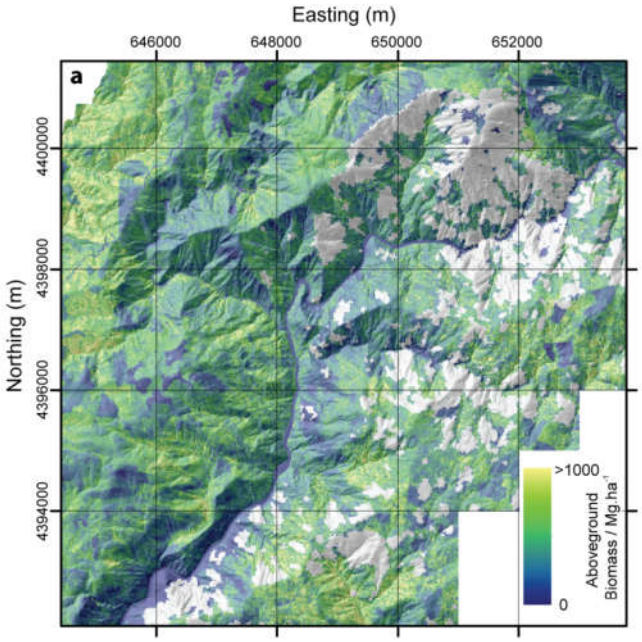
Easting (m)
646000
648000
650000
652000
a
Northing (m)
4400000
4398000
4396000
4394000
>1000
0
Aboveground Biomass / Mg.ha⁻¹

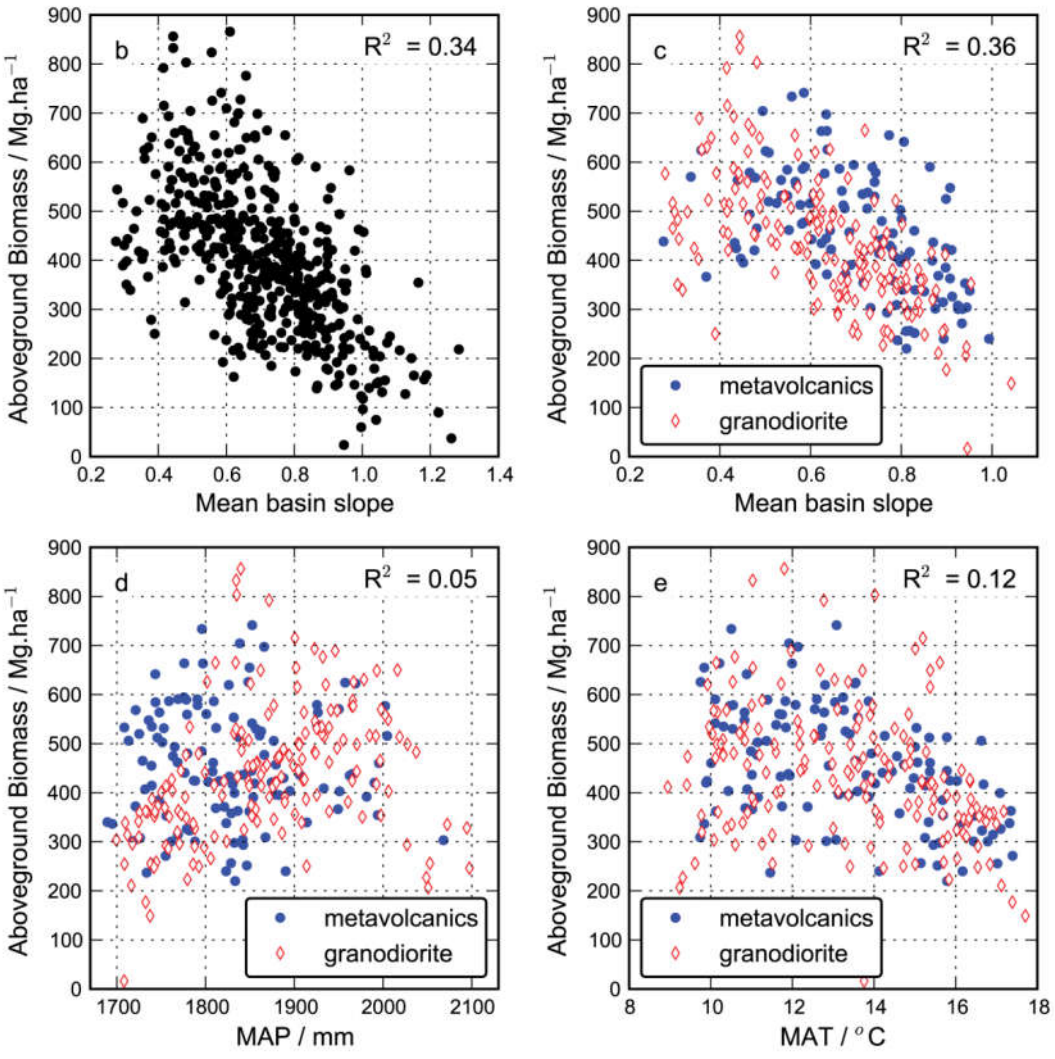
b
R² = 0.34
Aboveground Biomass / Mg.ha⁻¹
Mean basin slope
c
R² = 0.36
metavolcanics
granodiorite
d
R² = 0.05
MAP / mm
e
R² = 0.12
MAT / °C

strong that even including the regions severely affected by the 2008 fire, there is no major change in the relationship (R^2 for the univariate model changes from 0.32 to 0.34; parameters within standard error). Note that as both the climate and erosion gradients are at least partly topographically structured, a degree of autocorrelation of variables is unavoidable (Pearson's correlation coefficients: Mean basin slope-MAT = -0.02; Mean basin slope-MAP = -0.40; MAP-MAT = -0.14).

3.5 Discussion

The strong negative correlation between mean basin slope and basin averaged biomass (Figure 3.3) suggests that there is an important coupling between hillslope erosion rates and the process of succession and development of plant communities in this region. Whilst the simple linear models assumed in my analysis are likely an oversimplification of the true functional relationships between the variables, the models that explicitly incorporate the influence of erosion rate through spatial variations in mean basin slope perform significantly better than those without. The strength of the trends observed is remarkable given the degree of natural heterogeneity that one might expect, particularly as some parts of the plateau have been logged for timber, which is likely to have reduced the observed correlation. Erosion rates could influence AGB through a variety of mechanisms, but the most likely explanation I believe relates to its influence on the depth of soil and saprolite, and through this water storage and availability for plants.

In the Feather River region, previous work has focused on the geomorphological and geochemical evolution of the landscape. Hurst et al. [2012] observed that in response to increased fluvial incision at their base, hillslopes steepen and become increasingly

planar, focusing curvature at the ridge crest, consistent with theoretical and experimental models of non-linear hillslope sediment transport [*Roering et al.*, 1999, 2001a]. Decreasing residence times of material within the critical zone across this same transition are indicated by a decrease in the extent of weathering of both saprolite and soil [*Riebe et al.*, 2001a; *Yoo et al.*, 2011] and a corresponding drop in the soil clay content [*Yoo et al.*, 2011], again in agreement with theoretical [e.g. *Mudd and Yoo*, 2010b] and empirical observations from other rapidly eroding sites in California [*Dixon et al.*, 2012].

The change in residence time of material as it passes through the weathering zone is critical to understanding the functional link between erosion rate and biomass distribution in this setting. In the upland Sierra Nevada, water is the limiting factor in ecosystem productivity [*Urban et al.*, 2000]. Mixed conifer forests are typically established on relatively thin soils overlying strongly weathered saprolite [*Hubbert et al.*, 2001; *Witty et al.*, 2003]. Weathered granitic saprolite has an available water capacity of ~12%, which, whilst lower than that of soil (~20%), makes it a vital water store that continues to supply vegetation with moisture through the dry season long after the soil moisture has been exhausted [*Graham et al.*, 2010; *Bales et al.*, 2011].

Decreasing moisture storage as erosion rates increase, thus reducing water availability in the dry season, provides a compelling explanation for the observed trends. Water availability influences the tree species that can grow successfully, their growth and turnover rates, susceptibility to fire, drought and other disturbance, and ultimately the mean AGB of the resulting communities. My results suggest that trees are less likely to become large in high erosion rate areas, and will be more vulnerable in drought

years than those on lower erosion rate areas with enhanced soil and saprolite water availability. This conclusion is supported by the result that AGB was negatively correlated with temperature: drought sensitivity is increased by temperature [*Adams et al.*, 2009], and clearly this negative effect here outweighs any positive effect of increased radiation for photosynthesis.

Crossing the erosion gradient in the Feather River region, the landscape becomes increasingly inhospitable. Both the less extensively weathered saprolite and loss of clay from the soil as erosion rates increase [*Yoo et al.*, 2011] act to reduce the amount of water retained on the hillslope for ecological use, thus limiting forest productivity. The clear trends expressed in this landscape corroborate previous work elsewhere in the Sierra Nevada by Meyer et al., [2007], who noted that at the stand level, stand basal area was positively correlated with the combined thickness of the A and C horizons, which should obey an inverse relationship with erosion rate [*Dixon et al.*, 2012].

In more humid settings, moisture limitation ceases to place such strong constraints on ecosystem productivity, and erosion rates are more tightly coupled to the bio-availability of key nutrients [e.g. *Vitousek et al.*, 2003; *Porder et al.*, 2005a], though soil and saprolite water storage capacity has been implicated in explaining the vulnerability of trees to droughts even in normally very wet regions [*Slik et al.*, 2002]. At high erosion rates, it has been posited that productivity could be limited either by phosphorous limitation, due to a reduction in the weathering extent [*Porder et al.*, 2007], or nitrogen limitation, due to nitrogen loss through more frequent landslides [*Hilton et al.*, 2013]. In these settings it is likely that the relationship between erosion rate and the ecosystem properties may differ, depending on the pervasiveness and

efficiency of chemical weathering, and the primary mechanisms by which erosion occurs. Exploring how climate modulates this relationship remains an important challenge for future work quantifying eco-geomorphological coupling.

These findings have important implications for understanding longer term evolution of landscapes. By actively penetrating into bedrock, tree roots efficiently drive the physical formation of soil [*Gabet and Mudd*, 2010; *Roering et al.*, 2010]. Larsen et al. [2014a] postulated that the extremely high soil production rates they observed in the Western Alps of New Zealand, reaching 2.5mmyr^{-1}, were possible as a consequence of persistent active bioturbation by plant roots, maintaining soil mantled hillslopes at erosion rates reaching 10 mmyr^{-1}. In contrast, in the semi-arid San Gabriel Mountains of southern California, where moisture limitation is important and vegetation is thus likely to be more strongly controlled by erosion rate, maximum observed soil production rates are 0.37 mmyr^{-1}, an order of magnitude lower [*Heimsath et al.*, 2012].

3.6 Conclusions

In conclusion, empirical observations of AGB variations across a gradient of long-term erosion rates highlight geomorphic dynamics as a potentially important bottom-up control on the structural properties of the mixed conifer forests of the north-western Sierra Nevada Mountains. Specifically, increased erosion rates appear to be associated with lower AGB, a hitherto unconstrained relationship. In this setting, this relationship can be rationalised as being driven by moisture limitation as a direct consequence of the corresponding reduction in soil and saprolite development. This relationship is likely to exist elsewhere, but its strength and mechanism is likely to vary according to the range of erosion rates, bedrock lithology, climate and the presence and intensity of

natural or anthropogenic disturbance. I suggest that consideration of the underlying geomorphic setting is therefore important to consider when investigating variations in forest characteristics across landscapes.

3.7 Appendix - Extended Methods

3.7.1 Field Data

The study area occupies ~83 km^2, in the western Los Plumas National Forest. The full extent of the original LiDAR survey covers a total of ~208 km^2; it extends predominately to the south and southwest. My reason for limiting the analysis to the northern part of the survey area is that much of the excluded region has either been extensively cleared, or was very heavily damaged during the 2008 fires (either the 2008 Scotch or 2008 Friend/Darnell fires): as I do not have a map of land use history for the area, I am not be able to objectively account for the prevalence of anthropogenic clearing in the southern portions of the LiDAR survey. Since this occurs only in the more low-relief parts of the landscape, this would have obscured the influence of the natural landscape characteristics on the forest properties, which was the primary target of the study. Objective burn intensity maps were obtained from the USFS (accessed from http://www.fs.usda.gov/ on 14/11/2013) enabling me to identify regions that suffered significant fire damage to the structurally dominant vegetation [*Miller and Thode*, 2007; *Miller et al.*, 2009].

During the summers of 2012 and 2013 (post-dating the LiDAR collection by 4-5 years; LiDAR was collected in September 2008 by the National Center for Airborne Laser Mapping (NCALM - http://www.ncalm.org)), I undertook 31 10 m-radius tree inventory plots (locations indicated in Supplementary Figure 3.1), recording diameter at breast height (1.3 m), *DBH*, and species for all trees with *DBH* >10 cm. Plot positions were determined using a Trimble *Geo-XH* GPS device, which were post-processed giving positional uncertainties that were typically 20-50 cm. In an earlier

study quantifying uncertainty in biomass measurements, Gonzalez et al. [2010] estimated that errors in their measurement of *DBH* was typically ~3%, which I use as a guide for my uncertainty analysis. All plot locations were located within the footprint of the original LiDAR survey, but not confined to the region used in the study. As much as possible, I tried to avoid areas that burned severely in the 2008 fires. Two of the field inventory plots were taken from areas that had been cleared and therefore contained no trees. My justification for this is that some of the areas within the survey area had also been cleared, thus it was important to include some low biomass plots in my calibration.

3.7.2 Calculating plot biomass and estimating uncertainty

Plot biomass was estimated by calculating the aboveground biomass (AGB) for each tree surveyed using the DBH-based allometric equations [Supplementary Table 3.1; *Jenkins et al.*, 2003; *Návar*, 2009; *Halpern and Means*, 2011]. I used Nàvar's (2009) equation for *Quercus spp*. to estimate the biomass of *Quercus spp*, whilst I used the Jenkins et al. (2003) generalized equations for other tree species. As both the Jenkins et al. (2003) and the *Arctostaphylos spp.* [*Halpern and Means*, 2011] model estimates had to be back-transformed from log-units, I multiplied this by a correction factor, CF, to account for the back-transformation of the regression error (given by $CF=e^{MSE/2}$, where MSE is the mean square error) [*Baskerville*, 1972]. Uncertainty in the predictions from the back-transformed model, σ_A, can then be estimated by $\sigma_A = \left(\sqrt{CF^2 - 1}\right) \times AGB$ [*Chave et al.*, 2004]. For the Nàvar (2009) equation, the RMSE was reported in absolute units, so I converted this to a relative RMSE by taking this as a percentage of the mean biomass for the trees used to construct that particular

allometric equation, and used this as my estimate on the uncertainty of my predictions. No error estimates were given in the Halpern and Means database, so I assumed a relative error of 30% for *Arctostaphylos spp.* biomass calculations. Yanai et al. [2010] indicate that using the RMSE leads to an underestimate of the actual uncertainty in individual estimates, but the published equations did not provide the necessary statistics to calculate their preferred uncertainty estimate. Finally it is important to note that interpretation of the RMSE for the Jenkins et al. (2003) equations is complicated by the fact that these equations were derived by fitting "pseudo-data" produced from many different species specific equations, without propagating the uncertainties associated with each individual equation [*Jenkins et al.*, 2003]. It is therefore not a direct quantification of the uncertainty in the biomass estimates, but I use it in the absence of an alternative.

Uncertainty in the estimation of plot biomass stems from two sources: measurement error and errors in the prediction from the allometric equation. In order to account for the combined uncertainty in my plot based biomass I developed a Monte Carlo framework to simulate uncertainty in the measurement of DBH and biomass predictions from the allometric equations [*Gonzalez et al.*, 2010; *Yanai et al.*, 2010]. My treatment of errors in the allometric predictions is different to that used for measurement error; errors in measurement of DBH are assumed to be normally distributed and uncorrelated, whereas if there are errors in the allometric model, they are likely to be correlated for other trees of the same species within that plot [*Yanai et al.*, 2010]. Therefore, each iteration of the Monte Carlo procedure, errors in DBH are resampled from the probability distribution for each tree, but errors in the allometric

equations are sampled once for each iteration, and then the same equation set is used for all trees within the plot. I performed 1000 iterations of my Monte Carlo procedure, and used the mean and standard deviation to estimate the plot biomass and uncertainty respectively.

3.7.3 Calculation of LiDAR-derived biomass and uncertainty

LiDAR has been widely exploited as a tool to quantify spatial variations in AGB across a range of biomes [*Lefsky et al.*, 1999b, 2002; *Drake et al.*, 2003; *Næsset and Gobakken*, 2008; *Dahlin et al.*, 2011; *Asner et al.*, 2012; *Colgan et al.*, 2012b]. I use the mean return height, *MRH*, defined as the centroid of the canopy return profile for all returns within a 10m radius, as it combines information on both canopy height and canopy cover into a single variable. This is calibrated against the plot biomass estimates estimated for the 31 field inventory plots surveyed in the field region.

Uncertainty associated with this calibration arises from (i) errors in the plot biomass calculation, discussed above; (ii) positional error [*Frazer et al.*, 2011], from both the original LiDAR georeferencing and GPS measurement error; these errors are additive; (iii) temporal differences between the LiDAR survey and field surveys; (iv) canopy overlap with the edge of the field plot, creating a mismatch between trees identified within the field plots (stem localised) and the corresponding LiDAR point cloud (crown-delimited) [*Mascaro et al.*, 2011]. Of these, the latter two are very difficult to quantify, and I do not attempt to do this here. Positional errors were accounted for using a Monte Carlo sampling procedure; positional uncertainty was represented as a Gaussian distribution, from which I randomly sampled 1000 times, in each of the iterations extracting the MRH for each point cloud sample, and calculating the mean

and standard deviations to determine my estimate of plot MRH and its associated uncertainty. Relative errors associated with all these sources, from field plots [*Chave et al.*, 2003, 2004] to calibration of LiDAR-derived metrics [*Frazer et al.*, 2011; *Mascaro et al.*, 2011] are expected to be larger for small plot sizes, and are likely to contribute to significant scatter within my calibration dataset. One outlier is excluded from the regression analysis (marked as a hollow symbol in Figure 3.2 (b) and Supplementary Figure 3.2), as the plot biomass was skewed by the presence of one very large tree (*Quercus decurrens*, DBH > 1 m).

I use a simple linear relationship between plot biomass and MRH as my calibration model for the LiDAR-derived biomass map. Since there are appreciable uncertainties in both calibration variables, I use Standardized Major Axis (SMA) regression to fit the model [*Sokal and Rohlf*, 1995; *Warton et al.*, 2006] using the R package SMATR [*Warton et al.*, 2012]. I do not weight the regression, or propagate the estimated uncertainties through other methods such as Monte Carlo methods [e.g. *Gonzalez et al.*, 2010]. My reasoning for this is two-fold: I am not able to fully constrain the uncertainties in each of the variables; the distribution of errors may not be normal for every source of uncertainty. With this in mind, I accept that the absolute biomass values reported in this study have significant uncertainty; however, my calibrated LiDAR model explains 70% of the variance of the plot biomass, with most of the model biomass estimates agreeing with the calibration dataset within their estimated error. Thus the uncertainties are unlikely to affect the conclusions drawn from my subsequent geospatial analysis.

3.7.4 Topographic analysis

I investigate the geospatial co-variation in erosion rate and forest characteristics by analysing the topographic properties of second order drainage basins and their corresponding AGB (Supplementary Figure 3.3). Second order basins represent the catchment area for second order channels, as defined by Strahler stream order: first order channels represent stream reaches stretching from the channel head to the first tributary, at which they become second order channels; second order channel reaches terminate at the confluence with another second (or higher) order channel, and become third order (or higher) channels, etc. From a geomorphic perspective, drainage basins are a fundamental unit in landscape dynamics, as rivers set the lower boundary condition of hillslopes and thus have a first order control on the characteristics of their catchments. The network was extracted by locating channel heads using the DrEICH method developed by Clubb et al. [2014], which has been verified in this landscape [*Clubb et al.*, 2014], and subsequently routing flow via the steepest descent pathway. Extracted basins are shown in Supplementary Figure 3.3. The specific topographic metric that I use is mean basin slope, which provides a first order proxy for erosion rate [*Ahnert*, 1970; *Montgomery and Brandon*, 2002; *Hurst et al.*, 2012]. Following Hurst et al. (2012), slope is calculated at each pixel by fitting a six-term polynomial surface to a moving window with a 7m radius. This filters the effects of small wavelength noise present in high resolution DEMs, which does not reflect the long term evolution of topography.

3.7.5 Downscaling PRISM data

To enable me to account for the influence of climate gradients in my study site, I used the 800m resolution maps of Mean Annual Precipitation, MAP, and Mean Annual Temperature, MAT, from the PRISM Climate Group at Oregon State University (http://www.prismclimate.org). These maps are produced using the PRISM (Parameter-elevation Relationships on Independent Slopes Model) interpolation scheme which incorporates the effects of topography in a physically meaningful way, and has been subject to extensive peer review [e.g. *Daly et al.*, 2002, 2008]. Whilst this represents the highest resolution climate data available for my study region, it is based on an 800m resolution DEM, which is too coarse to account for the microclimatic effects of topography. To address this, I follow the method outlined by Chorover et al. [2011] to downscale this climate data [see also *Pelletier et al.*, 2013]. Both MAT and MAP were resampled to 10m resolution using spline interpolation, and then MAT was modified to account for the microclimatic effects of local topography on incoming solar radiation [*Yang et al.*, 2007].

3.7.6 Basin Lithology

The bedrock geology classification for each catchment was determined by selecting the dominant (i.e. >50%) lithology present in the basin, as determined from the USGS geological map of California [Supplementary Figure 3.3; from *Ludington et al.*, 2005]. To simplify the analysis of lithology, I used a binary classification splitting the basins into basins that are predominately underlain by granodiorite, and those underlain by other lithologies.

3.7.7 Statistical analysis of controls on AGB

I use a General Linear Model framework to explore the extent to which mean basin slope, basin-averaged MAP and MAT, and bedrock lithology can explain the variance in the AGB for the second order basins extracted for the landscape, using the statistical computing environment R [*R Core Team*, 2013]. In total, 16 different models were tested, the results of which are presented in Supplementary Tables 3.2 and 3.3. In order to account for the effects of the 2008 Scotch Fire, I focused on a sub-set of catchments, in which the biomass map was first filtered to remove parts of the forest that were categorized as suffering moderate/high severity fire damage in the USFS burn severity map, and any basins for which >50% of their area was affected were removed from the sample. The exceptions are Model 1 and Model 2, which use the full dataset. Since the fire only affected granodiorite catchments, I only tested the impact of lithology in the filtered dataset, as otherwise the results would very likely be biased by the impact of the fire damage on the levels of AGB in affected catchments.

Supplementary Table 3.1 Allometric equations used to estimate biomass of individual trees in the field inventory plots

Source	Species Group	Equation	Species
Jenkins et al., 2003	Cedar/Larch	ln (AGB) = -2.0336 + 2.2592*ln(DBH)	*Calocedrus Decurrens*
	Douglas Fir	ln (AGB) = -2.2304+ 2.4435*ln(DBH)	*Pseudotsuga Menziesii*
	Pine	ln (AGB) = -2.5356 + 2.4349*ln(DBH)	*Pinus Lambertiana, Pinus Ponderosa*
	Soft Maple/Birch	ln (AGB) = -1.9123 + 2.3651*ln(DBH)	*Acer Macrophyllum*
	Mixed Hardwood	ln (AGB) = -2.4800 + 2.4835*ln(DBH)	*Cornus Nuttalli*
Návar, 2009	Mixed *Quercus spp.*	$AGB = 0.0890*DBH^{2.5226}$	*Quercus Kelloggii, Quercus Chrysolepis*
Halpern & Means, 2011	*Arctostaphylos spp.*	ln(AGB) = 3.466 + 2.421*ln(DBA)	*Arctostaphylos spp.*

Notes: **Abbreviations: DBH: Diameter at Breast Height (1.3m), in cm; DBA: Diameter at Base, in cm; AGB: Aboveground Biomass, in kg.**

Supplementary Table 3.2 The results from 16 different GLM analyses exploring the controls on the variation of mean AGB for all 2nd order drainage basins within the study region.

	Model	Nº. Basins	Adj. R^2	F-statistic	p-value
1	AGB ~ MBS †	374	0.34	194.6	$<2.2\times10^{-16}$
2	AGB ~ MBS*MAP*MAT †	374	0.47	47.68	$<2.2\times10^{-16}$
3	AGB ~ MBS	287	0.32	137.2	$<2.2\times10^{-16}$
4	AGB ~ MAP	287	0.04	12.8	0.0004
5	AGB ~ MAT	287	0.12	40.4	8.1×10^{-10}
6	AGB ~ MBS*MAP	287	0.39	60.6	$<2.2\times10^{-16}$
7	AGB ~ MBS*MAT	287	0.35	51.9	$<2.2\times10^{-16}$
8	AGB ~ MAP*MAT	287	0.18	22.3	5.5×10^{-16}
9	AGB ~ MBS*MAP*MAT	287	0.44	32.9	$<2.2\times10^{-16}$
10	AGB ~ MBS*MAP*MAT + factor(Lithology)	287	0.46	31.3	$<2.2\times10^{-16}$
11	AGB ~ MBS + factor(Lithology)	287	0.36	81.2	$<2.2\times10^{-16}$
12	AGB ~ MAP + factor(Lithology)	287	0.05	8.6	0.00023
13	AGB ~ MAT + factor(Lithology)	287	0.12	21.0	3.0×10^{-09}
14	AGB ~ MBS*MAP + factor(Lithology)	287	0.38	44.3	$<2.2\times10^{-16}$
15	AGB ~ MBS*MAT + factor(Lithology)	287	0.42	52.4	$<2.2\times10^{-16}$
16	AGB ~ MAP*MAT + factor(Lithology)	287	0.19	17.6	6.2×10^{-13}

Notes: **† full dataset; for all other models, the analysis excluded areas that suffered moderate-severe canopy disturbance during the 2008 Scotch fire, and completely excludes basins for which the affected area accounted for >50% of the total catchment area. Abbreviations: MBS = mean basin slope; MAP = mean annual precipitation; MAT = mean annual temperature. Lithology factor varies according to dominant bedrock lithology: 1 = granodiorite; 0 = meta-volcanics**

Supplementary Table 3.3 Full results from the GLM analysis exploring controls on the variation of mean AGB for all 2nd order drainage basins. This includes full suite of models explored including and excluding lithology as a factor.

Model	**1**		**2**		**3**		**4**		**5**		**6**		**7**		**8**	
Adj. R^2	0.34		0.47		0.32		0.04		0.12		0.39		0.34		0.18	
p-value	$<2.2 \times 10^{-16}$		$<2.2 \times 10^{-16}$		$<2.2 \times 10^{-16}$		0.0004		8.2×10^{-16}		$<2.2 \times 10^{-16}$		$<2.2 \times 10^{-16}$		5.5×10^{-13}	
Parameter	Coefficient	p	Coefficient	p	Coefficient	p	Coefficient	p	Coefficient	p	Coefficient	p	Coefficient	p	Coefficient	p
(Intercept) ($Mg.ha^{-1}$)	721.07	***	1.308×10^4	***	729.76	***	105.61	0.49	713.59	***	2695.62	***	892.94	***	3807.45	***
MBS	-461.91	***	-1.426×10^4	***	-432.62	***	-	-	-	-	-3127.03	***	-380.17	0.12	-	-
MAP	-	-	-6.245	***	-	-	0.30	***	-	-	-1.0389	***	-	-	-1.700	***
MAT	-	-	-734.8	**	-	-	-	-	-20.11	***	-	-	-13.93	0.31	-289.13	***
MBS x MAP	-	-	7.012	**	-	-	-	-	-	-	1.4285	***	-	-	-	-
MBS x MAT	-	-	825.1	*	-	-	-	-	-	-	-	-	-1.343	0.94	-	-
MAP x MAT	-	-	0.367	**	-	-	-	-	-	-	-	-	-	-	0.147	***
MBS x MAP x MAT	-	-	-0.416	*	-	-	-	-	-	-	-	-	-	-	-	-
Lithology Factor 1 = granodiorite; 0 = meta-volcanics	-	-	-	-	-	-	-	-	-	-	-	-	-	-	-	-

Supplementary Table 3.2 (*continued*)

Model	**9**		**10**		**11**		**12**		**13**		**14**		**15**		**16**	
Adj. R^2	0.44		0.46		0.36		0.05		0.12		0.38		0.42		0.19	
p-value	$<2.2 \times 10^{-16}$		$<2.2 \times 10^{-16}$		$<2.2 \times 10^{-16}$		0.0002		3.0×10^{-9}		$<2.2 \times 10^{-16}$		$<2.2 \times 10^{-16}$		6.2×10^{-13}	
Parameter	Coefficient	p	Coefficient	p	Coefficient	p	Coefficient	p	Coefficient	p	Coefficient	p	Coefficient	p	Coefficient	p
(Intercept) ($Mg.ha^{-1}$)	10687.86	**	1.125×10^4	**	782.37	***	-159.50		724.26	***	2464.12	***	890.23	***	3701.55	***
MBS	-9727.56	.	-1.088×10^4	*	-465.46	***	-	-	-	-	-2854.92	***	-346.79		-	-
MAP	-5.028	*	-5.361	**	-	-	0.337	***	-	-	-0.893	**	-	-	-1.636	***
MAT	-606.33	*	-669.2	*	-	-	-	-	-20.105	***	-	-	-9.903		-284.46	***
MBS x MAP	4.685	.	-40.72	***	-	-	-	-	-	-	1.273	***	-	-	-	-
MBS x MAT	504.59		5.363	.	-	-	-	-	-	-	-	-	-6.248		-	-
MAP x MAT	0.302	.	617.7		-	-	-	-	-	-	-	-	-	-	-25.490	***
MBS x MAP x MAT	-0.248		0.3398	*	-	-	-	-	-	-	-	-	-	-	-	-
Lithology Factor 1 = granodiorite; 0 = meta-volcanics	-	-	-0.3143		-52.98	***	-32.208	*	-18.383		-47.908	**	-50.551	***		.

***Notes*: Models numbered according to Table S2. Abbreviations: MBS = mean basin slope; MAP = mean annual precipitation; MAT = mean annual temperature. Lithology factor varies according to dominant bedrock lithology: 1 = granodiorite; 0 = meta-volcanics. Significance codes: *** p<0.001; ** p<0.01; * p<0.05; . p<0.01.**

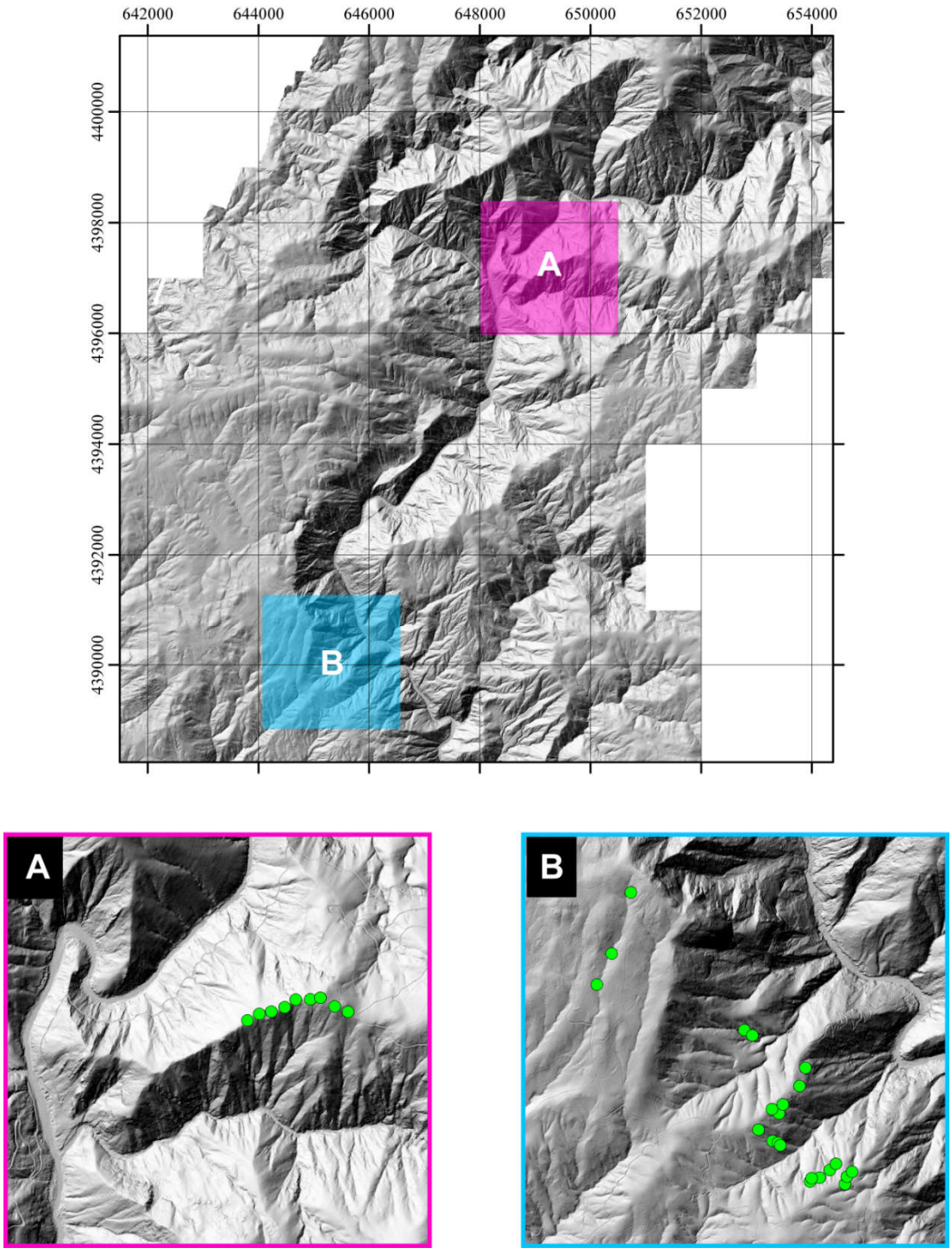

Supplementary Figure 3.1 A shaded relief map indicating the locations of the field inventory plots (green), from which I calculated plot biomass to calibrate the LiDAR-derived biomass estimates. The coordinate system is UTM Zone 10N.

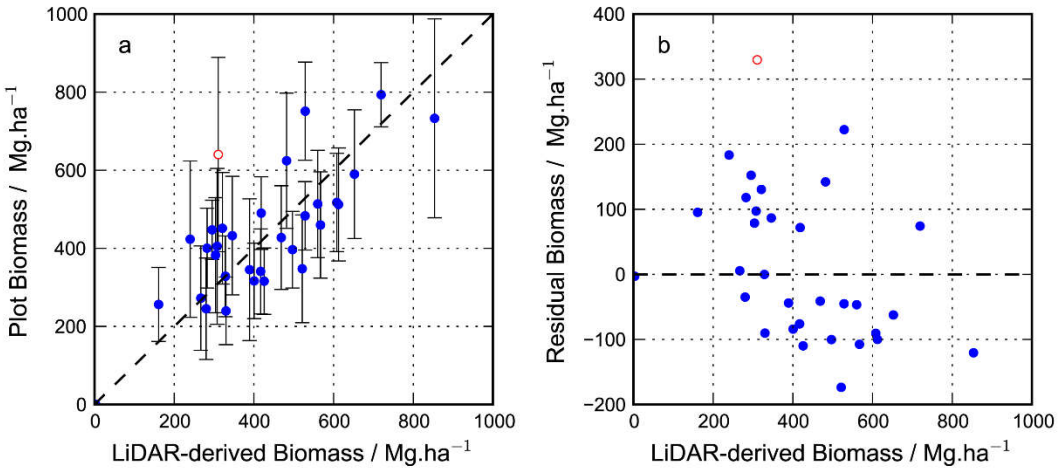

Supplementary Figure 3.2 (a) Comparison of plot-based biomass and LiDAR-derived biomass estimates. (b) Residual plot for the regression model. In both cases the outlier (marked by the hollow symbol) was excluded from the regression (see text for discussion).

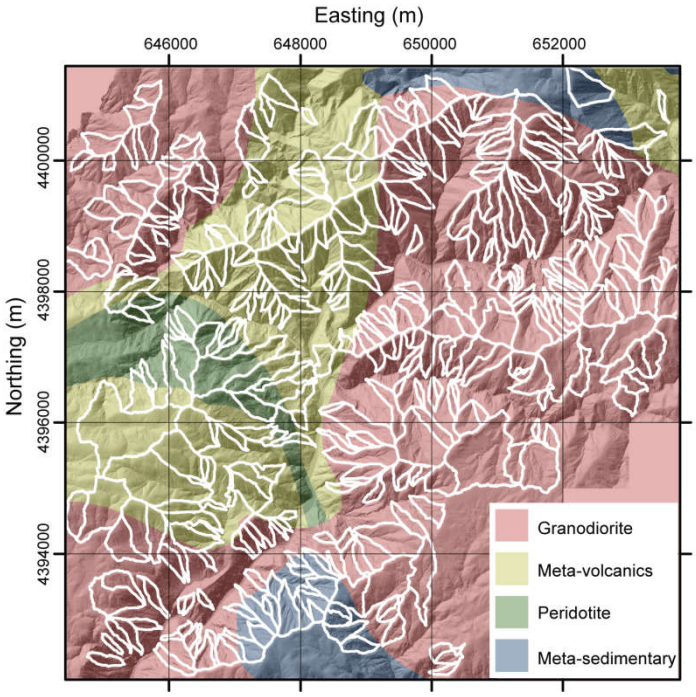

Supplementary Figure 3.3 A geological map of the study region [*Ludington et al.*, 2005], with the outlines of second order drainage basins analysed in this study outlined in white. The coordinate system is UTM Zone 10N.

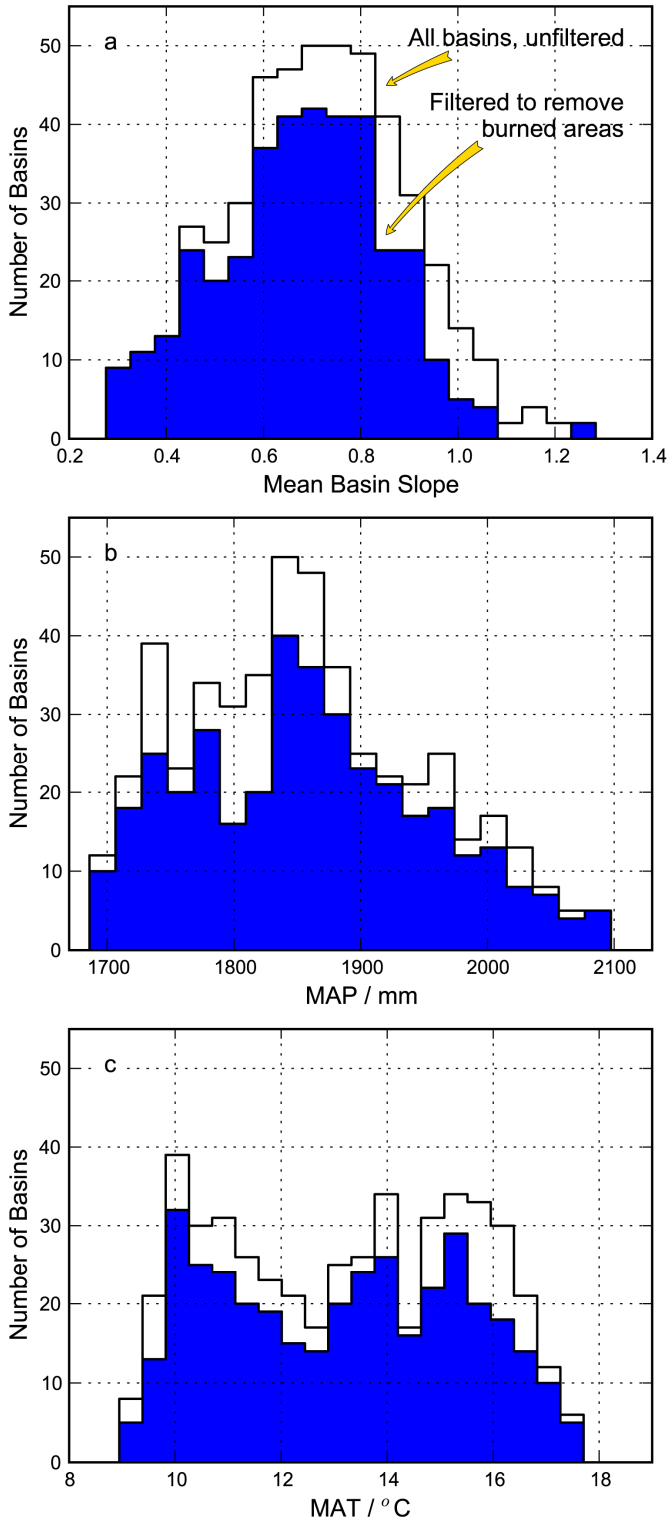

Supplementary Figure 3.4 Histograms of the explanatory variables: (a) MBS; (b) MAP; (c) MAT. The population distribution of both the full, unfiltered dataset of basins greater than 20,000m2 (black outline) and filtered dataset of basins (blue, filled) in which areas badly affected by the 2008 fire are removed, are shown.

3.8 Appendix – Summary of Forest Inventory Plot Data

PLOT	X	Y	POSITION ERROR (m)	AGB (kg(C) m^{-2})	±	MRH (m)	±
CAR2.1	649419.6	4397287.9	0.5	58.9	15.8	17.25	0.12
CAR2.2	649486.3	4397325.9	0.6	43.2	14.6	9.15	0.17
CAR2.3	649557.2	4397338.9	0.8	64.0	24.0	8.21	0.24
CAR2.4	649633.5	4397364.5	0.5	45.1	13.8	8.49	0.17
CAR2.5	649782.0	4397410.2	0.6	23.9	8.4	8.73	0.08
CAR2.6	649697.5	4397408.3	0.5	32.8	10.0	8.69	0.06
CAR2.7	649840.4	4397418.9	0.6	25.6	9.2	4.26	0.06
CAR2.8	649923.0	4397368.8	0.7	31.6	8.2	11.26	0.25
CAR2.9	649999.7	4397337.2	0.6	38.2	14.3	8.03	0.09
BR4.11	645372.8	4390131.6	0.6	51.4	14.1	16.20	0.29
BR4.12	645418.4	4390100.1	5.0	73.3	17.6	22.57	0.95
BR4.18	645807.2	4389278.0	1.1	31.7	9.5	10.60	0.04
BR4.20	645865.4	4389322.6	0.8	39.7	10.5	13.14	0.13
BR4.22	645901.7	4389359.3	0.7	34.1	8.5	11.03	0.18
BR4.23	645953.6	4389241.9	0.6	48.4	12.6	13.98	0.34
BR5.3	645453.4	4389556.1	0.7	42.4	13.0	6.35	0.05
BR5.8	645531.4	4389674.8	0.6	42.8	12.9	12.40	0.31
BR5.10	644717.7	4390925.5	2.8	79.4	19.3	19.03	0.99
BR5.12	644605.7	4390572.3	0.8	27.2	7.3	7.06	0.26
BR5.13	644520.6	4390393.2	0.8	40.5	9.9	8.14	0.08
BR2013_1.1	645724.8	4389912.8	0.5	44.7	13.3	7.81	0.04
BR2013_1.2	645691.6	4389808.5	0.6	40.0	13.2	7.47	0.22
BR2013_1.3	645595.0	4389701.3	0.7	51.3	13.4	14.82	0.59
BR2013_2.1	645761.2	4389275.3	0.8	45.9	12.2	15.00	0.06
BR2013_2.2	645966.0	4389284.9	0.6	34.8	9.0	13.79	0.20
BR2013_2.3	645995.7	4389312.9	0.7	51.7	12.1	16.08	0.31
BR2013_3.1	645535.5	4389491.0	0.5	49.0	16.7	11.07	0.25
BR2013_3.2	645566.1	4389480.7	0.6	75.1	24.7	13.99	0.04
BR2013_3.4	645579.6	4389465.2	0.9	62.3	19.3	12.75	0.20
Car_cascade	650057.0	4397311.0	0.3	0.0	0.0	0.08	0.02
Car_baldrock	645289.5	4389532.9	0.3	0.0	0.0	0.08	0.00

Chapter 4. Topographic Roughness as a Signature of the Emergence of Bedrock in Eroding Landscapes

Published in Earth Surface Dynamics: D.T. Milodowski, S.M. Mudd, and E.T.A. Mitchard (2015b), Earth Surface Dynamics, 3(2), 371–416, doi:10.5194/esurfd-3-371-2015.

Abstract

Rock is exposed at the Earth surface when rates of erosion locally exceed rates of soil production. The thinning of soils and emergence of bedrock has implications spanning geomorphology, ecology and hydrology. Soil mantled hillslopes are typically shaped by diffusion-like sediment transport processes that act to smooth topography through time, generating the familiar smooth, convex hillslope profiles that are common in low relief landscapes. Other processes, however, can roughen the landscape. Bedrock emergence can produce rough terrain; in this contribution I exploit the contrast between rough patches of bedrock outcrop and smooth, diffusion dominated soil to detect bedrock outcrops. Specifically, I demonstrate that the local variability of surface normal vectors, measured from 1 m resolution airborne LiDAR data, can be used as a topographic signature to identify areas within landscapes where rock exposure is present. I then use this roughness metric to investigate the transition from soil mantled to bedrock hillslopes as erosion rates increase in two transient landscapes, Bald Rock Basin, which drains into the Middle Fork Feather River, California, and Harrington Creek, a tributary of the Salmon River, Idaho. Rather than being abrupt,

as predicted by traditional soil production models, in both cases the transition from fully soil mantled to bedrock hillslopes is gradual and spatially heterogeneous, with rapidly eroding hillslopes supporting a patchwork of bedrock and soil that is well documented by changes in topographic roughness, highlighting the utility of this metric for testing hypotheses concerning the emergence of bedrock and adding to a growing body of evidence that indicates the persistence of partial soil mantles in steep, rapidly eroding landscapes.

4.1 Introduction

The geomorphic transition from hillslopes with a continuous soil mantle to rugged bedrock is a key phase in the evolution of eroding landscapes. Many slowly eroding landscapes feature sediment transport processes that act to diffuse and dampen short wavelength features of the topography, generating smooth, soil mantled hillslopes [*Gilbert*, 1909; *Carson and Kirkby*, 1972]. Bedrock becomes exposed at the surface when the rate of erosion exceeds the maximum rate of soil production [*Carson and Kirkby*, 1972; *Heimsath et al.*, 1997, 2012]. This transition is gradual, and spatially variable, reflecting the fact that both soil production and sediment transport are spatially heterogeneous, and typically operate via discrete events [*Wilkinson et al.*, 2005; *Strudley et al.*, 2006a, 2006b; *Gabet and Mudd*, 2010; *Furbish and Roering*, 2013]. The emergence of bedrock signifies a fundamental change in the dynamics of sediment transport, which become increasingly stochastic as mobile colluvium is stripped away and the hillslope sediment flux becomes detachment limited [e.g. *Binnie et al.*, 2007]. Furthermore, the establishment of terrestrial ecosystems is dependent on a hospitable substrate: the mosaic of bedrock and soil that constitutes the hillslope

surface imposes a physical template on the development of terrestrial ecosystems [*Phillips and Marion*, 2004; *Pelletier and Rasmussen*, 2009b; *Gabet and Mudd*, 2010; *Sheffer et al.*, 2013]. The rate of erosion that is sufficient to completely strip soil may therefore represent a limiting threshold for ecosystem development [*Graham et al.*, 2010]. In addition, the presence or absence of bedrock outcrop may reveal important information about the availability of nutrients such as phosphorous in soil parent material [*Hahm et al.*, 2014a]. Equally, the transition between deep and shallower soils, signalled by the appearance of bedrock outcrops, is an ecological gradient allowing for niche specialisation, driving biodiversity and diversity within species, influencing ecosystem function, species creation and adaptability [*Smith et al.*, 1997]. Quantifying the spatial distribution of rock exposure and its relationship to the ecological and geomorphological characteristics of a landscape thus comprises an important challenge in understanding critical zone dynamics.

The advent of airborne Light Detection And Ranging (LiDAR) as a remote sensing technology over the last decade or so has driven a revolution in the fields of both geomorphology and ecology by providing high resolution (<1 m) observations of both canopy structure and sub-canopy topography, therefore enabling observations to be made at length-scales sufficiently small to analyse the geomorphic characteristics of hillslopes [*Roering et al.*, 2010; *DiBiase et al.*, 2012; *Hurst et al.*, 2012]. Higher resolution still (<1 cm) is possible using terrestrial LiDAR systems, permitting the analysis of multi-scale dimensionality from length scales of centimetres to several metres, enabling the objective classification of point clouds into specific features, such as vegetation and bedrock, with a high degree of accuracy [*Brodu and Lague*, 2012;

Lague et al., 2013]. Despite the obvious benefits of high resolution terrestrial LiDAR scanning, the greater spatial coverage permitted by airborne surveys maintains its utility for landscape scale applications, requiring the development of remote sensing methods with which it is possible to extract information about the geomorphic characteristics of hillslopes, such as the extent of rock exposure, from such comparatively low resolution data.

DiBiase et al. [2012] used airborne LiDAR data to investigate the impact of increasing erosion rates on hillslope morphology in the San Gabriel Mountains, CA, demonstrating that slope distributions became increasingly skewed towards higher gradients, as steep, bedrock slopes became increasingly abundant. They successfully developed the Rock Exposure Index (REI) as a topographic metric to map rock exposure in this landscape, defined as areas in which the local gradient exceeds a threshold steepness beyond which soil is no longer retained on the hillslope. DiBiase and Lamb [2013] exploited this metric to quantify sediment storage by vegetation on steep slopes, and thus assess the likely impact of wild fires on hillslope sediment fluxes. Marshall and Roering [2014] used a similar slope-based metric to map erosion resistant sandstone beds in the Oregon Coast Range.

However, slope-based metrics are not universally applicable. For example, when long term rates of erosion exceed the local maximum rate of soil production, bedrock will be exposed at the surface, irrespective of slope [*Carson and Kirkby*, 1972; *Heimsath et al.*, 1997, 2012]. Within a given setting, rates of soil production may be limited by factors such as climate, vegetation, lithology and soil thickness [e.g. *Pelletier and Rasmussen*, 2009b; *Chorover et al.*, 2011; *Goodfellow et al.*, 2014b]. It is evident that

in many landscapes rock exposure emerges in places even at low topographic gradients, and is particularly common in regions with thin regolith cover, where tor formation is common [*Anderson*, 2002; *Strudley et al.*, 2006b], on ridgelines [*Gabet et al.*, 2015], or where bedrock heterogeneities drive small-scale variation in weathering rates [*Goodfellow et al.*, 2014a].

Another method by which rock exposure might be mapped from high resolution topographic models of hillslopes is through changes in their textural characteristics. On hillslopes mantled by a veneer of soil, sediment transport is driven by the time-integrated effect of a suite of local-scale diffusive processes, including bioturbation, tree throw, dry ravel and rain splash [e.g. *Gabet*, 2003; *Gabet et al.*, 2003; *Yoo et al.*, 2005; *Furbish et al.*, 2007]. The net efficiency of these processes in transporting material increases with topographic gradient – they are diffusion-like [*Furbish et al.*, 2009] – such that they act to dampen the amplitude of local topography, particularly when viewed at length-scales greater than those at which the dominant sediment transport rates operate. The resultant hillslopes therefore typically exhibit smooth, convex surfaces that are ubiquitous to many soil mantled landscapes [*Gilbert*, 1909; *Culling*, 1963, 1965; *Carson and Kirkby*, 1972; *McKean et al.*, 1993]. The emergence of bedrock at the surface potentially drives a significant increase in roughness, because there is a fundamental change in the dynamics of sediment transport at this location within the landscape: sediment transport is detachment limited [*Dietrich et al.*, 2003] and the local relief structure is governed by the characteristics of the bedrock (fracture density and orientation, bedding and foliation, weathering behaviour).

In this paper I exploit this idea and develop a new technique to identify areas of rock exposure from high resolution LiDAR data, based on short-wavelength topographic roughness. This method is validated in two granitoid landscapes by comparing the results to rock exposure mapped independently from high resolution orthophotographs, highlighting its utility and limitations. Finally, as a case study, I apply the algorithm in two strongly transient landscapes – the first in the Feather River region of the northern Sierra Nevada, California; the second in the Salmon River region SW of the Bitterroot Mountains, Idaho – in order to illustrate the transition from diffusive, soil mantled hillslopes to rough, bedrock hillslopes as erosion rates increase in both settings.

4.2 Methods – Quantifying Surface Roughness

Sediment fluxes on soil mantled hillslopes have been shown to be well approximated by a linear relationship with the topographic slope [*Ahnert*, 1970; *Carson and Kirkby*, 1972], becoming non-linear as erosion rates increase and steepen hillslopes towards a limiting slope beyond which mobile colluvium is unstable [*Roering et al.*, 1999]. The resultant topography is diffusive: hillslope processes act to dampen the amplitude of local micro-topography generating characteristically smooth hillslope topography. My method starts from the hypothesis that the emergence of bedrock through the soil mantle should be detectable as an increase in the local roughness of the topographic surface, due to a geomorphic process transition away from diffusion-like hillslope processes.

Specifically I analyse surface roughness using the variability of the orientation of local slope normal vectors, using the eigenvalues of an orientation tensor, derived from the

vectors normal to the topographic surface. A similar approach has been used in a range of geological applications, notably in earthquake seismology [*Fara and Scheidegger*, 1963], analysing trends in geological structural data [*Woodcock*, 1977] and more recently as a method to objectively locate landslides from high resolution topographic data [*McKean and Roering*, 2004]. I note here that other metrics describing surface roughness, such as the standard deviation of slope, have been used in other geomorphic contexts, such as LiDAR-based mapping of volcanic deposits [*Whelley et al.*, 2014] and channel bed morphology [*Cavalli et al.*, 2008].

Initially a second order polynomial surface is fitted to a moving data window of 3x3 pixels [*Evans*, 1980]. This method of surface approximation to calculate topographic metrics has been widely utilised in the calculation of surface derivatives, predominately slope and curvature, for the extraction of geomorphic features such as hilltops [*Hurst et al.*, 2012], channel networks [*Pirotti and Tarolli*, 2010; *Sofia et al.*, 2011], landslides [*Tarolli et al.*, 2010; *Lin et al.*, 2013], and anthropogenic features on floodplains [*Sofia et al.*, 2014]. Using a larger length-scale would dampen the roughness signal, but may be necessary if the topographic data is noisy [*Sofia et al.*, 2011]. The surface can be described by

$$z = ax^2 + by^2 + cxy + dx + ey + f, \quad (1)$$

where z is the surface elevation, x and y are horizontal coordinates, and a, b, c, d, e, and f are empirical fitting coefficients. A similar approach was employed by Hurst et al. [2012] to calculate hilltop curvature, who found no significant difference between the results obtained using six or nine term polynomials in their surface fitting

algorithm. Consequently I use a six term polynomial as it maximises computational efficiency. The normal to a surface is given by:

$$\boldsymbol{n} = \nabla(f(x,y) - z). \tag{2}$$

For equation (1), using spherical coordinates (r, θ, φ) at the origin, the unit normal vector becomes:

$$\boldsymbol{n} = \left(1, \quad \tan^{-1}\left(\sqrt{d^2 - e^2}\right), \quad \tan^{-1}\left({}^{e}/_{d}\right)\right). \tag{3}$$

For N surface normal vectors, the orientation matrix, $\boldsymbol{T}$, can be constructed using the directional cosines l_i, m_i and n_i, as shown below:

$$\boldsymbol{T} = \begin{bmatrix} \sum_i^N {l_i}^2 & \sum_i^N l_i m_i & \sum_i^N l_i n_i \\ \sum_i^N m_i l_i & \sum_i^N {m_i}^2 & \sum_i^N m_i n_i \\ \sum_i^N n_i l_i & \sum_i^N n_i m_i & \sum_i^N {n_i}^2 \end{bmatrix}, \tag{4}$$

where the directional cosines for the unit normal vectors are given by:

$$l_i = \sin\theta\cos\varphi, \qquad m_i = \sin\theta\sin\varphi \quad \text{and} \quad n_i = \cos\theta \tag{5}$$

The orientation matrix can be solved to find the three eigenvectors $\mathbf{v}_1$, $\mathbf{v}_2$, $\mathbf{v}_3$, which define the principal axes of the distribution of local normal vectors, and their corresponding eigenvalues, λ_1, λ_2, λ_3, which describe the degree of clustering of the normal vectors about these axes [*Watson*, 1966]. Following Woodcock [1977], I normalise the eigenvalues by the number of observations (N):

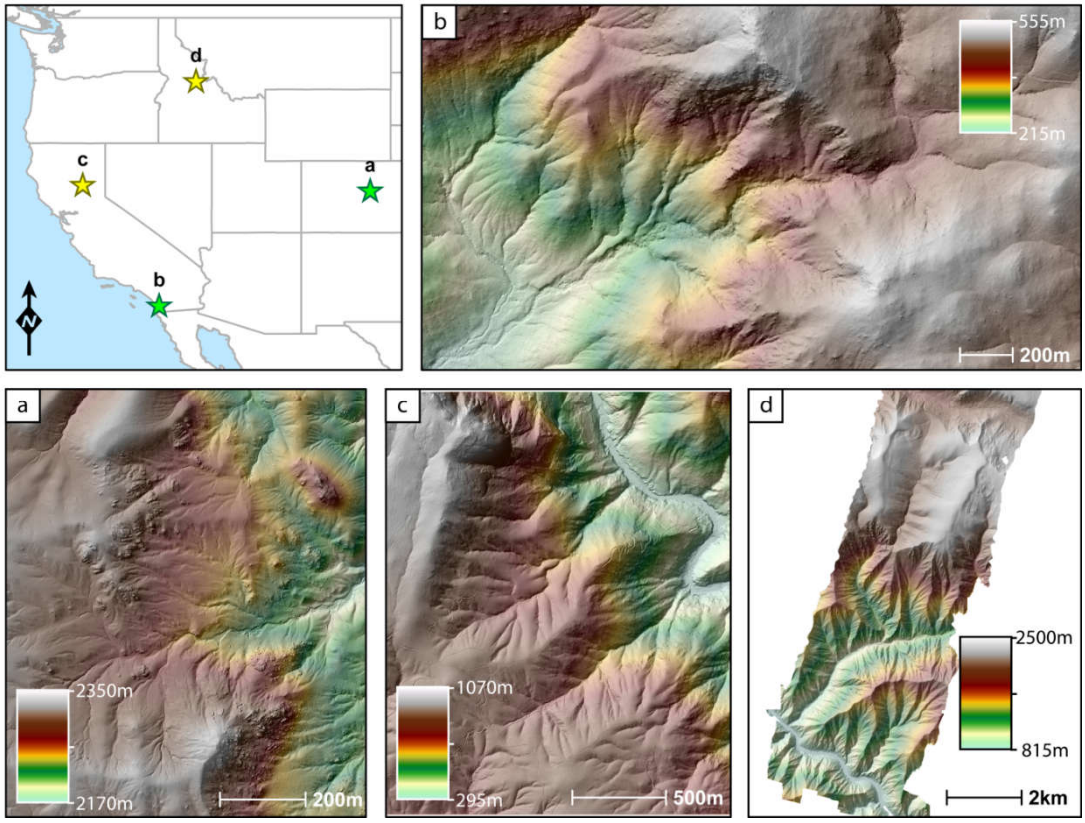

Figure 4.1 Field sites used in this study; (a) headwaters of the Spring Creek catchment, ~2.7 km SW of Rayleigh Peak, in the Colorado Front Ranges; (b) Poway Creek, California; (c) Bald Rock Basin, draining into the Middle Fork Feather River, Californian Sierra Nevada; (d) Harrington Creek, which drains into the Salmon River, Idaho. Sites (a) and (b) were used to validate my algorithm; sites (c) and (d) were subsequently analysed to investigate the transition from soil-mantled to bedrock hillslopes in transient landscapes.

$$S_1 = {}^{\lambda_1}/_{N}, \qquad S_2 = {}^{\lambda_2}/_{N}, \qquad S_3 = {}^{\lambda_3}/_{N}. \tag{6}$$

S_1 ($\frac{1}{3} \leq S_1 \leq 1$) describes the clustering around the major axis, S_2 ($0 \leq S_2 \leq \frac{1}{2}$) the intermediate axis, and S_3 ($0 \leq S_3 \leq \frac{1}{3}$) the minor axis. These normalised eigenvalues can be used to describe the morphology of a given surface [*Woodcock*, 1977]: for a smooth surface, the local surface normal vectors will have similar orientations, thus they will cluster tightly around the major axis, $\mathbf{v}_1$, and S_1 will be large, whereas the degree of clustering around the minor axis, $\mathbf{v}_3$, will thus be very small (low S_3). Conversely, for a rough surface, the normal vectors will be more randomly orientated; there will be a

weaker degree of clustering around $\mathbf{v}_1$ (low S_1), whilst the clustering around $\mathbf{v}_3$ will be relatively high (therefore high S_3).

A moving data kernel is passed over the dataset to analyse the variability of the surface normal vectors within the local (circular) neighbourhood. The radius of this kernel determines the length-scale over which the roughness of the surface is quantified. Identifying the correct length-scale in this case is critical – too large, and long wavelength variations in the topography (i.e. ridge-valley topography) will dominate, obscuring any signal from rock exposure; too small, and then the measured roughness will pick out locally smooth surfaces within an exposure of bedrock. I discuss determining the optimal length-scale in the Validation section (for results, see Section 4.3.4).

Table 4.1 Summary of datasets used in this chapter

Airborne LiDAR				
Region	**Acquisition date**	**Areal extent used (km^2)**	**Point Density (pts m^{-2})**	**Dataset Acknowledgement**
Rayleigh Peak, CO	May 2010	23	10.1	*1*
Poway Creek, CA	January 2005	1.4	1.4	*2*
Bald Rock Basin, CA	September 2008	4.0	9.8	*1*
Harrington Creek, ID	August 2011	49.0	4.6	*1*
Orthophotographs				
Region	**Acquisition date**	**Resolution / m**	**Sensor type**	**Dataset Acknowledgement**
Rayleigh Peak, CO	March 2010	0.30	*Colour Near-Infrared*	*3*
Poway Creek, CA	May 2012	0.15	*Colour Near-Infrared*	*3*

1 National Center for Airborne Laser Mapping (NCALM – http://www.ncalm.org); 2 USGS Center for LiDAR Information Coordination and Knowledge (CLICK – http://lidar..cr.usgs.gov/; via OpenTopography); 3 USGS (via EarthExplorer http://earthexplorer.usgs.gov/)

4.3 Validation of the surface roughness algorithm

4.3.1 Validation sites

In order to test the surface roughness metric described above as a measure of rock exposure, I selected two validation sites in Western USA (Figure 4.1) based on the availability of co-located LiDAR and high resolution (<30 cm) orthophotographs. A further requirement for validation sites was that the degree of vegetation cover was minimal, to permit the objective classification of rock outcrop in the imagery (Section 4.3.2). All LiDAR datasets and orthophotographs used in the study are freely available from either the National Science Foundation's OpenTopography service (www.opentopography.org) or from the United States Geological Survey (USGS; earthexplorer.usgs.gov/). Technical details for the datasets have been collated in Table 4.1.

4.3.1.1 Rayleigh Peak, Colorado

The first validation site is located in the headwaters of the Spring Creek catchment, in the central Colorado Frontal Range, which drains into the South Platte River ~40 km SSW of Denver (Figure 4.1a). The climate is semi-arid with frequent intense summer storms. Mean Annual Precipitation (MAP) of 440 mm, and average monthly temperatures varying from a maximum (minimum) of 27.7(10.8)^{0}C in summer to 6.0(-9.0)^{0}C in winter (http://www.prismclimate.org). Vegetation comprises grassland and sparse coniferous forest, of which Ponderosa Pine and Douglas Fir are the principal components, and the distribution of which is dominated by the impact of the 1996 Buffalo Creek wildfire, in which 79% of the Spring Creek catchment suffered severe burn damage [*Moody and Martin*, 2001], so that forest canopy now covers only a small

proportion of the landscape. The bedrock geology comprises Pikes Peak Granite [*Ruleman et al.*, 2011], which forms large, blocky outcrops. The degree of rock outcrop at the site varying from almost full exposure on hillslopes around Rayleigh Peak, which dominates the topography, to fully soil mantled hillslopes that are now predominately covered by grassland.

4.3.1.2 Poway Creek, California

The second study site is located in the Poway Creek catchment, located just east of the city of Poway, north of San Diego (Figure 4.1b). MAP is 825 mm and temperatures typically range from 29.1(14.1)^{0}C in summer to 11.5(-0.2)^{0}C in winter (http://www.prismclimate.org). The bedrock geology is principally composed of granodiorite with dacitic-andesitic extrusive rocks underlying the eastern margin [*Todd et al.*, 2004]. There is a gradient in rock exposure from predominately soil mantled, grassy hillslopes that are frequently gullied, to abundant rock outcrop in the steep, rugged headwaters. Due to classification errors in the original dataset, the LiDAR point cloud was reclassified using the multi-scale curvature algorithm incorporated within the MCC-LiDAR tool [*Evans and Hudak*, 2007].

4.3.2 Objective identification of rock exposure from high resolution orthophotographs

The high resolution orthophotographs were classified using the supervised classification toolbox available within the ENVI 4.8 processing environment. Specifically I utilised the Support Vector Machine classification method [*Wu et al.*, 2004], trained using a series of manually selected sample Regions Of Interest (ROIs) for each class. The classes used to analyse each orthophotograph comprised: “Rock”,

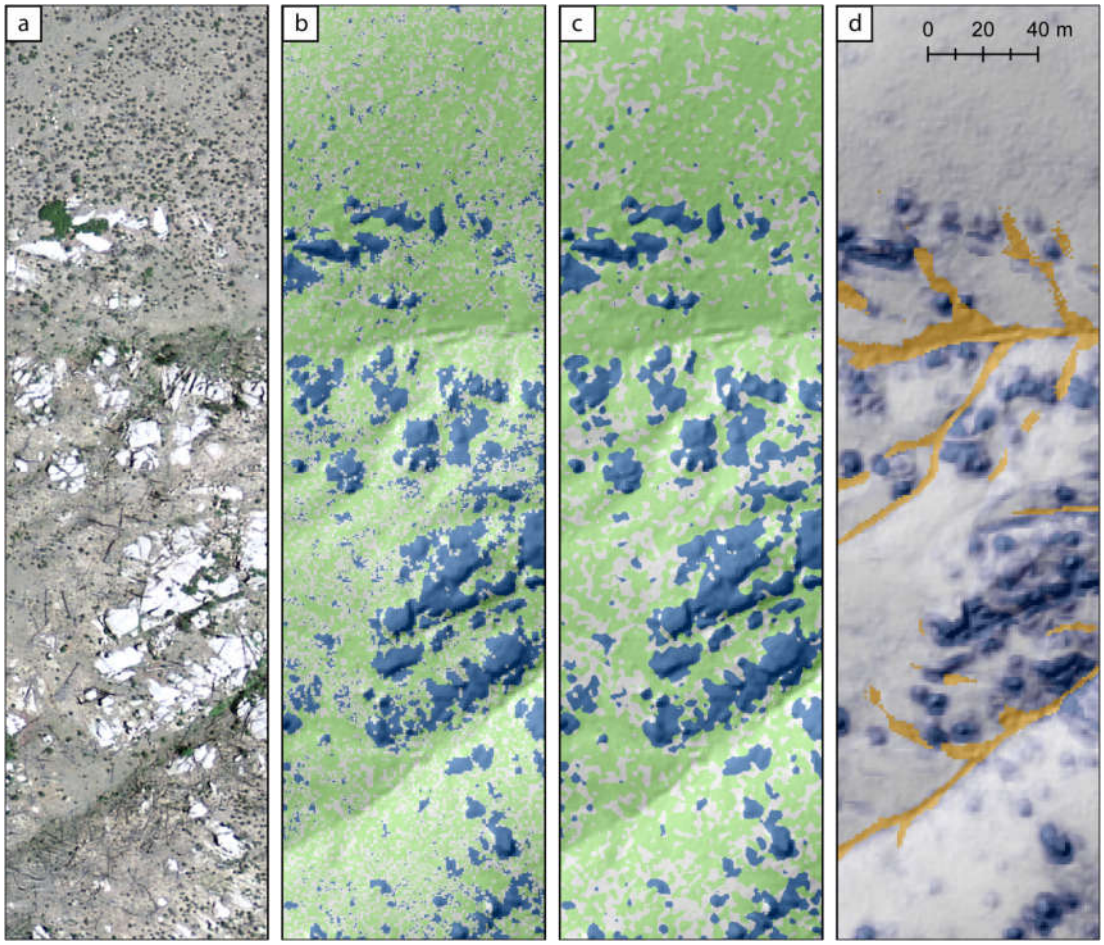

Figure 4.2 Validation procedure illustrated for the Rayleigh Peak site: (a) high resolution colour-near infrared orthophotograph; (b) results from the SVM classification procedure – rock = blue, soil mantled/vegetation = green; (c) classified image following the subsequent majority filter; (d) map of S_3, which I use as a measure of surface roughness, measured using a neighbourhood window radius of 3m. Orange pixels mark areas identified as being channelized.

"Vegetation", "Bare Earth" and "Shadow". With the exception of the "Shadow" class, which was not as spatially extensive, each ROI had a minimum of 10,000 pixels. The SVM classification was implemented to analyse the imagery at two pyramid levels, with a Pyramid Reclassification Threshold (i.e. the probability threshold required to reclassify a pixel, if given a different class at a finer resolution) of 0.90. As the avoidance of false positives within my validation dataset was of paramount importance, pixels were left unclassified if the confidence level for the final class fell below 95%. Subsequently a 7x7 pixel majority filter was employed to reduce the noise

in the classified image Figure 4.2. As my focus is on comparing soil mantled and rocky hillslopes, I combine the vegetation and bare earth classes, and treat areas that are in shadow as unclassified.

The quality of the classification scheme for each image was judged based both with a visual inspection of the classification results to ensure that there were no systematic errors located away from the training ROIs, and using the error matrices for each classification, providing a quantitative assessment of the scheme's ability to correctly reproduce the classification of the initial ROIs. At the 95% confidence interval, the SVM scheme discarded 9.4% of the ROI pixels as unclassified in the Rayleigh Peak dataset and 12.0% in the Poway Creek dataset. At the Rayleigh Peak site, the classification scheme was able to replicate the rock ROIs with a commission error (ratio of non-rock pixels classified as rock to the total number of pixels in the rock ROI) of 0.23% and an omission error (ratio of rock pixels incorrectly classified to the total number of pixels in the rock ROI) of 0.01%. At the Poway Creek site, the ROIs were replicated with a commission error of 0.01% and an omission error of 0.13%. Across the region as a whole, at both of my validation sites, the classification scheme struggled in areas where there are large changes in the saturation of the imagery (Figures 4.3-4.4), due to aspect-driven differences in illumination: as a result some areas have an increased proportion of unclassified pixels. This problem is endemic to image classification in high relief terrain, and is very hard to correct even with good topographic data and bi-directional reflectance function (BDRF-driven) models, as there is often no information captured in the brightest and darkest parts of the image[e.g. *Teillet et al.*, 1982; *Colby*, 1991; *Hale and Rock*, 2003].

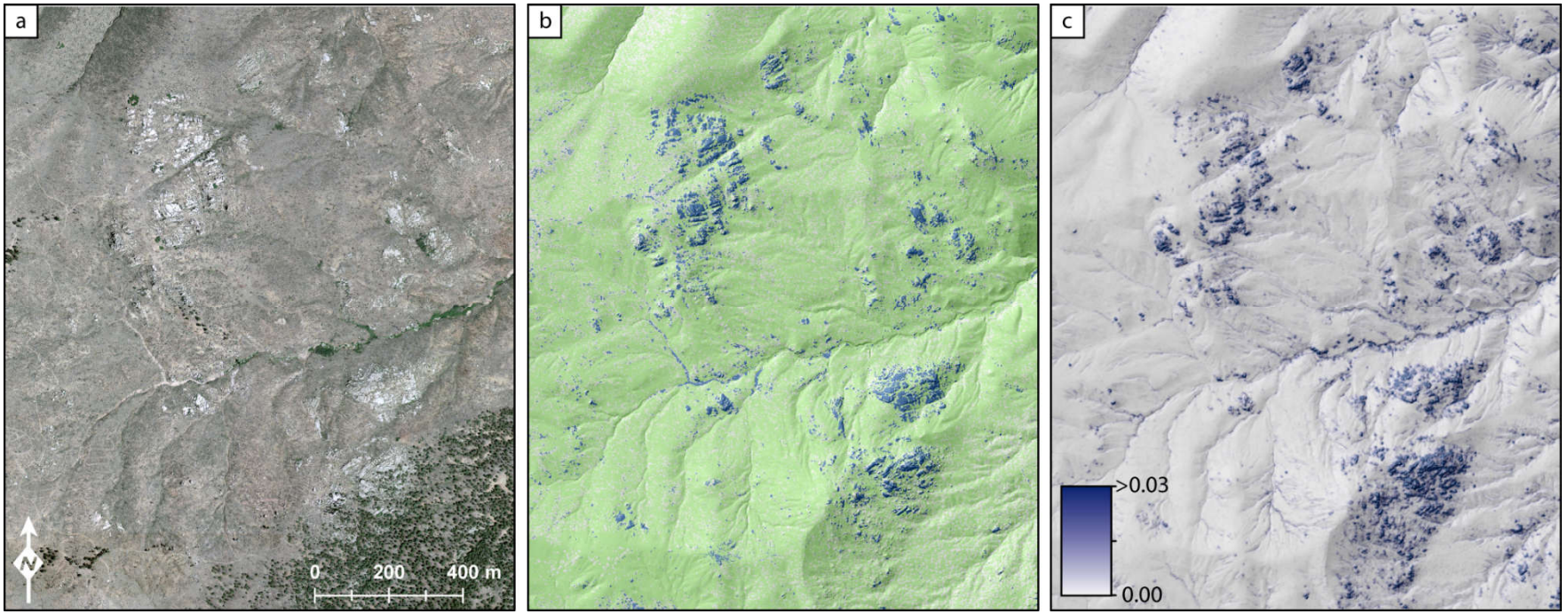

Figure 4.3 Validation maps for the Rayleigh Peak site: (a) high resolution, colour-near infrared orthophotograph; (b) results from combined classification procedure: rock = blue, soil mantled/vegetation = green; (c) map of S_3, which I use as a measure of surface roughness, measured using a neighbourhood window radius of 3m. To maximise the clarity of the maps, channelized portions of the landscape have not been masked.

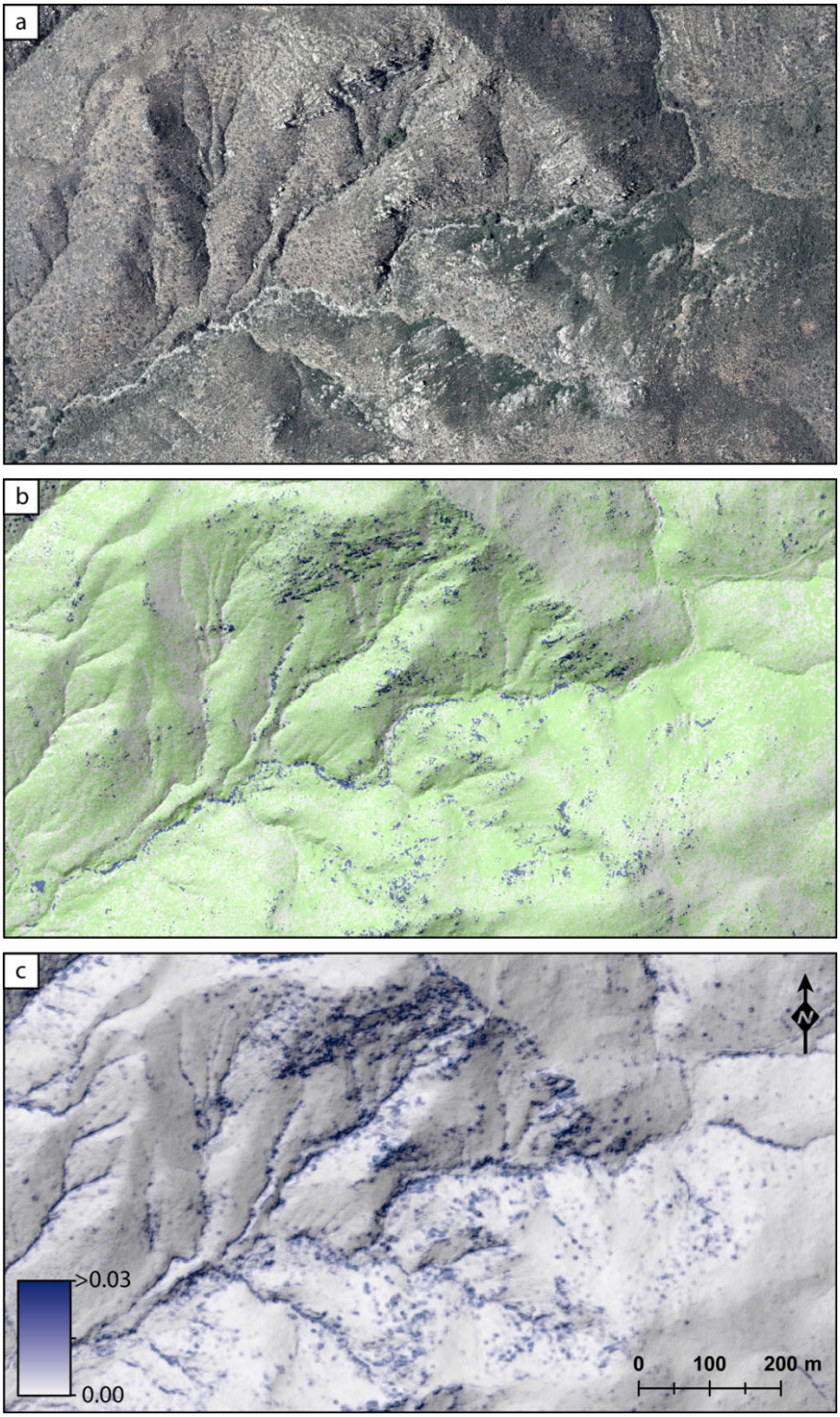

Figure 4.4 Validation maps for the Poway Creek site: (a) high resolution, colour-near infrared orthophotograph; (b) results from combined classification procedure: rock = blue, soil mantled/vegetation = green; (c) map of S_3, which I use as a measure of surface roughness, measured using a neighbourhood window radius of 3m. To maximise the clarity of the maps, channelized portions of the landscape have not been masked.

Again, this highlights the potential advantages of landscape classification techniques based on the morphological characteristics of the topographic surface. In addition, it is evident that there are still some areas where the image classification provides an incorrect classification. Nevertheless, the classification is sufficiently successful to provide two large test datasets with which to validate my roughness metric. Errors in the validation datasets will, if anything, lead to an underestimate of the accuracy of my topographically derived metric; it is hard to imagine how errors in the classification could inflate the accuracy of the topographic roughness metric, as the datasets are entirely independent and any errors unlikely to be co-located.

4.3.3 Validation procedure

I used the rock exposure maps from the classifications described above to perform the validation of the roughness algorithm in each of the four test landscapes. Since channels are often topographically rough, I first restricted my analysis to the hillslope domain. Several methods have been proposed to identify channel pixels in high resolution topography [e.g. *Lashermes et al.*, 2007; *Passalacqua et al.*, 2010a; *Pelletier*, 2013]; in each landscape I have used the method of Lashermes et al. [2007], in which the topography is filtered using a Gaussian filter, and then a curvature threshold to define the extent of the channel network is obtained statistically by looking for the departure from the expectations of a Gaussian distribution. This approach produces visibly satisfactory results across the range of landscapes used here.

After isolating the hillslopes, I searched through the parameter space for the S_3 eigenvalue, performing a pixel-pixel comparison with the orthophotograph classifications to ascertain whether the algorithm produced a true positive (TP), false

positive (FP), true negative (TN) or false negative (FN) for a given roughness threshold. In order to objectively assess the performance of the algorithm and determine an optimum threshold value to delineate areas with rock exposure, I calculated five test statistics: (i) true positive rate (= TP/(TP+FN)); (ii) false positive rate (= FP/(TN+FP)); (iii) commission error (= FP/(TP+FN)); (iv) omission errors (= FN/(TP+FN)); and (v) the overall accuracy (= (TP+TN)/Total); to objectively assess the performance of the algorithm and determine an optimum threshold value to delineate areas with rock exposure. In order to avoid bias in the aforementioned statistics towards either class, the larger of the two classes was randomly subsampled to the same number of test pixels as the smaller of the two before proceeding with the calculations. I repeated this procedure for three neighbourhood radii (3 m, 5 m and 7 m) in each of the two field sites to assess the influence of neighbourhood size on the measured surface roughness. An important consideration when interpreting the validation results is that the surface roughness represents a spatially aggregated metric, representing a blend of the topographic characteristics within the circumference of the neighbourhood window. Consequently, it is unlikely that this metric will discriminate between small areas of patchy soil interspersed between rugged rock outcrops at length scales smaller than the neighbourhood window. This effect becomes increasingly significant as the window size increases and is an inevitable outcome from neighbourhood statistical approaches. As a result, I eliminate from my validation dataset areas that are not classed as rock exposure that lie within 7 m (the largest neighbourhood radius used) of mapped rock exposure. For comparison, I also report the same statistics for the full dataset.

Table 4.2 Summary of validation results for three different threshold values of the eigenvalue S_3. These represent a subsample from the data displayed in figures 5 and 6. TPR = True Positive Rate; FPR = False Positive Rate; CE = Commission Error; OE = Omission Error; OA = Overall Accuracy (for definitions see text). As the surface roughness metric is spatially aggregated, this pixel-wise comparison was conducted avoiding soil-mantled pixels that were located proximal to areas of rock exposure (see text). Including these results in an increase in the false positive rate and commission errors, and corresponding drop in overall accuracy (see also Figures 4 and 6); however these errors are collocated with areas of rock exposure, and arise as a consequence of this proximity.

	TPR			FPR			CE			OE			OA		
Neighbourhood Window Radius	**3m**	**5m**	**7m**	**3m**	**5m**	**7m**	**3m**	**5m**	**7m**	**3m**	**5m**	**7m**	**3m**	**5m**	**7m**
$S_{3,\ threshold}$	**Rayleigh Peak**														
0.005	0.68	0.76	0.80	0.05	0.11	0.16	0.05	0.11	0.16	0.32	0.24	0.20	0.81	0.83	0.82
0.010	0.50	0.59	0.64	0.01	0.03	0.04	0.01	0.03	0.04	0.50	0.41	0.36	0.74	0.78	0.80
0.015	0.37	0.46	0.50	<0.01	0.01	0.01	<0.01	0.01	0.01	0.63	0.54	0.49	0.68	0.73	0.75
$S_{3,\ threshold}$	**Poway Creek**														
0.005	0.69	0.83	0.88	0.09	0.15	0.23	0.09	0.15	0.23	0.31	0.17	0.12	0.80	0.84	0.83
0.010	0.43	0.60	0.68	0.03	0.05	0.07	0.03	0.05	0.07	0.57	0.40	0.32	0.70	0.78	0.81
0.015	0.28	0.42	0.50	0.01	0.02	0.03	0.01	0.02	0.03	0.72	0.58	0.50	0.63	0.70	0.73

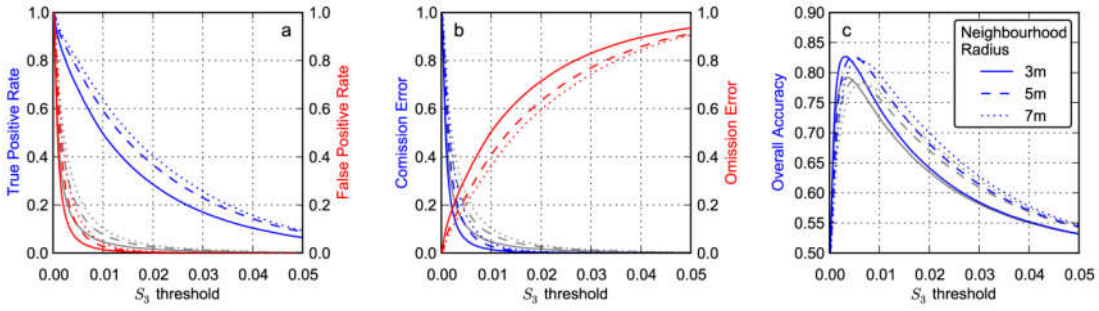

Figure 4.5 Validation statistics for Rayleigh Peak site as a function of the roughness threshold used to delimit rock exposure for three different neighbourhood window radii: (a) true positive and false positive rates; (b) commission and omission errors; (c) overall accuracy. These tests were conducted twice – the red and blue lines illustrate the results from tests in which the pixels classified as soil mantled pixels were filtered to avoid localities proximal to rock exposure (see text), therefore is more representative of the roughness signature of a pure soil mantled hillslope; the grey lines illustrate the same tests, but without this prior filtering step.

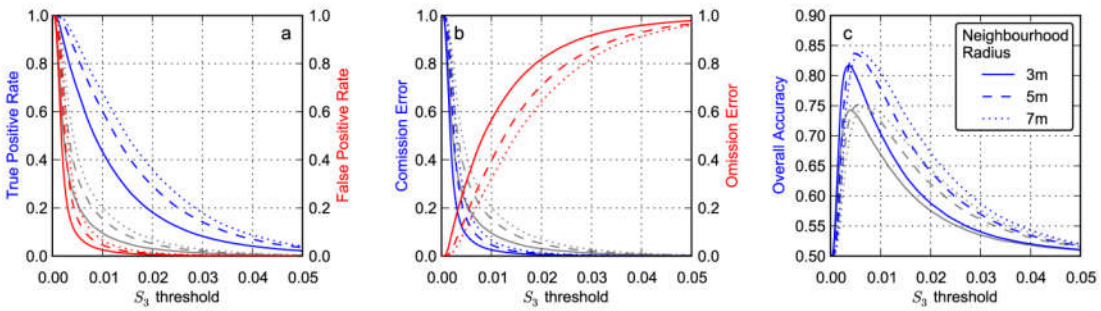

Figure 4.6 Validation statistics for Poway Creek site as a function of the roughness threshold used to delimit rock exposure for three different neighbourhood window radii: (a) true positive and false positive rates; (b) commission and omission errors; (c) overall accuracy. These tests were conducted twice – the red and blue lines illustrate the results from tests in which the soil mantled samples were filtered to avoid localities proximal to rock exposure, therefore is more representative of the roughness signature of a pure soil mantled hillslope; the grey lines illustrate the same tests, but without this prior filtering step.

4.3.4 Validation Results

In both landscapes, the close correspondence between the topographically derived roughness maps against the rock exposure mapped from the high resolution orthophotographs attests to a qualitatively good agreement between the two (Figures 4.3 and 4.4). Hillslopes that are covered by a continuous mantle of soil map consistently as areas that are topographically smooth, having locally consistent normal vector orientations; in contrast the emergence of bedrock drives a significant increase in the roughness of the affected hillslopes that is clearly picked up by my algorithm.

In the Rayleigh Peak example, both areas with widespread rock outcrop and more isolated exposures are picked out (Figure 4.3). The primary area of discordance lies in the SW corner of the image. Here the roughness algorithm predicts a much greater extent of rock exposure than the classified image. Inspection of the orthophotograph in this area reveals significant vegetation cover, obscuring areas where there is clearly bedrock, thus severely hampering the optical classification in this location. Areas of enhanced roughness running laterally along the trunk channel, which flows from west

to east here, provide another potential false positive in the roughness map; this highly localised roughness signature marks the banks of the incised channel. The validation statistics similarly show a distinct difference between soil-mantled hillslopes and areas with rock exposure (Figure 4.5; Table 4.2). The FPR rapidly decreases as the value of S_3 used to discriminate between the two characteristics increases, with a maximum accuracy (taking into account both false positives and false negatives) of >80% for ~0.003 ≤ $S_{3,\ threshold}$ ≤ ~0.005. The TPR also decreases across this interval, which is likely to be driven by areas of rock exposure where the rock surfaces have a low fracture density, therefore appear smooth, and the fact that my test dataset is not perfect (see discussion in section 4.3.2).

I stress here that the imperfections in the validation dataset derived from the orthophotographs will lead to a conservative estimate of the true accuracy of the roughness algorithm. Critically from the perspective of mapping out areas of rock exposure, the rate at which the TPR decreases with increasing values of $S_{3,\ threshold}$ is much lower than that of the FPR. Increasing the size of the neighbourhood window over which the surface roughness is characterised acts to increase the number of true positives for a given threshold, but there is a trade-off, as this improvement is accompanied by an increase in the number of false positives (Figures 4.5 and 4.6; Table 4.2). This is probably due to the "leakage" of the roughness signal from areas where there is rock exposure into the expanded neighbourhoods of proximal soil pixels (Figure 4.7), and also due to the fact that the longer wavelength topographic structure imposed by the ridge-valley architecture starts to influence the variability in the

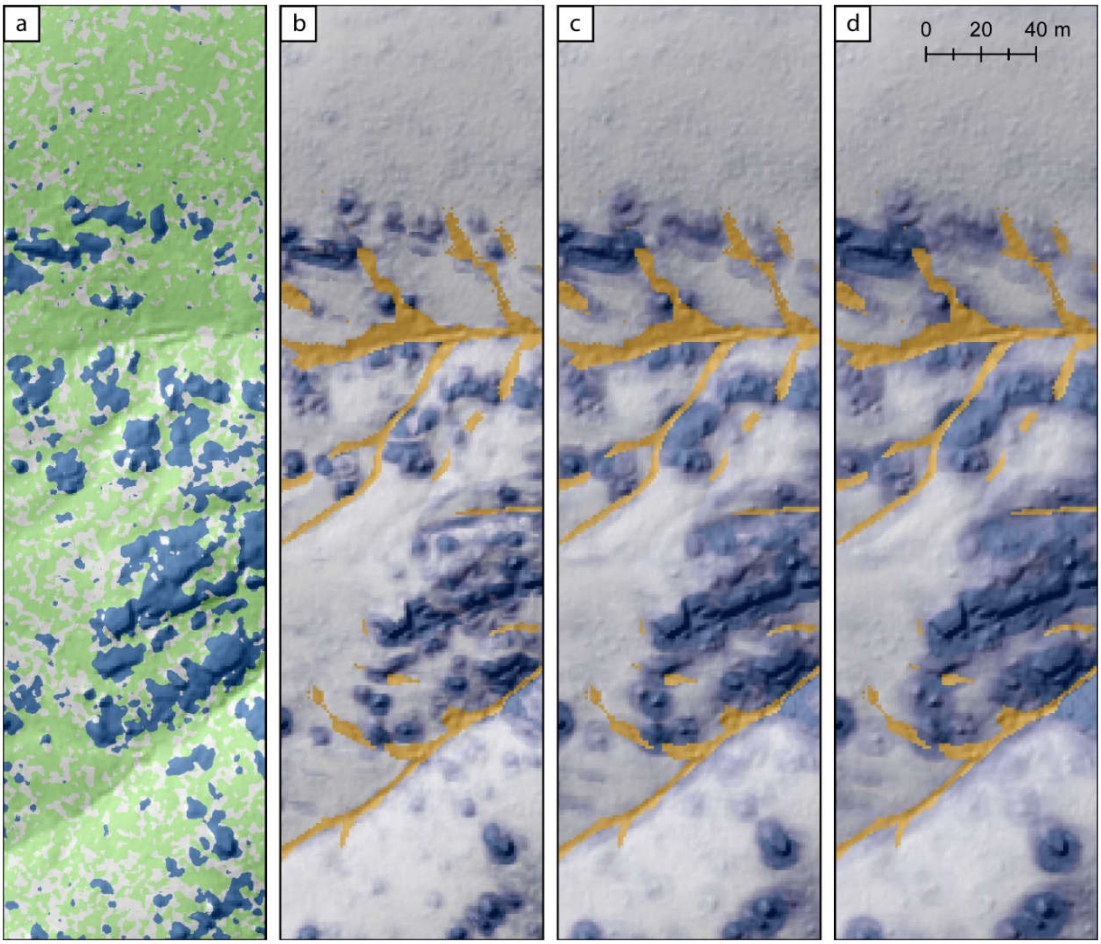

Figure 4.7 Illustration of the impact of the effect of changing neighbourhood window radius on the roughness signal that is measured: (a) results from combined classification procedure – rock = blue, soil mantled/vegetation = green; (b-d) maps of S3 using a neighbourhood window radius of (a) 3 m; (b) 5 m; and (c) 7 m. Orange pixels mark areas identified as being channelized. Note the increase in the leakage of the roughness signal into proximal areas as the neighbourhood radius is increased.

distribution of surface normal vectors; the latter case is particularly prevalent in areas that area located close to gullies and channels.

The pattern that emerges from the Poway Creek site is very similar; again, the maps of rock exposure do a qualitatively good job at locating hillslopes with rock outcrops, although the visual comparison is hindered by the spatially variable success of the classification scheme (Figure 4.4). Again, the network of channels and gullies provides additional sources of roughness in the landscape. The performance in the

quantitative tests exhibits very similar patterns to those obtained for the Rayleigh Peak site (Figure 4.6; Table 4.2).

4.3.5 Implications for use of topographic roughness in other settings

The fact that the roughness signatures of both validation landscapes display strikingly similar characteristics (Figures 4.5 and 4.6), suggests that surface roughness is a promising tool for mapping the extent of bedrock outcrop on hillslopes. As with existing methods [e.g. REI; *DiBiase et al.*, 2012], an important caveat is that full calibration is dependent on the *a posteriori* knowledge of threshold values, obtained, for example, through comparison against rock exposure mapped from high resolution photographs [*DiBiase et al.*, 2012; this study]. This is non-trivial in areas with significant vegetation cover due to the difficulty in resolving the ground surface; indeed, in areas with significant tree cover a significant portion of exposed rock is always hidden. Greater uncertainty will arise in areas where prior calibration against orthophotographs is not possible. A further element of caution is required, as my validation sites are limited to low-moderate relief, granitoid settings, but nevertheless, I expect that the methodology can be used judiciously in other landscapes. A number of important considerations are necessary in doing so, given that in many scenarios it will not be possible to use aerial imagery to independently judge the performance of the algorithm.

Firstly, it is evident from Figures 4.3-4.6 that a minor portion of landscapes mapped as rock exposure is topographically smooth. Variations in bedrock morphology present a challenge for the textural classification of topography. Errors may be introduced in areas where a significant proportion of the bedrock has been polished,

or where the bedrock is massive and exhibits sparse jointing. The latter case is illustrated by smooth, massive granitoid domes, where the distribution of fractures is dominated by surface parallel exfoliation joints [*Gilbert*, 1904; *Migoń*, 2006]. In such cases the textural characteristics of bedrock hillslopes may be indistinguishable from those with a continuous soil mantle. In the case of layered rocks, slopes parallel to the structural fabric may be smooth, whereas slopes that cross-cut the layering will appear rougher. This may drive variable accuracy in the results of textural classification metrics. However, large areas of smooth bedrock should be readily visible in satellite/aerial imagery because such conditions are unlikely to support significant vegetation cover [*Graham et al.*, 2010; *Hahm et al.*, 2014a]. Furthermore, where smooth surfaces form steep structures, a slope-based metric such as the REI [*DiBiase et al.*, 2012] can easily be employed alongside surface roughness to catch these false negatives. Combinations of topographic metrics in this way may potentially permit more robust feature extraction from high resolution data.

Secondly, bedrock exposure is not unique in adding roughness elements to landscapes, as surface roughness may potentially be generated by other processes. At length scales of 11 – 50 m, topographic roughness may be dominated by the signature of deep seated landslides, if present [*Booth et al.*, 2009], while other features associated with landslides may generate roughness at shorter wavelengths [*McKean and Roering*, 2004; *Tarolli et al.*, 2010]; Roughness at small length scales (typically <7.5 m) can also be generated via tree throw where this process is prevalent [*Roering et al.*, 2010; *Marshall and Roering*, 2014]. Moreover a degree of familiarity with target landscapes is likely essential in order to critically evaluate the results, although this criteria is not

unique to this method and should apply to all geomorphic feature extraction techniques, particularly at short wavelengths. Furthermore, in more complex landscapes with multiple roughness generation mechanisms, the spatial distribution of roughness generated by different processes may still allow useful quantitative information to be extracted (for example, instances of tree throw are likely to be quasi-random, or at least spatially discrete events, whereas exposure of bedrock in hillslopes is likely to generate connected "clusters" of roughness), although I do not extend my analysis in this manner here.

The size of the polynomial surface-fitting window should ideally be comparable to the feature being extracted. In landscapes where other roughening elements are present, or when the LiDAR data is noisy, a larger window can be employed, or the topography can be smoothed, with the limitation that as the degree of smoothing increases, the textural information that distinguished bedrock hillslopes from soil mantled hillslopes is progressively lost [*Albani et al.*, 2004; *Sofia et al.*, 2013]. Finally, the neighbourhood size used to quantify surface roughness will dictate the resolution at which you can discriminate between soil and rock outcrop (Figure 4.7).

For many applications, whether making an assessment of shallow landslide hazard, or testing hypotheses concerning the transition from soil mantled-bedrock topography, avoiding false positives is particularly important. For neighbourhood radii of 3-5 m, a threshold value of $S_3 = 0.01$ limits the occurrence of false positives to <5% (Figure 4.5), decreasing to <2% for $S_3 = 0.015$. Omission errors decrease substantially by increasing the radius of the neighbourhood window, but there is a trade-off against an increasing frequency of commission errors (Figures 4.5 and 4.6).

In Figure 4.8, I illustrate an alternative approach to mapping rock exposure using the surface roughness metric introduced above. Specifically I assess the fraction of pixels within a local neighbourhood that have a value of S_3 greater than a specified threshold value. Employing a sufficiently high threshold, I can thus express the expected rock exposure within that neighbourhood. This provides a conservative estimate of the degree of rock outcrop for a given portion of hillslope. In all cases, there is a positive correlation between the rock exposure mapped from the orthophotographs and the roughness of the topographic surface (Figure 4.8). However, when the S_3 threshold is set too low, the frequency of false positives leads to an overestimation of the rock exposure in a given portion of the landscape, as expected from my previous analysis (Figures 4.3-4.7). In the Rayleigh Peak site, there is a good agreement between the degree of rock exposure mapped by the two methods using a S_3 threshold of 0.010, if roughness is quantified with a neighbourhood radius of 3 m, and 0.015 if quantified with a neighbourhood radius of 5 m. Again this conforms to the expectations arising from the validation tests (Figure 4.5). In Poway Creek, there appears to be a systematic over-estimation of the rock exposure. The Poway Creek catchment presents a more challenging landscape to classify for three reasons: (i) Gullies are common, and many of the channels show evidence of recent incision; the channel banks in these incised localities generate false positives due to the sharp break in slope. There may be bedrock exposed in the terrace walls, but if present may be obscured by overhanging vegetation. (ii) Changing insolation conditions across the image made classification using the optical data more difficult (Figure 4.5). (iii) The original LiDAR point cloud was relatively sparse (Table 4.1), as a consequence of which discrimination of ground returns from those hitting low lying shrubs is more difficult.

As a general point I emphasise that although the high resolution orthophotographs provide the best means of objectively testing my algorithm, the resulting validation datasets are not perfect, and classification errors will result in under-estimation of the success of the roughness metric.

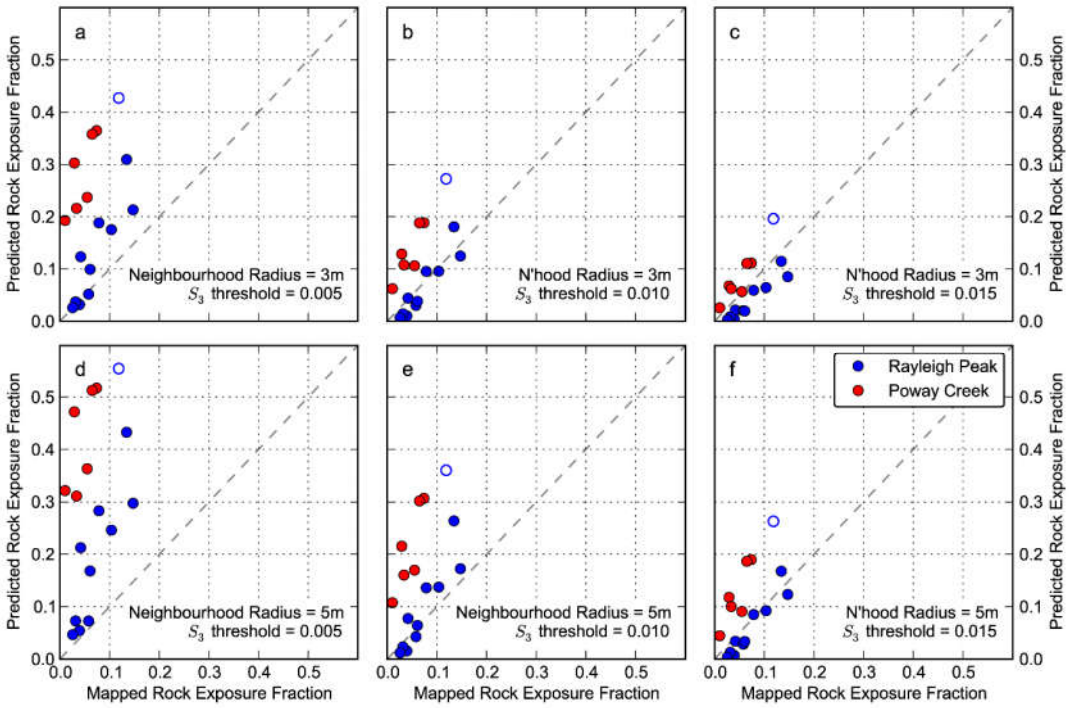

Figure 4.8 A comparison of the rock exposure classified from the orthophotographs against the expected fraction of rock exposure predicted using different thresholds of the surface roughness metric, S_3, for a series of the validation sites near Rayleigh Peak, Colorado, and Poway Creek, California. Each data point represents the rock exposure mapped within a 401 m x 401 m square region within a regularly spaced grid. (a-c) S_3 mapped using a neighbourhood radius of 3 m; (d-f) S_3 mapped using a neighbourhood radius of 5 m. The hollow symbol outlined in blue is from the SE corner of the Rayleigh Peak site, where the rock exposure mapped from the orthophotographs significantly under-predicts the true degree of rock exposure due to a combination vegetation cover and variable insolation conditions.

4.4 Application of the roughness algorithm to transient landscapes – investigating the soil-bedrock transition in Bald Rock Basin, California, and Harrington Creek, Idaho

4.4.1 Study sites

I investigate the variations in hillslope characteristics exhibited in two landscapes – Bald Rock Basin, in the Californian Sierra Nevada, and the Harrington Creek catchment, a tributary of the Salmon River, Idaho – which both exhibit strongly transient states of landscape evolution, under different climate regimes.

4.4.1.1 Bald Rock Basin, California

The Bald Rock Basin catchment drains into Middle Fork Feather River, in the north-western Sierra Nevada Mountains, California (Figure 4.1c). The regional climate in this locality is strongly seasonal, with maximum (minimum) temperatures range from 30(12)^{0}C in the summer to 9(-1)^{0}C in the winter, and mean annual precipitation typically ~1750 mm, a substantial majority of which falls between October and April, whereas the summer months are dry (http://www.prismclimate.org). Geologically, the catchment is underlain by the Bald Rock Pluton, a trondhjemite-tonalite intrusion of mid-late Mesozoic age [*Compton*, 1955; *Saucedo and Wagner*, 1992]. The landscape is close to fully vegetated by mixed conifer forest that is typical of the mid-elevation Sierra Nevada [*Barbour and Billings*, 2000]. The notable exception to this is Bald Rock Dome, which rises precipitously from the Feather River Canyon to form a broad, smooth, bare bedrock dome to the north of Bald Rock Basin. Although outside of the study catchment, it hints at the possibility of significant compositional

or structural heterogeneity within the pluton that is imposing a localised bottom-up restriction on forest growth in some parts of the landscape [*Hahm et al.*, 2014a].

Landscape transience in the Feather River region is driven by a wave of fluvial incision that is presently propagating up the channel network [*Hurst et al.*, 2012]. The resultant range of erosion rates spans an order of magnitude, placing fundamental controls on the nature of the hillslopes [*Hurst et al.*, 2012, 2013b], soils [*Yoo et al.*, 2011; *Attal et al.*, 2015; *Gabet et al.*, 2015] and biosphere [Chapter 3; *Milodowski et al.*, 2015a]. Rates of erosion in the inner canyon, driven by fluvial incision along the main-stem Feather River, reach ~250 mm ka^{-1} [*Riebe et al.*, 2000; *Hurst et al.*, 2012]. Bald Rock Basin has not fully adjusted to this elevated rate of fluvial incision, with a prominent topographic knickpoint marking the transition to lower relief topography that is eroding much more slowly at 30-40 mm ka^{-1} [*Riebe et al.*, 2000; *Hurst et al.*, 2012].

Moving across this gradient in erosion rates, hillslope form changes from being low-gradient and convex to steep and planar in the rejuvenated parts of the landscape below the knickpoint [*Hurst et al.*, 2012], consistent with the expectations of models of non-linear, diffusion-like sediment transport [*Roering et al.*, 1999]. Within Bald Rock Basin itself, Yoo et al. [2011] investigated changes in substrate characteristics between a series of transects across this transition, indicating that the increase in erosion rate drives a reduction in the residence time of material within the weathering zone, highlighted by a decrease in the extent of weathering of both the soil and saprolite. Consistent with these observations, a more detailed inventory of soil grain size distributions from soil pits throughout Bald Rock Basin indicate a marked increase in the coarser grain fraction in more rapidly eroding parts of the basin [*Attal et al.*, 2015].

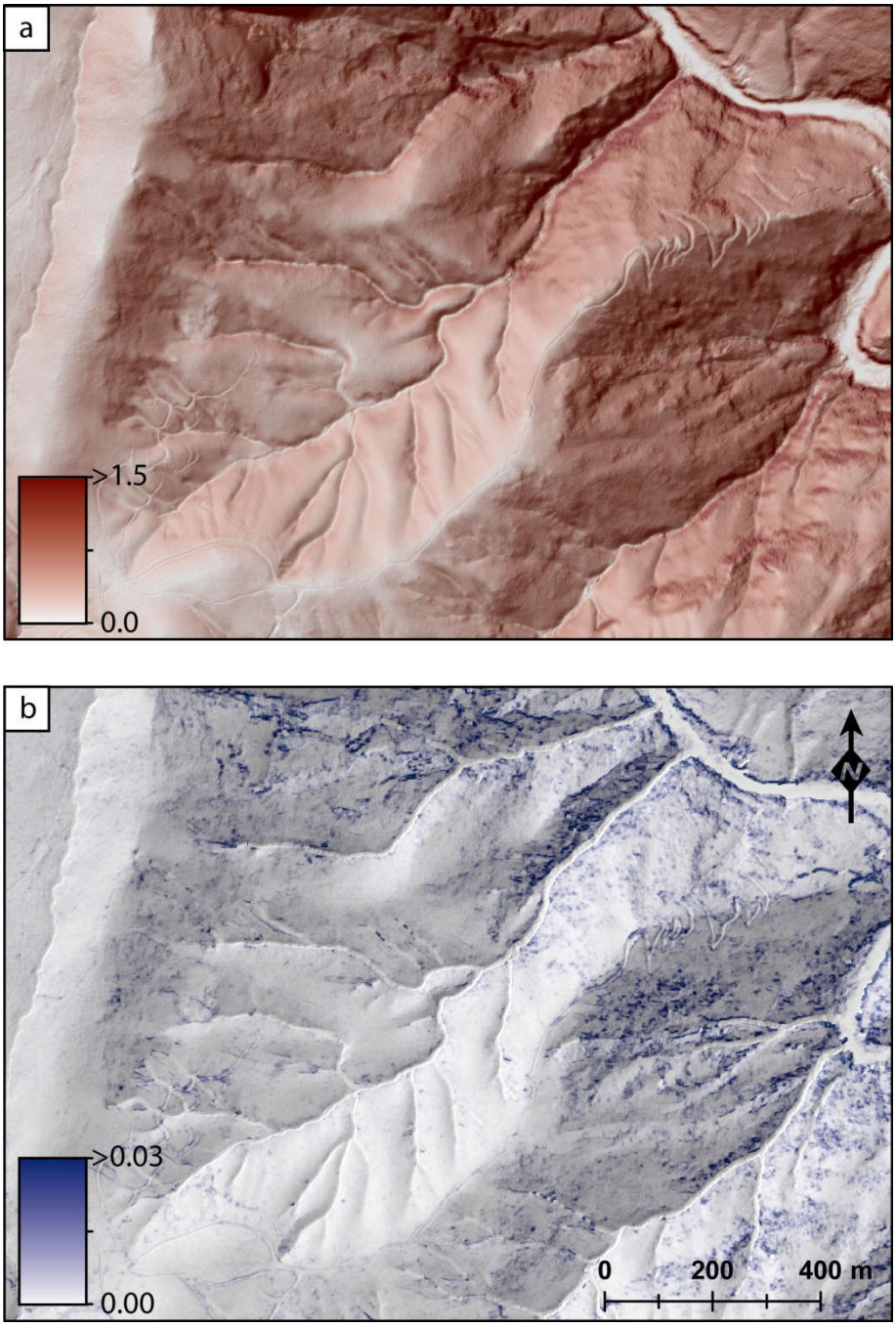

Figure 4.9 Maps displaying (a) topographic slope, and (b) S_3 for Bald Rock Basin, Californian Sierra Nevada. The Middle Fork Feather River is located in the NE corner of each map, flowing from NW to SE.

I use the surface roughness algorithm introduced above, to expand on this earlier work and further characterise changes in the bedrock exposure across the geomorphic transition.

4.4.1.2 Harrington Creek, Idaho

The Harrington Creek catchment drains into Main Salmon River, around 40km SSW of the Bitterroot Mountains, Idaho (Figure 4.1d). The regional climate is continental, with maximum (minimum) temperatures range from 26.2(6.2)^{0}C in the summer to 0.0(-10.8)^{0}C in the winter, whereas precipitation is more evenly distributed throughout the year, with mean annual precipitation typically ~630mm (http://www.prismclimate.org). Vegetation in the catchment comprises coniferous forest with variable canopy cover [*Barbour and Billings*, 2000]. The catchment is underlain by plutonic rocks related to the Idaho Batholith, with small inclusions of Eocene dykes of rhyolitic-dacitic composition [*Lewis and Stanford*, 2002]. Analysis of fission tracks in apatite and zircon grains from the Idaho Batholith suggest that exhumation rates have varied from 0.03-0.1 mm yr^{-1} between 50-10 Ma to 0.32±0.10 mm yr^{-1} from 10 Ma-present, associated with canyon-forming fluvial incision along the Salmon River [*Sweetkind and Blackwell*, 1989; *Ferrier et al.*, 2012]. Point measurements of regolith production rates, based on cosmogenic ^{10}Be concentrations, suggest erosion rates integrated over 10^3 – 10^4 years of up to 0.12 mm yr^{-1} [*Ferrier et al.*, 2012]. Associated with this fluvial incision are a series of knickpoints that are propagating up the tributaries of the Salmon River, including Harrington Creek, and mark the transition from a slowly eroding, relict landscape to steep, rapidly eroding, rejuvenated topography that is actively adjusting to the elevated incision rates below the fluvial knickpoint [*Wood*, 2013]. The Harrington Creek region has been subject to significantly less research relative to Bald Rock Basin; I use the same methods for this site to investigate changes in the geomorphic characteristics of the hillslopes across this transition.

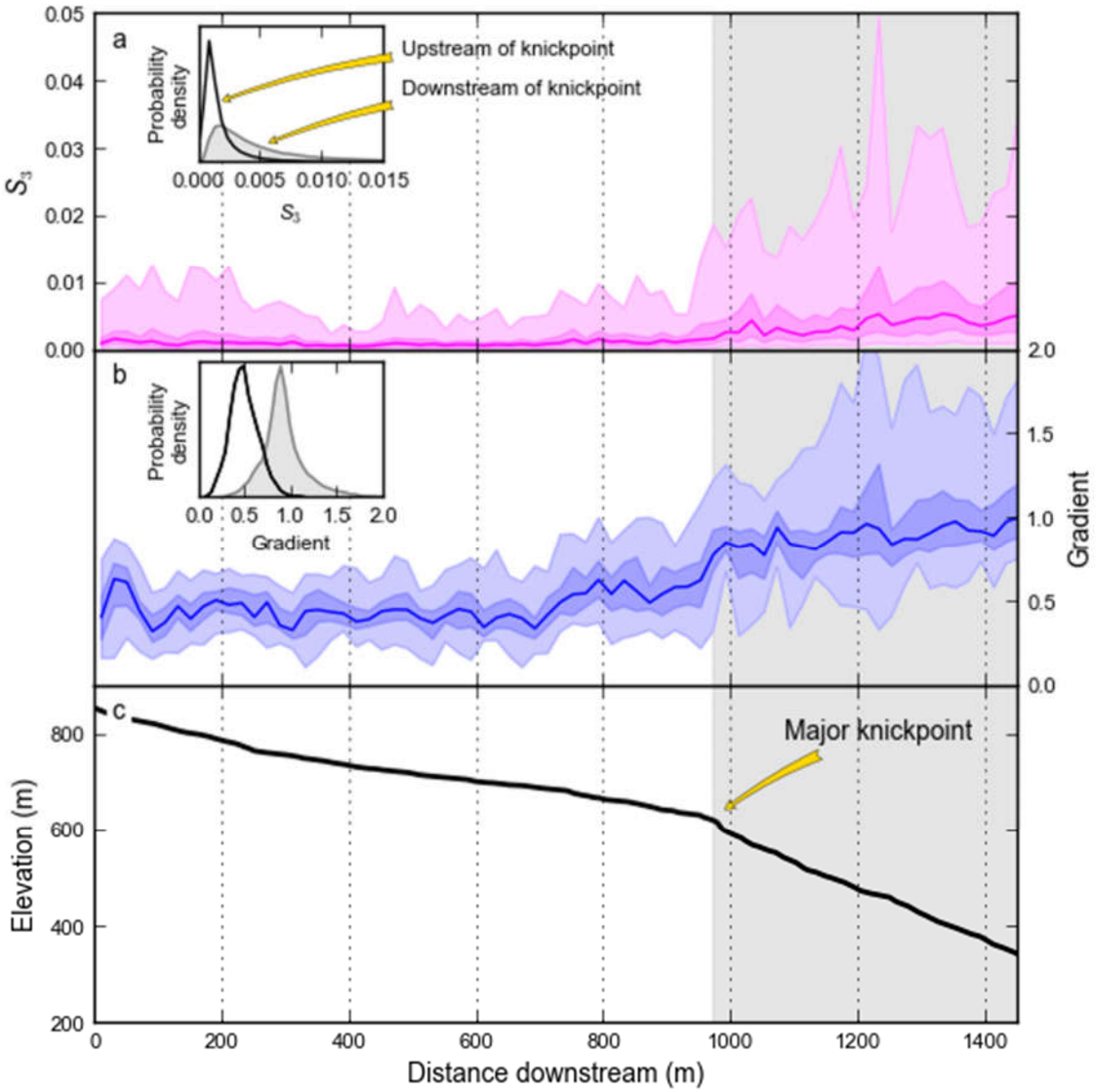

Figure 4.10 Changes in topographic characteristics along a longitudinal swath centred on the trunk channel draining Bald Rock Basin: (a) surface roughness, S_3; (b) topographic gradient; (c) the longitudinal channel profile. The principal knickpoint has been highlighted, with the inset histograms summarising the distributions of the topographic metrics above and below. Upstream of the major knickpoint, smaller deviations from the typical graded profile indicate a series of smaller knickpoints. The swath has a half width of 250 m, and has been binned into 50 m intervals. In plates (a) and (b), the median has been plotted with the shaded intervals bounded by the 25th-75th quantiles and 2.5th-97.5th quantiles. S_3 was calculated using a 3 m radius neighbourhood window.

4.4.2 Topographic analysis

Changing bedrock exposure across the knickzones was mapped utilising the surface roughness method as described in Section 4.2, using a circular neighbourhood with a radius of 3 m, which was shown to perform well, with limited false positives, in my previous validation (Section 4.3). Topographic gradient was also measured using the slope of the best fitting six term polynomial surface, defined by a least squares regression to a circular neighbourhood with 7 m radius [*Hurst et al.*, 2012]. In order to map changes in hillslope characteristics along the length of the trunk channel, I use longitudinal swath profiles, following a similar approach to the implementation of the generalised swath profile algorithm described by Hergarten et al. [2014], to map each point on the hillslope to the nearest location in the channel network. This method allows frequently used swath profile analysis to be undertaken using curvilinear features, such as river channels, as the baseline rather than requiring linear features. The trunk channels themselves were defined using the DrEICH algorithm [*Clubb et al.*, 2014], which searches for the upstream limit of the topographic signature of fluvial incision to define the fluvial network within the channelized domain. To first order, the longitudinal swath profiles should link hillslopes to the section of channel that sets their lower boundary condition, enabling us to link geomorphic changes in fluvial incision.

4.4.3 Results

In both Bald Rock Basin (Figures 4.9 & 4.10) and Harrington Creek (Figures 4.11 & 4.12), there are clearly distinct, contrasting topographic domains separated by major knickpoints. Moving across this transition, hillslope morphology changes from low

gradient, convex hillslopes (modal gradients above principal knickpoints are ~0.5 and ~0.4 within the headwaters of Bald Rock Basin and Harrington Creek respectively), to steep, planar hillslopes downstream of the knickpoints: respective modal gradients are ~0.9 and ~0.8. However, in addition to the changes in the hillslope profile across this transition there are concomitant textural changes to the hillslopes pertaining to the widespread emergence of bedrock. In both landscapes, the low gradient headwaters are also characterised by smooth topography indicative of a continuous soil mantle: within Bald Rock Basin, 1.5% of hillslope pixels have $S_3 > 0.010$; <1% have $S_3 > 0.015$; within Harrington Creek, 3% have $S_3 > 0.010$; 1.5% have $S_3 > 0.015$. In contrast, in the rejuvenated parts of the landscape, the increased dominance of bedrock is indicated by elevated topographic roughness: in the lower reaches of Bald Rock Basin 15% of hillslope pixels have $S_3 > 0.010$; 7% have $S_3 > 0.015$, while in the equivalent parts of the Harrington Creek drainage, 29% have $S_3 > 0.010$; 19% have $S_3 > 0.015$.

Critically, the emergence of bedrock is not uniform across the steeper parts of the landscape. Rather, the steep hillslopes present a rugged patchwork of bedrock outcrops and discontinuous soil cover. Likewise, across the upper part of Bald Rock Basin, there are a number of isolated patches of elevated roughness that can be picked out from the prevailing smooth terrain (Figure 4.9). Field inspection of these selected "rough spots" indicated that they corresponded to isolated rock outcrops, whereas instances of tree throw mounds, which could also generate roughness at short wavelengths, were comparatively rare.

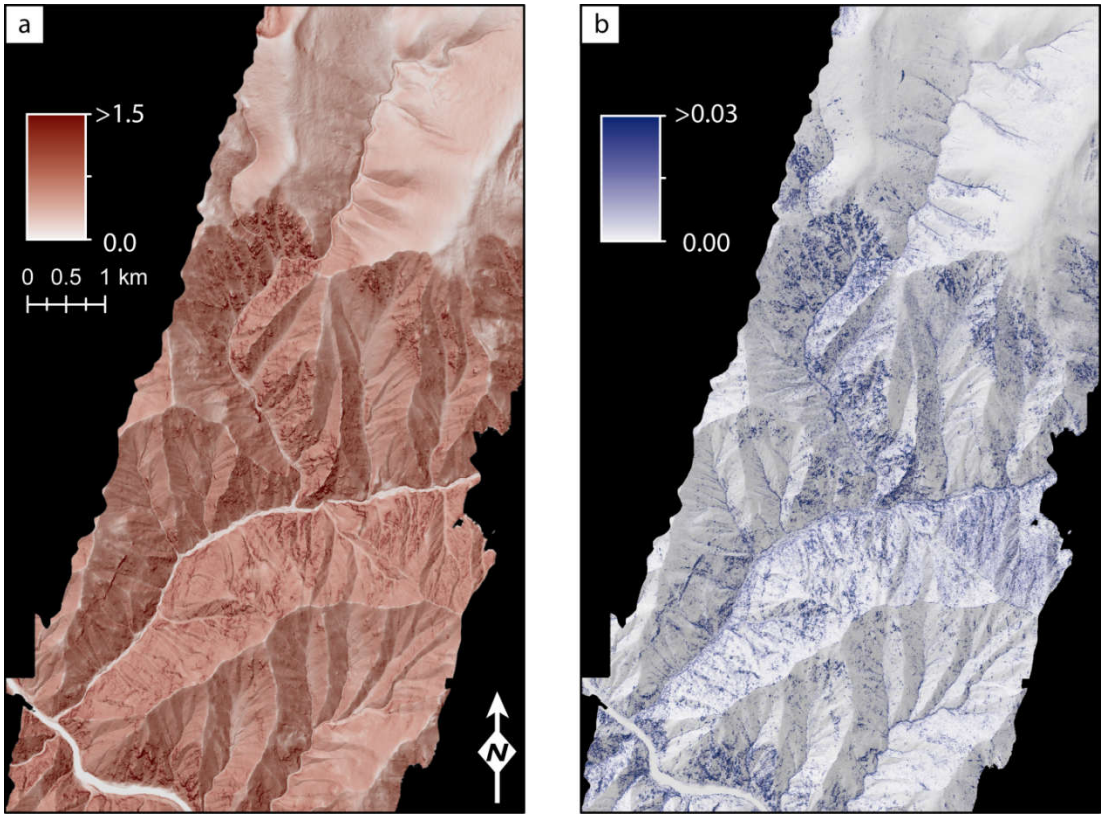

Figure 4.11 Maps displaying (a) topographic slope, and (b) S3, for a sub-catchment of Harrington Creek, Idaho. S_3 was calculated using a 3 m radius neighbourhood window.

4.4.4 Discussion

In both Bald Rock Basin and Harrington Creek, topographic knickpoints mark the domain transitions between a slowly eroding "relict" landscape, and rejuvenated topography responding to elevated rates of fluvial incision [*Hurst et al.*, 2012, 2013a; *Wood*, 2013]. Both landscapes exhibit similar hillslope responses to this geomorphic forcing. In this contribution I have deployed my new roughness algorithm to quantify the dynamics of the soil to bedrock transition. Specifically, in both landscapes the transition from soil-mantled to bedrock hillslopes is gradual and patchy. Furthermore, the steep hillslopes do not appear to be completely stripped of soil; the persistence of topographically smooth areas that manage to sustain a forest canopy [Chapter 3; *Milodowski et al.*, 2015a] indicates that patchy soil cover persists at high erosion rates.

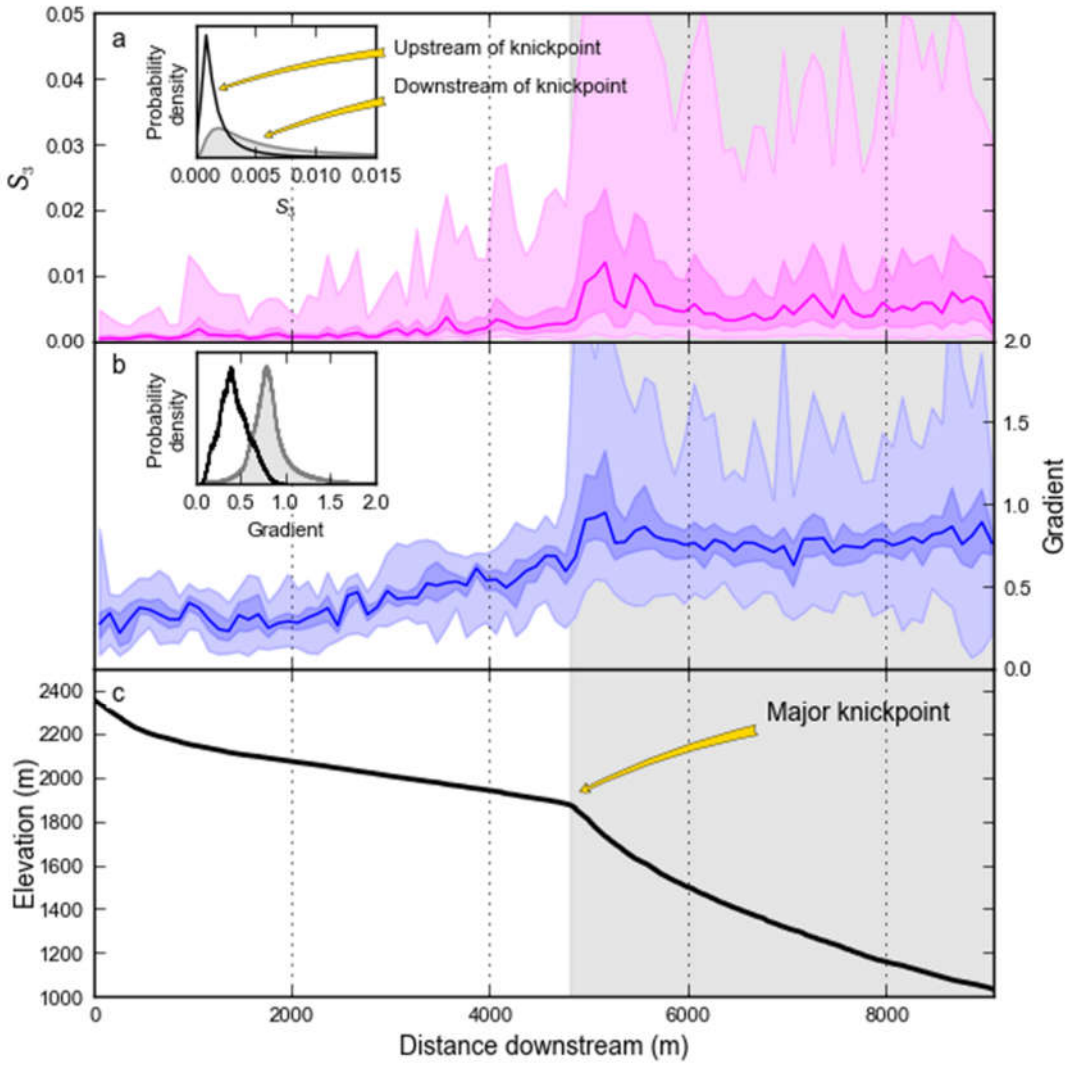

Figure 4.12 Changes in topographic characteristics along a longitudinal swath centred on the trunk channel draining the principal tributary to Harrington Creek: (a) surface roughness, S_3; (b) topographic gradient; (c) the longitudinal channel profile. The principal knickpoint has been highlighted, with the inset histograms summarising the distributions of the topographic metrics above and below. Upstream of the major knickpoint, smaller deviations from the typical graded profile indicate a series of smaller knickpoints. The swath has a half width of 350 m, and has been binned into 50 m intervals. In plates (a) and (b), the median has been plotted along with the shaded intervals bounded by the 25th-75th quantiles and 2.5th-97.5th quantiles.

In the Feather River Region, aboveground biomass hosted by the hillslopes has been shown to decrease with increasing erosion rates [Chapter 3; *Milodowski et al.*, 2015a], but biogenic soil production is still able to keep pace with elevated rates of erosion to maintain a partial soil mantle. This is in agreement with observations from soil depth

transects within the basin that show little difference in soil depths measured above the knickpoint, ranging from 40-80 cm, to those measured below the knickpoint, which ranged from 30-60 cm [*Yoo et al.*, 2011].

The nature of the soil-bedrock transition observed at these two sites aligns closely with the observations from the San Gabriel Mountains in California [*DiBiase et al.*, 2012]. A gradual, patchy transition is significant because it is at odds with the expectations from widely used models of soil production, in which the rate of production decays exponentially with depth from a maximum production rate for a bare bedrock surface [e.g. *Heimsath et al.*, 1997], which in this framework represents a threshold erosion rate defining a sharp transition from soil-mantled to bedrock topography. The patchy transition observed may be driven in part by structural or compositional controls on the rate at which bedrock breaks down to form mobile regolith, but can also be rationalised by models of soil production that consider the processes driving soil production and sediment transport as occurring in discrete events [*Strudley et al.*, 2006a, 2006b; *Gabet and Mudd*, 2010]. Understanding whether these patches are stationary in time or dynamic is important in understanding the longer term evolution of steep landscapes and how this evolution is shaped by the coupling of geomorphic and ecological processes. Finally, while clearly important from a hillslope perspective, there are broader implications for landscape evolution: the dynamics of sediment transport in bedrock landscapes are very different to those in soil mantled landscapes [e.g. *Dietrich et al.*, 2003; *Binnie et al.*, 2007], impacting on the calibre [*Whittaker et al.*, 2010; *Attal et al.*, 2015] and temporal variability [*Hicks et al.*, 2000; *Hovius et al.*, 2000] of sediment supplied to the channel network; therefore the nature of the soil-

bedrock transition impacts on the nature of hillslope-channel coupling, modulating the fluvial response to changes in base level.

4.5 Overall Discussion and Conclusions

The structure of topographic relief is controlled by different processes operating at different spatial scales [*Perron et al.*, 2008b]: at wavelengths greater than ~100 m, topography is dominated by the spacing of ridges and valleys [*Perron et al.*, 2008b, 2009]; at the sub-hillslope length-scale, other processes generate detectable topographic signatures [e.g. *McKean and Roering*, 2004; *Roering et al.*, 2010]. Booth et al. [2009] exploited spectral analysis to show that areas affected by deep-seated landslides exhibit significantly greater power at intermediate wavelengths (~11-50 m), enabling the objective classification of regions in which deep-seated landslides were prevalent. At shorter length-scales, Roering et al. [2010] suggested that roughness generated at small length-scales (<7.5 m) in the Oregon Coast Ranges could be attributed to the presence of tree throw mounds; similar analysis of topographic profiles extracted from contrasting catchments in the same setting found a lack of spectral power at these short wavelengths for resistant bedrock hillslopes in comparison to soil-mantled hillslopes, attributed to a diminished biotic contribution to weathering [*Marshall and Roering*, 2014].

I propose that short wavelength surface roughness, quantified using the same roughness algorithms introduced by McKean and Roering [2004], can be used to make inferences about hillslope characteristics specifically pertaining to the exposure of bedrock. Comparison against rock exposure measured independently and objectively from high-resolution orthophotographs from multiple landscapes suggests that the

emergence of bedrock in hillslopes produces a detectable topographic signature that distinguishes it from hillslopes that have a continuous soil mantle. I applied this technique to forested landscapes in California and Idaho, highlighting the ability of LiDAR surveys to resolve high resolution features of the topography through canopy. Thus I propose surface roughness as a new method for mapping rock exposure from LiDAR data that complements previously published metrics [*DiBiase et al.*, 2012], and is likely to be of particular benefit in landscapes in which rock outcrops are present at topographic gradients lower than the angle of repose.

I caveat this finding with the statement that rock exposure is not the only mechanism of generating topographic roughness at short length-scales; for example, gullying and slumping provide two mechanisms by which the smooth parabolic morphology associated with ideal, diffusive soil mantled hillslopes may be modified [*Tarolli and Dalla Fontana*, 2009]; likewise small-scale features associated with deep-seated landslides, such as folds and scarps, generate a roughness signal at similar length-scales to rock outcrop [*McKean and Roering*, 2004; *Tarolli et al.*, 2010]. In addition, while many soil mantled sediment transport processes act to diffuse topography, they typically do so through discrete events (e.g. tree throw) [*Furbish et al.*, 2009; *Gabet and Mudd*, 2010]. While the fingerprint that these individual events leave on the landscape is transient, they provide a potentially important roughness signature at the relevant length-scale for that mode of disturbance [*Roering et al.*, 2010]. An additional factor to consider is that bedrock morphology is itself variable, and therefore certain mechanisms of generating rock exposure may not generate significant roughness; this would be exemplified by, for example, low gradient, glacially polished surfaces, or by

massive granitoid bedrock with very low fracture density in which jointing is restricted to approximately surface parallel exfoliation planes. Consequently, interpretation of surface roughness metrics should critically take into account the presence of other geomorphic processes that are potentially operating within the landscape and the characteristics of the bedrock itself. Indeed, this principal applies to the interpretation of any topographic metric obtained from remotely sensed data; in complex geomorphic settings, isolation of specific hillslope characteristics from a single textural attributes may be impossible at the data resolution presently available from airborne surveys; ultimately a combination of metrics, covering a broader range of morphological characteristics may well be necessary.

The characterisation of hillslopes is of importance across a diverse range of surface processes research, providing a better understanding of controls on hydrological flow routing, sediment production and transport processes and ecosystem development. The utility of topographic data to aid this endeavour is strongly dependent on the resolution of these datasets. In the case of hillslope characteristics, such as rock exposure, roughness is expressed at the metre scale; using 1m-resolution DEMs, it is possible to examine variations in hillslope form at sufficient levels of detail that it is possible to distinguish between soil and bedrock hillslopes; this information is rapidly lost as the data resolution is coarsened [*DiBiase et al.*, 2012]. However these shorter length scales are particularly susceptible to noise in the dataset [*Albani et al.*, 2004; *Sofia et al.*, 2013]. This highlights the requirement for high quality, high resolution surveys, which permit accurate classification of vegetation and ground returns prior to surface creation. LiDAR surveys with higher shot spacing are therefore likely to

provide a disproportionately greater level of detail on hillslope characteristics [*Brodu and Lague*, 2012], and this should be taken into account when planning airborne surveys. In particular, the continued development of unmanned aerial vehicles (UAVs) as a platform for airborne LiDAR collection will increasingly make higher resolution surveys accessible to the research community [e.g. *Lin et al.*, 2011].

Finally, my analysis of the geomorphic changes driven by changing rates of erosion in two different landscapes reveals a number of significant conclusions regarding the nature of the soil-bedrock transition. In both cases, the transition from soil mantled hillslopes to bedrock dominated hillslopes is clearly gradual, with areas of patchy soil coverage persistent on steep, rapidly eroding hillslopes. A "patchy" transition from soil-mantled to bedrock hillslopes challenges prevailing modelling approaches towards soil production, but is in agreement with conclusions from previous studies of soil production in rapidly eroding landscapes – the European Alps [*Norton et al.*, 2008], San Gabriel Mountains, California [*Heimsath et al.*, 2012] and Southern Alps, New Zealand [*Larsen et al.*, 2014a] – each of which observe the coexistence of soil and bedrock on rapidly eroding hillslopes., This has been attributed in part to efficient biogenic soil production [*Larsen et al.*, 2014a], which facilitates the rapid generation and stabilisation of soil between landslide events, and lithological susceptibility to weathering processes [*Norton et al.*, 2008]. The hypothesis of a biogenically mediated soil-bedrock transition is supported by the observation in these landscapes that patchy vegetation cover persists on the steeper hillslopes where trees have maintained a foothold, and is in agreement with expectations from numerical modelling of soil production by discrete events [*Gabet and Mudd*, 2010]. Capturing the salient aspects

of these models within larger-scale landscape evolution models represents a key challenge in simulating the evolution of mixed-bedrock landscapes that are typical of many upland settings.

Chapter 5. Lithology, vegetation and sources of complexity in the coupled geomorphic and ecological response of hillslopes to incision

In preparation for submission to Journal of Geophysical Research: Earth Surface: D.T. Milodowski, S.M. Mudd, and E.T.A. Mitchard (in prep.)

Abstract

I investigate how the coupling of ecology and geomorphology influences the response of hillslopes to fluvial incision rates in the Feather River region of the Californian Sierra Nevada. Specifically, I address the soil-bedrock transition, and the role that lithology and vegetation play in mediating this transition, using high resolution, LiDAR-derived topographic and forest structural data. I demonstrate that increasing rates of erosion, which range from 20 – 250 mm kyr^{-1}, drive a reduction in aboveground biomass and concomitant increase in rock exposure on hillslopes. The transition from soil mantled to bedrock hillslopes is gradual and patchy, with a high degree of spatial variability driven by both inter- and intra-lithological heterogeneity. Coupling the co-dependence of soil production processes and vegetation into a simplified numerical model, I illustrate that feedbacks between soil thickness and biotic soil production are capable of generating a complex response to geomorphic forcing, such that hillslopes possess multiple stable states: for intermediate rates of erosion, equilibrium hillslopes may be either soil mantled or bedrock. The evolution of hillslopes in response to changing base level is therefore path-dependent; in response to cyclic forcing, the evolution trajectory of hillslope soils may display

pronounced hysteresis. This behaviour is particularly marked when hillslopes are forced across the soil-bedrock transition: the recovery hillslopes stripped of soil is inhibited by a lack of biotic soil production, leading to the persistence of bedrock hillslopes once significant exposure has been generated.

5.1 Introduction

The emergent picture of the Critical Zone [*National Research Council*, 2001] – the domain spanning from the lowermost depths of the weathering front to the uppermost extent of the canopy – portrays a complex series of interconnected geomorphic, hydrological and bio-geochemical process that link the atmosphere, biosphere and geosphere [*Amundson et al.*, 2007; *Chorover et al.*, 2011]. Deciphering the functional relationships between topography, climate, vegetation, soils and erosion remains a critical challenge for developing a quantitative understanding of the behaviour of this system, and is required to make predictions of how landscapes will respond to environmental change. Important insights into these linkages can be gained through exploring the geomorphic and ecological significance of gradients in environmental conditions such as climate [*Pelletier et al.*, 2013] and lithology [*Hahm et al.*, 2014b; *Marshall and Roering*, 2014].

In addition to climate and lithology, another fundamental control on the characteristics of the Critical Zone is the rate of erosion. Typically, erosion in upland landscapes is governed by the coupling of hillslopes and channels [*Gilbert*, 1877; *Arrowsmith et al.*, 1996]. Hillslopes are coupled to the channel network as their local base level is set directly by their proximal channel. Consequently, the history of fluvial incision imposes a major control on the dynamics of erosion and sediment transport on hillslopes [*Mudd and Furbish*, 2007b; *Hurst et al.*, 2013a; *Bilderback et al.*, 2015]. As incision rates increase, hillslopes steepen and become increasingly planar, raising the sediment flux so that it re-equilibrates with the elevated rate of base-level fall at their lower boundary [e.g. *Roering et al.*, 1999]. In very steep landscapes, in which hillslope

gradients approach the limit of stability, landslides become the increasingly dominant mode of sediment transfer [*Hovius et al.*, 1997; *Larsen and Montgomery*, 2012].

The erosion of overlying hillslope material drives the advection of pristine, un-weathered bedrock towards the surface, exposing it to physical and chemical weathering processes [*West et al.*, 2005; *Ferrier and Kirchner*, 2008; *Gabet and Mudd*, 2009; *Rempe and Dietrich*, 2014]. The weathering of bedrock produces saprolite and ultimately soil; in so doing, this creates a hospitable, porous substrate from which plants can extract moisture and nutrients [*Vitousek et al.*, 2003; *Porder et al.*, 2007; *Graham et al.*, 2010]. Conversely, vegetation is itself an active geomorphological agent: plants play a direct role in both the physical and chemical break down of soil [*Bonneville et al.*, 2009; *Gabet and Mudd*, 2010; *Roering et al.*, 2010], and in the subsequent transport of this soil across hillslopes [*Gabet et al.*, 2003]. The presence of this thin veneer of life that mantles much of the terrestrial surface of our planet therefore has a profound impact on the characteristics and evolution of landscapes [*Dietrich and Perron*, 2006; *Amundson et al.*, 2015] and possesses a potentially important role in modulating the response of hillslopes to changes in climate, land cover or base level [e.g. *Roering et al.*, 2002; *Hughes et al.*, 2009; *Dosseto et al.*, 2010].

Soil characteristics are also strongly coupled to erosion rates: as erosion rates increase, the residence time of material within the critical zone decreases [*Mudd and Yoo*, 2010a]. Consequently soils that develop on more rapidly eroding hillslopes are likely to be thinner and less well developed [*Heimsath et al.*, 1997, 2012; *Attal et al.*, 2015; *Gabet et al.*, 2015], thus providing a mechanism through which changes in erosion rate propagate to impact on the characteristics of ecosystems [Chapter 3; *Milodowski et al.*,

2015a]. Where rates of erosion outstrip rates of soil production, we observe a transition from a continuous soil-mantle to bedrock hillslopes [*DiBiase et al.*, 2012; *Heimsath et al.*, 2012; *Milodowski et al.*, 2015b] and hillslope sediment fluxes becomes detachment limited [*Dietrich et al.*, 2003; *Binnie et al.*, 2007]. In steep, detachment-limited landscapes, the dynamics of the soil-bedrock are complicated by the episodic landslides, which dominate hillslope sediment fluxes [*Hovius et al.*, 1997; *Larsen and Montgomery*, 2012]. Soil production in these settings is complicated by the stochastic stripping bedrock and any overlying soil cover from hillslopes, and subsequent recovery of soil and vegetation on exposed bedrock [*Guariguata*, 1990; *Heimsath et al.*, 2012; *Larsen et al.*, 2014a; *Stark and Passalacqua*, 2014].

Soil production rates are themselves intimately connected to a number of substrate properties. Weathering rates vary with bedrock texture and mineralogy [e.g. *Goldich*, 1938; *Pye*, 1986; *Heckman and Rasmussen*, 2011; *Bazilevskaya et al.*, 2013] and water availability [e.g. *Gabet et al.*, 2006; *Maher*, 2010; *Maher and Chamberlain*, 2014]. Fractures provide conduits along which water can penetrate deeper into underlying bedrock [*Anderson et al.*, 2002; *Goodfellow et al.*, 2014b] and weaknesses that can be exploited by root networks, facilitating the physical break down of bedrock [e.g. *Zwieniecki and Newton*, 1995; *Gabet and Mudd*, 2010; *Larsen et al.*, 2014a]. In turn, the fracture distribution within the substrate varies according to both topographic position and stress history [*Molnar et al.*, 2007; *Clarke and Burbank*, 2010; *Clair et al.*, 2015]. Variations in substrate properties between geological units – here termed intra-lithological heterogeneity – therefore has the potential to modify the dynamics of soil production and sediment transport on hillslopes. Dosseto et al. [2012] found

significant differences in the rates of regolith formation between neighbouring ridgelines underlain by volcanic and granitic bedrock. However, even within comparatively similar bedrock types there may be large differences in the dynamics of soil production. In the granitoid landscape of the Sierra Nevada, Hahm et al. [2014b] found that sharp ecotones, marking a transition from fully forested hillslopes to low relief bedrock surfaces, corresponded with pluton boundaries across which there were sharp drops in phosphorous availability. Conversely, in the Oregon Coast Ranges, diagenetic variations in sedimentary sequences control local relief structure and bedrock outcrop patterns [*Marshall and Roering*, 2014]. Likewise textural differences within plutonic rocks can also influence their weathering behaviour and hence the distribution of rock outcrop in a landscape [*Goodfellow et al.*, 2014a; *Migoń and Vieira*, 2014]. In addition to inter-lithological differences, variability in grain size, fracture density, diagenesis and composition, may all be exhibited within a given lithological unit – here termed intra-lithological heterogeneity – which again may modify the efficacy of soil production and sediment transport processes, in addition to the hospitability of the substrate towards supporting vegetation.

Thus, there are manifold pathways through which lithology may influence the soil-bedrock transition. Landscapes in which rates of erosion vary through space provide opportunities to examine in detail their control on characteristics of Critical Zone architecture. The Feather River catchment, located in the Northern Sierra Nevada of California, represents one excellent candidate in this regard. Erosion rates in this region have been shown to vary over an order of magnitude from 20 to >250 mm ka^{-1} [e.g. *Riebe et al.*, 2000; *Hurst et al.*, 2012]. The hallmarks of this geomorphic

disequilibrium are clearly imprinted on the topography, which exhibits a striking geomorphic gradient that juxtaposes steep, rugged canyons against lower relief valleys that possess smooth, convex, soil-mantled hillslopes [*Hurst et al.*, 2012; *Milodowski et al.*, 2015b]. Using high resolution (1 m) airborne Light Detection And Ranging (LiDAR) data, Hurst et al. [2012] indicated that the geomorphic signature of this landscape transience was consistent with being driven by an upstream migration of a wave of elevated fluvial incision through the Feather River and its tributaries, driving the steepening of hillslopes and concentration of curvature at the ridge-crest.

Moving across this geomorphic gradient, increasing rates of hillslope erosion have been shown to drive a reduction in the extent of weathering, with a marked drop in clay content of the soil and concurrent increase in the coarse grain fraction [*Yoo et al.*, 2011; *Attal et al.*, 2015], decreased soil thickness [*Gabet et al.*, 2015], and a reduction in the extent of saprolite development [*Yoo et al.*, 2011], all consistent with expectations for a reduction in the residence time of material moving through the critical zone [*Mudd and Yoo*, 2010a; *Dixon et al.*, 2012]. Correspondingly, increasing surface roughness at high erosion rates indicates the gradual, patchy emergence of bedrock [Chapter 4; *Milodowski et al.*, 2015b]. The first order impact of these geomorphological changes on the mixed conifer forest ecosystem was explored in Chapter 3 [*Milodowski et al.*, 2015a], in which I demonstrated that aboveground biomass decreases as erosion rates increase.

My approach in this chapter builds on this previous work, taking a more holistic perspective that encompasses both changes in the physical characteristics of hillslopes – hillslope morphology, bedrock exposure and lithology – and changes in the

ecological characteristics of the forest that mantles them. Specifically I address the following research questions:

i. As erosion rates increase, how does lithology impact the transition from soil mantled to bedrock hillslopes?
ii. In this hillslope response, what degree of heterogeneity is exhibited both between hillslopes underlain different lithologies (inter-lithological heterogeneity) and within a single lithological unit (intra-lithological heterogeneity)?
iii. How do the coupled ecological and geomorphic changes modulate the hillslope response to fluvial incision?

5.2 Study Site

The study site is located along the Middle Fork of the Feather River, the catchment of which drains the northernmost portion of the Sierra Nevada Mountains (Figure 5.1). In 2008, the region was subject to an airborne LiDAR survey by the National Center for Airborne Laser Mapping (NCALM). The survey yielded a high resolution point cloud, with a point density of ~9.8 pts m^{-2}, from which was derived a 1 m "bare-earth" Digital Elevation Model (DEM). This data is freely available through the National Science Foundation's OpenTopography service (http://www.opentopography.org/).

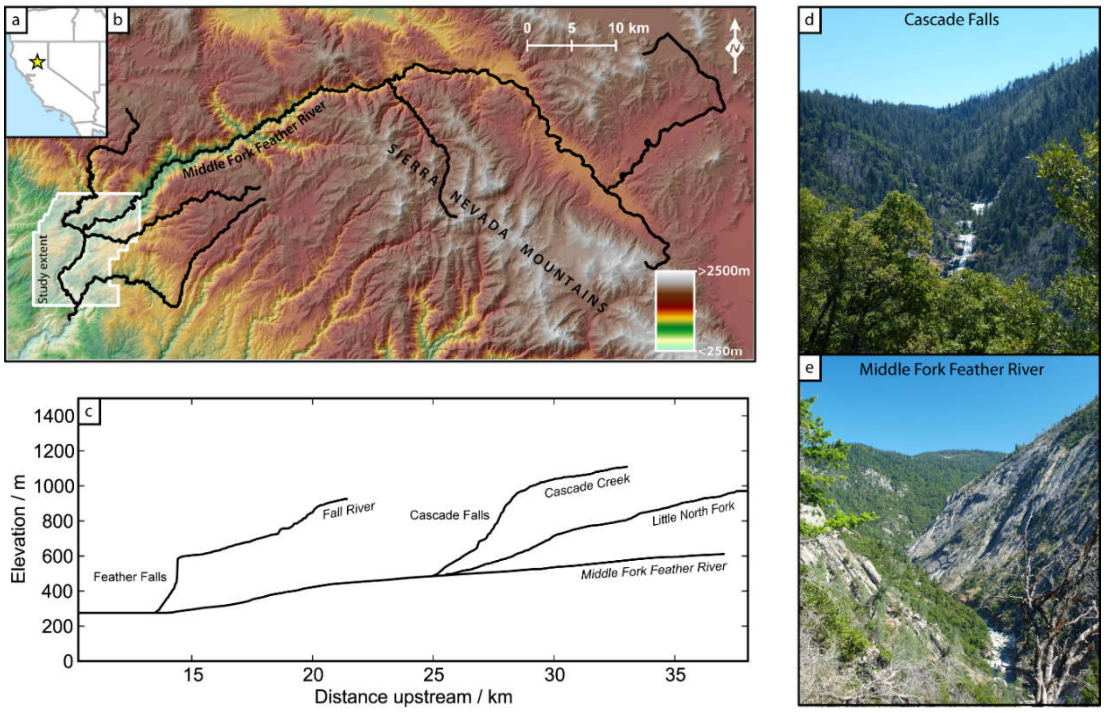

Figure 5.1 Field site and regional context: (a) Location map; (b) Middle Fork Feather River, with footprint of LiDAR survey indicated by the polygon outlined in white; (c) channel profiles for the Middle Fork Feather River and principal tributaries within the extent of the study area; (d) Cascade Falls, located in the NE of the field site; (e) the inner gorge of the mainstem Middle Fork Feather River, flowing N-S through the central part of the field site.

The Feather River region is underlain by bedrock comprising a suite of granitoid plutons belonging to the Sierra Nevada batholith – the exposed root of the Cordilleran magmatic arc active during the Jurassic-Cretaceous [*Ducea*, 2001; *Cecil et al.*, 2012] – intruded into metamorphosed sedimentary, volcanic and ophiolitic rocks associated with the Triassic-Jurassic Slate Creek and Fiddle Creek complexes [*Saucedo and Wagner*, 1992; *Day and Bickford*, 2004]. Within the spatial extent of the LiDAR survey the geology (Figure 5.2) is dominated by the presence of three coarse-grained granitoid plutons: (i) Cascade Pluton (CP), grading from quartz diorite at the margin to tonalite towards the core in the central eastern part of the pluton [*Hietanen*, 1976];

(ii) Bald Rock Pluton (BRP), a trondhjemite pluton that grades towards granodiorite and tonalite at the margins [*Hietanen*, 1951; *Compton*, 1955]; (iii)

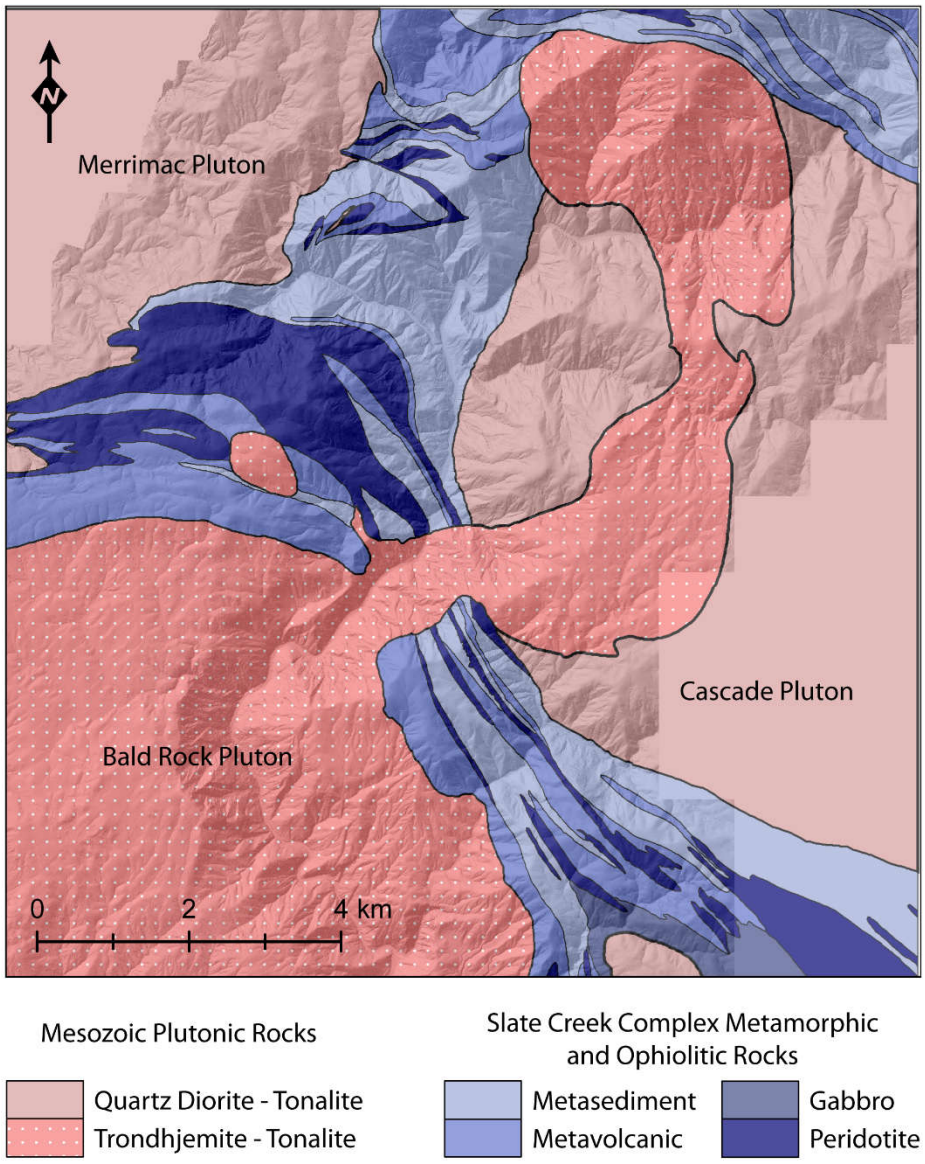

Figure 5.2 Bedrock geology of the study area; redrawn and adapted from existing geological maps by Hietanen (1976) and Saucedo and Wagner (1992).

Merrimac Pluton, which just encroaches into the north-western part of the surveyed area, and is similar in composition to the Cascade Pluton, grading from quartz-diorite to tonalite at the core [*Hietanen*, 1951, 1976]. All the plutons exhibit fairly high angle

(~50-90°) jointing and flow banding [*Compton*, 1955; *Hietanen*, 1976]. The surrounding bedrock encompass an assortment of metamorphosed intrusive (peridotite/serpentinite, gabbro), sedimentary (predominately quartzite/phyllite with some marble), and volcanic (calc-alkaline lavas/tuffs) rocks of the Slate Creek Complex (SCC) [*Hietanen*, 1976; *Saucedo and Wagner*, 1992]. These units have been deformed during emplacement of the granitoid plutons, distorting the structures and foliations from their regional trend such that they sweep round the pluton boundaries concordantly [*Compton*, 1955].

The present day climate is strongly seasonal: maximum (minimum) temperatures range from 9(-1)^{0}C in winter to 30(12)^{0}C at the height of summer; precipitation totals ~1750 mm annually, but >90% falls during the months between October and April and the region commonly experiences extended dry periods through the summer months (data from the PRISM Climate Group, Oregon State University; www.prism.oregonstate.edu/). Ecologically, the region is characterised by mixed conifer forests that are typical of the mid-elevation Sierra Nevada [*Barbour and Billings*, 2000]; the canopy is dominated by coniferous species, such as *Pseudotsuga menziesii, Pinus ponderosa, Calocedrus decurrens* and *Pinus lambertiana*, with some hardwood species also present, including *Quercus Kellogi*, in addition to *Arctostaphylos* shrubs [Chapter 3; *Milodowski et al.*, 2015a]. This mixed forest cover mantles much of the topography in the field site, with the exceptions of areas that have been logged, and notably the occurrence of exposed bedrock surfaces, the most prominent of which forms Bald Rock Dome.

In common with many of the rivers draining the northern Sierra Nevada, the Feather River has carved out a deep, precipitous canyon into a lower relief plateau that descends gradually from the range-crest, towards the eastern margin of the range, to the Central Valley in the west (Figure 5.1). Studies of cosmogenic nuclides indicate a landscape in a state of transience, with higher erosion rates (>250 mm ka^{-1}) proximal to the canyon, and slow erosion rates (20 - 40 mm ka^{-1}) in the tributary catchments draining the plateau [*Riebe et al.*, 2000; *Hurst et al.*, 2012], consistent with the upstream migration of a wave of elevated incision rates [*Hurst et al.*, 2012]. The propagation of this incision wave is clearly imprinted on the distribution of topographic gradients, with actively adjusting hillslopes below the knickpoint steepening in response to the higher incision rates [*Hurst et al.*, 2012]. Questions regarding the origins of these canyons have intrigued scientists for over a century [e.g. *Lindgren*, 1911; *Wahrhaftig*, 1965], but a recent appraisal of geomorphological and stratigraphic evidence suggests that they have been in existence since at least the Eocene-Oligocene [*Gabet*, 2014 and references therein], consistent with paleo-climatic reconstructions that suggest the northern Sierra Nevada had high elevations for much of the Cenozoic [e.g. *Mulch et al.*, 2006; *Cassel et al.*, 2009].

5.3 Methods

5.3.1 Overview

In order to explore the eco-geomorphic response of the Feather River landscape to changing fluvial incision, I employ a range of topographic analysis techniques to extract quantitative information regarding:

i. Changes in the morphological characteristics of hillslopes associated with these gradients in fluvial incision, from hillslope gradients and curvature to the emergence of bedrock at the topographic surface. Specifically I characterise variations in topographic slope, curvature and topographic roughness, permitting the isolation of hillslopes upslope of colluvial and fluvial channels [*Passalacqua et al.*, 2010a; *Pelletier*, 2013] and assess spatial variations in hillslope erosion rates [*Hurst et al.*, 2012, 2013a], and map the spatial distribution of rock exposure [Chapter 4; *Milodowski et al.*, 2015b].

ii. Changes in forest characteristics, specifically utilising the canopy information recorded within the LiDAR point cloud to quantify spatial variations in aboveground biomass [Chapter 3; *Milodowski et al.*, 2015a].

5.3.2 Isolation of Hillslope Domain

Recent advances have seen significant progress made in the analysis of hillslope form to characterise hillslopes and place constraints on the rate at which they erode [*Roering et al.*, 2007; *Pelletier et al.*, 2011; *DiBiase et al.*, 2012; *Hurst et al.*, 2012; *Milodowski et al.*, 2015b]. However, a prerequisite to the successful quantification of hillslope morphology and dynamics is the extraction of geomorphic process domains that delineate hillslopes and the channel network. The initial stage in my topographic analysis is thus the identification of hillslope and channel domains. Several methods have previously been proposed in this endeavour, broadly grouped into two categories: (i) geometric-based methods, which isolate the channel network by identifying convergent portions of the landscape [*Passalacqua et al.*, 2010a, 2010b; *Sofia et al.*, 2011; *Pelletier*, 2013]; (ii) process-based methods that search for a shift in the scaling

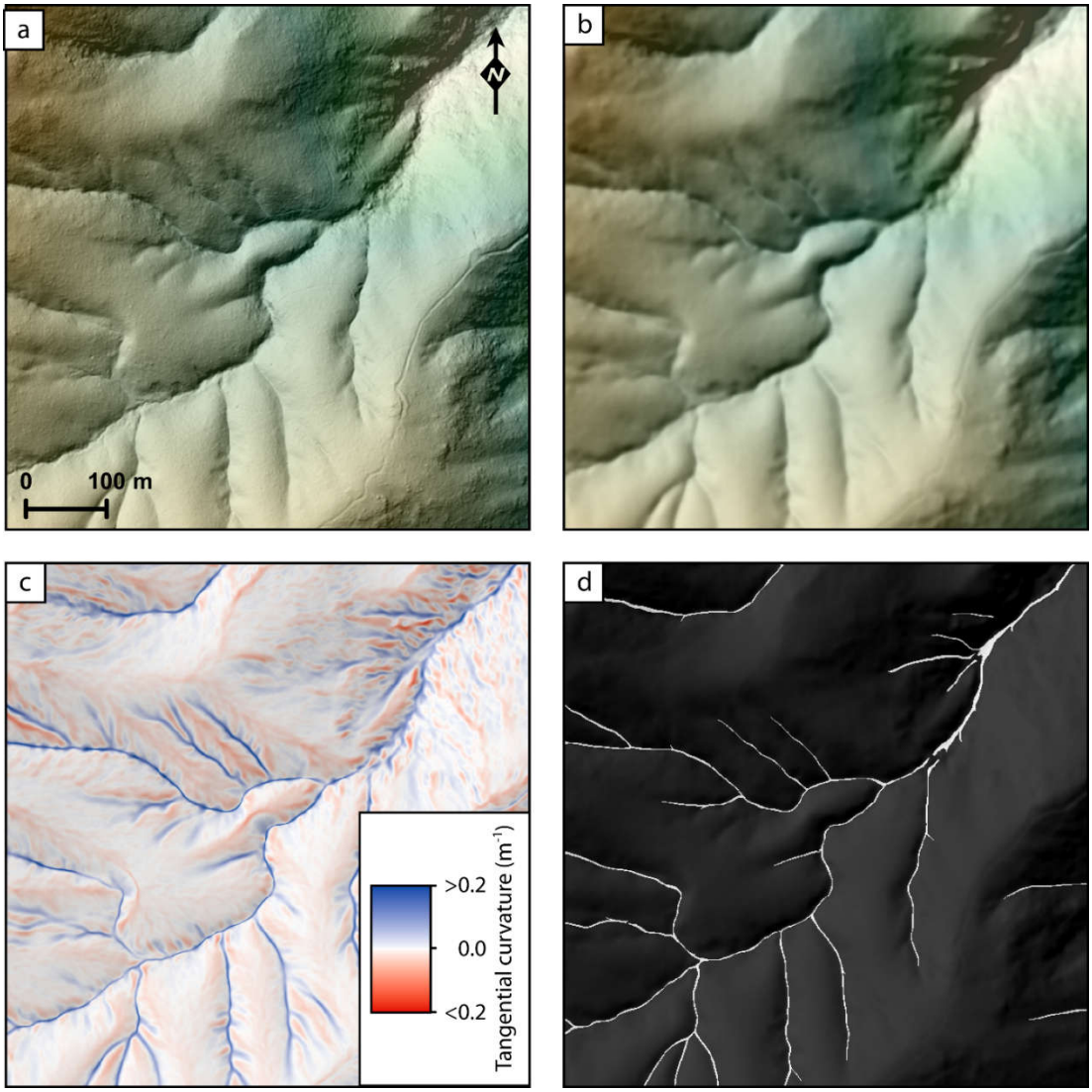

Figure 5.3 Isolation of hillslope and channel domain: (a) original 1 m resolution LiDAR-derived DEM; (b) DEM after being filtered with a Wiener filter; (c) tangential curvature distribution for filtered DEM; (d) extracted channel mask.

of the landscapes relief structure indicating a transition from fluvial to non-fluvial sediment transport, thus defining the fluvial network [*DiBiase et al.*, 2012; *Clubb et al.*, 2014]. Importantly, the hillslope-fluvial transition is frequently "fuzzy", as the upper reaches of convergent, channelized topography are often colluvial and/or debris flow features [e.g. *Stock and Dietrich*, 2003]. As the subsequent hillslope analyses depend on isolation of the eroding portions of the hillslopes upslope of colluvial

hollows and channels, I utilise a geometric-based method to extract a channel network thus including, as far as possible the colluvial portions of the network.

The specific method employed here combines elements suggested previously by Passalacqua et al. [2010a] and Pelletier [2013] and is illustrated in Figure 5.3. I first filter the topographic data using a Wiener filter [*Wiener*, 1949; *Pelletier*, 2013] – a non-linear, signal enhancing spectral filter. Tangential curvature is then quantified by taking the respective derivative of the filtered topography from a two dimensional surface fitted to a moving circular neighbourhood with a radius of 3 m [*Evans*, 1980]. Following Passalacqua et al. [2010a], a curvature threshold defining the channel network is determined statistically using a quantile-quantile plot, and both a connected component threshold and an accumulated area threshold (calculated using the D-Infinity algorithm [*Tarboton*, 1997]) are used to filter out small isolate concave patches that remain on the hillslopes. The upstream tips of this multi-pixel network are used to define the channel network following the method described by Grieve et al. [in review, 2016].

5.3.3 Hillslope Characteristics

5.3.3.1 Slope and Curvature

Slope and curvature are calculated for each pixel based on their respective derivatives of a six-term polynomial surface:

$$z = ax^2 + by^2 + cxy + dx + ey + f \quad (5.1),$$

fitted using least squares regression to a moving circular neighbourhood [*Evans*, 1980]. I employ a neighbourhood with a radius of 6 m [*Hurst et al.*, 2012], which acts

to smooth over micro-topographic noise. This process permits the extraction of topographic metrics that relate to the long term geomorphic development of the landscape, rather than topographic noise and small length-scale features such as tree throw pits, which relate to the occurrence of individual events (e.g. a tree throw mound) [*Roering et al.*, 2010; *Hurst et al.*, 2012; *Sofia et al.*, 2013].

5.3.3.2 Hilltop curvature and spatial variations in erosion rate

In soil mantled landscapes, the relationship between hillslope form and sediment flux can be approximated using a model in which the erosion rate, E [L T^{-1}] (dimensions of [M]ass, [L]ength and [T]ime denoted in square brackets), increases with hillslope gradient, ∇z, in a non-linear fashion as the hillslope steepens towards a limiting gradient, S_c [dimensionless] [*Andrews and Bucknam*, 1987; *Roering et al.*, 1999]:

$$E = -\frac{\rho_s}{\rho_r}\kappa\frac{\nabla^2 z}{1-\left(\left|\frac{\nabla z}{S_c}\right|\right)^2} \quad (5.2),$$

where ρ_s and ρ_s are the respective densities of soil and bedrock [M L^{-3}], and κ [L^2 T^{-1}] is the sediment transport coefficient, and z is the elevation of the surface [L].

Previous work by Hurst et al. [2012] suggests that this geomorphic transport function provides a good description of the time-integrated hillslope sediment transport at this site. At low topographic gradients ($\nabla z < 0.4$), the denominator in Equation 5.2 approaches unity and erosion rate scales approximately linearly with topographic curvature ($\nabla^2 z$). Since this condition is typically met by hilltops, and given that soil mantled hillslopes typically respond rapidly to changes in base level, hilltop curvature,

C_{HT} [L^{-1}], can therefore be used as a proxy for erosion rate [*Roering et al.*, 2007; *Hurst et al.*, 2012, 2013a, 2013c]:

$$E = -\frac{\rho_s}{\rho_r}\kappa C_{HT} \quad (5.3).$$

Topographic curvature is calculated using the moving window approach as described above. The ridge network is defined using the channel network delineated created in section 5.3.2., following the methodology described by Grieve et al. [in review, 2016]. Spatial variations in C_{HT}, and other metrics, are quantified using second order catchment averages.

In using C_{HT} as a proxy for erosion rate, it is important to note the caveat that this assumes that κ is constant across the range of erosion rates present in the landscape. Several studies have suggested that κ may vary inversely with soil depth [*Heimsath et al.*, 2005; *Roering*, 2008; *Pelletier et al.*, 2011]. While the majority of the ridgelines in the field site retain a soil mantle [*Yoo et al.*, 2011; *Hurst et al.*, 2012, 2013c], measurements of soil thickness spanning the erosion gradient along Cascade Ridge, in the north of the site, indicate that soil thickness is decreases as erosion rates increase, and also vary with local ridgeline topography [*Gabet et al.*, 2015]. Nevertheless, Hurst et al. [2012] found that ~70% of the variance in catchment average C_{HT} at this locality could be explained by variations in catchment-wide erosion rates, quantified using concentrations of ^{10}Be from fluvial sediments. Thus while spatial variations in soil thickness are likely to add to noise in the observed eco-geomorphic relationships, C_{HT} should be a good indicator, at least of relative changes in erosion rate.

5.3.3.3 Rock exposure

Two methods have presently been proposed to locate areas of hillslope in which rock is exposed at the surface: short wavelength topographic roughness, quantified using the local variability of the local topographic surface [*Milodowski et al.*, 2015b], and the Rock Exposure Index (REI), in which bedrock areas are identified based on a threshold topographic gradient, S_c [*DiBiase et al.*, 2012]. Previous authors have implemented the REI using S_c = 45° [*DiBiase et al.*, 2012; *Marshall and Roering*, 2014], although Marshall and Roering [2014] did not calibrate their metrics against independently mapped rock exposure. In Chapter 4, I investigated the spatial correspondence of surface roughness and rock exposure in a range of granitoid landscapes, and found that the degree of clustering around the minor axis (S_3; see Section 4.2) of the distribution of surface normal vectors within a 5 m radius neighbourhood provided good results (S_3 = 0.05) [*Milodowski et al.*, 2015b]. The limitations of both techniques are discussed in detail in Chapter 3 [*Milodowski et al.*, 2015b]; the advantage of the surface roughness approach is that it is able to locate areas of rock exposure in low relief settings. However, there are also cases, such as Bald Rock Dome, in which there are significant exposures of plutonic bedrock that are topographically smooth, with the prevailing fractures limited to exfoliation sheets. As a result, I use the combination of surface roughness and REI metrics to reduce the likelihood of false negatives: I consider a pixel bedrock if either S_3 >= 0.015 (this is a conservative threshold, see Section 4.3), or the local slope exceeds 45°.

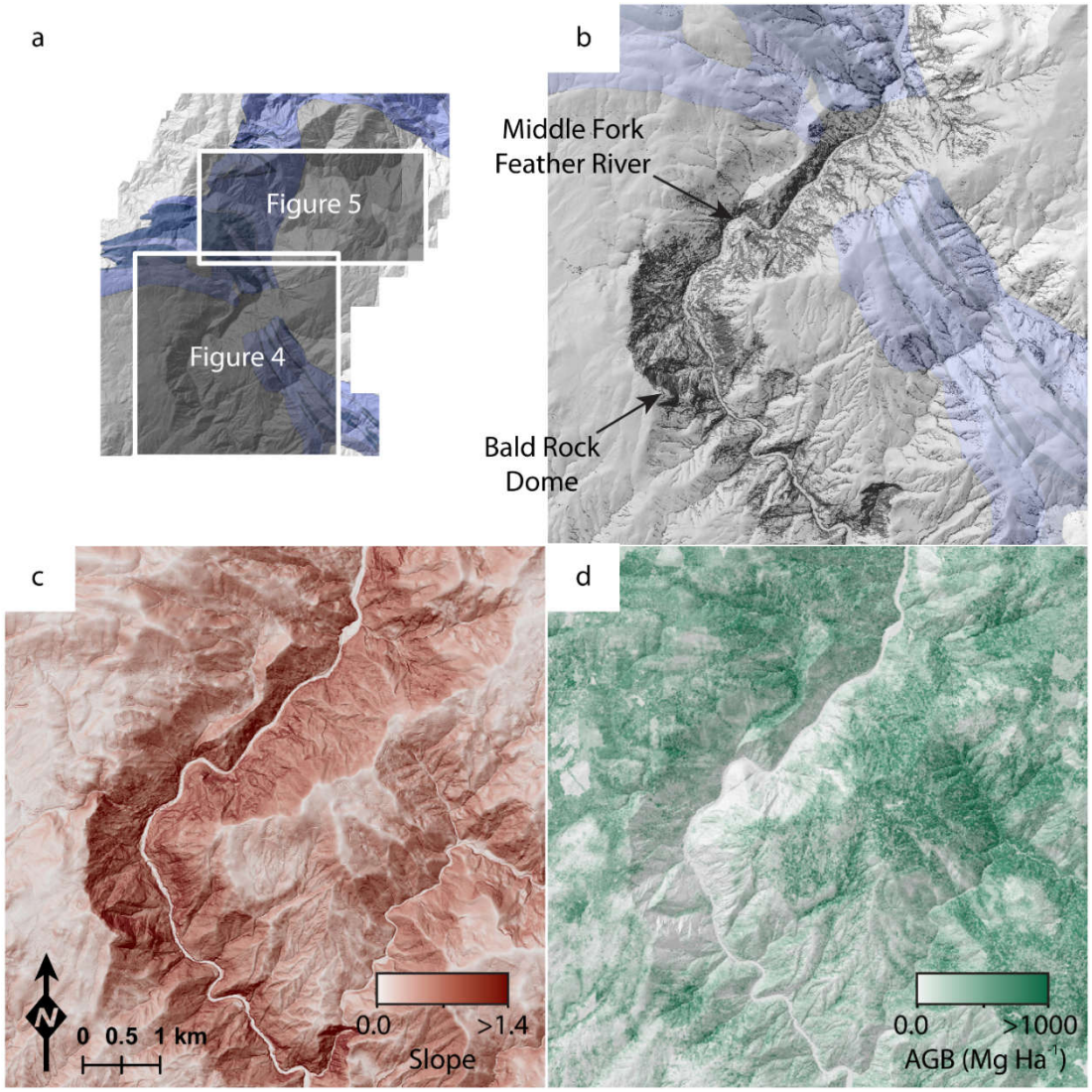

Figure 5.4 (a) Map of field site indicating locations of the maps presented in this figure and in Figure 5. (b) Rock exposure, (c) slope, and (d) AGB for the southern portion of the field site. Note the extensive areas of low biomass away from the inner canyon, in the SW of the image in particular, which correspond to areas particularly badly affected by the 2008 Scotch Fire, and patches of forest that have been cleared.

5.3.3.4 Aboveground biomass

LiDAR has been widely employed to estimate spatial variations in the structural characteristics of forest ecosystems in a range of biomes [*Lefsky et al.*, 2002; *Asner et al.*, 2012; *Hwang et al.*, 2015; *Milodowski et al.*, 2015a]. I quantify the distribution of aboveground biomass (AGB) across the landscape using the mean return height

(MRH) of the LiDAR point cloud based on a calibration developed using field inventory plots undertaken at this site [Chapter 3; *Milodowski et al.*, 2015a].

5.4 Results

5.4.1 Rock exposure and erosion rate

The amount of rock exposure present on hillslopes increases as erosion rates (C_{HT}) increase in our study area. This transition from a full soil mantle to rugged bedrock hillslopes is clearly gradual, with rapidly eroding hillslopes proximal to the inner canyon typically supporting a patchwork of bedrock outcrop coexisting with a partial to intermittent coverage of soil (Figures 5.4, 5.5). Lithology evidently places a significant control on the emergence of bedrock in this setting. This lithology control is particularly notable in the hillslopes draining directly into the trunk channel of the Middle Fork Feather River, and principal tributaries, the Little North Fork and Cascade Creek (Figures 5.4, 5.5): bedrock exposure in the inner canyon hillslopes on Bald Rock Pluton in the south is much more extensive and continuous, in contrast to the sparse, patchier distribution in the northern part of the area underlain by CP and SCC rocks, where hillslopes commonly retain a near-full soil mantle. Likewise, moving along Cascade Ridge in the north of the site, the trondhjemite tongue of BRP is coincident with an increase in the occurrence of bedrock outcrop, compared neighbouring CP hillslopes (Figure 5.4).

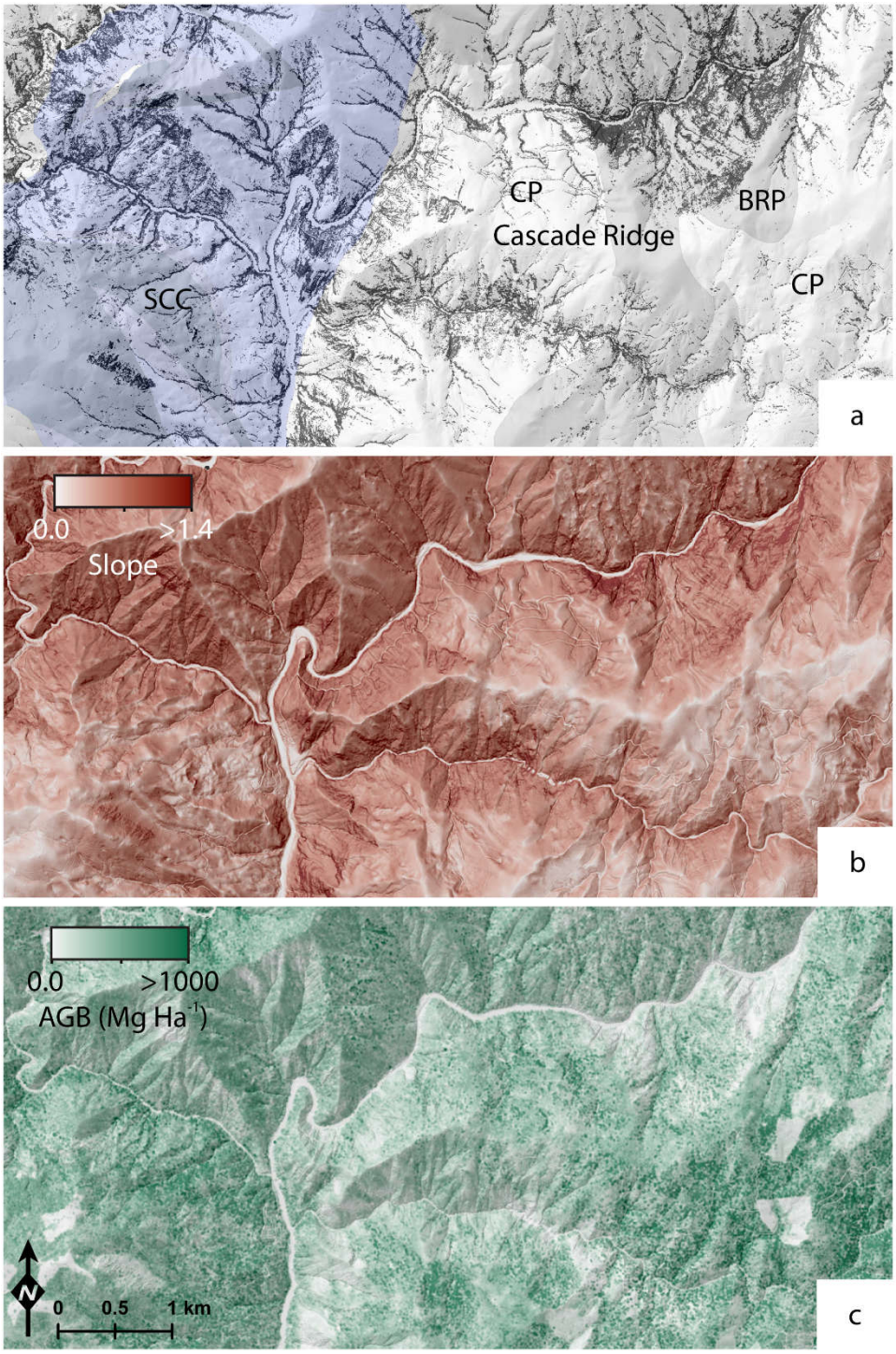

Figure 5.5 Maps of (a) bedrock outcrop, (b) slope, and (c) AGB in the Cascade Ridge region of the study site. In panel (a), the bedrock geology has been overlain over the rock exposure map. Along Cascade Ridge, erosion rates increase from east to west [*Hurst et al.*, 2012]. Note prominent changes in both rock exposure and AGB associated with this gradient, and changes in rock exposure coincident with lithological contacts.

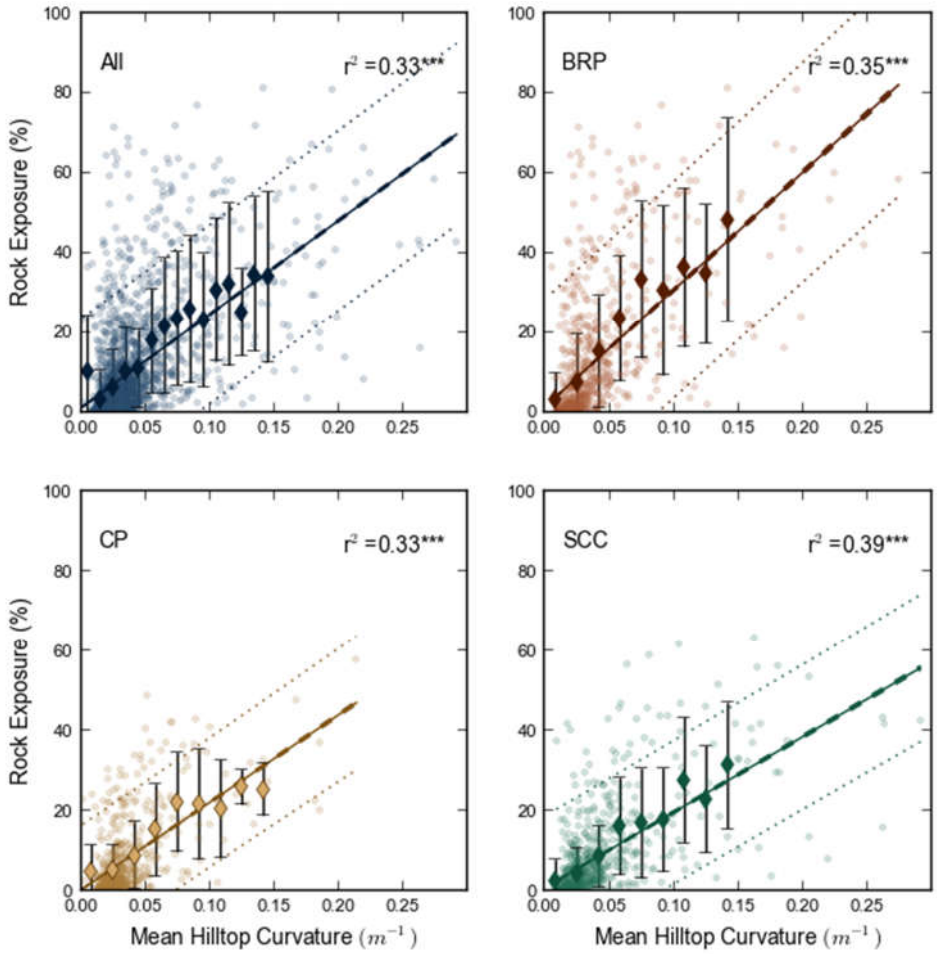

Figure 5.6 Trends between average C_{HT} and percentage rock exposure for 2nd order catchments. In the first panel, all catchments wthin the field site are included; in the remaining three, catchments are split by the dominant bedrock likthology. In each plot, the regression line (solid line) , based on a linear fit to the un-binned data, alongside the 95% confidence interval for the regression line (dashed line) and 95% prediction interval (dotted line). Error bars on the binned data represent the standard deviation within each bin. P-values for the regressions are reported after the r^2 value: *** $p < 0.001$. While there is a large uncertainty associated with the prediction interval, the regression line is well constrained for all lithology groups.

Considering the attributes of second order catchments across the field site, the relationship between C_{HT} and fraction of bedrock cover is well approximated by a positive linear relationship (Figure 5.6), with variations in catchment average C_{HT} accounting for 33% of the variance in rock exposure. Splitting the catchments according to the dominant lithology this increases to up to 39%. For all cases the

relationship is significant at the 99.9% confidence interval. These observations of a broadly linear increase in rock exposure with erosion rate corroborate those of the soil-bedrock transition in the San Gabriel Mountains ~700 km to the south [*DiBiase et al.*, 2012; *Heimsath et al.*, 2012].

The role of lithology again stands out, corroborating my earlier qualitative observations. Catchments draining Bald Rock Pluton (BRP), in particular, have systematically greater levels of rock exposure than those underlain by either Cascade Pluton (CP) or Slate Creek Complex (SCC) rock (Figures 5.6, 5.7). While the relationships observed in CP and SCC catchments are broadly similar, the gradient of

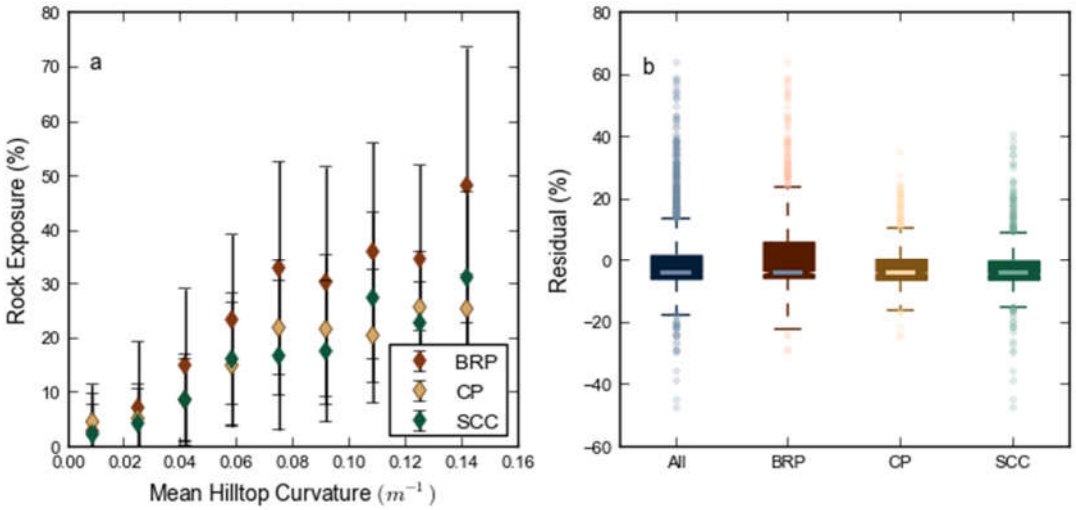

Figure 5.7(a) Summary of rock exposure vs. catchment mean hilltop curvature, showing all three lithology groups; error bars indicate the standard deviation of the observations within each bin. (b) Boxplots indicating the residuals for each lithology group, following the removal of trend between rock exposure and mean hilltop curvature for all 2nd order catchments. Note the similarity of the distributions of residuals for CP and SCC catchments, wheras the distribution of residual rock exposure for BRB catchments has much greater skew, with a heavy tail extending to higher residual rock exposure fractions.

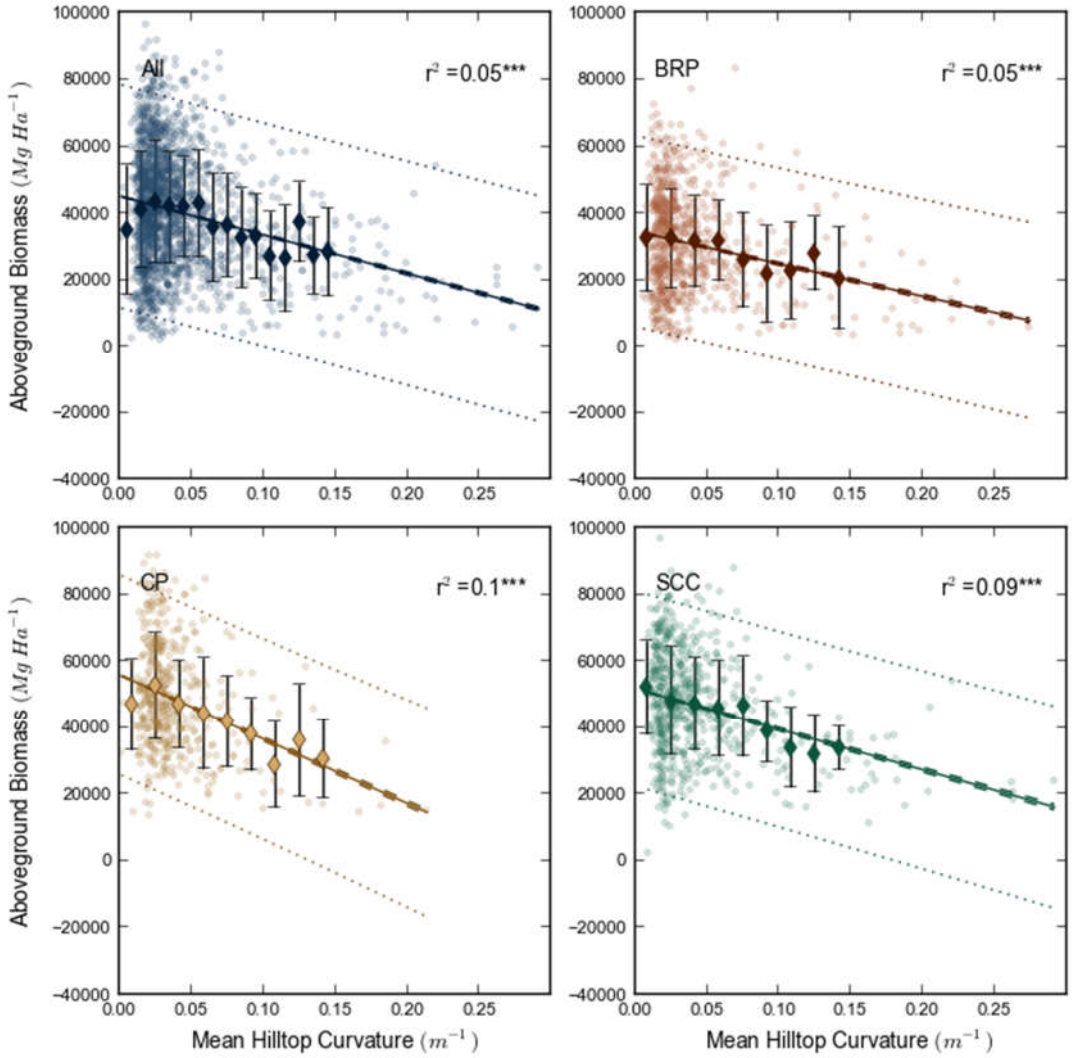

Figure 5.8 Trends between average hilltop curvature and AGB for 2nd order catchments. In the first panel, all catchments within the field site are included; in the remaining three, catchments are split by the dominant bedrock lithology present. In each of the plots, the regression line (solid line), 95% confidence interval for the regression line (dashed line) and 95% prediction interval (dotted line) for the un-binned dataset are displayed. The error bars on the binned data represent the standard deviation within each bin. P-values for the regressions are reported after the r^2 value: *** p < 0.001.

the relationship between C_{HT} and rock exposure is greater for BRP catchments, indicating a more rapid increase in the fraction of hillslopes with rock outcrop for catchments underlain by this lithology (Figure 5.6). Likewise, when the overall trend observed across all lithology groups is removed, the residuals for BRP catchments

exhibit a much heavier tail towards higher residual rock exposure compared to the other rock types (Figure 5.7).

5.4.2 Aboveground biomass and erosion rate

AGB is negatively correlated with erosion rate (Figure 5.8). The relationship is again broadly linear, but with significant variance; r^2 is limited to between 0.05 and 0.10. All relationships presented are significant at the 99.9% confidence interval. This first order trend matches previous observations from the north-western portion of the field site around Cascade Ridge [*Gabet et al.*, 2015; Chapter 3; *Milodowski et al.*, 2015a]. Some patches of very low biomass correlate with areas severely affected by fires in 2008, which particularly affected BRP hillslopes, and areas of the plateau that have been cleared or are actively logged (Figures 5.4, 5.5) [Chapter 3; *Milodowski et al.*, 2015a]. This undoubtedly adds a potential source of bias into the results when comparing across lithologies: AGB is systematically lower in catchments underlain by BRP bedrock relative to both CP and SCC across all erosion rates (Figure 5.9), although interpretation of lithological controls on ecosystem structure are complicated by the fact that the 2008 burn severity was highest in the SW and north of the site, areas prevailingly underlain by BRP bedrock. This bias does not negate the regional negative trend in AGB observed across the erosion rate gradient [Chapter 3; *Milodowski et al.*, 2015a]; however, the impact of this forest disturbance contributes to the large scatter observed in the dataset for low C_{HT} catchments, particularly those located in the southwest of the field site. This is primarily responsible for the decreased correlation observed at the scale of the full field site, compared to trends observed to a sub-section of the area to the northwest, where the degree of forest

disturbance is less severe, and hence geomorphic controls on forest structure are more clearly evident in the AGB distribution [Chapter 3; *Milodowski et al.*, 2015a].

For the same second order catchments, average AGB and fraction of bedrock exposure exhibit a statistically significant negative correlation (r^2 = 0.05), with a monotonic decrease in biomass for the binned data across the range of rock exposures present (Figure 5.10). A high degree of variance is observed in soil mantled catchments on the plateau, which are affected by the aforementioned logging and clearance, or were more severely impacted by the 2008 fire; these both contribute towards catchments with much lower than expected AGB, despite possessing an extensive soil mantle.

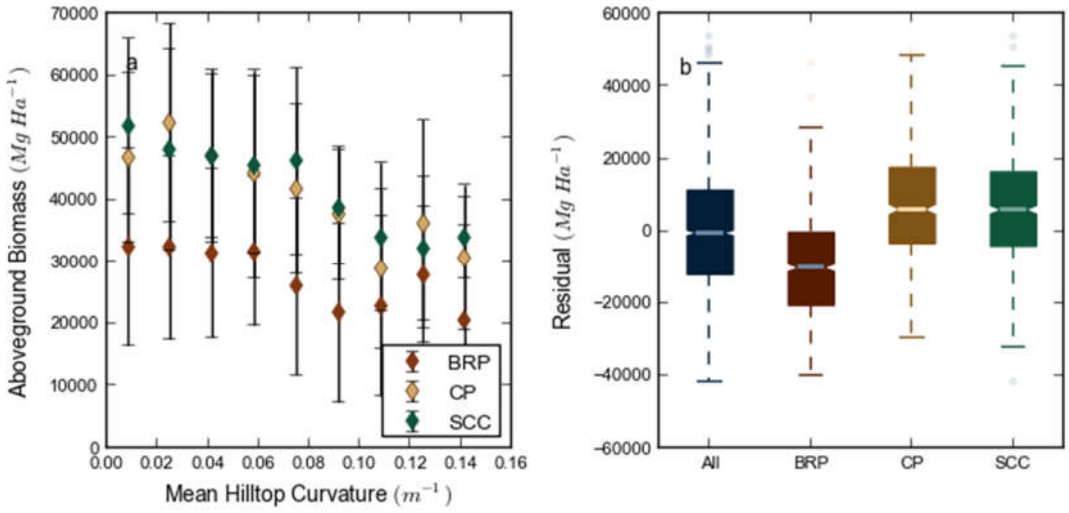

Figure 5.9(a) Summary of catchment mean hilltop curvature vs. AGB showing all three lithology groups; (b) boxplots indicating the residual AGB for each lithology group, following the removal of trend between AGB and mean hilltop curvature for all 2nd order catchments in the field site. Note that the residuals are systematically lower for BRP catchments compared to both CP and SCC catchments.

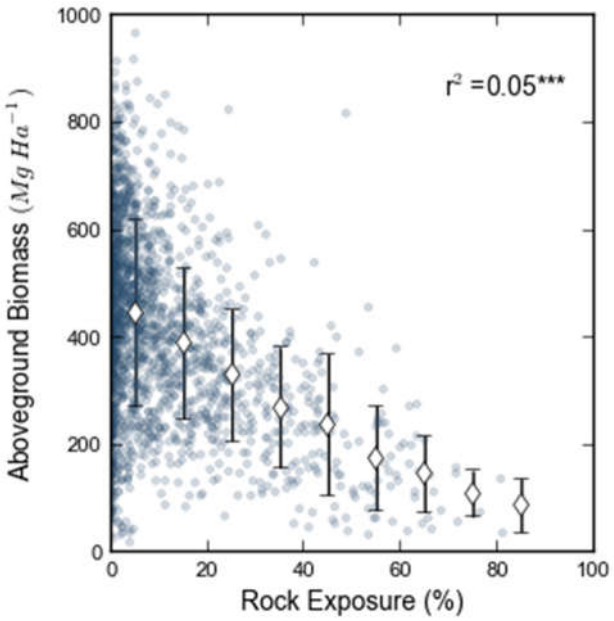

Figure 5.10 Relationship between rock exposure percentage and AGB for all second order catchments. The statistical significance of the relationship is indicated after the r^2 value (* $p < 0.001$), calculated for the un-binned dataset.**

5.5 Discussion

5.5.1 Lithological control on the soil-bedrock transition

The transition from soil mantled to bedrock hillslopes is the expected geomorphic response to increased fluvial incision rates once erosion rates outpace the rate at which soil can be produced [e.g. *Heimsath et al.*, 1997, 2012]. The gradual, patchy nature of this transition has been illustrated previously, both in this setting [Chapter 4; *Milodowski et al.*, 2015b] and across erosion rate gradients present in other landscapes [*DiBiase et al.*, 2012; *Heimsath et al.*, 2012; Chapter 4; *Milodowski et al.*, 2015b]. However, these previous studies have not otherwise considered how bedrock type impacts on this transition. The trends observed in this site suggest that bedrock exposure increases more rapidly for hillslopes established on BRP (trondhjemite-tonalite) relative to CP (quartz diorite) and SCC (metamorphic/ophiolitic) rocks,

suggestive of an earlier transition from soil mantled-bedrock hillslopes. The rate of physical and chemical weathering of bedrock is fundamentally dependent on its texture, mineralogy and fracture distribution [*Goldich*, 1938; *Pye*, 1986; *White et al.*, 2001; *Buss et al.*, 2008; *Heckman and Rasmussen*, 2011; *Bazilevskaya et al.*, 2013], therefore the dependence of the soil-bedrock transition on lithology should not come as a surprise [*Hahm et al.*, 2014b]. Intuitively, one might expect greater similarities between similar bedrock types. It is therefore interesting that the controls on bedrock exposure for CP hillslopes are apparently so much more similar to SCC hillslopes rather than those established on the granitoid bedrock of BRP.

Using high resolution topography and geological maps alone, I am not able to say exactly what mechanism drives the differences in the erosion rate and bedrock exposure. Existing studies of regolith variations across the erosion rate gradient in this landscape have revealed a complex relationship between erosion rate and soil thickness. In Bald Rock Basin, a tributary catchment to the Feather River that drains BRP, a series of hillslope transects across the erosion rate gradient relatively consistent regolith thicknesses despite erosion rates increasing almost threefold [*Yoo et al.*, 2011; *Hurst et al.*, 2012]. In contrast, along Cascade Ridge, predominately underlain by CP, regolith thicknesses measured along the ridgeline decreased from East to West from >1 m to ~10 cm, associated with an increase in estimated erosion rates from ~60 mm ka^{-1} to ~520 mm ka^{-1} [*Gabet et al.*, 2015]. Variable dynamics of soil production are a feature common to granitoid rocks, for which differences in both the mineralogy and grain size can have a large impact on the susceptibility of the bedrock to weathering [*Godard et al.*, 2001; *Migoń*, 2006; *Bazilevskaya et al.*, 2013]. Variations in the

occurrence of rock exposure within granitoid landscapes often coincide with pluton boundaries [*Hahm et al.*, 2014b; *Migoń and Vieira*, 2014], where minerology and grain size can change over relatively short distances. Chemical differences between plutons may also impact on the physical production of soil from bedrock as a consequence of feedbacks linking nutrient availability and vegetation [*Hahm et al.*, 2014a]. Of particular important to ecosystems is the availability of phosphorous: the principal source of phosphorous to the soil is the underlying bedrock [*Walker and Syers*, 1976; *Vitousek et al.*, 2010; *Mage and Porder*, 2013; *Porder and Ramachandran*, 2013]. Differences in phosphorous concentration across pluton boundaries have been advocated as one potential mechanism controlling sharp ecotones across pluton boundaries and the emergence of prominent balds elsewhere in the Sierra Nevada [*Hahm et al.*, 2014a]. Geochemical analyses of plutons in the Feather River Region [*Hietanen*, 1976] suggest lower phosphorous concentrations in BRP compared to CP. Paired with greater rock exposure on BRP, this is consistent with an element of nutrient limitation on soil production, however the presently available data is insufficient to test this hypothesis further.

Alternatively, differences in the degree of fracturing may also be at least partly responsible for the lithological control observed here. The importance of fractures in the weathering and breakdown of bedrock is clear: fractures provide conduits for water, thus facilitating the penetration of the weathering front deep into the subsurface [*Anderson et al.*, 2002; *Buss et al.*, 2008; *Ma et al.*, 2010; *Goodfellow et al.*, 2014b]; the presence of fractures also limits the bulk strength of hillslopes and thus their ability to maintain relief [*Schmidt and Montgomery*, 1995; *Molnar et al.*, 2007], while also

providing footholds that enable the establishment of vegetation, the root networks of which act to further enhance weathering and the production of soils [*Gabet and Mudd*, 2010; *Roering et al.*, 2010].

The prevalence of fractures is dependent on a range of controls, including inherited structures, topographic stresses and the cumulative deformation imposed by the history of tectonic and plutonic activity [*Molnar et al.*, 2007; *Clarke and Burbank*, 2010; *Clair et al.*, 2015]. Tectonic deformation acts as a "rock crusher" [*Molnar et al.*, 2007; *Clarke and Burbank*, 2010; *Clair et al.*, 2015], driving pervasive fracturing. Conversely, post-tectonic intrusive rocks found in arc settings commonly exhibit much less pervasive fracturing, enabling the formation of domes, and precipitous high relief bedrock walls [*Gilbert*, 1904; *Molnar et al.*, 2007; *Clarke and Burbank*, 2010]. Bald Rock Dome, in the SE of this field site provides a good example of this, with flaw-free bedrock walls rising steeply from the inner canyon [*Compton*, 1955] (Figure 5.5). In contrast, the older SCC rocks are extensively faulted and fractured, while the intrusion of the plutonic units has also imposed its own clear deformation imprint of the structure of the country rock [*Hietanen*, 1951, 1976; *Compton*, 1955]. Within CP, foliations are particularly well developed towards the pluton margins, and contact relationships with BRP indicate that it is likely to have been emplaced after the solidification of the earlier CP pluton [*Hietanen*, 1976]. The consequent deformation of CP may be partly responsible for the differences observed here.

5.5.2 Lithological control on forest structure

The trend for decreasing AGB across the erosion rate gradient in this landscape substantiates previous work in the NE of the area [*Gabet et al.*, 2015; Chapter 3;

Milodowski et al., 2015a]. This has been attributed to reduced moisture storage capacity of the soil and saprolite, as a result of the more rapid advection of material through the critical zone, limiting the time available for weathering and soil production [Chapter 3; *Milodowski et al.*, 2015a]; elsewhere in the Northern Sierras observations indicate a significant relationship between the combined thickness of the A and C horizons and stand density [*Meyer et al.*, 2007]. The coupling of AGB to moisture storage capacity to AGB in this landscape is likely to be particularly strong because of the requirement for groundwater to supply vegetation with moisture through the long, dry summer [*Rose et al.*, 2003; *Graham et al.*, 2010; *Kelly and Goulden*, 2016]; in the thin soils characteristic of the Sierra Nevada, roots penetrate saprolite within the first few years of growth [*Witty et al.*, 2003]. In catchments where bedrock outcrops at the surface, there is an additional limitation imposed on forest structure, which becomes increasingly constrained by the patchiness of the soil [*Gabet and Mudd*, 2010; *Sheffer et al.*, 2013] (Figure 5.10).

There is a significant degree of variability in AGB for slowly eroding catchments draining the plateau (Figures 5.8, 5.10), which acts to reduce the quality of the regression. This variance is driven to a large extent by the impact of the 2008 Scotch fire, which severely affected parts of the study site, while parts of the landscape have also been logged or deforested, particularly in the southwest (Figures 5.4, 5.5). Moreover, the areas affected are significantly biased towards slowly eroding catchments draining the plateau; anthropogenic clearance is absent from steeper parts of the landscape. Accounting for the impact of this disturbance footprint on present

day forest structure, I found a much tighter coupling of AGB to the erosion gradient [Chapter 3; *Milodowski et al.*, 2015a].

Lithology also appears to play a significant role in the distribution of AGB, although the observation of reduced AGB on BRP is caveated by the fact that areas underlain by the Bald Rock Pluton were predominately affected by the aforementioned fire. Furthermore, parts of this landscape, particularly plateau areas in the southwest beyond the borders of the Plumas National Forest, have been logged or deforested. This undoubtedly adds a significant source of bias to my observations. Nevertheless, the greater extent of bedrock exposure towards the inner canyon in areas underlain by BRP is suggestive of shallower soils that may support a reduced carrying capacity for the landscape on BRP hillslopes compared to other lithologies present.

While the gradual reduction in AGB observed across the erosion gradient would be the expected result of thinning soil and saprolite, assuming that biotic soil production scales in some way with AGB, then biotic soil production is also likely to decrease across this erosion gradient, providing a positive feedback through which the control that erosion rate places on soil thickness is amplified. Moreover, this assumption is supported by observations that AGB is typically correlated with belowground root biomass [*Hwang et al.*, 2015], and bedrock fracture by tree throw is more prevalent where trees are larger [*Gabet and Mudd*, 2010].

5.5.3 Intra-lithological heterogeneity

Even accounting for lithology, variations in C_{HT} can only account for 33-39% of the variance in rock exposure exhibited at this site. While some of the unexplained variance may be accounted for due to spatial variations in the relationship between C_{HT}

and erosion rate, driven for example by variability in the sediment transport coefficient, κ, it is unlikely that this can solely account for this (note the relatively strong relationship between C_{HT} and erosion rate observed by Hurst et al. [2012] in this locality). Intra-lithological heterogeneity – variability in bedrock characteristics exhibited within a given lithologic unit – therefore appears to be significant in modulating the hillslope response to fluvial incision in this region. Neighbouring catchments commonly possess contrasting hillslope characteristics despite having a similar bedrock type (Figure 5.4, 5.5); predominately bedrock catchments can be located next to others with a near continuous soil mantle. Likewise, the relationships observed between AGB and C_{HT} also display a large degree of variability, although a significant portion of this variability is likely to reflect shorter term ecological dynamics, including fire-driven tree mortality and anthropogenic disturbance [*Lydersen and North*, 2012; *Anderson and Stillick*, 2013; *Milodowski et al.*, 2015a].

5.5.4 Eco-geomorphic coupling and the occurrence of mixed soil-bedrock hillslopes in rapidly eroding landscapes

Development of a mechanistic understanding of why hillslopes exhibit contrasting hillslope evolution trajectories in response to similar histories of geomorphic forcing represents a major challenge for models of hillslope evolution [*Heimsath et al.*, 2012; *Larsen et al.*, 2014a]. For example, an important distinction from a hillslope evolution perspective is whether the occurrence of mosaics of soil and bedrock is a manifestation of lithological variability alone, or whether there are geomorphic boundary conditions for which multiple stable states exist at which a hillslope may either be mantled by soil mantle, or host exposed bedrock depending on the history of erosion and disturbance.

Given that the presence and production of soil is intimately entwined with the fate of the vegetation that it supports [*Gabet and Mudd*, 2010; *Graham et al.*, 2010; *Roering et al.*, 2010; *Amundson et al.*, 2015], changes in soil thickness associated with varying rates of erosion are highly likely to be coupled with changes to the biosphere [*Gabet et al.*, 2015; Chapter 3; *Milodowski et al.*, 2015a]. In order to explore how the linkages between biology and soil production could mediate the hillslope response to changing erosion rates, I utilise a simple dynamical systems model for a hillslope [e.g. *Stark and Passalacqua*, 2014], focusing specifically on soil production and changes in soil thickness. This approach, in which the dynamics of the system in question are simplified to an approximated, low-dimensional set of differential equations, is amenable to examining the coupling between vegetation and hillslope processes: the emergent behaviour of these models is relatively easy to understand, as a result of the simplicity of their implementation [*Thornes*, 1983, 1985; *Stark and Passalacqua*, 2014; *Pelak et al.*, 2016].

The starting point for my model implementation closely follows that of Stark and Passalacqua [2014]. The model element represents a hillslope "patch". Within the hillslope patch, the evolution of soil thickness, $h[t]$, and vegetation, here modelled as biomass, $v(t)$, are governed by two differential equations. The rate of change of soil thickness, $\partial h/\partial t$, is determined by the competition between erosion, $E(t)$ [L T^{-1}], and soil production, $P(h)$ [L T^{-1}]:

$$\frac{\partial h}{\partial t} = P - E \qquad (5.4).$$

Note that sediment transport is not modelled at the process level, rather a specified erosion rate is applied to the hillslope patch. In the case of a bedrock hillslope ($h = 0$), where erosion rates exceed soil production rates, all soil produced in the time-step is removed. Soil production is modelled as decreasing exponentially with increasing soil depth from a maximum soil production rate, $P_0[v]$, at zero soil depth [*Heimsath et al.*, 1997, 1999, 2001]:

$$P = P_0 \exp(-\lambda h) \tag{5.5}.$$

The exponent λ [L^{-1}] determines the rate of decay of P with depth. The maximum rate of soil production is expected to vary with vegetation, as plants actively drive the physical and chemical breakdown of bedrock to produce soil [e.g. *Berner et al.*, 2003; *Bonneville et al.*, 2009; *Taylor et al.*, 2009; *Gabet and Mudd*, 2010; *Roering et al.*, 2010]. Additionally, weathering rates are strongly dependent on the presence of water, particularly in granitoid landscapes [e.g. *Godard et al.*, 2001; *Gabet et al.*, 2006; *Migoń*, 2006]. By stabilising soil on hillslopes, vegetation further promotes weathering reactions by prolonging the timescale of water-rock interactions. Following Stark and Passalacqua [2014], I incorporate this vegetation dependence by partitioning P_0 into a biotic and abiotic component:

$$P_0 = P_{0,abiotic}\left(1 + \frac{\varphi v}{v_{max}}\right) \tag{5.6}.$$

In this instance, φ is a dimensionless scalar that modifies the relative efficacy of biogenic soil production, $v(h,t)$ [$M L^{-2}$] represents biomass and v_{max} [$M L^{-2}$] represents the maximum landscape carrying capacity.

Table 5.1 Parameter definitions for simple hillslope model

Parameter	Symbol	Value
Maximum abiotic soil production rate	$P_{0,abiotic}$	2.5 mm yr^{-1}
Decay constant in soil production function	λ	2.0 m^{-1}
Scaling factor for biotic contribution to soil production rate	φ	4.0
Growth rate factor	α	5.0
Maximum biomass carrying capacity of landscape	v_{max}	500 Mg Ha^{-1}
Constant controlling scaling of v_{cc} with h	γ	5.0 m^{-1}

Biomass growth, $\partial v/\partial t$, is treated as a logistic growth function [*Stark and Passalacqua*, 2014], in which the biomass approaches the local landscape carrying capacity $v_{cc}[h]$ ($v_{cc} <= v_{max}$) according to a growth rate factor, α [T^{-1}]:

$$\frac{\partial v}{\partial t} = \alpha v \left(1 - \frac{v}{v_{cc}}\right) \quad (5.7),$$

The two differential equations (Equations 5.4 & 5.7) provide the core of my dynamical hillslope system. Within this framework soil and vegetation are coupled. Additionally, in many landscapes the local carrying capacity, v_{cc}, is likely to be dependent on the thickness of the soil, as this provides the substrate from which plants can extract nutrients and moisture [*Graham et al.*, 2010; *Vitousek et al.*, 2010]; within the Californian Sierra Nevada, where the soil and saprolite moisture store are critical through the extended summers, aboveground biomass and stand density correlate with

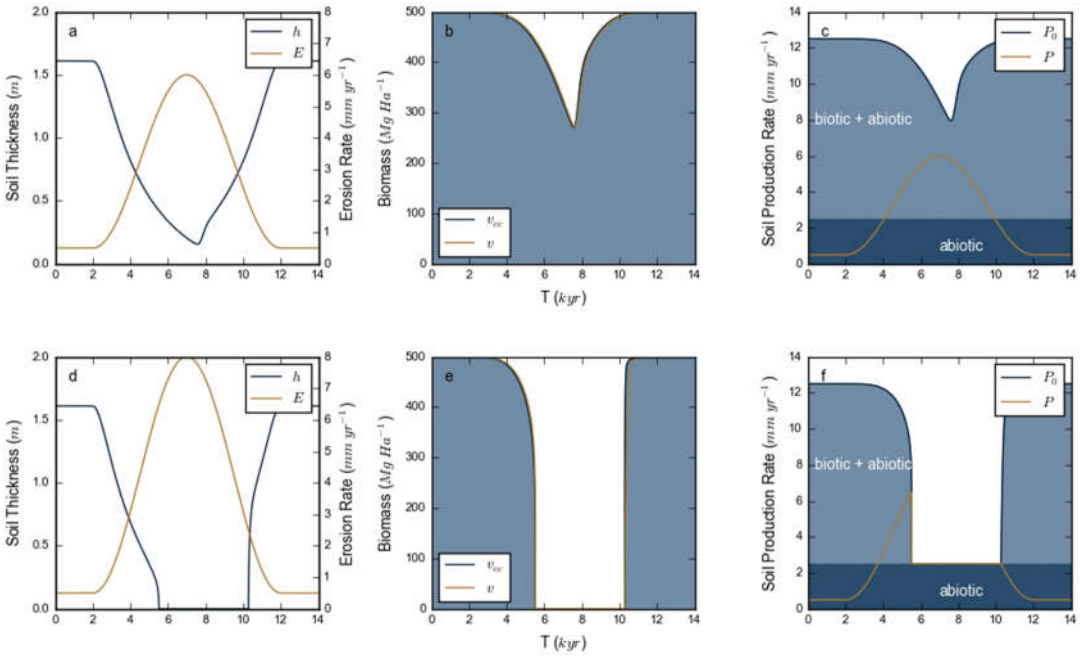

Figure 5.11 Evolution of model hillslope for two differing erosion rate histories; (a,d) soil thickness and erosion rate; (b,e) biomass and landscape carrying capacity; (c,f) Actual production rate and maximum production rate. In the first scenario (a-c), erosion rates are not sufficiently high to pass the soil-bedrock transition; in the second (d-f), this threshold is crossed.

soil thickness and are inversely correlated with erosion rates [*Meyer et al.*, 2007; *Gabet et al.*, 2015; Chapter 3; *Milodowski et al.*, 2015a]. I use a heuristic relationship to model this aspect of eco-geomorphic coupling in my model hillslope patch, in which the carrying capacity increases quickly as soil depths increase from zero, then approaches a regional limiting value, v_{max} [M L^{-2}], asymptotically as soil thickness ceases to be the limiting factor on landscape carrying capacity:

$$v_{cc} = v_{max}\left(1 - \exp(-\gamma h)\right) \quad (5.8).$$

The constant γ governs the rate at which carrying capacity increases with soil thickness, and therefore the range of soil thicknesses over which vegetation is sensitive

to change. A similar formulation was used by Pelak et al. [2016] to investigate the role of vegetation removal for agriculture on the stability of soils.

To explore the basic behaviour of this simplified model, I ran two simulations indicated in Figure 5.11, to test the response of the model hillslope to changing rates of erosion. In the initial model scenario, the erosion rate applied to the hillslope is increased, but not sufficiently to strip the soil, then decreased, according to a sinusoidal function (Figure 5.11a); in the latter scenario, I repeat the same experiment, but in this case increase the rate of erosion further, so that I drive the hillslope across the soil-bedrock transition (Figure 5.11d). In both cases, I start with a soil mantled hillslope that is fully vegetated (full details of the model parameters used are given in Table 5.1). The model is spun up so that h and v reach a steady state for the initial boundary conditions.

The coevolution of h, P, v and v_{cc} are illustrated in Figure 5.11a-c for the first model experiment, in which the hillslope maintains its soil mantle, and 5.11d-f, in which there is a soil-bedrock transition. In the first model scenario, in which a soil mantle is maintained, soil thickness on the hillslope patch gradually diminishes as the erosion rate increases, before recovering along a similar, albeit opposite, evolution pathway. In contrast, in second case, the evolution trajectory of the hillslope is markedly different. The response to increasing rates of erosion is similar, up to the point at which h (and therefore v_{cc}) decrease to such an extent that the soil is stripped completely. In both cases, the evolution pathways for the hillslope system exhibit hysteresis, but this effect is much more marked when the increase in erosion rates is sufficient to move the hillslope system across the soil-bedrock transition (Figure 5.12).

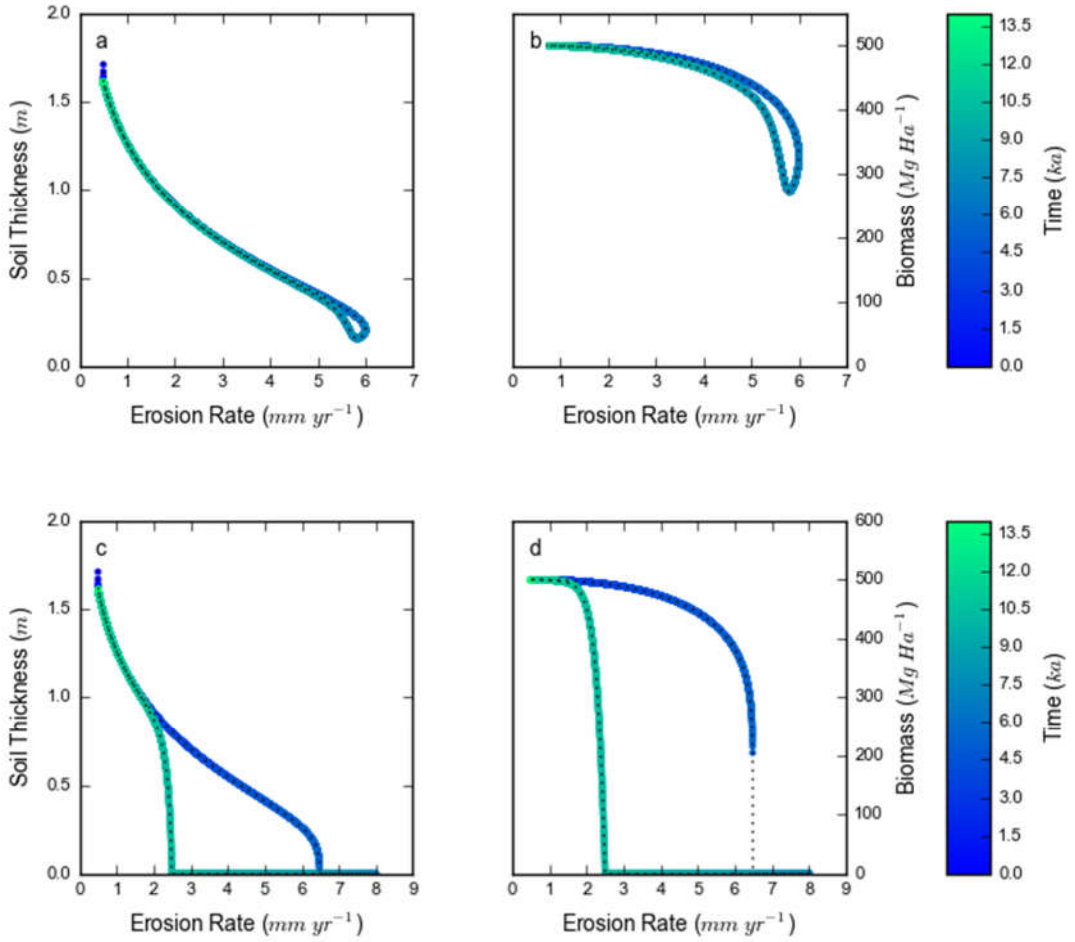

Figure 5.12 Evolution pathways for the two model scenarios: (a,c) coevolution of soil thickness and erosion rate; (b,d) coevolution of biomass and erosion rate. The upper plots (a,b) represent the evolution of the hillslope patch in the incomplete soil loss scenario; the lower plots (c,d) represent the total soil loss scenario. Both scenarios exhibit hysteresis, however the hysteresis loop is much more pronounced in the second (c,d) in which soil is completely stripped away at the highest erosion rates.

Without soil, the hillslope is not able to support vegetation; without the biogenic contribution towards soil production, the soil mantle (and v_{cc}) does not recover until much lower rates of erosion. Mapping out the evolution of h as a function of erosion rate through the simulation reveals that the model hillslope system exhibits multiple stable states at intermediate erosion rates, which are similarly evident in the phase

portraits for this system (Figure 5.13). As a result of the vegetation dependence of soil production rates built into the model, at these intermediate erosion rates a hillslope may either be soil mantled or bedrock depending on the base level change history.

The model developed here is clearly a gross simplification of real hillslopes. In particular, my approach does not model the lateral transfer of sediment across hillslopes, by which soil may gradually encroach onto neighbouring expanses of bedrock [*Gabet and Mudd*, 2010; *Deligne et al.*, 2013]. Likewise, I do not consider fractures in bedrock hillslopes, which provide potential footholds for vegetation, and thus may provide focal points from which a soil mantle gradually recovers more readily than would be suggested by this model [*Gabet and Mudd*, 2010]. This would undoubtedly add more complexity to the dynamics of the hillslope response, compared to those indicated here. Furthermore, using a more complex treatment of erosion, such as a stochastic disturbance regime to drive changes in vegetation and soil thickness [e.g. *Stark and Passalacqua*, 2014], may provide further insights into the stability of soils in rapidly eroding landscapes, and remains a target for future work. Nevertheless, the basic observations that (i) coexistence of bedrock and soil hillslopes is possible at intermediate rates of erosion without having to invoke small wavelength changes in the weathering dynamics of the substrate (although I do not refute that substrate variations are also important), and (ii) the path dependence of hillslope characteristics and resultant hysteresis exhibited in response to fluctuations in erosion rate, are both

features that I anticipate would be revealed by more complex model formulations and will be significant in the evolution of real landscapes.

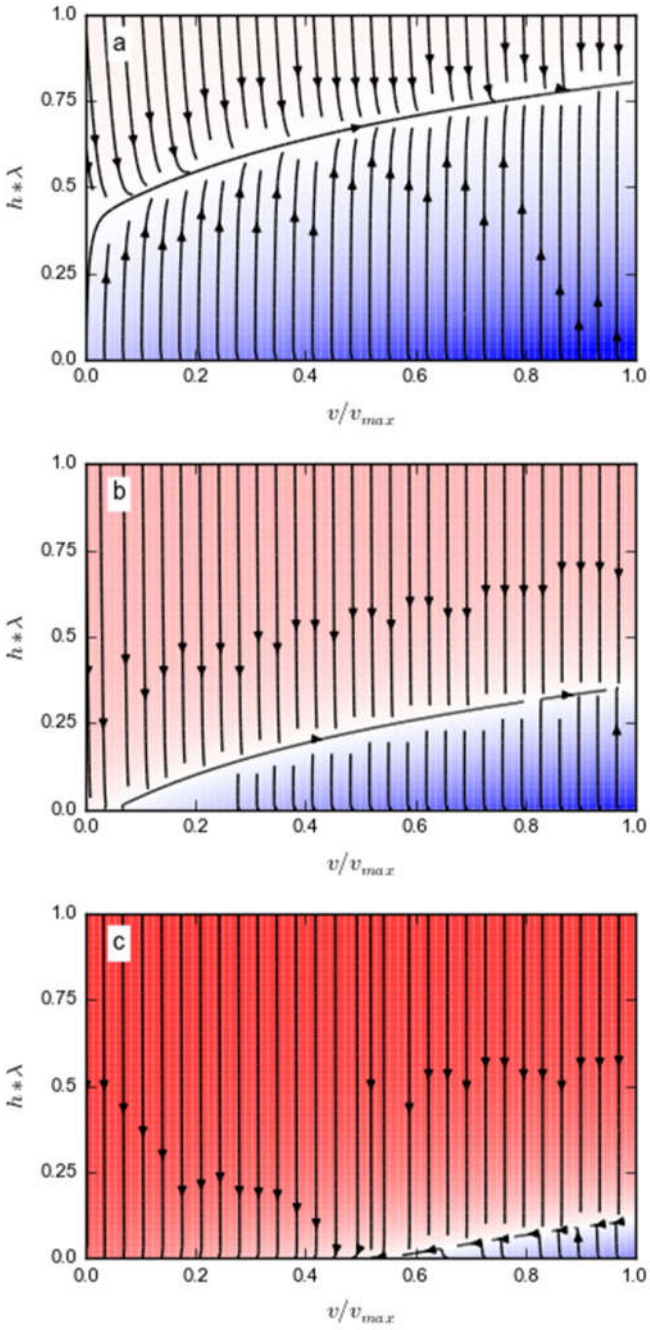

Figure 5.13 Phase portraits illustrating possible evolution trajectories for the model hillslope system under three erosion rates: (a) E = 0.5 mm yr^{-1}; (b) E = 3.0 mm yr^{-1}; (c) E = 8.0 mm yr^{-1}. A red background indicates parts of the parameter space in which soil thickness is decreasing; blue indicates soil thickness increasing.

5.5.5 Hillslope response times revisited

Perhaps one of the most significant impacts of the soil-bedrock transition suggested by this simple model is that of modifying the hillslope response time. Sediment transport on soil mantled landscapes can be well approximated by non-linear diffusive models [*Roering et al.*, 1999, 2001a; *Roering*, 2008; *Hurst et al.*, 2012]. Due to the presence of a continuous blanket of mobile colluvium, perturbations in base level readily propagate upslope [*Culling*, 1963, 1965]. In such systems, it is possible to calculate an expected hillslope response time based on estimated values of L_H, S_c and κ [*Roering et al.*, 2001b]. At the Feather River site, Hurst et al. [2012] thus estimated that the response time of soil mantled hillslopes in this landscape was of the order of 10^3 years and thus respond rapidly to the upstream propagation of base level changes through the channel network. However, once bedrock outcrops at the surface, the dynamics of sediment transport are constrained by bedrock properties [e.g. *Gilbert*, 1877; *Selby*, 1980; *Korup and Schlunegger*, 2009; *Larsen et al.*, 2010], which control the detachment of material from the substrate. Of particular importance in dictating bulk rock strength at the hillslope length scale is the abundance of fractures within the bedrock, providing an important link between present day geomorphic dynamics and bedrock deformation history [*Molnar et al.*, 2007; *Clarke and Burbank*, 2010].

Bedrock hillslopes will be differentially coupled to channel incision compared to soil mantled hillslopes, their timescale of response controlled by their progressive weakening through weathering, and erosion through mass wasting processes (bedrock landslides and rock falls) [*Moore et al.*, 2009]. If bedrock is structurally weak, or weathers rapidly, hillslopes may still

respond relatively quickly to changes in fluvial incision; however, if the bedrock is capable of withholding stresses over long timescales, the evolution of hillslopes may effectively be decoupled from fluctuations in fluvial incision, with bedrock canyon walls potentially persisting through multiple cycles of incision and aggradation [e.g. *Molnar et al.*, 2007; *Gabet*, 2014].

5.6 Conclusions

The Feather River catchment in the northern Sierra Nevada has become a well-established site for studying the effects of landscape disequilibrium, as a result of the striking gradient in erosion rates that spans an order of magnitude (20 – 250 mm kyr^{-1}) [*Riebe et al.*, 2000; *Yoo et al.*, 2011; *Hurst et al.*, 2012, 2013c; *Gabet et al.*, 2015; *Milodowski et al.*, 2015a, 2015b]. In this chapter I examined the ecological and geomorphic implications of the erosion rate gradient and the transition from soil mantled to bedrock hillslopes, specifically focusing on the role that lithology and biota play in mediating this transition. Echoing previous studies mapping the transition from soil-mantled to bedrock hillslopes [*DiBiase et al.*, 2012; *Heimsath et al.*, 2012; *Milodowski et al.*, 2015b], I find that the transition observed across the Feather River Site is gradual and patchy, and exhibits strong heterogeneity, whereby bedrock hillslopes frequently coexist adjacent to hillslopes with a near continuous soil mantle, despite their presumably similar base level histories.

Bedrock lithology is found to have a significant effect on both the ecological and geomorphological expression of the erosion rate gradient. Generalising the underlying geology into three primary lithology groups: two granitoid plutons, Bald Rock Pluton (trondhjemite-tonalite; BRP) and Cascade Pluton (quartz diorite; CP), intruded into

older Slate Creek Complex metamorphic and ophiolitic rocks (SCC), I find that BRP hillslopes typically possess higher degrees of rock exposure at a given rate of erosion compared to the other lithologies present. Interestingly, despite the similarity of CP to BRP in terms of age and petrogenesis, the characteristics of the soil-bedrock transition on hillslopes established on this pluton are much closer in resemblance to those of SCC. Likewise, hillslopes established on BRP bedrock support systematically lower levels of AGB.

Through my remotely sensed observations alone, I am not able to isolate a process level mechanism through which this pattern has become manifest in the landscape. Nevertheless, I suggest that hillslope characteristics may be strongly sensitive to the structure, texture and/or composition of plutonic rocks [e.g. *Godard et al.*, 2001; *Migoń*, 2006; *Hahm et al.*, 2014b; *Migoń and Vieira*, 2014]. Ultimately, to move beyond speculative arguments for the trends observed, the LiDAR-based datasets presented here need to be tied to other observations that can provide more insight into the characteristics of the underlying bedrock. Significant recent advances have been made using geophysical surveying techniques [*Clarke and Burbank*, 2010; *Holbrook et al.*, 2014; *Clair et al.*, 2015; *Parsekian et al.*, 2015], and detailed geochemical analyses [*Hahm et al.*, 2014b]. Integrating such techniques with high resolution topographic analyses permitted by airborne LiDAR provides an opportunity to explore the relationships between erosion, ecology and the processes of soil production in much greater detail. Additionally I note that after I have accounted for the effects of lithology, landscapes often display a profound degree of heterogeneity. Capturing the essence of this natural variability in numerical models of landscape evolution is a

major challenge, and understanding the source and nature of this variability presently represents a fundamental barrier to the development of predictive models.

The gradual emergence of bedrock in this landscape attests to the thinning of soils as hillslopes erode more rapidly. The negative correlation observed between hillslope erosion rates and AGB has a number of implications. Firstly, AGB and primary productivity scale in many landscapes [*Keeling and Phillips*, 2007], thus productivity and the capacity of the forest ecosystem to sequester carbon are likely to be diminished in more rapidly eroding parts of the landscape. Secondly, as variations in AGB also likely reflect variations in belowground biomass [*Hwang et al.*, 2015], I suggest a positive feedback whereby the capacity for biotic soil production decreases as erosion rates increase, exacerbating the resultant thinning of soil. Incorporating this coupling of vegetation and soil production into a highly simplified dynamical system model of a hillslope, I illustrate that hillslopes are inherently complex systems that possess multiple stable states, such that for intermediate rates of erosion, equilibrium hillslopes may be either soil mantled or bedrock. While the model developed in this study is clearly a simplification of real hillslopes, it leads to a number of potentially important conclusions. The evolution of hillslopes in response to base level forcing is path-dependent, and in response to cyclic forcing, the evolution trajectory of hillslope soils may therefore be highly nonlinear and display pronounced hysteresis. This has implications in considering the response time of hillslopes and their sensitivity to short timescale fluctuations in fluvial incision. In particular, in landscapes where a significant component of overall soil production is of biotic origin, hillslope responses may be much slower for hillslopes in which soil is stripped away, thus limiting biotic

soil production, compared to hillslopes that manage to retain a soil mantle, leading to the persistence of bedrock features observed in many landscapes.

Chapter 6. Discussion & Conclusions

6.1 Overview & Synthesis

This thesis explores how erosion, integrated over many thousands of years, dictates the geomorphic and ecological characteristics of hillslopes. In Section 1.2, I outlined a series of hypotheses regarding different aspects of the interconnectivity that exists between processes of soil production and erosion on hillslopes, and the vegetation that mantles them:

H1 Rapidly eroding hillslopes support forests with smaller canopies and lower aboveground biomass compared to hillslopes eroding at slower rates.

H2 As erosion rates increase and soil thickness consequently decreases, the degree of bedrock exposed on hillsides increases. At the landscape scale, this soil-bedrock transition is gradual and patchy, rather than abrupt.

H3 The expression of the above relationships, if present, in the Sierra Nevada landscape is modulated by lithology.

H4 Biotic soil production in forested landscapes helps maintain a soil mantle on rapidly eroding hillslopes.

In order to do this, I have exploited metre-scale, LiDAR-derived models of topography and canopy structure, permitting ecological and geomorphological observations to be made at the length scales that are relevant to hillslope processes, and developed a numerical model to investigate the coupling between erosion and biotic soil production. The focal point for this thesis is the landscape drained by the Middle Fork Feather River and tributaries in the northwest Sierra Nevada. This landscape exhibits

striking geomorphic gradients in relief, rock outcrop, hillslope gradient and hilltop curvature associated with spatial variations in erosion rate, ranging from 25 mm ka^{-1} to over 250 mm ka^{-1} [*Riebe et al.*, 2000; *Hurst et al.*, 2012]. The first order patterns in relief structure have been previously identified [*Riebe et al.*, 2000; *Hurst*, 2012; *Hurst et al.*, 2012, 2013b], with a low relief landscape typified by gentle, concave hillslopes, juxtaposed against a precipitous, high relief inner canyon, centred on the Middle Fork Feather River and its principal tributaries. The conclusions from this thesis build on this earlier work to provide a richer insight into the ecological impact of this erosion rate gradient in addition to exploring processes of soil production and the dynamics of the soil-bedrock transition. I address the key conclusions from the thesis below, before exploring their wider importance and implications (Section 6.2) and opportunities for future research (Section 6.3).

6.1.1 *H1*: Rapidly eroding hillslopes support forests with smaller canopies and lower aboveground biomass compared to hillslopes eroding at slower rates.

I demonstrate that spatial variations in erosion rate, integrated over millennial timescales, are a key driver of variance in the mixed conifer forests of the Northern Sierra Nevada. Long term erosion rates of small catchments in the Feather River Region, mapped using mean basin slope as an erosion rate proxy, are shown to explain a significantly greater proportion of the variance (32%) in the distribution of aboveground biomass (AGB) of the mixed conifer forest compared to other ecologically important variables such as microclimate and lithology. Observations from the north of the Feather River site by Gabet et al. [2015], made concurrently to

this thesis, indicate a reduction in AGB by approximately two thirds moving along a ridgeline transect along which apparent erosion rates, mapped with ridgeline curvature, decrease from ~60 mm ka^{-1} to ~520 mm ka^{-1}. This finding has a number of important implications, discussed in detail in Section 6.2.

Firstly, geomorphic gradients provide a potentially important source of variance in ecosystem. Hillslopes experiencing higher rates of erosion are shown to host lower forest AGB; AGB itself strongly correlates with rates of primary production in many landscapes [*Keeling and Phillips*, 2007; *Wang et al.*, 2011], therefore erosion rates are not only important from the perspective of carbon storage in vegetation, but are also likely important drivers of variability in productivity. Furthermore, vegetation is an active agent of soil production [*Gabet and Mudd*, 2010; *Hahm et al.*, 2014a; *Amundson et al.*, 2015] and has been suggested to play a key role in a maintaining soil mantle in rapidly eroding settings [*Heimsath et al.*, 2012; *Larsen et al.*, 2014a]. If the decrease in AGB is accompanied by a similar drop in the power of biotic soil production, this presents a potentially important feedback modulating the response of hillslope soils to changes in erosion rate.

6.1.2 *H2*: As erosion rates increase and soil thickness consequently decreases, the degree of bedrock exposed on hillsides increases. At the landscape scale, this soil-bedrock transition is gradual and patchy, rather than abrupt.

I developed a novel method to map rock exposure on hillslopes from high resolution digital elevation models based on surface roughness, characterised using the local

variability of surface normal vectors. This was shown to be a powerful tool to locate areas of rock outcrop emerging through a smooth soil mantle that complements existing methods based solely on local topographic slope [*DiBiase et al.*, 2012]. I then show that in both the Feather River landscape, and another transient landscape in Idaho, the soil-bedrock transition is gradual and patchy, with the steep slopes of the more rapidly eroding parts topography supporting a patchwork of rock outcrop and soil. This patchy transition from soil mantled to bedrock hillslopes contradicts the expectation from the traditional models for soil production employed in landscape evolution models, in which soil production is treated as a continuum the rate of soil production is considered to decrease exponentially with increasing soil depth. However, it corroborates observations of a patchy soil-bedrock transition in the San Gabriel Mountains [*DiBiase et al.*, 2012; *Heimsath et al.*, 2012], and finds agreement with the expectations from hillslope models in which the formulation of soil production includes a representation of biotic processes [*Gabet and Mudd*, 2010; *Stark and Passalacqua*, 2014; *Pelak et al.*, 2016].

6.1.3 *H3*: The expression of the above relationships, if present, in the Sierra Nevada landscape is modulated by lithology.

Exploring the eco-geomorphic response to variations in fluvial incision in more detail, I demonstrate that there are marked differences in the hillslope characteristics that cannot be explained solely due to changes in erosion rate: bedrock lithology is an important determinant of both the ecological and geomorphological properties of hillslopes. The geology of the Feather River site comprises two granitoid plutons (Bald Rock Pluton, BRP, and Cascade Pluton, CP) of Jurassic age, intruded into early

Jurassic metamorphic and ophiolitic rocks of the Slate Creek Complex (SCC). Rock exposure is significantly more abundant above BRP, with AGB systematically lower, whereas there is greater similarity in the characteristics of CP and SCC hillslopes. While the role of lithology is particularly evident across lithological boundaries, significant heterogeneity is also exhibited by hillslopes within a single geologic unit, indicating that substrate variance manifest within the same geological unit may also be important.

6.1.4 *H4*: Biotic soil production in forested landscapes helps maintain a soil mantle on rapidly eroding hillslopes.

Considering (i) the decrease in AGB observed across the erosion gradient in the Feather River site; (ii) that belowground biomass tends to scale with the aboveground component [e.g. *Hwang et al.*, 2015]; and (iii) that decreases in soil thickness in the Sierra Nevada correlate with reduced stand density [*Meyer et al.*, 2007] and AGB [*Gabet et al.*, 2015], I posit that biotic soil production becomes limited as erosion rates increase. Incorporating this eco-geomorphic coupling of soil production into a simplified dynamical systems model [e.g. *Stark and Passalacqua*, 2014], I demonstrate that soils, and the forests they support may exhibit multiple stable states: at relatively slow erosion rates, hillslopes are uniformly soil mantled; at very high erosion rates, hillslopes are uniformly bedrock; at intermediate erosion rates, both bedrock and soil mantled hillslopes are stable hillslope configurations. Thus, hillslope evolution, and the soil-bedrock transition, is path dependent; once exposed at the surface, significant patches of bedrock exposure may persist over a wide range of incision rates.

6.2 Importance & Wider Implications

6.2.1 Geomorphic controls on forest structure and ecology

Within the geomorphology community, rates of erosion have been widely acknowledged as one of the fundamental controls on topographic form and on critical zone characteristics such as soil thickness and weathering extent (see review in Section 1.3, and references therein), offering several pathways through which they may place a "bottom-up" control on ecosystem properties. However, the ecological importance of erosion rates was previously unconstrained.

In the Feather River Region, the structure of the mixed conifer forest is intimately tied to the physical characteristics of the landscape. In part, this is due to the annual climatic undulations between wet winters and hot, dry summers, which require vegetation to source water from the substrate throughout a significant proportion of the year [*Jones and Graham*, 1993; *Royce and Barbour*, 2001; *Rose et al.*, 2003; *Witty et al.*, 2003; *Graham et al.*, 2010; *Goulden et al.*, 2012; *Holbrook et al.*, 2014; *Kelly and Goulden*, 2016]. The extent of saprolite weathering and the thickness of soils, and therefore the magnitude of these moisture stores, is closely tied to erosion rates, due to the fundamental control of the latter on residence times of material in the critical zone [e.g. *Heimsath et al.*, 1997, 2012; *Pelletier and Rasmussen*, 2009b; *Mudd and Yoo*, 2010a; *Yoo et al.*, 2011; *Rempe and Dietrich*, 2014; *Attal et al.*, 2015; *Gabet et al.*, 2015]. Within the Feather River site, observations of the chemical depletion of saprolite at the base of soil pits indicates that weathering extent in this setting confirm this expected inverse relationship between saprolite development and erosion rate [*Yoo et al.*, 2011]. Tile probe surveys along a ridgeline in the north of the site (Cascade

Ridge), which spans the erosion gradient present, indicate a general decrease in soil thickness from >1 m to <30 cm as erosion rates increase [*Gabet et al.*, 2015]. Superimposed on this negative trend, both soil moisture content and residual soil thickness oscillate according to the local topographic position along the ridgeline: topographic nobs are typically dryer, with shallower soils; saddles generally host thicker soils with a higher moisture content [*Gabet et al.*, 2015]. Higher regolith moisture content promotes weathering and development of porosity in bedrock [*Graham et al.*, 2010], increasing the hospitability of the substrate to vegetation, promoting a positive feedback in which further weathering, facilitated by both moisture and vegetation, increases local moisture storage [*Gabet et al.*, 2015].

Thus, in landscapes, such as the Sierra Nevada, where vegetation is strongly reliant on groundwater moisture storage [*Graham et al.*, 2010; *Kelly and Goulden*, 2016], I postulate that the control on water availability is the most likely causal mechanism through which the evidently strong correlation between AGB and erosion rates is manifest. In doing so, I acknowledge that other mechanisms (such as nutrient limitation and disturbance) may also provide significant linkages both in this and other settings [e.g. *Porder et al.*, 2007, 2015; *Porder and Chadwick*, 2009; *Dislich and Huth*, 2012; *Hilton et al.*, 2013; *Hahm et al.*, 2014a]. The relative strengths of these competing controls, both relative to each other, and climatic or anthropogenic factors, are likely to vary significantly depending on the climatic and geologic setting. By controlling moisture availability, gradients in erosion rate may also drive spatial variability in the sensitivity of forest communities to drought in water limited

environments. In turn, this may drive differences in drought mortality and susceptibility of trees to diseases and pests [*Dale et al.*, 2001].

Alternatively, variations in erosion rate may drive changes in forest community composition such that drought tolerant species are favoured on more rapidly eroding hillslopes, just as the species composition of forest ecosystems is sensitive to microclimate in moisture or temperature limited conditions [*Stephenson*, 1990; *Urban et al.*, 2000; *Franklin*, 2003]. Casual observations within the Feather River landscape suggest that compositional gradients are also present, spanning the erosion rate gradient that is so prominent in the landscape, with xeric manzanita (*Arctostaphylos spp.*) shrubs more prevalent along rapidly eroding ridgelines, gradually replaced by an increasing abundance of oaks (*Querqus kelloggii, Querqus chrysolepis*) and more mesic conifers (*Pinus spp., Pseudotsuga menziesii, Calocedrus decurrens*) [*Gabet et al.*, 2015; *Milodowski et al.*, 2015a]. The plot sizes used in this study for the LiDAR calibration [Chapter 3; *Milodowski et al.*, 2015a] are too small, and too few in number, to make robust inferences regarding changes in species composition [*Chave et al.*, 2003], but this could become a target for future LiDAR-based investigation.

6.2.2 Lithology and eco-geomorphic feedbacks modulate soil-bedrock transition

The traditional approach by which soil production processes are incorporated into landscape evolution models is to consider the rate of lowering of the bedrock-soil interface as decreasing exponentially with soil thickness [e.g. *Heimsath et al.*, 1997]. In this scenario, the maximum soil production rate serves as a threshold erosion rate beyond which soil is stripped. The expectation in this scenario is that there should be

an abrupt soil-bedrock transition as erosion rates increase across this threshold. I find limited evidence to support this. Rather, the transition is spatially heterogeneous, even at the hillslope scale, with a patchy transition from soil mantle to bedrock. Models that incorporate erosion and soil production as discrete events [e.g. *Strudley et al.*, 2006a, 2006b; *Gabet and Mudd*, 2010] are able to simulate the patchy transition, and some workers have hypothesised that the maintenance of a soil mantle is permissible as a consequence of efficient biogenic soil production [*Gabet and Mudd*, 2010; *Yoo et al.*, 2011; *Heimsath et al.*, 2012; *Larsen et al.*, 2014a; *Gabet et al.*, 2015]. Variations in bedrock structure and composition, arising through both inter- and intra-lithological heterogeneity, may also impose localised variability on the efficacy of soil production processes [*Ahnert*, 1987; *Norton et al.*, 2008; *Hahm et al.*, 2014a].

The decrease in AGB observed across the erosion rate gradient may also have significant feedbacks into the dynamics of soil production. Vegetation promotes the formation and maintenance of soils, both through root networks raising reinforcement, binding together and therefore stabilising disaggregated material on hillslopes [e.g. *Schmidt et al.*, 2001; *Gray and Barker*, 2004; *Hales et al.*, 2009], and through actively driving the physical [e.g. *Bennie*, 1991; *Zwieniecki and Newton*, 1995; *Gabet and Mudd*, 2010; *Roering et al.*, 2010] and chemical [e.g. *Bonneville et al.*, 2009; *Taylor et al.*, 2009] breakdown of bedrock. Canopy height and AGB strongly correlate with below ground root biomass [*Lefsky et al.*, 2005; *Hwang et al.*, 2015]. While the functional relationship linking vegetation, soil thickness and soil production rates is likely to be complex, spatial variations in AGB are likely to drive spatial variations in the biotic contribution to the production of soil from bedrock. All else being equal,

soil production rates under a forest canopy are therefore likely to be greater than on un-vegetated hillslopes [*Gabet and Mudd*, 2010; *Amundson et al.*, 2015]. A clear bedrock dependence on the soil-bedrock transition is therefore expected. For example, where bedrock is weak or highly fractured, the relative ease with which vegetation can become established will enable more rapid recovery of soils following disturbance [*Gabet and Mudd*, 2010; *Larsen et al.*, 2014a], while enhanced rates of both biotic and abiotic soil production will help to sustain a soil mantle at higher erosion rates [*Marshall and Roering*, 2014; *Rempe and Dietrich*, 2014].

This coupling of vegetation and hillslopes, arising through the reliance of plants on having a hospitable substrate from which to extract both nutrients and water, and through the active role in soil production and maintenance performed by plants gives rise to complexity in the evolution of hillslopes in response to geomorphic forcing. In this thesis, I have only begun to explore this aspect, considering the impact of a gradual increase and decrease in erosion rates on the coevolution of hillslope soils and vegetation. However, these simple experiments illustrate a strong path dependence of the characteristics and evolution trajectories of hillslope systems, with a range of erosion rates over which bare bedrock hillslopes may coexist with soil mantled hillslopes, without having to appeal to variations in the parameterisation of soil production processes. Hysteresis in the evolution of soil thickness and biomass is observed in the behaviour of both the model experiments presented in Chapter 5, however this is much more pronounced when erosion rates are increased sufficiently to strip soil and expose bedrock. Note that this is a different mechanism to that which caused the hysteresis observed by Hurst et al. [2013a], who noted that the transient

adjustment of soil mantled hillslopes responding to changes in base level forcing was also path dependent. Superimposing the observations in the eco-geomorphic dynamics of soil production, one might expect that this latter hysteresis behaviour to be even more pronounced if erosion rates are increased sufficiently to force hillslopes across the soil-bedrock transition; extensive bedrock hillslopes are a persistent feature in many landscapes following periods of canyon incision [e.g. *Molnar et al.*, 2007; *DiBiase et al.*, 2014b; *Gabet*, 2014; *Baynes et al.*, 2015]. Moreover, emergent landscapes nonlinearities in the evolution of hillslopes poses a challenge in the development of predictive landscape evolution models, since relatively small changes in climatic, anthropogenic or geomorphic forcing may generate abrupt and potentially long lasting responses, depending on the stability of the hillslope system [*Schumm*, 1979; *Thornes*, 1983; *Scheffer et al.*, 2001].

In real landscapes, erosion typically occurs in discrete events during which parcels of sediment are entrained and transported downslope [e.g. *Benda and Dunne*, 1997; *Hovius et al.*, 2000; *Strudley et al.*, 2006a; *Gabet and Mudd*, 2010; *Tucker and Bradley*, 2010]. Likewise, forest ecosystems are periodically disturbed, as a result of storms, fires, disease, drought and geomorphic disturbances [e.g. *Dale et al.*, 2001; *Breshears et al.*, 2005]. Incorporating a more realistic, stochastic treatment of the dynamics of both erosion and vegetation within the simple dynamical system presented in Chapter 5 may yield some further insights into the complexity of hillslope systems, and the role of disturbance regimes in driving landscape heterogeneity [*Stark and Passalacqua*, 2014].

6.2.3 Limitations for topographic analysis

The evolution of landscape reflects the time-integrated effect of competing geomorphic processes that sculpt topography through the erosion, transport and deposition of sediment [*Tucker and Bras*, 1998; *Perron et al.*, 2009]. One of the fundamental challenges within quantitative geomorphology is to uncover and exploit functional relationships between the resultant topographic form and geomorphic process. Such relationships can potentially be used to make inferences into past and future landscape dynamics, for example, to predict rates of geomorphic change and to constrain other physical properties of landscapes, such as soil thickness [e.g. *Ahnert*, 1970; *Kirby and Whipple*, 2001; *Roering et al.*, 2007; *Pelletier and Rasmussen*, 2009a; *Perron et al.*, 2009; *DiBiase and Whipple*, 2011; *Hurst et al.*, 2012; *Crouvi et al.*, 2013].

By resolving the morphology of the earth surface at the sufficiently high resolution required to resolve active geomorphic processes, LiDAR greatly facilitates the extraction of meaningful topographic metrics [e.g. *Slatton et al.*, 2007; *Perron et al.*, 2009; *Roering et al.*, 2010; *Hurst et al.*, 2012]. However, in the absence of repeat surveys, inference of landscape evolution histories often requires ergodic assumptions [e.g. *Hurst et al.*, 2013a]. Thus, the predictive capacity of these approaches are limited by the fact that real landscapes are inherently complex, whereas the theoretical models that underpin process-based topographic approaches are necessarily simplified; sources of heterogeneity are poorly understood, and any constraints on the amplitude of the resultant variability that these heterogeneities provide are at best weak. This problem is confounded given the stochastic nature of sediment transport processes

[*Benda and Dunne*, 1997; *Kirchner et al.*, 2001]. Additional challenges are posed by the emergence of bedrock, which indicates a major process transition away from hillslopes for which sediment transport is transport limited, towards hillslopes that are detachment limited, their evolution governed by the bulk strength and rate of breakdown of the constituent rock [*Schmidt and Montgomery*, 1995; *Dietrich et al.*, 2003; *Binnie et al.*, 2007]; this presents further complications that are only beginning to be addressed [*Molnar et al.*, 2007; *Clarke and Burbank*, 2010; *Hahm et al.*, 2014a; *Clair et al.*, 2015].

In the case of hillslopes, significant progress has been made within individual soil mantled landscapes, where relatively close agreement has been demonstrated between theoretical models that treat sediment transport as a non-linear diffusive flux (approximating a linear diffusion flux at low topographic gradients) [*Roering et al.*, 2007; *Roering*, 2008; *Pelletier and Rasmussen*, 2009b; *Pelletier et al.*, 2011; *Hurst et al.*, 2012, 2013a, 2013b; *Ma et al.*, 2013; *West et al.*, 2013, 2014; *McGuire et al.*, 2014]; however we lack the functional understanding to extrapolate calibrated models into landscapes with differing climate, vegetation, lithology [*Hurst et al.*, 2013b]. This body of research directly addresses this knowledge gap: in showing that the soil-bedrock transition associated with increasing erosion rates is gradual and patchy, I provide an important test for models of soil production; in exploring how lithology is modulating this transition, I add to a growing body of recent research that is highlighting sources of rich heterogeneity in the dynamics of landscape evolution [e.g. *Heckman and Rasmussen*, 2011; *Dosseto et al.*, 2012; *Hahm et al.*, 2014a; *Marshall and Roering*, 2014].

In Chapter 5, I have demonstrated that in the northern Californian Sierra Nevada, lithological variations drive significant heterogeneity is exhibited both in terms of the ecological and geomorphic characteristics of hillslopes. A bedrock control on both forest ecosystems and rock exposure has been illustrated, with marked differences across the contacts of granitoid plutons with differing phosphorous availability [*Hahm et al.*, 2014a]. However, I also show that after accounting for variations in erosion rate, there is a strong degree of heterogeneity *within* an individual geological unit – exposed bedrock walls sit side by side with fully vegetated, soil mantled hillslopes. Such striking heterogeneity may be driven either through non-linear coupling of ecological and geomorphic processes, as illustrated by the numerical model presented in Chapter 5, through small scale variations in the structure or composition of the substrate, or – as I suspect is most likely – both. This intrinsic variability limits the predictive capacity of geomorphic models, and thus topographic analysis techniques for which they underpin because ergodic assumptions break down; uncertainties are exacerbated if methods are extrapolated to other landscapes without independent constraints to parameterise the relevant functional relationships.

6.2.4 LiDAR as a tool for exploring the critical zone

The majority of the research encompassed in this thesis is underpinned by quantitative analysis of high resolution data describing sub-metre scale variations in topographic form and canopy architecture derived from LiDAR surveys. The detail LiDAR surveys provide regarding both topography and forest structure make this technology ideally suited to interdisciplinary research bridging Geomorphology and Ecology [e.g. *Lefsky et al.*, 2002; *Lim et al.*, 2003; *Slatton et al.*, 2007; *Harpold et al.*, 2015;

Passalacqua et al., 2015; *Taylor et al.*, 2015], as outlined in detail in Section 1.5. LiDAR is an incredibly powerful tool for generating empirical observations and trends with which to test theoretical relationships, and explore new hypotheses; in this thesis, I was able to map out the covariations of hillslope form, rock exposure, aboveground biomass and erosion rate; the emergent trends illustrate important aspects concerning the dynamics of hillslope evolution, soil production and vegetation.

However, there are a number of notable limitations that should be considered in research design, but nevertheless provide opportunities for future work [e.g. *Roering et al.*, 2013]. In particular, while LiDAR captures both detailed canopy structure and surface topography in three dimensions, the lower extent of the critical zone descends below the surface. The characteristics of this belowground component, such as the thickness and variability of soil, and the composition and mechanical properties of the underlying saprolite, cannot be interrogated directly using LiDAR data alone. Based on our understanding of how the architecture of the critical zone functions, it is possible to make informed hypotheses as to the underlying mechanism driving emergent geomorphological and ecological trends picked out by LiDAR surveys. However, in order to provide more concrete constraints there is a clear and present need to integrate a wider range of technologies to generate a fuller picture of critical zone architecture. Geophysical techniques that provide are able to provide an image of what lies beneath our feet, in particular shallow seismic refraction surveys and ground penetrating radar, offer tremendous potential in this regard [*Clarke and Burbank*, 2010, 2011; *Roering et al.*, 2010; *Holbrook et al.*, 2014; *Clair et al.*, 2015; *Parsekian et al.*, 2015]. Likewise, the development of full-waveform, multispectral

LiDAR [e.g. *Mallet and Bretar*, 2009] has the potential to yield greater insights into the nutrient and moisture status of vegetation [*Wallace et al.*, 2012, 2014], which in turn enables more detailed links to be made regarding landscape scale controls on forest ecosystems [e.g. *Asner et al.*, 2015].

6.3 Research Opportunities & Future Work

6.3.1 Constraining mechanistic links between hillslope erosion rates, weathering, soil production and ecosystem function

In the Feather River landscape, I demonstrate that hillslope erosion rates are strongly coupled to the biosphere: as erosion rates increase across the geomorphic gradient, hillslopes support less AGB, and there are fewer large trees. The underlying mechanism linking forest structure to erosion rates was hypothesised to be a driven by reduced moisture storage capacity in more rapidly eroding parts of the landscape, as a result of the reduced residence time of material moving through the critical zone, during which it is exposed to weathering. This hypothesis is supported by existing observations of soil thickness [*Gabet et al.*, 2015] and saprolite weathering extent [*Yoo et al.*, 2011] across the erosion rate gradient. Forests in the Sierra Nevada are particularly sensitive to levels of accessible groundwater storage because vegetation is reliant on this moisture store through the dry summer months [*Rose et al.*, 2003; *Graham et al.*, 2010; *Bales et al.*, 2011; *Kelly and Goulden*, 2016]. Future work in this area should attempt to test this hypothesis by utilising alternative, complimentary methodologies that are able to yield more specific detail into variations in soil and saprolite thickness and the temporal dynamics of moisture usage by trees.

Geophysical surveys that are able to provide an image of the subsurface promise have the potential to be particularly powerful tools to constrain the characteristics of the soil, saprolite and underlying bedrock [*Parsekian et al.*, 2015]. Weathering of bedrock acts to increase porosity and leads to the alteration of primary minerals to secondary weathering products, such as clays. These act reduce the propagation velocity of seismic waves, and tend to reduce the electrical resistivity [*Olona et al.*, 2010]. As a result, both shallow seismic refraction and electrical resistance tomography surveys have the potential to investigate spatial variations of regolith thickness [*Befus et al.*, 2011; *Holbrook et al.*, 2014]. In the Colorado Frontal Ranges, Befus et al. [2011] used a series of geophysical survey transects in two contrasting catchments to test how both microclimate and fluvial incision impact on regolith thickness. Geophysical surveys have also been used to provide constraints on the distribution and pervasiveness of bedrock fractures [*Clarke and Burbank*, 2010, 2011; *Clair et al.*, 2015], which may help to tease apart the underlying causes of the lithological control on the geomorphic and ecological characteristics of hillslopes in the Feather River site.

In addition to geophysical surveys, a more detailed picture of the architecture of the critical zone would be gained by a more detailed consideration of the vegetation changes. In this thesis, variations in forest structural characteristics were explored using relatively simple canopy-based metrics. More complex treatments of the canopy point cloud, for example the segmentation of individual trees [e.g. *Brandtberg*, 2007; *Li et al.*, 2012; *Jakubowski et al.*, 2013; *Khosravipour et al.*, 2014], or quantification of canopy gap dynamics [*Koukoulas and Blackburn*, 2004; *Schliemann and Bockheim*, 2011; *Asner et al.*, 2013], coupled with rigorous field surveys documenting variations

in species composition, would help to highlight how forest communities adapt to differing rates of erosion in the Feather River landscape.

Further insight could be obtained through analysis of the thickness and isotopic composition of tree rings [*McCarroll and Loader*, 2004], which could indicate temporal variations in growth rates and moisture provenance through the growing season [*Tang and Feng*, 2001; *Marshall and Monserud*, 2006; *Brooks et al.*, 2010; *Singer et al.*, 2013]. In Sierra Nevada forests, soil moisture tends to be exhausted before saprolite moisture is depleted [*Rose et al.*, 2003; *Graham et al.*, 2010]. Using changes in the isotopic composition of tree rings, it may be possible to document how the source of moisture utilised by trees varies according to tree species [*Marshall and Monserud*, 2006] and how this changes through the course of the summer dry season [*Singer et al.*, 2013]. If the water source can be isolated using the isotopic composition of tree rings, it should be possible to investigate how the temporal dynamics of water use vary across the erosion rate gradient, and test whether vegetation established on more rapidly eroding hillslopes is more sensitive to drought stress.

A corollary of the hypothesis proposed here that moisture-limitation links erosion rates and ecosystems is that this mechanism should be sensitive to climate. The Feather River site annually receives ~1750 mm of rainfall a year, with an extended hot, dry summer; drier climates, such as those found 700 km to the south in the San Bernardino and San Gabriel Mountains, ecosystems are potentially more acutely tied to the geomorphic evolution of landscapes; in wetter climates. Where moisture is available throughout the year, this proposed mechanism may well be weaker, although even in tropical environments covariation of AGB and topography suggests that the

availability of water is still an important factor governing the growth and productivity of forests [*Detto et al.*, 2013], while water storage capacity also mediates the impact of droughts on tree mortality [*Slik et al.*, 2002]. Undertaking comparative studies along erosion rate gradients in additional landscapes has the potential to start testing these hypotheses and in doing so, help to constrain one aspect of the interconnectivity that exists between geomorphology, climate and ecosystems.

6.3.2 Eco-geomorphic cascades: the ecological impact of geomorphic gradients in other settings

Geomorphic controls on moisture availability is just one mechanistic pathway through which the dynamics of landscape evolution may cascade through the biosphere. In tropical regions, gradients in erosion rate and soil age drive variations in landscape biogeochemistry, disturbance frequency and nutrient availability that in turn impact on plant functional traits, forest biomass and biodiversity [*Vitousek et al.*, 2003; *Porder et al.*, 2005a, 2007, 2015; *van de Weg et al.*, 2009; *Hilton et al.*, 2011, 2013; *Asner et al.*, 2014, 2015; *Weintraub et al.*, 2014; *Brocard et al.*, 2015]. Differences in the functional traits of forest ecosystems [*Asner et al.*, 2014, 2015] imposed by their geomorphic setting, could potentially drive both inter- and intra-landscape heterogeneity in their resilience and response to environmental pressures, such as climate change [*Ostle et al.*, 2009]. In the Amazon-Andes corridor, a 3300m elevation gradient stretching from the Amazon lowlands into the Andes Mountains, plant functional traits exhibit marked gradients: moving upwards in elevation, canopy heights (and therefore likely AGB) decrease, with a structural shift towards smaller plants, increased understory and increasing incidence of canopy gaps, reflecting

changes in disturbance by landslides, light availability, soil fertility and temperature [*Gentry*, 1988; *Asner et al.*, 2014]. While elevation is often the dominant control at the macro-scale, elevation gradients such as these commonly exhibit significant levels of geomorphic and lithological variability not only moving upslope, but critically, also within a given elevation range [*Stephenson*, 1990; *Urban et al.*, 2000; *Macias-Fauria and Johnson*, 2013; *Asner et al.*, 2014; *Hahm et al.*, 2014a; *Brocard et al.*, 2015; *Taylor et al.*, 2015]. One well documented ecosystem response of vegetation in response to climate change is the gradual upslope movement of forest communities, tracking the shift in their optimal climate window [*Feeley et al.*, 2011]. Therefore, understanding geomorphic and lithological controls on plant functional traits and biodiversity is not only important when considering the impacts on ecosystem response to changes in climate in their present location, but also in understanding how the structure, composition and resilience of forest communities may change in the future as they shift in response to these changes.

Until recently, investigating the coupling of ecological and landscape dynamics has been hugely challenging, due to the difficulties in sampling sufficiently across relevant landscape scales. LiDAR-based studies, including this thesis, have demonstrated huge potential to start addressing this knowledge gap and are starting to provide important constraint on landscape controls on ecosystem function and composition [*Porder et al.*, 2005b; *Vitousek et al.*, 2009; *Kellner et al.*, 2011; *Detto et al.*, 2013; *Asner et al.*, 2014, 2015; *Gabet et al.*, 2015; *Harpold et al.*, 2015; *Taylor et al.*, 2015]. Moreover, the role that geomorphology plays in the development of ecosystems and their sensitivity to change is only beginning to be explored; this linkage between landscape

dynamics, climate and the biosphere, both in tropical forests and elsewhere, provides a critical avenue for future research. As availability of worldwide LiDAR datasets increases, facilitated by recent movements towards increasing the level of open access to data within the USA and Europe in particular, many more opportunities are opening up to examine the connections between life and landscape.

6.3.3 Numerical modelling of eco-geomorphic coupling

Inversion of landscapes to inform geomorphic dynamics is inherently difficult because we only see a "snapshot" of a landscapes evolution through time, whereas sediment transport processes are stochastic and therefore it unlikely to be adequately represented in observational records [*Hicks et al.*, 2000; *Hovius et al.*, 2000; *Kirchner et al.*, 2001]. Numerical models therefore provide an important means of exploring the temporal dynamics of landscape evolution that complement observations made in real landscapes [*Dietrich et al.*, 2003; *Tucker and Hancock*, 2010]. In chapter 5, I introduced a simple dynamical systems model for a hillslope that incorporated the co-dependency of vegetation and soil production. Incorporating a more realistic, stochastic erosion and disturbance regime into this would permit the investigation of how disturbance processes, such as fire and landslides [*Stark and Passalacqua*, 2014], or land use change [*Pelak et al.*, 2016], potentially couple into soil production on hillslopes, and on the post-disturbance recovery of soils and vegetation.

6.4 Conclusions

The principal conclusions from this thesis are:

1. *Geomorphic gradients drive ecological gradients*

   Within the mixed conifer forests of the Californian Sierra Nevada, pronounced gradients in erosion rate impose a fundamental control on forest structure: hillslopes eroding more rapidly support lower aboveground biomass. In environments where precipitation is strongly seasonal, this is likely to be driven, at least in part, through diminished moisture storage capacity in soil and saprolite underlying rapidly eroding hillslopes.

2. *Topographic roughness provides a topographic signature of the emergence of bedrock*

   The emergence of bedrock on hillslopes indicates a process transition from transport-limited to detachment-limited sediment transport processes. This generates a diagnostic increase in the local roughness of the surface, which can be exploited to map out the spatial distribution of bedrock outcropping at the surface.

3. *As erosion rates increase, hillslopes gradually expose more bedrock*

   Hillslopes in rapidly eroding landscapes comprise a mosaic of soil and bedrock; the transition from a continuous soil mantle to full bedrock hillslopes is gradual and patchy. These dynamics cannot be captured by simple

exponential models of soil production [e.g. *Heimsath et al.*, 1997] and thus represent a challenge for models of landscape evolution.

4. *Lithology is an important determinant of the ecological and geomorphological properties of hillslopes*

   Both the dynamics of the soil-bedrock transition and forest structure are dependent on the nature of the underlying geology. The underlying mechanism through which this dependence is imposed remains to be determined by future work; however, differences in texture, composition and fracture density may all drive variability in susceptibility of bedrock to weathering and its hospitability to vegetation. Significant heterogeneity is also exhibited at the intra-lithological level.

5. *Coupling of vegetation and soil production drives complexity in the hillslope response to base level change*

   Vegetation is an active geomorphic agent, driving soil production and stabilising soil on hillslopes. Positive feedbacks between biotic soil production and soil thickness generate complex, path-dependent responses to geomorphic forcing; in response to cyclic forcing, the evolution trajectory of hillslope soils may display pronounced hysteresis, particularly if forced across the soil-bedrock transition. Eco-geomorphic coupling therefore provides a potentially important and non-linear impact on the evolution of hillslopes.

References

Adams, H. D., M. Guardiola-Claramonte, G. A. Barron-Gafford, J. C. Villegas, D. D. Breshears, C. B. Zou, P. A. Troch, and T. E. Huxman (2009), Temperature sensitivity of drought-induced tree mortality portends increased regional die-off under global-change-type drought, *Proc. Natl. Acad. Sci.*, *106*(17), 7063–7066, doi:10.1073/pnas.0901438106.

Ahnert, F. (1970), Functional Relationships Between Denudation, Relief, and Uplift in Large Mid-Latitude Drainage Basins, *Am. J. Sci.*, *268*(3), 243–263.

Ahnert, F. (1987), Approaches to dynamic equilibrium in theoretical simulations of slope development, *Earth Surf. Process. Landf.*, *12*(1), 3–15, doi:10.1002/esp.3290120103.

Albani, M., B. Klinkenberg, D. W. Andison, and J. P. Kimmins (2004), The choice of window size in approximating topographic surfaces from Digital Elevation Models, *Int. J. Geogr. Inf. Sci.*, *18*(6), 577–593, doi:10.1080/13658810410001701987.

Allen, P. A. (2008), From landscapes into geological history, *Nature*, *451*(7176), 274–276.

Almond, P., J. Roering, and T. C. Hales (2007), Using soil residence time to delineate spatial and temporal patterns of transient landscape response, *J. Geophys. Res. Earth Surf.*, *112*(F3), F03S17, doi:10.1029/2006JF000568.

Amundson, R., A. T. Austin, E. a. G. Schuur, K. Yoo, V. Matzek, C. Kendall, A. Uebersax, D. Brenner, and W. T. Baisden (2003), Global patterns of the isotopic composition of soil and plant nitrogen, *Glob. Biogeochem. Cycles*, *17*(1), 1031, doi:10.1029/2002GB001903.

Amundson, R., D. D. Richter, G. S. Humphreys, E. G. Jobbágy, and J. Gaillardet (2007), Coupling between Biota and Earth Materials in the Critical Zone, *Elements*, *3*(5), 327–332, doi:10.2113/gselements.3.5.327.

Amundson, R. et al. (2012), Geomorphologic evidence for the late Pliocene onset of hyperaridity in the Atacama Desert, *Geol. Soc. Am. Bull.*, *124*(7-8), 1048–1070, doi:10.1130/B30445.1.

Amundson, R., A. Heimsath, J. Owen, K. Yoo, and W. E. Dietrich (2015), Hillslope soils and vegetation, *Geomorphology*, *234*, 122–132, doi:10.1016/j.geomorph.2014.12.031.

Anderson, R. S. (2002), Modeling the tor-dotted crests, bedrock edges, and parabolic profiles of high alpine surfaces of the Wind River Range, Wyoming, *Geomorphology*, *46*(1-2), 35–58, doi:10.1016/S0169-555X(02)00053-3.

Anderson, R. S., and S. P. Anderson (2010), *Geomorphology: the mechanics and chemistry of landscapes*, Cambridge University Press, Cambridge ; New York.

Anderson, R. S., and R. D. Stillick (2013), 800 years of vegetation change, fire and human settlement in the Sierra Nevada of California, USA, *Holocene*, *23*(6), 823–832, doi:10.1177/0959683612471985.

Anderson, S. P., W. E. Dietrich, and G. H. Brimhall (2002), Weathering profiles, mass-balance analysis, and rates of solute loss: Linkages between weathering and erosion in a small, steep catchment, *Geol. Soc. Am. Bull.*, *114*(9), 1143–1158, doi:10.1130/0016-7606(2002)114<1143:WPMBAA>2.0.CO;2.

Andrews, D. J., and R. C. Bucknam (1987), Fitting degradation of shoreline scarps by a nonlinear diffusion model, *J. Geophys. Res. Solid Earth*, *92*(B12), 12857–12867, doi:10.1029/JB092iB12p12857.

Arrowsmith, J. R., D. D. Pollard, and D. D. Rhodes (1996), Hillslope development in areas of active tectonics, *J. Geophys. Res. Solid Earth*, *101*(B3), 6255–6275, doi:10.1029/95JB02583.

Asner, G. P. (2009), Tropical forest carbon assessment: integrating satellite and airborne mapping approaches, *Environ. Res. Lett.*, *4*(3), 034009, doi:10.1088/1748-9326/4/3/034009.

Asner, G. P., and J. Mascaro (2014), Mapping tropical forest carbon: Calibrating plot estimates to a simple LiDAR metric, *Remote Sens. Environ.*, *140*, 614–624, doi:10.1016/j.rse.2013.09.023.

Asner, G. P., J. Mascaro, H. C. Muller-Landau, G. Vieilledent, R. Vaudry, M. Rasamoelina, J. S. Hall, and M. van Breugel (2012), A universal airborne LiDAR approach for tropical forest carbon mapping, *Oecologia*, *168*(4), 1147–1160, doi:10.1007/s00442-011-2165-z.

Asner, G. P., J. R. Kellner, T. Kennedy-Bowdoin, D. E. Knapp, C. Anderson, and R. E. Martin (2013), Forest Canopy Gap Distributions in the Southern Peruvian Amazon, *PLoS ONE*, *8*(4), e60875, doi:10.1371/journal.pone.0060875.

Asner, G. P., C. B. Anderson, R. E. Martin, D. E. Knapp, R. Tupayachi, F. Sinca, and Y. Malhi (2014), Landscape-scale changes in forest structure and functional traits along an Andes-to-Amazon elevation gradient, *Biogeosciences*, *11*(3), 843–856, doi:10.5194/bg-11-843-2014.

Asner, G. P., C. B. Anderson, R. E. Martin, R. Tupayachi, D. E. Knapp, and F. Sinca (2015), Landscape biogeochemistry reflected in shifting distributions of chemical traits in the Amazon forest canopy, *Nat. Geosci.*, *8*(7), 567–573, doi:10.1038/ngeo2443.

Attal, M., G. E. Tucker, A. C. Whittaker, P. A. Cowie, and G. P. Roberts (2008), Modeling fluvial incision and transient landscape evolution: Influence of dynamic channel adjustment, *J. Geophys. Res. Earth Surf.*, *113*(F3), F03013, doi:10.1029/2007JF000893.

Attal, M., P. A. Cowie, A. C. Whittaker, D. Hobley, G. E. Tucker, and G. P. Roberts (2011), Testing fluvial erosion models using the transient response of bedrock rivers to tectonic forcing in the Apennines, Italy, *J. Geophys. Res.-Earth Surf.*, *116*, doi:10.1029/2010JF001875.

Attal, M., S. M. Mudd, M. D. Hurst, B. Weinman, K. Yoo, and M. Naylor (2015), Impact of change in erosion rate and landscape steepness on hillslope and fluvial sediments grain size in the Feather River basin (Sierra Nevada, California), *Earth Surf. Dyn.*, *3*(1), 201–222, doi:10.5194/esurf-3-201-2015.

Bagnold, R. (1977), Bed Load Transport by Natural Rivers, *Water Resour. Res.*, *13*(2), 303–312, doi:10.1029/WR013i002p00303.

Bales, R. C., J. W. Hopmans, A. T. O'Geen, M. Meadows, P. C. Hartsough, P. Kirchner, C. T. Hunsaker, and D. Beaudette (2011), Soil Moisture Response to Snowmelt and Rainfall in a Sierra Nevada Mixed-Conifer Forest, *Vadose Zone J.*, *10*(3), 786–799, doi:10.2136/vzj2011.0001.

Barbour, M. G., and W. D. Billings (2000), *North American terrestrial vegetation / edited by Michael G. Barbour, William Dwight Billings*, Cambridge, England ; New York, N.Y. : Cambridge University Press.

Baskerville, G. L. (1972), Use of Logarithmic Regression in the Estimation of Plant Biomass, *Can. J. For. Res.*, *2*(1), 49–53, doi:10.1139/x72-009.

Baynes, E. R. C., M. Attal, S. Niedermann, L. A. Kirstein, A. J. Dugmore, and M. Naylor (2015), Erosion during extreme flood events dominates Holocene canyon evolution in northeast Iceland, *Proc. Natl. Acad. Sci.*, *112*(8), 2355–2360, doi:10.1073/pnas.1415443112.

Bazilevskaya, E., M. Lebedeva, M. Pavich, G. Rother, D. Y. Parkinson, D. Cole, and S. L. Brantley (2013), Where fast weathering creates thin regolith and slow weathering creates thick regolith, *Earth Surf. Process. Landf.*, *38*(8), 847–858, doi:10.1002/esp.3369.

Befus, K. M., A. F. Sheehan, M. Leopold, S. P. Anderson, and R. S. Anderson (2011), Seismic Constraints on Critical Zone Architecture, Boulder Creek Watershed, Front Range, Colorado, *Vadose Zone J.*, *10*(3), 915, doi:10.2136/vzj2010.0108.

Benda, L., and T. Dunne (1997), Stochastic forcing of sediment supply to channel networks from landsliding and debris flow, *Water Resour. Res.*, *33*(12), 2849–2863, doi:10.1029/97WR02388.

Bennie, A. T. P. (1991), *Growth and mechanical impedence. In "Plant roots: The hidden half".(Eds Y Waisel, A Eshel, U Kafhaki) pp. 393–414*, Marcel Dekker Inc.: New York.

Berner, E. K., R. A. Berner, and K. L. Moulton (2003), 5.06 - Plants and Mineral Weathering: Present and Past, in *Treatise on Geochemistry*, edited by H. D. H. K. Turekian, pp. 169–188, Pergamon, Oxford.

Bilderback, E. L., J. R. Pettinga, N. J. Litchfield, M. Quigley, M. Marden, J. J. Roering, and A. S. Palmer (2015), Hillslope response to climate-modulated river incision in the Waipaoa catchment, East Coast North Island, New Zealand, *Geol. Soc. Am. Bull.*, *127*(1-2), 131–148, doi:10.1130/B31015.1.

Binnie, S. A., W. M. Phillips, M. A. Summerfield, and L. K. Fifield (2007), Tectonic uplift, threshold hillslopes, and denudation rates in a developing mountain range, *Geology*, *35*(8), 743–746, doi:10.1130/G23641A.1.

Binnie, S. A., W. M. Phillips, M. A. Summerfield, L. K. Fifield, and J. A. Spotila (2010), Tectonic and climatic controls of denudation rates in active orogens: The San Bernardino Mountains, California, *Geomorphology*, *118*(3-4), 249–261, doi:10.1016/j.geomorph.2010.01.005.

Bonneville, S., M. M. Smits, A. Brown, J. Harrington, J. R. Leake, R. Brydson, and L. G. Benning (2009), Plant-driven fungal weathering: Early stages of mineral alteration at the nanometer scale, *Geology*, *37*(7), 615–618, doi:10.1130/G25699A.1.

Booth, A. M., J. J. Roering, and J. T. Perron (2009), Automated landslide mapping using spectral analysis and high-resolution topographic data: Puget Sound lowlands, Washington, and Portland Hills, Oregon, *Geomorphology*, *109*(3-4), 132–147, doi:10.1016/j.geomorph.2009.02.027.

Booth, A. M., J. J. Roering, and A. W. Rempel (2013), Topographic signatures and a general transport law for deep-seated landslides in a landscape evolution model, *J. Geophys. Res. Earth Surf.*, *118*(2), 603–624, doi:10.1002/jgrf.20051.

Bornyasz, M. A., R. C. Graham, and M. F. Allen (2005), Ectomycorrhizae in a soil-weathered granitic bedrock regolith: linking matrix resources to plants, *Geoderma*, *126*(1–2), 141–160, doi:10.1016/j.geoderma.2004.11.023.

Brandtberg, T. (2007), Classifying individual tree species under leaf-off and leaf-on conditions using airborne lidar, *ISPRS J. Photogramm. Remote Sens.*, *61*(5), 325–340, doi:10.1016/j.isprsjprs.2006.10.006.

Brantley, S. L. et al. (2011), Twelve testable hypotheses on the geobiology of weathering, *Geobiology*, *9*(2), 140–165, doi:10.1111/j.1472-4669.2010.00264.x.

Braun, J., X. Robert, and T. Simon-Labric (2013), Eroding dynamic topography, *Geophys. Res. Lett.*, *40*(8), 1494–1499, doi:10.1002/grl.50310.

Braun, J., T. Simon-Labric, K. E. Murray, and P. W. Reiners (2014), Topographic relief driven by variations in surface rock density, *Nat. Geosci.*, *7*(7), 534–540, doi:10.1038/ngeo2171.

Breshears, D. D. et al. (2005), Regional vegetation die-off in response to global-change-type drought, *Proc. Natl. Acad. Sci. U. S. A.*, *102*(42), 15144–15148, doi:10.1073/pnas.0505734102.

Brocard, G. Y., J. K. Willenbring, F. N. Scatena, and A. H. Johnson (2015), Effects of a tectonically-triggered wave of incision on riverine exports and soil mineralogy in the Luquillo Mountains of Puerto Rico, *Appl. Geochem.*, *63*, 586–598, doi:10.1016/j.apgeochem.2015.04.001.

Brodu, N., and D. Lague (2012), 3D terrestrial lidar data classification of complex natural scenes using a multi-scale dimensionality criterion: Applications in geomorphology,

ISPRS J. Photogramm. Remote Sens., *68*, 121–134, doi:10.1016/j.isprsjprs.2012.01.006.

Brooks, J. R., H. R. Barnard, R. Coulombe, and J. J. McDonnell (2010), Ecohydrologic separation of water between trees and streams in a Mediterranean climate, *Nat. Geosci.*, *3*(2), 100–104, doi:10.1038/ngeo722.

Buades, A., B. Coll, and J. M. Morel (2004), On image denoising methods, *CMLA Prepr.*, *5*.

Burbank, D. W., J. Leland, E. Fielding, R. S. Anderson, N. Brozovic, M. R. Reid, and C. Duncan (1996), Bedrock incision, rock uplift and threshold hillslopes in the northwestern Himalayas, *Nature*, *379*(6565), 505–510.

Busby, C. J., and K. Putirka (2009), Miocene evolution of the western edge of the Nevadaplano in the central and northern Sierra Nevada: palaeocanyons, magmatism, and structure, *Int. Geol. Rev.*, *51*(7-8), 670–701, doi:10.1080/00206810902978265.

Buss, H. L., P. B. Sak, S. M. Webb, and S. L. Brantley (2008), Weathering of the Rio Blanco quartz diorite, Luquillo Mountains, Puerto Rico: Coupling oxidation, dissolution, and fracturing, *Geochim. Cosmochim. Acta*, *72*(18), 4488–4507, doi:10.1016/j.gca.2008.06.020.

Carson, M. A., and M. J. Kirkby (1972), *Hillslope form and process*, Cambridge University Press Cambridge.

Cassel, E. J., and S. A. Graham (2011), Paleovalley morphology and fluvial system evolution of Eocene–Oligocene sediments ("auriferous gravels"), northern Sierra Nevada, California: Implications for climate, tectonics, and topography, *Geol. Soc. Am. Bull.*, *123*(9-10), 1699–1719, doi:10.1130/B30356.1.

Cassel, E. J., S. A. Graham, and C. P. Chamberlain (2009), Cenozoic tectonic and topographic evolution of the northern Sierra Nevada, California, through stable isotope paleoaltimetry in volcanic glass, *Geology*, *37*(6), 547–550, doi:10.1130/G25572A.1.

Cassel, E. J., S. A. Graham, C. P. Chamberlain, and C. D. Henry (2012), Early Cenozoic topography, morphology, and tectonics of the northern Sierra Nevada and western Basin and Range, *Geosphere*, *8*(2), 229–249, doi:10.1130/GES00671.1.

Cassel, E. J., D. O. Breecker, C. D. Henry, T. E. Larson, and D. F. Stockli (2014), Profile of a paleo-orogen: High topography across the present-day Basin and Range from 40 to 23 Ma, *Geology*, G35924.1, doi:10.1130/G35924.1.

Catté, F., P. Lions, J. Morel, and T. Coll (1992), Image Selective Smoothing and Edge Detection by Nonlinear Diffusion, *SIAM J. Numer. Anal.*, *29*(1), 182–193, doi:10.1137/0729012.

Cavalli, M., P. Tarolli, L. Marchi, and G. Dalla Fontana (2008), The effectiveness of airborne LiDAR data in the recognition of channel-bed morphology, *CATENA*, *73*(3), 249–260, doi:10.1016/j.catena.2007.11.001.

Cecil, M. R., M. N. Ducea, P. W. Reiners, and C. G. Chase (2006), Cenozoic exhumation of the northern Sierra Nevada, California, from (U-Th)/He thermochronology, *Geol. Soc. Am. Bull.*, *118*(11-12), 1481–1488, doi:10.1130/B25876.1.

Cecil, M. R., G. L. Rotberg, M. N. Ducea, J. B. Saleeby, and G. E. Gehrels (2012), Magmatic growth and batholithic root development in the northern Sierra Nevada, California, *Geosphere*, *8*(3), 592–606, doi:10.1130/GES00729.1.

Chadwick, O. A., J. J. Roering, A. M. Heimsath, S. R. Levick, G. P. Asner, and L. Khomo (2013), Shaping post-orogenic landscapes by climate and chemical weathering, *Geology*, *41*(11), 1171–1174, doi:10.1130/G34721.1.

Chamberlain, C. P., H. T. Mix, A. Mulch, M. T. Hren, M. L. Kent-Corson, S. J. Davis, T. W. Horton, and S. A. Graham (2012), The Cenozoic climatic and topographic evolution of the western North American Cordillera, *Am. J. Sci.*, *312*(2), 213–262, doi:10.2475/02.2012.05.

Chase, M. N., E. A. Johnson, and Y. E. Martin (2012), The influence of geomorphic processes on plant distribution and abundance as reflected in plant tolerance curves, *Ecol. Monogr.*, *82*(4), 429–447, doi:10.1890/11-2145.1.

Chave, J., R. Condit, S. Lao, J. P. Caspersen, R. B. Foster, and S. P. Hubbell (2003), Spatial and temporal variation of biomass in a tropical forest: results from a large census plot in Panama, *J. Ecol.*, *91*(2), 240–252.

Chave, J., R. Condit, S. Aguilar, A. Hernandez, S. Lao, and R. Perez (2004), Error propagation and scaling for tropical forest biomass estimates., *Philos. Trans. R. Soc. B Biol. Sci.*, *359*(1443), 409–420.

Chave, J. et al. (2005), Tree allometry and improved estimation of carbon stocks and balance in tropical forests, *Oecologia*, *145*(1), 87–99, doi:10.1007/s00442-005-0100-x.

Chen, Q. (2015), Modeling aboveground tree woody biomass using national-scale allometric methods and airborne lidar, *ISPRS J. Photogramm. Remote Sens.*, *106*, 95–106, doi:10.1016/j.isprsjprs.2015.05.007.

Chen, Q., D. Baldocchi, P. Gong, and M. Kelly (2006), Isolating Individual Trees in a Savanna Woodland Using Small Footprint Lidar Data, *Photogramm. Eng. Remote Sens.*, *72*(8), 923–932, doi:10.14358/PERS.72.8.923.

Chorover, J. et al. (2011), How Water, Carbon, and Energy Drive Critical Zone Evolution: The Jemez–Santa Catalina Critical Zone Observatory, *Vadose Zone J.*, *10*(3), 884–899, doi:10.2136/vzj2010.0132.

Clair, J. S., S. Moon, W. S. Holbrook, J. T. Perron, C. S. Riebe, S. J. Martel, B. Carr, C. Harman, K. Singha, and D. deB Richter (2015), Geophysical imaging reveals topographic stress control of bedrock weathering, *Science*, *350*(6260), 534–538, doi:10.1126/science.aab2210.

Clark, D. B., and J. R. Kellner (2012), Tropical forest biomass estimation and the fallacy of misplaced concreteness, *J. Veg. Sci.*, *23*(6), 1191–1196, doi:10.1111/j.1654-1103.2012.01471.x.

Clarke, B. A., and D. W. Burbank (2010), Bedrock fracturing, threshold hillslopes, and limits to the magnitude of bedrock landslides, *Earth Planet. Sci. Lett.*, *297*(3-4), 577–586, doi:10.1016/j.epsl.2010.07.011.

Clarke, B. A., and D. W. Burbank (2011), Quantifying bedrock-fracture patterns within the shallow subsurface: Implications for rock mass strength, bedrock landslides, and erodibility, *J. Geophys. Res.*, *116*(F4), F04009.

Clubb, F., S. Mudd, and D. Milodowski (2015), Reply to comment by P. Passalacqua and E. Foufoula-Georgiou on "Objective extraction of channel heads from high-resolution topographic data," *Water Resour. Res.*, *51*(2), 1377–1379, doi:10.1002/2014WR016603.

Clubb, F. J., S. M. Mudd, D. T. Milodowski, M. D. Hurst, and L. J. Slater (2014), Objective extraction of channel heads from high-resolution topographic data, *Water Resour. Res.*, *50*(5), 4283–4304, doi:10.1002/2013WR015167.

Cohen, D., P. Lehmann, and D. Or (2009), Fiber bundle model for multiscale modeling of hydromechanical triggering of shallow landslides, *Water Resour. Res.*, *45*, doi:10.1029/2009WR007889.

Cohen, D., M. Schwarz, and D. Or (2011), An analytical fiber bundle model for pullout mechanics of root bundles, *J. Geophys. Res. Earth Surf.*, *116*(F3), F03010, doi:10.1029/2010JF001886.

Colby, J. (1991), Topographic Normalization in Rugged Terrain, *Photogramm. Eng. Remote Sens.*, *57*(5), 531–537.

Colgan, M. S., G. P. Asner, and T. Swemmer (2012a), Harvesting tree biomass at the stand level to assess the accuracy of field and airborne biomass estimation in savannas, *Ecol. Appl.*, *23*(5), 1170–1184, doi:10.1890/12-0922.1.

Colgan, M. S., G. P. Asner, S. R. Levick, R. E. Martin, and O. A. Chadwick (2012b), Topo-edaphic controls over woody plant biomass in South African savannas, *Biogeosciences*, *9*(5), 1809–1821, doi:10.5194/bg-9-1809-2012.

Compton, R. R. (1955), Trondhjemite Batholith Near Bidwell Bar, California, *Geol. Soc. Am. Bull.*, *66*(1), 9–44, doi:10.1130/0016-7606(1955)66[9:TBNBBC]2.0.CO;2.

Constantine, J. A., M.-J. Schelhaas, E. Gabet, and S. M. Mudd (2012), Limits of windthrow-driven hillslope sediment flux due to varying storm frequency and intensity, *Geomorphology*.

Coops, N. C., T. Hilker, M. A. Wulder, B. St-Onge, G. Newnham, A. Siggins, and J. A. (Tony) Trofymow (2007), Estimating canopy structure of Douglas-fir forest stands from discrete-return LiDAR, *Trees*, *21*(3), 295–310, doi:10.1007/s00468-006-0119-6.

Cox, N. J. (1980), On the relationship between bedrock lowering and regolith thickness, *Earth Surf. Process.*, *5*(3), 271–274, doi:10.1002/esp.3760050305.

Crouvi, O., J. D. Pelletier, and C. Rasmussen (2013), Predicting the thickness and aeolian fraction of soils in upland watersheds of the Mojave Desert, *Geoderma*, *195–196*, 94–110, doi:10.1016/j.geoderma.2012.11.015.

Culling, W. (1963), Soil Creep and the Development of Hillside Slopes, *J. Geol.*, *71*(2), 127–161.

Culling, W. E. H. (1960), Analytical theory of erosion, *J. Geol.*, 336–344.

Culling, W. E. H. (1965), Theory of Erosion on Soil-Covered Slopes, *J. Geol.*, *73*(2), 230–254.

Cyr, A. J., D. E. Granger, V. Olivetti, and P. Molin (2010), Quantifying rock uplift rates using channel steepness and cosmogenic nuclide–determined erosion rates: Examples from northern and southern Italy, *Lithosphere*, *2*(3), 188 –198, doi:10.1130/L96.1.

Dahlin, K. M., G. P. Asner, and C. B. Field (2011), Environmental filtering and land-use history drive patterns in biomass accumulation in a mediterranean-type landscape, *Ecol. Appl.*, *22*(1), 104–118, doi:10.1890/11-1401.1.

Dale, V. H. et al. (2001), Climate Change and Forest Disturbances, *BioScience*, *51*(9), 723–734, doi:10.1641/0006-3568(2001)051[0723:CCAFD]2.0.CO;2.

Daly, C., W. P. Gibson, G. H. Taylor, G. L. Johnson, and P. Pasteris (2002), A knowledge-based approach to the statistical mapping of climate, *Clim. Res.*, *22*(2), 99–113.

Daly, C., M. Halbleib, J. I. Smith, W. P. Gibson, M. K. Doggett, G. H. Taylor, J. Curtis, and P. P. Pasteris (2008), Physiographically sensitive mapping of climatological temperature and precipitation across the conterminous United States, *Int. J. Climatol.*, *28*(15), 2031–2064, doi:10.1002/joc.1688.

Davis, W. M. (1892), The Convex Profile of Bad-Land Divides, *Science*, *20*(508), 245–245.

Day, H. W., and M. E. Bickford (2004), Tectonic setting of the Jurassic Smartville and Slate Creek complexes, northern Sierra Nevada, California, *Geol. Soc. Am. Bull.*, *116*(11-12), 1515–1528.

Day, H. W., E. M. Moores, and A. C. Tuminas (1985), Structure and tectonics of the northern Sierra Nevada, *Geol. Soc. Am. Bull.*, *96*(4), 436–450, doi:10.1130/0016-7606(1985)96<436:SATOTN>2.0.CO;2.

DeCelles, P. G. (2004), Late Jurassic to Eocene evolution of the Cordilleran thrust belt and foreland basin system, western U.S.A., *Am. J. Sci.*, *304*(2), 105–168, doi:10.2475/ajs.304.2.105.

Deligne, N. I., K. V. Cashman, and J. J. Roering (2013), After the lava flow: The importance of external soil sources for plant colonization of recent lava flows in the central Oregon Cascades, USA, *Geomorphology*, *202*, 15–32, doi:10.1016/j.geomorph.2012.12.009.

Densmore, A. L., M. A. Ellis, and R. S. Anderson (1998), Landsliding and the evolution of normal fault-bounded mountains., *J. Geophys. Res. Solid Earth*, *103*(B7), 15203–15219.

Detto, M., H. C. Muller-Landau, J. Mascaro, and G. P. Asner (2013), Hydrological Networks and Associated Topographic Variation as Templates for the Spatial Organization of Tropical Forest Vegetation, *PLoS ONE*, *8*(10), e76296, doi:10.1371/journal.pone.0076296.

DiBiase, R., A. M. Booth, V. Ganti, J. S. Scheingross, and M. P. Lamb (2014a), Field experiments of nonlocal sediment transport on a steep hillslope, *AGU Fall Meet. Abstr.*, *32*.

DiBiase, R. A., and M. P. Lamb (2013), Vegetation and wildfire controls on sediment yield in bedrock landscapes, *Geophys. Res. Lett.*, *40*(6), 1093–1097, doi:10.1002/grl.50277.

DiBiase, R. A., and K. X. Whipple (2011), The influence of erosion thresholds and runoff variability on the relationships among topography, climate, and erosion rate, *J. Geophys. Res.*, doi:10.1029/2011JF002095.

DiBiase, R. A., K. X. Whipple, A. M. Heimsath, and W. B. Ouimet (2010), Landscape form and millennial erosion rates in the San Gabriel Mountains, CA, *Earth Planet. Sci. Lett.*, *289*(1-2), 134–144, doi:10.1016/j.epsl.2009.10.036.

DiBiase, R. A., A. M. Heimsath, and K. X. Whipple (2012), Hillslope response to tectonic forcing in threshold landscapes, *Earth Surf. Process. Landf.*, *37*(8), 855–865, doi:10.1002/esp.3205.

DiBiase, R. A., K. X. Whipple, M. P. Lamb, and A. M. Heimsath (2014b), The role of waterfalls and knickzones in controlling the style and pace of landscape adjustment in the western San Gabriel Mountains, California, *Geol. Soc. Am. Bull.*, B31113.1, doi:10.1130/B31113.1.

Dickinson, W. R. (2004), Evolution of the North American Cordillera, *Annu. Rev. Earth Planet. Sci.*, *32*(1), 13–45, doi:10.1146/annurev.earth.32.101802.120257.

Dietrich, W. E., and T. Dunne (1978), Sediment budget for a small catchment in a mountainous terrain, *Z. Für Geomorphol. Suppl.*, *29*, 191–206.

Dietrich, W. E., and J. T. Perron (2006), The search for a topographic signature of life, *Nature*, *439*(7075), 411–418, doi:10.1038/nature04452.

Dietrich, W. E., C. J. Wilson, D. R. Montgomery, and J. McKean (1993), Analysis of Erosion Thresholds, Channel Networks, and Landscape Morphology Using a Digital Terrain Model, *J. Geol.*, *101*(2), 259–278.

Dietrich, W. E., R. Reiss, M. L. Hsu, and D. R. Montgomery (1995), A process-based model for colluvial soil depth and shallow landsliding using digital elevation data, *Hydrol. Process.*, *9*(3-4), 383–400.

Dietrich, W. E., D. G. Bellugi, L. S. Sklar, J. D. Stock, A. M. Heimsath, and J. J. Roering (2003), Geomorphic transport laws for predicting landscape form and dynamics, *Geophys. Monogr.-Am. Geophys. UNION*, *135*, 103–132.

Dislich, C., and A. Huth (2012), Modelling the impact of shallow landslides on forest structure in tropical montane forests, *Ecol. Model.*, *239*, 40–53, doi:10.1016/j.ecolmodel.2012.04.016.

Dixon, J. L., A. M. Heimsath, J. Kaste, and R. Amundson (2009a), Climate-driven processes of hillslope weathering, *Geology*, *37*(11), 975 –978, doi:10.1130/G30045A.1.

Dixon, J. L., A. M. Heimsath, and R. Amundson (2009b), The critical role of climate and saprolite weathering in landscape evolution, *Earth Surf. Process. Landf.*, *34*(11), 1507–1521, doi:10.1002/esp.1836.

Dixon, J. L., A. S. Hartshorn, A. M. Heimsath, R. A. DiBiase, and K. X. Whipple (2012), Chemical weathering response to tectonic forcing: A soils perspective from the San Gabriel Mountains, California, *Earth Planet. Sci. Lett.*, *323–324*, 40–49, doi:10.1016/j.epsl.2012.01.010.

D'Odorico, P., and S. Fagherazzi (2003), A probabilistic model of rainfall-triggered shallow landslides in hollows: A long-term analysis, *Water Resour. Res.*, *39*(9), 1262, doi:10.1029/2002WR001595.

Dosseto, A., P. P. Hesse, K. Maher, K. Fryirs, and S. Turner (2010), Climatic and vegetation control on sediment dynamics during the last glacial cycle, *Geology*, *38*(5), 395–398, doi:10.1130/G30708.1.

Dosseto, A., H. Buss, and P. O. Suresh (2011), The delicate balance between soil production and erosion, and its role on landscape evolution, *Appl. Geochem.*, *26*, S24–S27, doi:10.1016/j.apgeochem.2011.03.020.

Dosseto, A., H. L. Buss, and P. O. Suresh (2012), Rapid regolith formation over volcanic bedrock and implications for landscape evolution, *Earth Planet. Sci. Lett.*, *337–338*, 47–55, doi:10.1016/j.epsl.2012.05.008.

Drake, J. B., R. G. Knox, R. O. Dubayah, D. B. Clark, R. Condit, J. B. Blair, and M. Hofton (2003), Above-ground biomass estimation in closed canopy Neotropical forests using lidar remote sensing: factors affecting the generality of relationships, *Glob. Ecol. Biogeogr.*, *12*(2), 147–159, doi:10.1046/j.1466-822X.2003.00010.x.

Ducea, M. (2001), The California arc: Thick granitic batholiths, eclogitic residues, lithospheric-scale thrusting, and magmatic flare-ups, *GSA Today*, *11*(11), 4.

Dunne, T. (1991), Stochastic aspects of the relations between climate, hydrology and landform evolution, *Trans. Jpn. Geomorphol. Union 地形*, *12*, 1–24.

Dunne, T., and B. F. Aubry (1985), Evaluation of Horton's theory of sheetwash and rill erosion on the basis of field experiments, in *Hillslope processes*, edited by A. D. Abrahams, pp. 31–53, Allen and Unwin Inc., London.

Dunne, T., D. V. Malmon, and S. M. Mudd (2010), A rain splash transport equation assimilating field and laboratory measurements, *J. Geophys. Res. Earth Surf.*, *115*(F1), F01001, doi:10.1029/2009JF001302.

Dunne, T., D. V. Malmon, and K. B. J. Dunne (2016), Limits on the morphogenetic role of rain splash transport in hillslope evolution, *J. Geophys. Res. Earth Surf.*, 2015JF003737.

Edelman, S. H., H. W. Day, and M. E. Bickford (1989), Implications of U-Pb zircon ages for the tectonic settings of the Smartville and Slate Creek complexes, northern Sierra Nevada, California, *Geology*, *17*(11), 1032–1035, doi:10.1130/0091-7613(1989)017<1032:IOUPZA>2.3.CO;2.

Eger, A., P. C. Almond, and L. M. Condron (2011), Pedogenesis, soil mass balance, phosphorus dynamics and vegetation communities across a Holocene soil chronosequence in a super-humid climate, South Westland, New Zealand, *Geoderma*, *163*(3–4), 185–196, doi:10.1016/j.geoderma.2011.04.007.

Egerton-Warburton, L. M., R. C. Graham, and K. R. Hubbert (2003), Spatial variability in mycorrhizal hyphae and nutrient and water availability in a soil-weathered bedrock profile, *Plant Soil*, *249*(2), 331–342, doi:10.1023/A:1022860432113.

Ekström, G., and C. P. Stark (2013), Simple Scaling of Catastrophic Landslide Dynamics, *Science*, *339*(6126), 1416–1419, doi:10.1126/science.1232887.

Elser, J. J., M. E. S. Bracken, E. E. Cleland, D. S. Gruner, W. S. Harpole, H. Hillebrand, J. T. Ngai, E. W. Seabloom, J. B. Shurin, and J. E. Smith (2007), Global analysis of nitrogen and phosphorus limitation of primary producers in freshwater, marine and terrestrial ecosystems, *Ecol. Lett.*, *10*(12), 1135–1142, doi:10.1111/j.1461-0248.2007.01113.x.

Evans, I. S. (1980), An integrated system of terrain analysis and slope mapping, *Z Geomorphol*, (36), 274–295.

Evans, J. S., and A. T. Hudak (2007), A Multiscale Curvature Algorithm for Classifying Discrete Return LiDAR in Forested Environments, *Geosci. Remote Sens. IEEE Trans. On*, *45*(4), 1029 –1038, doi:10.1109/TGRS.2006.890412.

Fara, H. D., and A. E. Scheidegger (1963), An Eigenvalue Method for the Statistical Evaluation of Fault Plane Solutions of Earthquakes, *Bull. Seismol. Soc. Am.*, *53*(4), 811–816.

Farr, T. G. et al. (2007), The Shuttle Radar Topography Mission, *Rev. Geophys.*, *45*(2), RG2004, doi:10.1029/2005RG000183.

Faure Walker, J. P., G. P. Roberts, P. A. Cowie, I. Papanikolaou, A. M. Michetti, P. Sammonds, M. Wilkinson, K. J. W. McCaffrey, and R. J. Phillips (2012), Relationship between topography, rates of extension and mantle dynamics in the actively-extending Italian Apennines, *Earth Planet. Sci. Lett.*, *325–326*, 76–84, doi:10.1016/j.epsl.2012.01.028.

Feeley, K. J., M. R. Silman, M. B. Bush, W. Farfan, K. G. Cabrera, Y. Malhi, P. Meir, N. S. Revilla, M. N. R. Quisiyupanqui, and S. Saatchi (2011), Upslope migration of Andean trees, *J. Biogeogr.*, *38*(4), 783–791, doi:10.1111/j.1365-2699.2010.02444.x.

Fernandes, N. F., and W. E. Dietrich (1997), Hillslope evolution by diffusive processes: The timescale for equilibrium adjustments, *Water Resour. Res.*, *33*(6), 1307–1318, doi:10.1029/97WR00534.

Ferrier, K. L., and J. W. Kirchner (2008), Effects of physical erosion on chemical denudation rates: A numerical modeling study of soil-mantled hillslopes, *Earth Planet. Sci. Lett.*, *272*(3–4), 591–599, doi:10.1016/j.epsl.2008.05.024.

Ferrier, K. L., J. W. Kirchner, and R. C. Finkel (2012), Weak influences of climate and mineral supply rates on chemical erosion rates: Measurements along two altitudinal transects in the Idaho Batholith, *J. Geophys. Res. Earth Surf.*, *117*(F2), F02026, doi:10.1029/2011JF002231.

Fielding, E., B. Isacks, M. Barazangi, and C. Duncan (1994), How flat is Tibet?, *Geology*, *22*(2), 163–167, doi:10.1130/0091-7613(1994)022<0163:HFIT>2.3.CO;2.

Fisher, G. B., B. Bookhagen, and C. B. Amos (2013), Channel planform geometry and slopes from freely available high-spatial resolution imagery and DEM fusion: Implications for channel width scalings, erosion proxies, and fluvial signatures in tectonically active landscapes, *Geomorphology*, *194*, 46–56, doi:10.1016/j.geomorph.2013.04.011.

Flageollet, J. C. (1977), *Origine des reliefs, altérations et formations superficielles contribution à l'étude géomorphologique des massifs anciens cristallins: l'exemple du Limousin et de la Vendée du nord-ouest*, École nationale supérieure de géologie appliquée et de prospection minière du centre de recherches pétrographiques et géochimiques (CNRS) et des Laboratoires des sciences de la terre de l'Université.

Foody, G. M., D. S. Boyd, and M. E. J. Cutler (2003), Predictive relations of tropical forest biomass from Landsat TM data and their transferability between regions, *Remote Sens. Environ.*, *85*(4), 463–474, doi:10.1016/S0034-4257(03)00039-7.

Foufoula-Georgiou, E., V. Ganti, and W. E. Dietrich (2010), A nonlocal theory of sediment transport on hillslopes, *J. Geophys. Res.-Earth Surf.*, *115*, doi:10.1029/2009JF001280.

Fox, M., L. Goren, D. A. May, and S. D. Willett (2014), Inversion of fluvial channels for paleo–rock uplift rates in Taiwan, *J. Geophys. Res. Earth Surf.*, 2014JF003196, doi:10.1002/2014JF003196.

Fox, M., T. Bodin, and D. L. Shuster (2015), Abrupt changes in the rate of Andean Plateau uplift from reversible jump Markov Chain Monte Carlo inversion of river profiles, *Geomorphology*, *238*, 1–14, doi:10.1016/j.geomorph.2015.02.022.

Franklin, J. (2003), Clustering Versus Regression Trees for Determining Ecological Land Units in the Southern California Mountains and Foothills, *For. Sci.*, *49*(3), 354–368.

Frazer, G. W., S. Magnussen, M. A. Wulder, and K. O. Niemann (2011), Simulated impact of sample plot size and co-registration error on the accuracy and uncertainty of LiDAR-derived estimates of forest stand biomass, *Remote Sens. Environ.*, *115*(2), 636–649, doi:10.1016/j.rse.2010.10.008.

Furbish, D. J., and S. Fagherazzi (2001), Stability of creeping soil and implications for hillslope evolution, *Water Resour. Res.*, *37*(10), 2607–2618, doi:10.1029/2001WR000239.

Furbish, D. J., and P. K. Haff (2010), From divots to swales: Hillslope sediment transport across divers length scales, *J. Geophys. Res. Earth Surf.*, *115*(F3), F03001, doi:10.1029/2009JF001576.

Furbish, D. J., and J. J. Roering (2013), Sediment disentrainment and the concept of local versus nonlocal transport on hillslopes, *J. Geophys. Res. Earth Surf.*, *118*(2), 937–952, doi:10.1002/jgrf.20071.

Furbish, D. J., K. K. Hamner, M. Schmeeckle, M. N. Borosund, and S. M. Mudd (2007), Rain splash of dry sand revealed by high-speed imaging and sticky paper splash targets, *J. Geophys. Res. Earth Surf.*, *112*(F1), F01001, doi:10.1029/2006JF000498.

Furbish, D. J., P. K. Haff, W. E. Dietrich, and A. M. Heimsath (2009), Statistical description of slope-dependent soil transport and the diffusion-like coefficient, *J Geophys Res*, *114*(F00A05), doi:10.1029/2009JF001267.

Gabet, E. J. (2000), Gopher bioturbation: Field evidence for non-linear hillslope diffusion, *Earth Surf. Process. Landf.*, *25*(13), 1419–1428, doi:10.1002/1096-9837(200012)25:13<1419::AID-ESP148>3.0.CO;2-1.

Gabet, E. J. (2003), Sediment transport by dry ravel, *J. Geophys. Res. Solid Earth*, *108*(B1), 2049, doi:10.1029/2001JB001686.

Gabet, E. J. (2007), A theoretical model coupling chemical weathering and physical erosion in landslide-dominated landscapes, *Earth Planet. Sci. Lett.*, *264*(1-2), 259–265, doi:10.1016/j.epsl.2007.09.028.

Gabet, E. J. (2014), Late Cenozoic uplift of the Sierra Nevada, California? A critical analysis of the geomorphic evidence, *Am. J. Sci.*, *314*(8), 1224–1257, doi:10.2475/08.2014.03.

Gabet, E. J., and M. K. Mendoza (2012), Particle transport over rough hillslope surfaces by dry ravel: Experiments and simulations with implications for nonlocal sediment flux, *J. Geophys. Res. Earth Surf.*, *117*(F1), F01019, doi:10.1029/2011JF002229.

Gabet, E. J., and S. M. Mudd (2009), A theoretical model coupling chemical weathering rates with denudation rates, *Geology*, *37*(2), 151–154, doi:10.1130/G25270A.1.

Gabet, E. J., and S. M. Mudd (2010), Bedrock erosion by root fracture and tree throw: A coupled biogeomorphic model to explore the humped soil production function and the persistence of hillslope soils, *J. Geophys. Res.*, *115*(F04005), doi:10.1029/2009JF001526.

Gabet, E. J., O. J. Reichman, and E. W. Seabloom (2003), The effects of bioturbation on soil processes and sediment transport, *Annu. Rev. Earth Planet. Sci.*, *31*(1), 249–273.

Gabet, E. J., R. Edelman, and H. Langner (2006), Hydrological controls on chemical weathering rates at the soil-bedrock interface, *Geology*, *34*(12), 1065–1068, doi:10.1130/G23085A.1.

Gabet, E. J., S. M. Mudd, D. T. Milodowski, K. Yoo, M. D. Hurst, and A. Dosseto (2015), Local topography and erosion rate control regolith thickness along a ridgeline in the Sierra Nevada, California, *Earth Surf. Process. Landf.*, *40*, 1779–1790, doi:10.1002/esp.3754.

Gaillardet, J., B. Dupré, P. Louvat, and C. J. Allegre (1999), Global silicate weathering and CO< sub> 2</sub> consumption rates deduced from the chemistry of large rivers, *Chem. Geol.*, *159*(1), 3–30.

Gallaway, J. M., Y. E. Martin, and E. A. Johnson (2009), Sediment transport due to tree root throw: integrating tree population dynamics, wildfire and geomorphic response, *Earth Surf. Process. Landf.*, *34*(9), 1255–1269.

Gallen, S. F., K. W. Wegmann, K. L. Frankel, S. Hughes, R. Q. Lewis, N. Lyons, P. Paris, K. Ross, J. B. Bauer, and A. C. Witt (2011), Hillslope response to knickpoint migration in the Southern Appalachians: implications for the evolution of post-orogenic landscapes, *Earth Surf. Process. Landf.*, *36*(9), 1254–1267, doi:10.1002/esp.2150.

Gentry, A. H. (1988), Changes in Plant Community Diversity and Floristic Composition on Environmental and Geographical Gradients, *Ann. Mo. Bot. Gard.*, *75*(1), 1–34, doi:10.2307/2399464.

Gesch, D., M. Oimoen, S. Greenlee, C. Nelson, M. Steuck, and D. Tyler (2002), The national elevation dataset, *Photogramm. Eng. Remote Sens.*, *68*(1), 5–32.

Gilbert, G. (1909), The convexity of hilltops, *J. Geol.*, *17*(4), 344–350.

Gilbert, G. K. (1877), *Report on the Geology of the Henry Mountains*, 2029, Department of the Interior, US Geographical and Geological Survey of the Rocky Mountain Region, Washington, D.C.

Gilbert, G. K. (1904), Domes and dome structure of the high Sierra, *Geol. Soc. Am. Bull.*, *15*(1), 29–36, doi:10.1130/GSAB-15-29.

Giletycz, S., N. Loget, C.-P. Chang, and F. Mouthereau (2015), Transient fluvial landscape and preservation of low-relief terrains in an emerging orogen: Example from Hengchun Peninsula, Taiwan, *Geomorphology*, *231*, 169–181, doi:10.1016/j.geomorph.2014.11.026.

Glennie, C. L., W. E. Carter, R. L. Shrestha, and W. E. Dietrich (2013), Geodetic imaging with airborne LiDAR: the Earth's surface revealed, *Rep. Prog. Phys.*, *76*(8), 086801, doi:10.1088/0034-4885/76/8/086801.

Godard, A., J.-J. Lagasquie, and Y. Lageat (2001), *Basement Regions*, Springer Science & Business Media.

Goldich, S. S. (1938), A Study in Rock-Weathering, *J. Geol.*, *46*(1), 17–58.

Goldsworthy, M., and J. Jackson (2001), Migration of activity within normal fault systems: examples from the Quaternary of mainland Greece, *J. Struct. Geol.*, *23*(2–3), 489–506, doi:10.1016/S0191-8141(00)00121-8.

Gonzalez, P., G. P. Asner, J. J. Battles, M. A. Lefsky, K. M. Waring, and M. Palace (2010), Forest carbon densities and uncertainties from Lidar, QuickBird, and field measurements in California, *Remote Sens. Environ.*, *114*(7), 1561–1575, doi:10.1016/j.rse.2010.02.011.

Goodfellow, B. W., G. E. Hilley, and M. S. Schulz (2011), Vadose zone controls on weathering intensity and depth: Observations from grussic saprolites, *Appl. Geochem.*, *26, Supplement*, S36–S39, doi:10.1016/j.apgeochem.2011.03.023.

Goodfellow, B. W., A. Skelton, S. J. Martel, A. P. Stroeven, K. N. Jansson, and C. Hättestrand (2014a), Controls of tor formation, Cairngorm Mountains, Scotland, *J. Geophys. Res. Earth Surf.*, *119*(2), 2013JF002862, doi:10.1002/2013JF002862.

Goodfellow, B. W., O. A. Chadwick, and G. E. Hilley (2014b), Depth and character of rock weathering across a basaltic-hosted climosequence on Hawai‘i, *Earth Surf. Process. Landf.*, *39*(3), 381–398, doi:10.1002/esp.3505.

Goren, L., M. Fox, and S. D. Willett (2014), Tectonics from fluvial topography using formal linear inversion: Theory and applications to the Inyo Mountains, California, *J. Geophys. Res. Earth Surf.*, 2014JF003079, doi:10.1002/2014JF003079.

Goulden, M. L., R. G. Anderson, R. C. Bales, A. E. Kelly, M. Meadows, and G. C. Winston (2012), Evapotranspiration along an elevation gradient in California’s Sierra Nevada, *J. Geophys. Res. Biogeosciences*, *117*(G3), G03028, doi:10.1029/2012JG002027.

Goward, S. N., and D. L. Williams (1997), Landsat and Earth Systems Science: Development of terrestrial monitoring, *Photogramm. Eng. Remote Sens.*, *63*(7), 887–900.

Graham, R., A. Rossi, and R. Hubbert (2010), Rock to regolith conversion: Producing hospitable substrates for terrestrial ecosystems, *GSA Today*, *20*(2), 4–9, doi:10.1130/GSAT57A.1.

Granger, D. E., J. W. Kirchner, and R. Finkel (1996), Spatially averaged long-term erosion rates measured from in situ-produced cosmogenic nuclides in alluvial sediment, *J. Geol.*, *104*(3), 249–257.

Gray, D., and D. Barker (2004), *Root-soil mechanics and interactions*, edited by S. Bennett and A. Simon, Amer Geophysical Union, Washington.

Grieve, S. W. D., S. M. Mudd, M. D. Hurst, and D. T. Milodowski (2016), A nondimensional framework for exploring the relief structure of landscapes, *Earth Surf. Dyn. Discuss.*, *2016*, 1–41, doi:10.5194/esurf-2015-53.

Guariguata, M. R. (1990), Landslide Disturbance and Forest Regeneration in the Upper Luquillo Mountains of Puerto Rico, *J. Ecol.*, *78*(3), 814–832, doi:10.2307/2260901.

Gutierrez-Jurado, H. A., E. R. Vivoni, E. Istanbulluoglu, and R. L. Bras (2007), Ecohydrological response to a geomorphically significant flood event in a semiarid catchment with contrasting ecosystems, *Geophys. Res. Lett.*, *34*(24), doi:10.1029/2007GL030994.

Gutiérrez-Jurado, H. A., E. R. Vivoni, C. Cikoski, J. B. J. Harrison, R. L. Bras, and E. Istanbulluoglu (2013), On the observed ecohydrologic dynamics of a semiarid basin with aspect-delimited ecosystems, *Water Resour. Res.*, *49*(12), 8263–8284, doi:10.1002/2013WR014364.

Hack, J. T. (1957), *Studies of longitudinal stream profiles in Virginia and Maryland*, Professional Paper, USGS Numbered Series, US Geological Survey.

Hack, J. T. (1960), Interpretation of Erosional Topography in Humid Temperate Regions, *Am. J. Sci.*, *258*, 80–97.

Hack, J. T., and J. C. Goodlett (1960), *Geomorphology and forest ecology of a mountain region in the central Appalachians*, Professional Paper, USGS Numbered Series, United States Government Printing Office, Washington, D.C.

Hahm, W. J., C. S. Riebe, C. E. Lukens, and S. Araki (2014a), Bedrock composition regulates mountain ecosystems and landscape evolution, *Proc. Natl. Acad. Sci.*, *111*(9), 3338–3343, doi:10.1073/pnas.1315667111.

Hahm, W. J., C. S. Riebe, C. E. Lukens, and S. Araki (2014b), Bedrock composition regulates mountain ecosystems and landscape evolution, *Proc. Natl. Acad. Sci.*, 201315667, doi:10.1073/pnas.1315667111.

Hale, S. R., and B. N. Rock (2003), Impact of Topographic Normalization on Land-Cover Classification Accuracy, *Photogramm. Eng. Remote Sens.*, *69*(7), 785–791, doi:10.14358/PERS.69.7.785.

Hales, T. C., C. R. Ford, T. Hwang, J. M. Vose, and L. E. Band (2009), Topographic and ecologic controls on root reinforcement, *J. Geophys. Res.-Earth Surf.*, *114*, doi:10.1029/2008JF001168.

Hales, T. C., K. M. Scharer, and R. M. Wooten (2012), Southern Appalachian hillslope erosion rates measured by soil and detrital radiocarbon in hollows, *Geomorphology*, *138*(1), 121–129, doi:10.1016/j.geomorph.2011.08.030.

Halpern, C., and J. Means (2011), Pacific Northwest Plant Biomass Component Equation Library., *Long-Term Ecol. Res. For. Sci. Data Bank Corvallis Database*. Available from: http://andrewsforest.oregonstate.edu/data/abstract.cfm?dbcode=TP072 (Accessed 6 March 2013)

Hanks, T. C. (2000), The age of scarplike landforms from diffusion-equation analysis, in *Quaternary Geochronology: Methods and Applications*, vol. 4, edited by J. S. Noller, J. M. Sowers, and W. R. Lettis, American Geophysical Union, Washington, D.C.

Hansen, M. C. et al. (2013), High-Resolution Global Maps of 21st-Century Forest Cover Change, *Science*, *342*(6160), 850–853, doi:10.1126/science.1244693.

Harpold, A. A. et al. (2015), Laser vision: lidar as a transformative tool to advance critical zone science, *Hydrol Earth Syst Sci*, *19*(6), 2881–2897, doi:10.5194/hess-19-2881-2015.

Heckman, K., and C. Rasmussen (2011), Lithologic controls on regolith weathering and mass flux in forested ecosystems of the southwestern USA, *Geoderma*, *164*(3–4), 99–111, doi:10.1016/j.geoderma.2011.05.003.

Heimsath, A. M., W. E. Dietrich, K. Nishiizumi, and R. C. Finkel (1997), The soil production function and landscape equilibrium, *Nature*, *388*(6640), 358–361, doi:10.1038/41056.

Heimsath, A. M., W. E. Dietrich, K. Nishiizumi, and R. C. Finkel (1999), Cosmogenic nuclides, topography, and the spatial variation of soil depth, *Geomorphology*, *27*(1-2), 151–172, doi:10.1016/S0169-555X(98)00095-6.

Heimsath, A. M., W. E. Dietrich, K. Nishiizumi, and R. C. Finkel (2001), Stochastic processes of soil production and transport: Erosion rates, topographic variation and cosmogenic nuclides in the Oregon Coast Range, *Earth Surf. Process. Landf.*, *26*(5), 531–552, doi:10.1002/esp.209.

Heimsath, A. M., D. J. Furbish, and W. E. Dietrich (2005), The illusion of diffusion: Field evidence for depth-dependent sediment transport, *Geology*, *33*(12), 949–952, doi:10.1130/G21868.1.

Heimsath, A. M., D. Fink, and G. R. Hancock (2009), The "humped" soil production function: eroding Arnhem Land, Australia, *Earth Surf. Process. Landf.*, *34*(12), 1674–1684, doi:10.1002/esp.1859.

Heimsath, A. M., R. A. DiBiase, and K. X. Whipple (2012), Soil production limits and the transition to bedrock-dominated landscapes, *Nat. Geosci.*, *5*(3), 210–214, doi:10.1038/ngeo1380.

Hergarten, S., J. Robl, and K. Stüwe (2014), Extracting topographic swath profiles across curved geomorphic features, *Earth Surf. Dyn.*, *2*(1), 97–104, doi:10.5194/esurf-2-97-2014.

Heritage, G., and D. Hetherington (2007), Towards a protocol for laser scanning in fluvial geomorphology, *Earth Surf. Process. Landf.*, *32*(1), 66–74, doi:10.1002/esp.1375.

Hicks, D. M., B. Gomez, and N. A. Trustrum (2000), Erosion thresholds and suspended sediment yields, Waipaoa River Basin, New Zealand, *Water Resour. Res.*, *36*(4), 1129–1142, doi:10.1029/1999WR900340.

Hietanen, A. (1951), Metamorphic and Igneous Rocks of the Merrimac Area, Plumas National Forest, California, *Geol. Soc. Am. Bull.*, *62*(6), 565–608, doi:10.1130/0016-7606(1951)62[565:MAIROT]2.0.CO;2.

Hietanen, A. M. (1976), *Metamorphism and plutonism around the middle and south forks of the Feather River, California*, Professional Paper, USGS Numbered Series, U.S. Govt. Print. Off.,.

Hilley, G. E., and J. R. Arrowsmith (2008), Geomorphic response to uplift along the Dragon's Back pressure ridge, Carrizo Plain, California, *Geology*, *36*(5), 367–370, doi:10.1130/G24517A.1.

Hilley, G. E., C. P. Chamberlain, S. Moon, S. Porder, and S. D. Willett (2010), Competition between erosion and reaction kinetics in controlling silicate-weathering rates, *Earth Planet. Sci. Lett.*, *293*(1–2), 191–199, doi:10.1016/j.epsl.2010.01.008.

Hilton, R. G., P. Meunier, N. Hovius, P. J. Bellingham, and A. Galy (2011), Landslide impact on organic carbon cycling in a temperate montane forest, *Earth Surf. Process. Landf.*, *36*(12), 1670–1679, doi:10.1002/esp.2191.

Hilton, R. G., A. Galy, N. Hovius, S.-J. Kao, M.-J. Horng, and H. Chen (2012), Climatic and geomorphic controls on the erosion of terrestrial biomass from subtropical mountain forest, *Glob. Biogeochem. Cycles*, *26*(3), n/a–n/a, doi:10.1029/2012GB004314.

Hilton, R. G., A. Galy, A. J. West, N. Hovius, and G. G. Roberts (2013), Geomorphic control on the δ15N of mountain forests, *Biogeosciences*, *10*(3), 1693–1705, doi:10.5194/bg-10-1693-2013.

Holbrook, W. S., C. S. Riebe, M. Elwaseif, J. L. Hayes, K. Basler-Reeder, D. L. Harry, A. Malazian, A. Dosseto, P. C. Hartsough, and J. W. Hopmans (2014), Geophysical constraints on deep weathering and water storage potential in the Southern Sierra Critical Zone Observatory, *Earth Surf. Process. Landf.*, *39*(3), 366–380, doi:10.1002/esp.3502.

Horton, T. W., D. J. Sjostrom, M. J. Abruzzese, M. A. Poage, J. R. Waldbauer, M. Hren, J. Wooden, and C. P. Chamberlain (2004), Spatial and temporal variation of Cenozoic surface elevation in the Great Basin and Sierra Nevada, *Am. J. Sci.*, *304*(10), 862–888, doi:10.2475/ajs.304.10.862.

House, M. A., B. P. Wernicke, and K. A. Farley (1998), Dating topography of the Sierra Nevada, California, using apatite (U–Th)/He ages, *Nature*, *396*(6706), 66–69, doi:10.1038/23926.

House, M. A., B. P. Wernicke, and K. A. Farley (2001), Paleo-Geomorphology of the Sierra Nevada, California, from (U-TH) /He Ages in Apatite, *Am. J. Sci.*, *301*(2), 77–102, doi:10.2475/ajs.301.2.77.

Hovius, N., C. P. Stark, and P. A. Allen (1997), Sediment flux from a mountain belt derived by landslide mapping, *Geology*, *25*(3), 231.

Hovius, N., C. P. Stark, C. Hao-Tsu, and L. Jiun-Chuan (2000), Supply and removal of sediment in a landslide-dominated mountain belt: Central Range, Taiwan, *J. Geol.*, *108*(1), 73–89.

Howard, A. (1994), A Detachment-Limited Model of Drainage-Basin Evolution, *Water Resour. Res.*, *30*(7), 2261–2285, doi:10.1029/94WR00757.

Hren, M. T., M. Pagani, D. M. Erwin, and M. Brandon (2010), Biomarker reconstruction of the early Eocene paleotopography and paleoclimate of the northern Sierra Nevada, *Geology*, *38*(1), 7–10, doi:10.1130/G30215.1.

Hubbert, K. R., R. C. Graham, and M. A. Anderson (2001), Soil and Weathered Bedrock, *Soil Sci. Soc. Am. J.*, *65*(4), 1255–1252, doi:10.2136/sssaj2001.6541255x.

Hughes, M. W., P. C. Almond, and J. J. Roering (2009), Increased sediment transport via bioturbation at the last glacial-interglacial transition, *Geology*, *37*(10), 919–922, doi:10.1130/G30159A.1.

Hurst, M. D. (2012), Hillslope morphology as an indicator of landscape evolution in tectonically active landscapes, University of Edinburgh, Edinburgh, United Kingdom.

Hurst, M. D., S. M. Mudd, R. Walcott, M. Attal, and K. Yoo (2012), Using hilltop curvature to derive the spatial distribution of erosion rates, *J. Geophys. Res.-Earth Surf.*, *117*(F02017), doi:10.1029/2011JF002057.

Hurst, M. D., S. M. Mudd, M. Attal, and G. Hilley (2013a), Hillslopes Record the Growth and Decay of Landscapes, *Science*, *341*(6148), 868–871, doi:10.1126/science.1241791.

Hurst, M. D., S. M. Mudd, K. Yoo, M. Attal, and R. Walcott (2013b), Influence of lithology on hillslope morphology and response to tectonic forcing in the northern Sierra Nevada of California, *J. Geophys. Res. Earth Surf.*, *118*(2), 832–851, doi:10.1002/jgrf.20049.

Hurst, M. D., S. M. Mudd, K. Yoo, M. Attal, and R. Walcott (2013c), Influence of lithology on hillslope morphology and response to tectonic forcing in the northern Sierra Nevada of California, *J. Geophys. Res. Earth Surf.*, *118*(2), 832–851, doi:10.1002/jgrf.20049.

Hwang, T., L. Band, and T. C. Hales (2009), Ecosystem processes at the watershed scale: Extending optimality theory from plot to catchment, *Water Resour. Res.*, *45*(11), W11425, doi:10.1029/2009WR007775.

Hwang, T., L. E. Band, T. C. Hales, C. F. Miniat, J. M. Vose, P. V. Bolstad, B. Miles, and K. Price (2015), Simulating vegetation controls on hurricane-induced shallow landslides with a distributed ecohydrological model, *J. Geophys. Res. Biogeosciences*, 2014JG002824, doi:10.1002/2014JG002824.

Iida, T. (1999), A stochastic hydro-geomorphological model for shallow landsliding due to rainstorm, *CATENA*, *34*(3–4), 293–313, doi:10.1016/S0341-8162(98)00093-9.

Isherwood, D., and A. Street (1976), Biotite-induced grussification of the Boulder Creek Granodiorite, Boulder County, Colorado, *Geol. Soc. Am. Bull.*, *87*(3), 366–370, doi:10.1130/0016-7606(1976)87<366:BGOTBC>2.0.CO;2.

Istanbulluoglu, E., and R. L. Bras (2005), Vegetation-modulated landscape evolution: Effects of vegetation on landscape processes, drainage density, and topography, *J. Geophys. Res.-Earth Surf.*, *110*(F2), doi:10.1029/2004JF000249.

Istanbulluoglu, E., and R. L. Bras (2006), On the dynamics of soil moisture, vegetation, and erosion: Implications of climate variability and change, *Water Resour. Res.*, *42*(6), doi:10.1029/2005WR004113.

Istanbulluoglu, E., O. Yetemen, E. R. Vivoni, H. A. Gutiérrez-Jurado, and R. L. Bras (2008), Eco-geomorphic implications of hillslope aspect: Inferences from analysis of landscape morphology in central New Mexico, *Geophys. Res. Lett.*, *35*(14), L14403, doi:10.1029/2008GL034477.

Jakubowski, M. K., W. Li, Q. Guo, and M. Kelly (2013), Delineating Individual Trees from Lidar Data: A Comparison of Vector- and Raster-based Segmentation Approaches, *Remote Sens.*, *5*(9), 4163–4186, doi:10.3390/rs5094163.

Jenkins, J. C., D. C. Chojnacky, L. S. Heath, and R. A. Birdsey (2003), National-scale biomass estimators for United States tree species, *For. Sci.*, *49*(1), 12–35.

Jenkins, J. C., D. C. Chojnacky, L. S. Heath, and R. A. Birdsey (2004), *Comprehensive database of diameter-based biomass regressions for North American tree species*.

Jones, D. P., and Graham (1993), Water-Holding Characteristics of Weathered Granitic Rock in Chaparral and Forest Ecosystems, *Soil Sci. Soc. Am. J. - SSSAJ*, *57*(1), doi:10.2136/sssaj1993.03615995005700010044x.

Kasischke, E. S., J. M. Melack, and M. Craig Dobson (1997), The use of imaging radars for ecological applications—A review, *Remote Sens. Environ.*, *59*(2), 141–156, doi:10.1016/S0034-4257(96)00148-4.

Keeling, H. C., and O. L. Phillips (2007), The global relationship between forest productivity and biomass, *Glob. Ecol. Biogeogr.*, *16*(5), 618–631, doi:10.1111/j.1466-8238.2007.00314.x.

Keller, M., M. Palace, and G. Hurtt (2001), Biomass estimation in the Tapajos National Forest, Brazil: Examination of sampling and allometric uncertainties, *For. Ecol. Manag.*, *154*(3), 371–382, doi:10.1016/S0378-1127(01)00509-6.

Kellner, J. R., G. P. Asner, P. M. Vitousek, M. A. Tweiten, S. Hotchkiss, and O. A. Chadwick (2011), Dependence of Forest Structure and Dynamics on Substrate Age and Ecosystem Development, *Ecosystems*, *14*(7), 1156–1167, doi:10.1007/s10021-011-9472-4.

Kelly, A. E., and M. L. Goulden (2016), A montane Mediterranean climate supports year-round photosynthesis and high forest biomass, *Tree Physiol.*, tpv131, doi:10.1093/treephys/tpv131.

Khosravipour, A., A. K. Skidmore, M. Isenburg, T. Wang, and Y. A. Hussin (2014), Generating Pit-free Canopy Height Models from Airborne Lidar, *Photogramm. Eng. Remote Sens.*, *80*(9), 863–872, doi:10.14358/PERS.80.9.863.

Kirby, E., and K. Whipple (2001), Quantifying differential rock-uplift rates via stream profile analysis, *Geology*, *29*(5), 415–418, doi:10.1130/0091-7613(2001)029<0415:QDRURV>2.0.CO;2.

Kirby, E., and K. X. Whipple (2012), Expression of active tectonics in erosional landscapes, *J. Struct. Geol.*, *44*, 54–75, doi:10.1016/j.jsg.2012.07.009.

Kirchner, J. W., R. C. Finkel, C. S. Riebe, D. E. Granger, J. L. Clayton, J. G. King, and W. F. Megahan (2001), Mountain erosion over 10 yr, 10 ky, and 10 my time scales, *Geology*, *29*(7), 591–594.

Kirkby, M. J. (1985), A basis for soil profile modelling in a geomorphic context, *J. Soil Sci.*, *36*(1), 97–121, doi:10.1111/j.1365-2389.1985.tb00316.x.

Koons, P. O. (1989), The topographic evolution of collisional mountain belts; a numerical look at the Southern Alps, New Zealand, *Am. J. Sci.*, *289*(9), 1041–1069, doi:10.2475/ajs.289.9.1041.

Korup, O., and F. Schlunegger (2009), Rock-type control on erosion-induced uplift, eastern Swiss Alps, *Earth Planet. Sci. Lett.*, *278*(3–4), 278–285, doi:10.1016/j.epsl.2008.12.012.

Koukoulas, S., and G. A. Blackburn (2004), Quantifying the spatial properties of forest canopy gaps using LiDAR imagery and GIS, *Int. J. Remote Sens.*, *25*(15), 3049–3072, doi:10.1080/01431160310001657786.

Lague, D., N. Brodu, and J. Leroux (2013), Accurate 3D comparison of complex topography with terrestrial laser scanner: Application to the Rangitikei canyon (N-Z), *ISPRS J. Photogramm. Remote Sens.*, *82*, 10–26, doi:10.1016/j.isprsjprs.2013.04.009.

Lal, D. (1991), Cosmic ray labeling of erosion surfaces: in situ nuclide production rates and erosion models, *Earth Planet. Sci. Lett.*, *104*(2–4), 424–439, doi:10.1016/0012-821X(91)90220-C.

Langbein, W. B., and S. A. Schumm (1958), Yield of sediment in relation to mean annual precipitation, *Eos Trans. Am. Geophys. Union*, *39*(6), 1076–1084, doi:10.1029/TR039i006p01076.

Larsen, I. J., and D. R. Montgomery (2012), Landslide erosion coupled to tectonics and river incision, *Nat. Geosci.*, *5*(7), 468–473, doi:10.1038/ngeo1479.

Larsen, I. J., D. R. Montgomery, and O. Korup (2010), Landslide erosion controlled by hillslope material, *Nat. Geosci.*, *3*(4), 247–251, doi:10.1038/ngeo776.

Larsen, I. J., P. C. Almond, A. Eger, J. O. Stone, D. R. Montgomery, and B. Malcolm (2014a), Rapid Soil Production and Weathering in the Southern Alps, New Zealand, *Science*, *343*(6171), 637–640, doi:10.1126/science.1244908.

Larsen, I. J., D. R. Montgomery, and H. M. Greenberg (2014b), The contribution of mountains to global denudation, *Geology*, G35136.1, doi:10.1130/G35136.1.

Lashermes, B., E. Foufoula-Georgiou, and W. E. Dietrich (2007), Channel network extraction from high resolution topography using wavelets, *Geophys. Res. Lett.*, *34*(23), L23S04, doi:10.1029/2007GL031140.

Lebedeva, M. I., and S. L. Brantley (2013), Exploring geochemical controls on weathering and erosion of convex hillslopes: beyond the empirical regolith production function, *Earth Surf. Process. Landf.*, *38*(15), 1793–1807, doi:10.1002/esp.3424.

Lebedeva, M. I., R. C. Fletcher, V. N. Balashov, and S. L. Brantley (2007), A reactive diffusion model describing transformation of bedrock to saprolite, *Chem. Geol.*, *244*(3-4), 624–645.

Lefsky, M. A., W. B. Cohen, S. A. Acker, G. G. Parker, T. A. Spies, and D. Harding (1999a), Lidar remote sensing of the canopy structure and biophysical properties of Douglas-fir western hemlock forests, *Remote Sens. Environ.*, *70*(3), 339–361, doi:10.1016/S0034-4257(99)00052-8.

Lefsky, M. A., D. Harding, W. . Cohen, G. Parker, and H. . Shugart (1999b), Surface Lidar Remote Sensing of Basal Area and Biomass in Deciduous Forests of Eastern Maryland, USA, *Remote Sens. Environ.*, *67*(1), 83–98, doi:10.1016/S0034-4257(98)00071-6.

Lefsky, M. A., W. B. Cohen, D. J. Harding, G. G. Parker, S. A. Acker, and S. T. Gower (2002), Lidar remote sensing of above-ground biomass in three biomes, *Glob. Ecol. Biogeogr.*, *11*(5), 393–399, doi:10.1046/j.1466-822x.2002.00303.x.

Lefsky, M. A., D. J. Harding, M. Keller, W. B. Cohen, C. C. Carabajal, F. Del Bom Espirito-Santo, M. O. Hunter, and R. de Oliveira (2005), Estimates of forest canopy height and aboveground biomass using ICESat, *Geophys. Res. Lett.*, *32*(22), L22S02, doi:10.1029/2005GL023971.

Lewis, R. S., and L. R. Stanford (2002), Geologic map compilation of the western half of the Nez Perce Pass 30 x 60 minute quadrangle, Idaho,

Lim, K., P. Treitz, M. Wulder, B. St-Onge, and M. Flood (2003), LiDAR remote sensing of forest structure, *Prog. Phys. Geogr.*, *27*(1), 88–106, doi:10.1191/0309133303pp360ra.

Lin, C.-W., C.-M. Tseng, Y.-H. Tseng, L.-Y. Fei, Y.-C. Hsieh, and P. Tarolli (2013), Recognition of large scale deep-seated landslides in forest areas of Taiwan using high resolution topography, *J. Asian Earth Sci.*, *62*, 389–400, doi:10.1016/j.jseaes.2012.10.022.

Lindgren, W. (1911), The tertiary gravels of the Sierra Nevada of California, *USGS Prof. Pap. 73*, 226 p.

Lin, Y., J. Hyyppa, and A. Jaakkola (2011), Mini-UAV-Borne LIDAR for Fine-Scale Mapping, *Ieee Geosci. Remote Sens. Lett.*, *8*(3), 426–430, doi:10.1109/LGRS.2010.2079913.

Li, W., Q. Guo, M. K. Jakubowski, and M. Kelly (2012), A New Method for Segmenting Individual Trees from the Lidar Point Cloud, *Photogramm. Eng. Remote Sens.*, *78*(1), 75–84.

Ludington, S., B. C. Moring, R. J. Miller, K. S. Flynn, P. A. Stone, and D. R. Bedford (2005), Preliminary integrated databases for the United States - Western States: California, Nevada, Arizona, and Washington,

Ludwig, J. A., B. P. Wilcox, D. D. Breshears, D. J. Tongway, and A. C. Imeson (2005), Vegetation patches and runoff-erosion as interacting ecohydrological processes in semiarid landscapes, *Ecology*, *86*(2), 288–297, doi:10.1890/03-0569.

Lydersen, J., and M. North (2012), Topographic Variation in Structure of Mixed-Conifer Forests Under an Active-Fire Regime, *Ecosystems*, *15*(7), 1134–1146, doi:10.1007/s10021-012-9573-8.

Macias-Fauria, M., and E. A. Johnson (2013), Warming-induced upslope advance of subalpine forest is severely limited by geomorphic processes, *Proc. Natl. Acad. Sci.*, *110*(20), 8117–8122, doi:10.1073/pnas.1221278110.

Mage, S. M., and S. Porder (2013), Parent Material and Topography Determine Soil Phosphorus Status in the Luquillo Mountains of Puerto Rico, *Ecosystems*, *16*(2), 284–294, doi:10.1007/s10021-012-9612-5.

Maher, K. (2010), The dependence of chemical weathering rates on fluid residence time, *Earth Planet. Sci. Lett.*, *294*(1–2), 101–110, doi:10.1016/j.epsl.2010.03.010.

Maher, K. (2011), The role of fluid residence time and topographic scales in determining chemical fluxes from landscapes, *Earth Planet. Sci. Lett.*, *312*(1–2), 48–58, doi:10.1016/j.epsl.2011.09.040.

Maher, K., and C. P. Chamberlain (2014), Hydrologic Regulation of Chemical Weathering and the Geologic Carbon Cycle, *Science*, *343*(6178), 1502–1504, doi:10.1126/science.1250770.

Ma, L., F. Chabaux, E. Pelt, E. Blaes, L. Jin, and S. Brantley (2010), Regolith production rates calculated with uranium-series isotopes at Susquehanna/Shale Hills Critical Zone Observatory, *Earth Planet. Sci. Lett.*, *297*(1–2), 211–225, doi:10.1016/j.epsl.2010.06.022.

Ma, L., F. Chabaux, N. West, E. Kirby, L. Jin, and S. Brantley (2013), Regolith production and transport in the Susquehanna Shale Hills Critical Zone Observatory, Part 1: Insights from U-series isotopes, *J. Geophys. Res. Earth Surf.*, *118*(2), 722–740, doi:10.1002/jgrf.20037.

Mallet, C., and F. Bretar (2009), Full-waveform topographic lidar: State-of-the-art, *ISPRS J. Photogramm. Remote Sens.*, *64*(1), 1–16, doi:10.1016/j.isprsjprs.2008.09.007.

Marshall, J. A., and J. J. Roering (2014), Diagenetic variation in the Oregon Coast Range: Implications for rock strength, soil production, hillslope form, and landscape evolution, *J. Geophys. Res. Earth Surf.*, *119*, 1395–1417, doi:10.1002/2013JF003004.

Marshall, J. A., J. J. Roering, P. J. Bartlein, D. G. Gavin, D. E. Granger, A. W. Rempel, S. J. Praskievicz, and T. C. Hales (2015), Frost for the trees: Did climate increase erosion in unglaciated landscapes during the late Pleistocene?, *Sci. Adv.*, *1*(10), e1500715, doi:10.1126/sciadv.1500715.

Marshall, J. D., and R. A. Monserud (2006), Co-occurring species differ in tree-ring δ18O trends, *Tree Physiol.*, *26*(8), 1055–1066, doi:10.1093/treephys/26.8.1055.

Martin, Y. E., E. A. Johnson, and O. Chaikina (2013), Interplay between field observations and numerical modeling to understand temporal pulsing of tree root throw processes, Canadian Rockies, Canada, *Geomorphology*, *200*, 89–105, doi:10.1016/j.geomorph.2013.04.017.

Mascaro, J., M. Detto, G. P. Asner, and H. C. Muller-Landau (2011), Evaluating uncertainty in mapping forest carbon with airborne LiDAR, *Remote Sens. Environ.*, *115*(12), 3770–3774, doi:10.1016/j.rse.2011.07.019.

McCarroll, D., and N. J. Loader (2004), Stable isotopes in tree rings, *Quat. Sci. Rev.*, *23*(7–8), 771–801, doi:10.1016/j.quascirev.2003.06.017.

McGuire, L. A., J. D. Pelletier, and J. J. Roering (2014), Development of topographic asymmetry: Insights from dated cinder cones in the western United States, *J. Geophys. Res. Earth Surf.*, *119*(8), 1725–1750, doi:10.1002/2014JF003081.

McKean, J., and J. Roering (2004), Objective landslide detection and surface morphology mapping using high-resolution airborne laser altimetry, *Geomorphology*, *57*(3-4), 331–351, doi:10.1016/S0169-555X(03)00164-8.

McKean, J. A., W. E. Dietrich, R. C. Finkel, J. R. Southon, and M. W. Caffee (1993), Quantification of soil production and downslope creep rates from cosmogenic 10Be accumulations on a hillslope profile, *Geology*, *21*(4), 343–346, doi:10.1130/0091-7613(1993)021<0343:QOSPAD>2.3.CO;2.

Means, J. E., S. A. Acker, B. J. Fitt, M. Renslow, L. Emerson, C. J. Hendrix, and others (2000), Predicting forest stand characteristics with airborne scanning lidar, *Photogramm. Eng. Remote Sens.*, *66*(11), 1367–1372.

Meyer, M., M. North, A. Gray, and H. Zald (2007), Influence of soil thickness on stand characteristics in a Sierra Nevada mixed-conifer forest, *Plant Soil*, *294*(1), 113–123, doi:10.1007/s11104-007-9235-3.

Migoń, P. (2006), *Granite Landscapes of the World*, Geomorphological Landscapes of the World, Oxford University Press, Oxford.

Migoń, P., and K. Lidmar-Bergström (2001), Weathering mantles and their significance for geomorphological evolution of central and northern Europe since the Mesozoic, *Earth-Sci. Rev.*, *56*(1–4), 285–324, doi:10.1016/S0012-8252(01)00068-X.

Migoń, P., and G. Vieira (2014), Granite geomorphology and its geological controls, Serra da Estrela, Portugal, *Geomorphology*, *226*, 1–14, doi:10.1016/j.geomorph.2014.07.027.

Miller, J. D., and A. E. Thode (2007), Quantifying burn severity in a heterogeneous landscape with a relative version of the delta Normalized Burn Ratio (dNBR), *Remote Sens. Environ.*, *109*(1), 66–80, doi:10.1016/j.rse.2006.12.006.

Miller, J. D., E. E. Knapp, C. H. Key, C. N. Skinner, C. J. Isbell, R. M. Creasy, and J. W. Sherlock (2009), Calibration and validation of the relative differenced Normalized Burn Ratio (RdNBR) to three measures of fire severity in the Sierra Nevada and Klamath Mountains, California, USA, *Remote Sens. Environ.*, *113*(3), 645–656, doi:10.1016/j.rse.2008.11.009.

Miller, S. R., R. L. Slingerland, and E. Kirby (2007), Characteristics of steady state fluvial topography above fault-bend folds, *J. Geophys. Res.*, *112*(F4), F04004.

Milodowski, D. T., S. M. Mudd, and E. T. A. Mitchard (2015a), Erosion rates as a potential bottom-up control of forest structural characteristics in the Sierra Nevada Mountains, *Ecology*, *96*(1), 31–38, doi:10.1890/14-0649.1.

Milodowski, D. T., S. M. Mudd, and E. T. A. Mitchard (2015b), Topographic roughness as a signature of the emergence of bedrock in eroding landscapes, *Earth Surf. Dyn.*, *3*(4), 483–499, doi:10.5194/esurf-3-483-2015.

Mitchard, E. T. A., S. S. Saatchi, I. H. Woodhouse, G. Nangendo, N. S. Ribeiro, M. Williams, C. M. Ryan, S. L. Lewis, T. R. Feldpausch, and P. Meir (2009), Using satellite radar backscatter to predict above-ground woody biomass: A consistent relationship across four different African landscapes, *Geophys. Res. Lett.*, *36*(23), L23401, doi:10.1029/2009GL040692.

Molnar, P., and P. England (1990), Late Cenozoic uplift of mountain ranges and global climate change: chicken or egg?, *Nature*, *346*(6279), 29–34, doi:10.1038/346029a0.

Molnar, P., R. S. Anderson, and S. P. Anderson (2007), Tectonics, fracturing of rock, and erosion, *J. Geophys. Res. Earth Surf.*, *112*(F3), F03014, doi:10.1029/2005JF000433.

Montgomery, D., and M. Brandon (2002), Topographic controls on erosion rates in tectonically active mountain ranges, *Earth Planet. Sci. Lett.*, *201*(3-4), 481–489, doi:10.1016/S0012-821X(02)00725-2.

Montgomery, D., and W. Dietrich (1988), Where Do Channels Begin, *Nature*, *336*(6196), 232–234, doi:10.1038/336232a0.

Montgomery, D. R., and W. E. Dietrich (1992), Channel Initiation and the Problem of Landscape Scale, *Science*, *255*(5046), 826–830, doi:10.1126/science.255.5046.826.

Montgomery, D. R., and W. E. Dietrich (1994), A physically based model for the topographic control on shallow landsliding, *Water Resour. Res.*, *30*(4), 1153–1171.

Montgomery, D. R., K. M. Schmidt, H. M. Greenberg, and W. E. Dietrich (2000), Forest clearing and regional landsliding, *Geology*, *28*(4), 311–314, doi:10.1130/0091-7613(2000)28<311:FCARL>2.0.CO;2.

Montgomery, D. R., G. Balco, and S. D. Willett (2001), Climate, tectonics, and the morphology of the Andes, *Geology*, *29*(7), 579–582, doi:10.1130/0091-7613(2001)029<0579:CTATMO>2.0.CO;2.

Moody, J. A., and D. A. Martin (2001), Initial hydrologic and geomorphic response following a wildfire in the Colorado Front Range, *Earth Surf. Process. Landf.*, *26*(10), 1049–1070, doi:10.1002/esp.253.

Moore, J. R., J. W. Sanders, W. E. Dietrich, and S. D. Glaser (2009), Influence of rock mass strength on the erosion rate of alpine cliffs, *Earth Surf. Process. Landf.*, *34*(10), 1339–1352, doi:10.1002/esp.1821.

Mudd, S. M., and D. J. Furbish (2004), Influence of chemical denudation on hillslope morphology, *J Geophys Res*, *109*(4).

Mudd, S. M., and D. J. Furbish (2005), Lateral migration of hillcrests in response to channel incision in soil-mantled landscapes, *J. Geophys. Res. Earth Surf.*, *110*(F4), F04026, doi:10.1029/2005JF000313.

Mudd, S. M., and D. J. Furbish (2007a), Responses of soil-mantled hillslopes to transient channel incision rates, *J. Geophys. Res. Earth Surf.*, *112*(F3), F03S18, doi:10.1029/2006JF000516.

Mudd, S. M., and D. J. Furbish (2007b), Responses of soil-mantled hillslopes to transient channel incision rates, *J. Geophys. Res. Earth Surf.*, *112*(F3), F03S18, doi:10.1029/2006JF000516.

Mudd, S. M., and K. Yoo (2010a), Reservoir theory for studying the geochemical evolution of soils, *J. Geophys. Res. Earth Surf.*, *115*(F3), F03030, doi:10.1029/2009JF001591.

Mudd, S. M., and K. Yoo (2010b), Reservoir theory for studying the geochemical evolution of soils, *J Geophys Res*, *115*(F03030), F03030.

Mudd, S. M., K. Yoo, and E. J. Gabet (2013), 7.5 Influence of Chemical Weathering on Hillslope Forms, in *Treatise on Geomorphology*, edited by J. F. Shroder, pp. 56–65, Academic Press, San Diego.

Mudd, S. M., M. Attal, D. T. Milodowski, S. W. D. Grieve, and D. A. Valters (2014), A statistical framework to quantify spatial variation in channel gradients using the integral method of channel profile analysis, *J. Geophys. Res. Earth Surf.*, *119*(2), 2013JF002981, doi:10.1002/2013JF002981.

Mulch, A., S. A. Graham, and C. P. Chamberlain (2006), Hydrogen Isotopes in Eocene River Gravels and Paleoelevation of the Sierra Nevada, *Science*, *313*(5783), 87–89, doi:10.1126/science.1125986.

Mulch, A., A. M. Sarna-Wojcicki, M. E. Perkins, and C. P. Chamberlain (2008), A Miocene to Pleistocene climate and elevation record of the Sierra Nevada (California), *Proc. Natl. Acad. Sci.*, *105*(19), 6819–6824, doi:10.1073/pnas.0708811105.

Murray, A. B., M. a. F. Knaapen, M. Tal, and M. L. Kirwan (2008), Biomorphodynamics: Physical-biological feedbacks that shape landscapes, *Water Resour. Res.*, *44*(11), W11301, doi:10.1029/2007WR006410.

Næsset, E., and T. Gobakken (2008), Estimation of above- and below-ground biomass across regions of the boreal forest zone using airborne laser, *Remote Sens. Environ.*, *112*(6), 3079–3090, doi:10.1016/j.rse.2008.03.004.

Næsset, E., T. Gobakken, S. Solberg, T. G. Gregoire, R. Nelson, G. Ståhl, and D. Weydahl (2011), Model-assisted regional forest biomass estimation using LiDAR and InSAR as auxiliary data: A case study from a boreal forest area, *Remote Sens. Environ.*, *115*(12), 3599–3614, doi:10.1016/j.rse.2011.08.021.

National Research Council (2001), *Basic Research Opportunities in Earth Science*, The National Academies Press, Washington, DC.

Návar, J. (2009), Allometric equations for tree species and carbon stocks for forests of northwestern Mexico, *For. Ecol. Manag.*, *257*(2), 427–434, doi:10.1016/j.foreco.2008.09.028.

Nelson, R., W. Krabill, and G. MacLean (1984), Determining forest canopy characteristics using airborne laser data, *Remote Sens. Environ.*, *15*(3), 201–212, doi:10.1016/0034-4257(84)90031-2.

Nicótina, L., D. G. Tarboton, T. K. Tesfa, and A. Rinaldo (2011), Hydrologic controls on equilibrium soil depths, *Water Resour. Res.*, *47*(4), W04517, doi:10.1029/2010WR009538.

Norman, S. A., R. J. Schaetzl, and T. W. Small (1995), Effects of slope angle on mass movement by tree uprooting, *Geomorphology*, *14*(1), 19–27, doi:10.1016/0169-555X(95)00016-X.

Norton, K. P., F. von Blanckenburg, F. Schlunegger, M. Schwab, and P. W. Kubik (2008), Cosmogenic nuclide-based investigation of spatial erosion and hillslope channel coupling in the transient foreland of the Swiss Alps, *Geomorphology*, *95*(3–4), 474–486, doi:10.1016/j.geomorph.2007.07.013.

Oberlander, T. M. (1972), Morphogenesis of granitic boulder slopes in the Mojave Desert, California, *J. Geol.*, 1–20.

Olona, J., J. A. Pulgar, G. Fernández-Viejo, C. López-Fernández, and J. M. González-Cortina (2010), Weathering variations in a granitic massif and related geotechnical properties through seismic and electrical resistivity methods, *Surf. Geophys.*, *8*(1750), doi:10.3997/1873-0604.2010043.

Osterkamp, W. R., T. J. Toy, and M. T. Lenart (2006), Development of partial rock veneers by root throw in a subalpine setting, *Earth Surf. Process. Landf.*, *31*(1), 1–14.

Osterkamp, W. R., C. R. Hupp, and M. Stoffel (2012), The interactions between vegetation and erosion: new directions for research at the interface of ecology and geomorphology, *Earth Surf. Process. Landf.*, *37*(1), 23–36, doi:10.1002/esp.2173.

Ostle, N. J. et al. (2009), Integrating plant–soil interactions into global carbon cycle models, *J. Ecol.*, *97*(5), 851–863, doi:10.1111/j.1365-2745.2009.01547.x.

Ouimet, W. B., K. X. Whipple, and D. E. Granger (2009), Beyond threshold hillslopes: Channel adjustment to base-level fall in tectonically active mountain ranges, *Geology*, *37*(7), 579–582, doi:10.1130/G30013A.1.

Owen, J. J., R. Amundson, W. E. Dietrich, K. Nishiizumi, B. Sutter, and G. Chong (2011), The sensitivity of hillslope bedrock erosion to precipitation, *Earth Surf. Process. Landf.*

Parsekian, A. D., K. Singha, B. J. Minsley, W. S. Holbrook, and L. Slater (2015), Multiscale geophysical imaging of the critical zone, *Rev. Geophys.*, *53*(1), 2014RG000465, doi:10.1002/2014RG000465.

Passalacqua, P., and E. Foufoula-Georgiou (2015), Comment on "Objective extraction of channel heads from high-resolution topographic data" by Fiona J. Clubb et al., *Water Resour. Res.*, *51*(2), 1372–1376, doi:10.1002/2014WR016412.

Passalacqua, P., T. Do Trung, E. Foufoula-Georgiou, G. Sapiro, and W. E. Dietrich (2010a), A geometric framework for channel network extraction from lidar: Nonlinear diffusion and geodesic paths, *J. Geophys. Res. Earth Surf.*, *115*(F1), F01002, doi:10.1029/2009JF001254.

Passalacqua, P., P. Tarolli, and E. Foufoula-Georgiou (2010b), Testing space-scale methodologies for automatic geomorphic feature extraction from lidar in a complex mountainous landscape, *Water Resour. Res.*, *46*(11), W11535, doi:10.1029/2009WR008812.

Passalacqua, P. et al. (2015), Analyzing high resolution topography for advancing the understanding of mass and energy transfer through landscapes: A review, *Earth-Sci. Rev.*, *148*, 174–193, doi:10.1016/j.earscirev.2015.05.012.

Paton, T. R. (1995), *Soils : a new global view*, UCL, London.

Pelak, N. F., A. J. Parolari, and A. Porporato (2016), Bistable plant–soil dynamics and biogenic controls on the soil production function, *Earth Surf. Process. Landf.*, n/a–n/a, doi:10.1002/esp.3878.

Pelletier, J. D. (2013), A robust, two-parameter method for the extraction of drainage networks from high-resolution digital elevation models (DEMs): Evaluation using synthetic and real-world DEMs, *Water Resour. Res.*, *49*(1), 75–89, doi:10.1029/2012WR012452.

Pelletier, J. D., and C. Rasmussen (2009a), Geomorphically based predictive mapping of soil thickness in upland watersheds, *Water Resour. Res.*, *45*(9), W09417, doi:10.1029/2008WR007319.

Pelletier, J. D., and C. Rasmussen (2009b), Quantifying the climatic and tectonic controls on hillslope steepness and erosion rate, *Lithosphere*, *1*(2), 73–80, doi:10.1130/L3.1.

Pelletier, J. D. et al. (2011), Calibration and testing of upland hillslope evolution models in a dated landscape: Banco Bonito, New Mexico, *J. Geophys. Res.*, *116*(F4), F04004.

Pelletier, J. D. et al. (2013), Coevolution of nonlinear trends in vegetation, soils, and topography with elevation and slope aspect: A case study in the sky islands of southern Arizona, *J. Geophys. Res. Earth Surf.*, *118*(2), 741–758, doi:10.1002/jgrf.20046.

Penck, A. (1905), Glacial features in the surface of the Alps, *J. Geol.*, *13*(1), 1–19.

Perona, P., and J. Malik (1990), Scale-space and edge detection using anisotropic diffusion, *IEEE Trans. Pattern Anal. Mach. Intell.*, *12*(7), 629–639, doi:10.1109/34.56205.

Perron, J. T., and L. Royden (2013), An integral approach to bedrock river profile analysis, *Earth Surf. Process. Landf.*, *38*(6), 570–576, doi:10.1002/esp.3302.

Perron, J. T., W. E. Dietrich, and J. W. Kirchner (2008a), Controls on the spacing of first-order valleys, *J. Geophys. Res.-Earth Surf.*, *113*(F4), doi:10.1029/2007JF000977.

Perron, J. T., J. W. Kirchner, and W. E. Dietrich (2008b), Spectral signatures of characteristic spatial scales and nonfractal structure in landscapes, *J. Geophys. Res.-Earth Surf.*, *113*(F4), doi:10.1029/2007JF000866.

Perron, J. T., J. W. Kirchner, and W. E. Dietrich (2009), Formation of evenly spaced ridges and valleys, *Nature*, *460*(7254), 502–505, doi:10.1038/nature08174.

Phillips, J. D. (2009), Biological energy in landscape evolution, *Am. J. Sci.*, *309*(4), 271–289, doi:10.2475/04.2009.01.

Phillips, J. D., and D. A. Marion (2004), Pedological memory in forest soil development, *For. Ecol. Manag.*, *188*(1-3), 363–380, doi:10.1016/j.foreco.2003.08.007.

Phillips, J. D., and D. A. Marion (2006), Biomechanical effects of trees on soil and regolith: Beyond treethrow, *Ann. Assoc. Am. Geogr.*, *96*(2), 233–247, doi:10.1111/j.1467-8306.2006.00476.x.

Pirotti, F., and P. Tarolli (2010), Suitability of LiDAR point density and derived landform curvature maps for channel network extraction, *Hydrol. Process.*, *24*(9), 1187–1197, doi:10.1002/hyp.7582.

Poage, M. A., and C. P. Chamberlain (2001), Empirical Relationships Between Elevation and the Stable Isotope Composition of Precipitation and Surface Waters: Considerations for Studies of Paleoelevation Change, *Am. J. Sci.*, *301*(1), 1–15, doi:10.2475/ajs.301.1.1.

Popescu, S. C. (2007), Estimating biomass of individual pine trees using airborne lidar, *Biomass Bioenergy*, *31*(9), 646–655, doi:10.1016/j.biombioe.2007.06.022.

Popescu, S. C., and R. H. Wynne (2004), Seeing the trees in the forest: using lidar and multispectral data fusion with local filtering and variable window size for estimating tree height, *Photogramm. Eng. Remote Sens.*, *70*(5), 589–604.

Porder, S., and O. A. Chadwick (2009), Climate and soil-age constraints on nutrient uplift and retention by plants, *Ecology*, *90*(3), 623–636, doi:10.1890/07-1739.1.

Porder, S., and S. Ramachandran (2013), The phosphorus concentration of common rocks—a potential driver of ecosystem P status, *Plant Soil*, *367*(1-2), 41–55, doi:10.1007/s11104-012-1490-2.

Porder, S., A. Paytan, and P. M. Vitousek (2005a), Erosion and landscape development affect plant nutrient status in the Hawaiian Islands, *Oecologia*, *142*(3), 440–449, doi:10.1007/s00442-004-1743-8.

Porder, S., G. P. Asner, and P. M. Vitousek (2005b), Ground-based and remotely sensed nutrient availability across a tropical landscape, *Proc. Natl. Acad. Sci. U. S. A.*, *102*(31), 10909–10912, doi:10.1073/pnas.0504929102.

Porder, S., P. Vitousek, O. Chadwick, C. Chamberlain, and G. Hilley (2007), Uplift, Erosion, and Phosphorus Limitation in Terrestrial Ecosystems, *Ecosystems*, *10*(1), 159–171, doi:10.1007/s10021-006-9011-x.

Porder, S., A. H. Johnson, H. X. Xing, G. Brocard, S. Goldsmith, and J. Pett-Ridge (2015), Linking geomorphology, weathering and cation availability in the Luquillo Mountains of Puerto Rico, *Geoderma*, *249–250*, 100–110, doi:10.1016/j.geoderma.2015.03.002.

Prince, P. S., J. A. Spotila, and W. S. Henika (2011), Stream capture as driver of transient landscape evolution in a tectonically quiescent setting, *Geology*, *39*(9), 823.

Pritchard, D., G. G. Roberts, N. J. White, and C. N. Richardson (2009), Uplift histories from river profiles, *Geophys. Res. Lett.*, *36*(24), L24301, doi:10.1029/2009GL040928.

Pye, K. (1986), Mineralogical and textural controls on the weathering of granitoid rocks, *CATENA*, *13*(1–2), 47–57, doi:10.1016/S0341-8162(86)80004-2.

Rabus, B., M. Eineder, A. Roth, and R. Bamler (2003), The shuttle radar topography mission—a new class of digital elevation models acquired by spaceborne radar, *ISPRS J. Photogramm. Remote Sens.*, *57*(4), 241–262, doi:10.1016/S0924-2716(02)00124-7.

Rasmussen, C., and N. J. Tabor (2007), Applying a quantitative pedogenic energy model across a range of environmental gradients, *Soil Sci. Soc. Am. J.*, *71*(6), 1719–1729, doi:10.2136/ssaj2007.0051.

Rasmussen, C., P. Troch, J. Chorover, P. Brooks, J. Pelletier, and T. Huxman (2011a), An open system framework for integrating critical zone structure and function, *Biogeochemistry*, *102*(1), 15–29, doi:10.1007/s10533-010-9476-8.

Rasmussen, C., S. Brantley, D. deB. Richter, A. Blum, J. Dixon, and A. F. White (2011b), Strong climate and tectonic control on plagioclase weathering in granitic terrain, *Earth Planet. Sci. Lett.*, *301*(3–4), 521–530, doi:10.1016/j.epsl.2010.11.037.

Rasmussen, C., J. D. Pelletier, P. A. Troch, T. L. Swetnam, and J. Chorover (2015), Quantifying Topographic and Vegetation Effects on the Transfer of Energy and Mass to the Critical Zone, *Vadose Zone J.*, *0*(0), 0, doi:10.2136/vzj2014.07.0102.

R Core Team (2013), *R: A language and environment for statistical computing.*, R Foundation for Statistical Computing, Vienna, Austria.

Reinhardt, L., D. Jerolmack, B. J. Cardinale, V. Vanacker, and J. Wright (2010), Dynamic interactions of life and its landscape: feedbacks at the interface of geomorphology and ecology, *Earth Surf. Process. Landf.*, *35*(1), 78–101, doi:10.1002/esp.1912.

Rempe, D. M., and W. E. Dietrich (2014), A bottom-up control on fresh-bedrock topography under landscapes, *Proc. Natl. Acad. Sci.*, *111*(18), 6576–6581, doi:10.1073/pnas.1404763111.

Reneau, S. L., and W. E. Dietrich (1991), Erosion rates in the southern oregon coast range: Evidence for an equilibrium between hillslope erosion and sediment yield, *Earth Surf. Process. Landf.*, *16*(4), 307–322, doi:10.1002/esp.3290160405.

Rengers, F. K., G. E. Tucker, J. A. Moody, and B. A. Ebel (2016), Illuminating wildfire erosion and deposition patterns with repeat terrestrial lidar, *J. Geophys. Res. Earth Surf.*, *121*(3), 2015JF003600, doi:10.1002/2015JF003600.

Reubens, B., J. Poesen, F. Danjon, G. Geudens, and B. Muys (2007), The role of fine and coarse roots in shallow slope stability and soil erosion control with a focus on root system architecture: a review, *Trees*, *21*(4), 385–402, doi:10.1007/s00468-007-0132-4.

Riebe, C. S., J. W. Kirchner, D. E. Granger, and R. C. Finkel (2000), Erosional equilibrium and disequilibrium in the Sierra Nevada, inferred from cosmogenic 26Al and 10Be in alluvial sediment, *Geology*, *28*(9), 803–806.

Riebe, C. S., J. W. Kirchner, D. E. Granger, and R. C. Finkel (2001a), Minimal climatic control on erosion rates in the Sierra Nevada, California, *Geology*, *29*(5), 447–450, doi:10.1130/0091-7613(2001)029<0447:MCCOER>2.0.CO;2.

Riebe, C. S., J. W. Kirchner, D. E. Granger, and R. C. Finkel (2001b), Strong tectonic and weak climatic control of long-term chemical weathering rates, *Geology*, *29*(6), 511.

Riebe, C. S., J. W. Kirchner, and R. C. Finkel (2004), Erosional and climatic effects on long-term chemical weathering rates in granitic landscapes spanning diverse climate regimes, *Earth Planet. Sci. Lett.*, *224*(3-4), 547–562.

Roberts, G. G., and N. White (2010), Estimating uplift rate histories from river profiles using African examples, *J. Geophys. Res. Solid Earth*, *115*(B2), B02406, doi:10.1029/2009JB006692.

Roering, J., and M. Gerber (2005), Fire and the evolution of steep, soil-mantled landscapes, *Geology*, *33*(5), 349–352, doi:10.1130/G21260.1.

Roering, J., J. Kirchner, L. Sklar, and W. Dietrich (2001a), Hillslope evolution by nonlinear creep and landsliding: An experimental study, *Geology*, *29*(2), 143–146, doi:10.1130/0091-7613(2001)029<0143:HEBNCA>2.0.CO;2.

Roering, J. J. (2008), How well can hillslope evolution models "explain" topography? Simulating soil transport and production with high-resolution topographic data, *Geol. Soc. Am. Bull.*, *120*(9-10), 1248–1262, doi:10.1130/B26283.1.

Roering, J. J., J. W. Kirchner, and W. E. Dietrich (1999), Evidence for nonlinear, diffusive sediment transport on hillslopes and implications for landscape morphology, *Water Resour. Res.*, *35*(3), 853–870, doi:10.1029/1998WR900090.

Roering, J. J., J. W. Kirchner, and W. E. Dietrich (2001b), Hillslope evolution by nonlinear, slope-dependent transport: Steady state morphology and equilibrium adjustment timescales, *J. Geophys. Res. Solid Earth*, *106*(B8), 16499–16513, doi:10.1029/2001JB000323.

Roering, J. J., P. Almond, P. Tonkin, and J. McKean (2002), Soil transport driven by biological processes over millennial time scales, *Geology*, *30*(12), 1115–1118, doi:10.1130/0091-7613(2002)030<1115:STDBBP>2.0.CO;2.

Roering, J. J., K. M. Schmidt, J. D. Stock, W. E. Dietrich, and D. R. Montgomery (2003), Shallow landsliding, root reinforcement, and the spatial distribution of trees in the Oregon Coast Range, *Can. Geotech. J.*, *40*(2), 237–253.

Roering, J. J., P. Almond, P. Tonkin, and J. McKean (2004), Constraining climatic controls on hillslope dynamics using a coupled model for the transport of soil and tracers: Application to loess-mantled hillslopes, South Island, New Zealand, *J. Geophys. Res.*, *109*(F1), F01010, doi:10.1029/2003JF000034.

Roering, J. J., J. T. Perron, and J. W. Kirchner (2007), Functional relationships between denudation and hillslope form and relief, *Earth Planet. Sci. Lett.*, *264*(1-2), 245–258, doi:10.1016/j.epsl.2007.09.035.

Roering, J. J., J. Marshall, A. M. Booth, M. Mort, and Q. Jin (2010), Evidence for biotic controls on topography and soil production, *Earth Planet. Sci. Lett.*, *298*(1-2), 183–190, doi:10.1016/j.epsl.2010.07.040.

Roering, J. J., B. H. Mackey, J. A. Marshall, K. E. Sweeney, N. I. Deligne, A. M. Booth, A. L. Handwerger, and C. Cerovski-Darriau (2013), "You are HERE": Connecting the dots with airborne lidar for geomorphic fieldwork, *Geomorphology*, *200*, 172–183, doi:10.1016/j.geomorph.2013.04.009.

Rose, K., R. Graham, and D. Parker (2003), Water source utilization by Pinus jeffreyi and Arctostaphylos patula on thin soils over bedrock, *Oecologia*, *134*(1), 46–54.

Rosenbloom, N. A., and R. S. Anderson (1994), Hillslope and channel evolution in a marine terraced landscape, Santa Cruz, California, *J. Geophys. Res. Solid Earth*, *99*(B7), 14013–14029, doi:10.1029/94JB00048.

Royce, E. B., and M. G. Barbour (2001), Mediterranean climate effects. I. Conifer water use across a Sierra Nevada ecotone, *Am. J. Bot.*, *88*(5), 911–918.

Royden, L., and J. T. Perron (2013), Solutions of the stream power equation and application to the evolution of river longitudinal profiles, *J. Geophys. Res. Earth Surf.*, *118*(2), 497–518, doi:10.1002/jgrf.20031.

Ruleman, C. A., R. G. Bohannon, B. Bryant, R. R. Shroba, and W. R. Premo (2011), Geologic Map of the Bailey 30' × 60' Quadrangle, North-Central Colorado,

Ruxton V, B. P., and L. Berry (1959), The basal rock surface on weathered granitic rocks, *Proc. Geol. Assoc.*, *70*(4), 285–290, doi:10.1016/S0016-7878(59)80010-9.

Saco, P. M., G. R. Willgoose, and G. R. Hancock (2007), Eco-geomorphology of banded vegetation patterns in arid and semi-arid regions, *Hydrol. Earth Syst. Sci.*, *11*(6), 1717–1730.

Saleeby, J. B., H. F. Shaw, S. Niemeyer, E. M. Moores, and S. H. Edelman (1989), U/Pb, Sm/Nd and Rb/Sr geochronological and isotopic study of northern Sierra Nevada ophiolitic assemblages, California, *Contrib. Mineral. Petrol.*, *102*(2), 205–220, doi:10.1007/BF00375341.

San, B. T., and M. L. Suzen (2005), Digital elevation model (DEM) generation and accuracy assessment from ASTER stereo data, *Int. J. Remote Sens.*, *26*(22), 5013–5027, doi:10.1080/01431160500177620.

Sankey, T., R. Shrestha, J. B. Sankey, S. Hardegree, and E. Strand (2013), Lidar-derived estimate and uncertainty of carbon sink in successional phases of woody encroachment, *J. Geophys. Res. Biogeosciences*, *118*(3), 1144–1155, doi:10.1002/jgrg.20088.

Sass, O., M. Heel, I. Leistner, F. Stöger, K.-F. Wetzel, and A. Friedmann (2012), Disturbance, geomorphic processes and recovery of wildfire slopes in North Tyrol, *Earth Surf. Process. Landf.*, *37*(8), 883–894, doi:10.1002/esp.3221.

Saucedo, G. J., and D. L. Wagner (1992), Geologic map of the Chico quadrangle,

Scheffer, M., S. Carpenter, J. A. Foley, C. Folke, and B. Walker (2001), Catastrophic shifts in ecosystems, *Nature*, *413*(6856), 591–596, doi:10.1038/35098000.

Schliemann, S. A., and J. G. Bockheim (2011), Methods for studying treefall gaps: A review, *For. Ecol. Manag.*, *261*(7), 1143–1151, doi:10.1016/j.foreco.2011.01.011.

Schmidt, K. M., and D. R. Montgomery (1995), Limits to Relief, *Science*, *270*(5236), 617–620, doi:10.1126/science.270.5236.617.

Schmidt, K. M., J. J. Roering, J. D. Stock, W. E. Dietrich, D. R. Montgomery, and T. Schaub (2001), The variability of root cohesion as an influence on shallow landslide susceptibility in the Oregon Coast Range, *Can. Geotech. J.*, *38*(5), 995–1024.

Schumm, S. A. (1979), Geomorphic Thresholds: The Concept and Its Applications, *Trans. Inst. Br. Geogr.*, *4*(4), 485–515, doi:10.2307/622211.

Schwarz, M., P. Lehmann, and D. Or (2010), Quantifying lateral root reinforcement in steep slopes - from a bundle of roots to tree stands, *Earth Surf. Process. Landf.*, *35*(3), 354–367, doi:10.1002/esp.1927.

Schwarz, M., D. Cohen, and D. Or (2011), Pullout tests of root analogs and natural root bundles in soil: Experiments and modeling, *J. Geophys. Res. Earth Surf.*, *116*(F2), F02007, doi:10.1029/2010JF001753.

Schwarz, M., D. Cohen, and D. Or (2012), Spatial characterization of root reinforcement at stand scale: Theory and case study, *Geomorphology*, *171–172*, 190–200, doi:10.1016/j.geomorph.2012.05.020.

Selby, M. J. (1980), A rock mass strength classification for geomorphic purposes: with tests from Antarctica and New Zealand, *Z. Für Geomorphol.*, *24*(1), 31–51.

Sheffer, E., J. von Hardenberg, H. Yizhaq, M. Shachak, and E. Meron (2013), Emerged or imposed: a theory on the role of physical templates and self-organisation for vegetation patchiness, *Ecol. Lett.*, *16*(2), 127–139, doi:10.1111/ele.12027.

Shrestha, R., W. Carter, C. Slatton, and W. Dietrich (2007), "Research-Quality" Airborne Laser Swath Mapping: The Defining Factors, *Natl. Cent. Airborne Laser Mapp. NCALM Httpwww Ncalm Ufl Edu*.

Singer, M. B., J. C. Stella, S. Dufour, H. Piégay, R. J. S. Wilson, and L. Johnstone (2013), Contrasting water-uptake and growth responses to drought in co-occurring riparian tree species, *Ecohydrology*, *6*(3), 402–412, doi:10.1002/eco.1283.

Sklar, L. S., and W. E. Dietrich (2001), Sediment and rock strength controls on river incision into bedrock, *Geology*, *29*(12), 1087.

Sklar, L. S., and W. E. Dietrich (2004), A mechanistic model for river incision into bedrock by saltating bed load, *Water Resour. Res.*, *40*(6), W06301.

Skole, D., and C. Tucker (1993), Tropical Deforestation and Habitat Fragmentation in the Amazon - Satellite Data from 1978 to 1988, *Science*, *260*(5116), 1905–1910, doi:10.1126/science.260.5116.1905.

Slatton, K. C., W. E. Carter, R. L. Shrestha, and W. Dietrich (2007), Airborne Laser Swath Mapping: Achieving the resolution and accuracy required for geosurficial research, *Geophys. Res. Lett.*, *34*(23), L23S10, doi:10.1029/2007GL031939.

Slik, J. W. F., R. W. Verburg, and P. J. A. Kessler (2002), Effects of fire and selective logging on the tree species composition of lowland dipterocarp forest in East Kalimantan, Indonesia, *Biodivers. Conserv.*, *11*(1), 85–98.

Small, E. E., R. S. Anderson, and G. S. Hancock (1999), Estimates of the rate of regolith production using 10Be and 26Al from an alpine hillslope, *Geomorphology*, *27*(1–2), 131–150, doi:10.1016/S0169-555X(98)00094-4.

Smith, T. B., R. K. Wayne, D. J. Girman, and M. W. Bruford (1997), A Role for Ecotones in Generating Rainforest Biodiversity, *Science*, *276*(5320), 1855–1857, doi:10.1126/science.276.5320.1855.

Snyder, N. P., K. X. Whipple, G. E. Tucker, and D. J. Merritts (2000), Landscape response to tectonic forcing: Digital elevation model analysis of stream profiles in the Mendocino triple junction region, northern California, *Geol. Soc. Am. Bull.*, *112*(8), 1250–1263, doi:10.1130/0016-7606(2000)112<1250:LRTTFD>2.3.CO;2.

Sofia, G., P. Tarolli, F. Cazorzi, and G. Dalla Fontana (2011), An objective approach for feature extraction: distribution analysis and statistical descriptors for scale choice and channel network identification, *Hydrol Earth Syst Sci*, *15*(5), 1387–1402, doi:10.5194/hess-15-1387-2011.

Sofia, G., F. Pirotti, and P. Tarolli (2013), Variations in multiscale curvature distribution and signatures of LiDAR DTM errors, *Earth Surf. Process. Landf.*, *38*(10), 1116–1134, doi:10.1002/esp.3363.

Sofia, G., G. D. Fontana, and P. Tarolli (2014), High-resolution topography and anthropogenic feature extraction: testing geomorphometric parameters in floodplains, *Hydrol. Process.*, *28*(4), 2046–2061, doi:10.1002/hyp.9727.

Sokal, R. R., and F. J. Rohlf (1995), Biometry: the principles and practice of statistics in biological sciences, *WH Freeman Co. N. Y. USA*.

Stark, C. P., and P. Passalacqua (2014), A dynamical system model of eco-geomorphic response to landslide disturbance, *Water Resour. Res.*, *50*(10), 8216–8226, doi:10.1002/2013WR014810.

Stark, C. P., and G. J. Stark (2001), A Channelization Model of Landscape Evolution, *Am. J. Sci.*, *301*(4-5), 486–512, doi:10.2475/ajs.301.4-5.486.

Stephenson, N. L. (1990), Climatic Control of Vegetation Distribution: The Role of the Water Balance, *Am. Nat.*, *135*(5), 649–670.

Stephenson, N. L. (1998), Actual evapotranspiration and deficit: biologically meaningful correlates of vegetation distribution across spatial scales, *J. Biogeogr.*, *25*(5), 855–870, doi:10.1046/j.1365-2699.1998.00233.x.

Stephens, S. L., and B. M. Collins (2004), Fire regimes of mixed conifer forests in the north-central Sierra Nevada at multiple spatial scales, *Northwest Sci.*, *78*(1), 12–23.

Stock, G. M., R. S. Anderson, and R. C. Finkel (2004), Pace of landscape evolution in the Sierra Nevada, California, revealed by cosmogenic dating of cave sediments, *Geology*, *32*(3), 193–196, doi:10.1130/G20197.1.

Stock, J., and W. E. Dietrich (2003), Valley incision by debris flows: Evidence of a topographic signature, *Water Resour. Res.*, *39*(4), 1089.

Stock, J. D., D. R. Montgomery, B. D. Collins, W. E. Dietrich, and L. Sklar (2005), Field measurements of incision rates following bedrock exposure: Implications for process controls on the long profiles of valleys cut by rivers and debris flows, *Geol. Soc. Am. Bull.*, *117*(1-2), 174–194, doi:10.1130/B25560.1.

Stoffel, M., S. Rice, and J. M. Turowski (2013), Process geomorphology and ecosystems: Disturbance regimes and interactions, *Geomorphology*, *202*, 1–3, doi:10.1016/j.geomorph.2013.06.018.

Strudley, M. W., A. B. Murray, and P. K. Haff (2006a), Emergence of pediments, tors, and piedmont junctions from a bedrock weathering–regolith thickness feedback, *Geology*, *34*(10), 805–808, doi:10.1130/G22482.1.

Strudley, M. W., A. B. Murray, and P. K. Haff (2006b), Regolith thickness instability and the formation of tors in arid environments, *J. Geophys. Res. Earth Surf.*, *111*(F3), F03010, doi:10.1029/2005JF000405.

Sweeney, K. E., J. J. Roering, P. Almond, and T. Reckling (2012), How steady are steady-state landscapes? Using visible–near-infrared soil spectroscopy to quantify erosional variability, *Geology*, doi:10.1130/G33167.1.

Sweetkind, D. S., and D. D. Blackwell (1989), Fission-track evidence of the Cenozoic thermal history of the Idaho batholith, *Tectonophysics*, *157*(4), 241–250, doi:10.1016/0040-1951(89)90142-X.

Tague, C., and H. Peng (2013), The sensitivity of forest water use to the timing of precipitation and snowmelt recharge in the California Sierra: Implications for a warming climate, *J. Geophys. Res. Biogeosciences*, *118*(2), 875–887, doi:10.1002/jgrg.20073.

Tang, K., and X. Feng (2001), The effect of soil hydrology on the oxygen and hydrogen isotopic compositions of plants' source water, *Earth Planet. Sci. Lett.*, *185*(3–4), 355–367, doi:10.1016/S0012-821X(00)00385-X.

Tarboton, D. G. (1997), A new method for the determination of flow directions and upslope areas in grid digital elevation models, *Water Resour. Res.*, *33*(2), 309–319, doi:10.1029/96WR03137.

Tarboton, D. G., R. L. Bras, and I. Rodriguez-Iturbe (1991), On the extraction of channel networks from digital elevation data, *Hydrol. Process.*, *5*(1), 81–100.

Tarolli, P. (2014), High-resolution topography for understanding Earth surface processes: Opportunities and challenges, *Geomorphology*, *216*, 295–312, doi:10.1016/j.geomorph.2014.03.008.

Tarolli, P., and G. Dalla Fontana (2009), Hillslope-to-valley transition morphology: New opportunities from high resolution DTMs, *Geomorphology*, *113*(1–2), 47–56, doi:10.1016/j.geomorph.2009.02.006.

Tarolli, P., G. Sofia, and G. D. Fontana (2010), Geomorphic features extraction from high-resolution topography: landslide crowns and bank erosion, *Nat. Hazards*, *61*(1), 65–83, doi:10.1007/s11069-010-9695-2.

Taylor, L. L., J. R. Leake, J. Quirk, K. Hardy, S. A. Banwart, and D. J. Beerling (2009), Biological weathering and the long-term carbon cycle: integrating mycorrhizal evolution and function into the current paradigm, *Geobiology*, *7*(2), 171–191, doi:10.1111/j.1472-4669.2009.00194.x.

Taylor, P. et al. (2015), Landscape-Scale Controls on Aboveground Forest Carbon Stocks on the Osa Peninsula, Costa Rica, *PLoS ONE*, *10*(6), e0126748, doi:10.1371/journal.pone.0126748.

Teillet, P. M., B. Guindon, and D. G. Goodenough (1982), On the Slope-Aspect Correction of Multispectral Scanner Data, *Can. J. Remote Sens.*, *8*(2), 84–106, doi:10.1080/07038992.1982.10855028.

Terwilliger, V., and L. Waldron (1991), Effects of Root Reinforcement on Soil-Slip Patterns in the Transverse Ranges of Southern California, *Geol. Soc. Am. Bull.*, *103*(6), 775–785, doi:10.1130/0016-7606(1991)103<0775:EORROS>2.3.CO;2.

Tesfa, T. K., D. G. Tarboton, D. G. Chandler, and J. P. McNamara (2009), Modeling soil depth from topographic and land cover attributes, *Water Resour. Res.*, *45*(10), W10438, doi:10.1029/2008WR007474.

Thomas, M. F. (1974), Tropical geomorphology: a study of weathering and landform development in warm climates,

Thornes, J. B. (1983), Evolutionary Geomorphology, *Geography*, *68*(3), 225–235.

Thornes, J. B. (1985), The Ecology of Erosion, *Geography*, *70*(3), 222–235.

Todd, V. R., R. M. Alvarez, and Techni Graphic Systems, Inc. (2004), Preliminary geologic map of the El Cajon 30’ X 60’ quadrangle, southern California,

Tucker, G. E. (2009), Natural experiments in landscape evolution, *Earth Surf. Process. Landf.*, *34*(10), 1450–1460, doi:10.1002/esp.1833.

Tucker, G. E., and D. N. Bradley (2010), Trouble with diffusion: Reassessing hillslope erosion laws with a particle-based model, *J. Geophys. Res.*, *115*, doi:10.1029/2009JF001264.

Tucker, G. E., and R. L. Bras (1998), Hillslope processes, drainage density, and landscape morphology, *Water Resour. Res.*, *34*(10), 2751–2764.

Tucker, G. E., and G. R. Hancock (2010), Modelling landscape evolution, *Earth Surf. Process. Landf.*, *35*(1), 28–50, doi:10.1002/esp.1952.

Urban, D. L., C. Miller, P. N. Halpin, and N. L. Stephenson (2000), Forest gradient response in Sierran landscapes: the physical template, *Landsc. Ecol.*, *15*(7), 603–620, doi:10.1023/A:1008183331604.

Vanacker, V., F. von Blanckenburg, G. Govers, A. Molina, J. Poesen, J. Deckers, and P. Kubik (2007), Restoring dense vegetation can slow mountain erosion to near natural benchmark levels, *Geology*, *35*(4), 303–306, doi:10.1130/G23109A.1.

Vanwalleghem, T., U. Stockmann, B. Minasny, and A. B. McBratney (2013a), A quantitative model for integrating landscape evolution and soil formation, *J. Geophys. Res. Earth Surf.*, *118*(2), 331–347, doi:10.1029/2011JF002296.

Vanwalleghem, T., U. Stockmann, B. Minasny, and A. B. McBratney (2013b), A quantitative model for integrating landscape evolution and soil formation, *J. Geophys. Res. Earth Surf.*, *118*(2), 331–347, doi:10.1029/2011JF002296.

Vitousek, P., O. Chadwick, P. Matson, S. Allison, L. Derry, L. Kettley, A. Luers, E. Mecking, V. Monastra, and S. Porder (2003), Erosion and the Rejuvenation of Weathering-derived Nutrient Supply in an Old Tropical Landscape, *Ecosystems*, *6*(8), 762–772, doi:10.1007/s10021-003-0199-8.

Vitousek, P., G. P. Asner, O. A. Chadwick, and S. Hotchkiss (2009), Landscape-level variation in forest structure and biogeochemistry across a substrate age gradient in Hawaii, *Ecology*, *90*(11), 3074–3086, doi:10.1890/08-0813.1.

Vitousek, P. M., S. Porder, B. Z. Houlton, and O. A. Chadwick (2010), Terrestrial phosphorus limitation: mechanisms, implications, and nitrogen–phosphorus interactions, *Ecol. Appl.*, *20*(1), 5–15, doi:10.1890/08-0127.1.

Waddell, K. L., B. A. Hiserote, and F. Inventory (2005), *The PNW -FIA Integrated Database User Guide: A Database of Forest Inventory Information for California, Oregon, and Washington : Forest Inventory & Analysis Program, Pacific Northwest Station, Portland Oregon*, Forest Inventory and Analysis Program, Pacific Northwest Research Station.

Wahrhaftig, C. (1965), Stepped Topography of the Southern Sierra Nevada, California, *Geol. Soc. Am. Bull.*, *76*(10), 1165–1190, doi:10.1130/0016-7606(1965)76[1165:STOTSS]2.0.CO;2.

Wainwright, J., A. J. Parsons, and A. D. Abrahams (2000), Plot-scale studies of vegetation, overland flow and erosion interactions: case studies from Arizona and New Mexico, *Hydrol. Process.*, *14*(16-17), 2921–2943, doi:10.1002/1099-1085(200011/12)14:16/17<2921::AID-HYP127>3.0.CO;2-7.

Walker, T. W., and J. K. Syers (1976), The fate of phosphorus during pedogenesis, *Geoderma*, *15*(1), 1–19, doi:10.1016/0016-7061(76)90066-5.

Wallace, A., C. Nichol, and I. Woodhouse (2012), Recovery of Forest Canopy Parameters by Inversion of Multispectral LiDAR Data, *Remote Sens.*, *4*(2), 509–531, doi:10.3390/rs4020509.

Wallace, A. M., A. McCarthy, C. J. Nichol, X. Ren, S. Morak, D. Martinez-Ramirez, I. H. Woodhouse, and G. S. Buller (2014), Design and Evaluation of Multispectral LiDAR for the Recovery of Arboreal Parameters, *IEEE Trans. Geosci. Remote Sens.*, *52*(8), 4942–4954, doi:10.1109/TGRS.2013.2285942.

Walther, S. C., J. J. Roering, P. C. Almond, and M. W. Hughes (2009), Long-term biogenic soil mixing and transport in a hilly, loess-mantled landscape: Blue Mountains of southeastern Washington, *Catena*, *79*(2), 170–178, doi:10.1016/j.catena.2009.08.003.

Wang, Y., J. Y. Fang, T. Kato, Z. D. Guo, B. Zhu, W. H. Mo, and Y. H. Tang (2011), Inventory-based estimation of aboveground net primary production in Japan's

forests from 1980 to 2005, *Biogeosciences*, *8*(8), 2099–2106, doi:10.5194/bg-8-2099-2011.

Waring, R., J. Way, E. Hunt, L. Morrissey, K. Ranson, J. Weishampel, R. Oren, and S. Franklin (1995), Biologists Toolbox - Imaging Radar for Ecosystem Studies, *Bioscience*, *45*(10), 715–723, doi:10.2307/1312677.

Warton, D. I., I. J. Wright, D. S. Falster, and M. Westoby (2006), Bivariate line-fitting methods for allometry, *Biol. Rev.*, *81*(2), 259–291, doi:10.1017/S1464793106007007.

Warton, D. I., R. A. Duursma, D. S. Falster, and S. Taskinen (2012), smatr 3– an R package for estimation and inference about allometric lines, *Methods Ecol. Evol.*, *3*(2), 257–259, doi:10.1111/j.2041-210X.2011.00153.x.

Watson, G. S. (1966), Statistics of orientation data, *J. Geol.*, *74*(5P2), 786–797.

van de Weg, M. J. van de, P. Meir, J. Grace, and O. K. Atkin (2009), Altitudinal variation in leaf mass per unit area, leaf tissue density and foliar nitrogen and phosphorus content along an Amazon-Andes gradient in Peru, *Plant Ecol. Divers.*, *2*(3), 243–254, doi:10.1080/17550870903518045.

Weintraub, S. R., P. G. Taylor, S. Porder, C. C. Cleveland, G. P. Asner, and A. R. Townsend (2014), Topographic controls on soil nitrogen availability in a lowland tropical forest, *Ecology*, *96*(6), 1561–1574, doi:10.1890/14-0834.1.

West, A. J., A. Galy, and M. Bickle (2005), Tectonic and climatic controls on silicate weathering, *Earth Planet. Sci. Lett.*, *235*(1–2), 211–228, doi:10.1016/j.epsl.2005.03.020.

West, N., E. Kirby, P. Bierman, R. Slingerland, L. Ma, D. Rood, and S. Brantley (2013), Regolith production and transport at the Susquehanna Shale Hills Critical Zone Observatory, Part 2: Insights from meteoric 10Be, *J. Geophys. Res. Earth Surf.*, *118*(3), 1877–1896, doi:10.1002/jgrf.20121.

West, N., E. Kirby, P. Bierman, and B. A. Clarke (2014), Aspect-dependent variations in regolith creep revealed by meteoric 10Be, *Geology*, G35357.1, doi:10.1130/G35357.1.

Whelley, P. L., L. S. Glaze, E. S. Calder, and D. J. Harding (2014), LiDAR-Derived Surface Roughness Texture Mapping: Application to Mount St. Helens Pumice Plain Deposit Analysis, *IEEE Trans. Geosci. Remote Sens.*, *52*(1), 426–438, doi:10.1109/TGRS.2013.2241443.

Whipple, K., and G. Tucker (1999), Dynamics of the stream-power river incision model: Implications for height limits of mountain ranges, landscape response timescales, and research needs, *J. Geophys. Res.-Solid Earth*, *104*(B8), 17661–17674, doi:10.1029/1999JB900120.

Whipple, K. X. (2004), Bedrock Rivers and the Geomorphology of Active Orogens, *Annu. Rev. Earth Planet. Sci.*, *32*(1), 151–185, doi:10.1146/annurev.earth.32.101802.120356.

Whipple, K. X., and G. E. Tucker (2002), Implications of sediment-flux-dependent river incision models for landscape evolution, *J. Geophys. Res.-Solid Earth*, *107*(B2), doi:10.1029/2000JB000044.

White, A. F., T. D. Bullen, M. S. Schulz, A. E. Blum, T. G. Huntington, and N. E. Peters (2001), Differential rates of feldspar weathering in granitic regoliths, *Geochim. Cosmochim. Acta*, *65*(6), 847–869, doi:10.1016/S0016-7037(00)00577-9.

Whittaker, A. C. (2012), How do landscapes record tectonics and climate?, *Lithosphere*, *4*(2), 160–164, doi:10.1130/RF.L003.1.

Whittaker, A. C., and S. J. Boulton (2012), Tectonic and climatic controls on knickpoint retreat rates and landscape response times, *J. Geophys. Res.*, *117*(F2), doi:10.1029/2011JF002157.

Whittaker, A. C., P. A. Cowie, M. Attal, G. E. Tucker, and G. P. Roberts (2007a), Bedrock channel adjustment to tectonic forcing: Implications for predicting river incision rates, *Geology*, *35*(2), 103–106, doi:10.1130/G20738.1.

Whittaker, A. C., P. A. Cowie, M. Attal, G. E. Tucker, and G. P. Roberts (2007b), Contrasting transient and steady-state rivers crossing active normal faults: new field observations from the Central Apennines, Italy, *Basin Res.*, *19*(4), 529–556, doi:10.1111/j.1365-2117.2007.00337.x.

Whittaker, A. C., M. Attal, P. A. Cowie, G. E. Tucker, and G. Roberts (2008), Decoding temporal and spatial patterns of fault uplift using transient river long profiles, *Geomorphology*, *100*(3-4), 506–526, doi:10.1016/j.geomorph.2008.01.018.

Whittaker, A. C., M. Attal, and P. A. Allenn (2010), Characterising the origin, nature and fate of sediment exported from catchments perturbed by active tectonics, *Basin Res.*, *22*(6), 809–828, doi:10.1111/j.1365-2117.2009.00447.x.

Wiener, N. (1949), *Extrapolation, interpolation, and smoothing of stationary time series*, MIT press Cambridge, MA.

Wilcox, B. P., D. D. Breshears, and C. D. Allen (2003), Ecohydrology of a resource-conserving semiarid woodland: Effects of scale and disturbance, *Ecol. Monogr.*, *73*(2), 223–239, doi:10.1890/0012-9615(2003)073[0223:EOARSW]2.0.CO;2.

Wilkinson, M. T., J. Chappell, G. S. Humphreys, K. Fifield, B. Smith, and P. Hesse (2005), Soil production in heath and forest, Blue Mountains, Australia: influence of lithology and palaeoclimate, *Earth Surf. Process. Landf.*, *30*(8), 923–934, doi:10.1002/esp.1254.

Wilkinson, M. T., P. J. Richards, and G. S. Humphreys (2009), Breaking ground: Pedological, geological, and ecological implications of soil bioturbation, *Earth-Sci. Rev.*, *97*(1–4), 257–272, doi:10.1016/j.earscirev.2009.09.005.

Willett, S. D., R. Slingerland, and N. Hovius (2001), Uplift, Shortening, and Steady State Topography in Active Mountain Belts, *Am. J. Sci.*, *301*(4-5), 455–485, doi:10.2475/ajs.301.4-5.455.

Willett, S. D., S. W. McCoy, J. T. Perron, L. Goren, and C.-Y. Chen (2014), Dynamic Reorganization of River Basins, *Science*, *343*(6175), 1248765, doi:10.1126/science.1248765.

Witty, J. H., R. C. Graham, K. R. Hubbert, J. A. Doolittle, and J. A. Wald (2003), Contributions of water supply from the weathered bedrock zone to forest soil quality, *Geoderma*, *114*, 389–400.

Wobus, C., K. X. Whipple, E. Kirby, N. Snyder, J. Johnson, K. Spyropolou, B. Crosby, and D. Sheehan (2006), Tectonics from topography: Procedures, promise, and pitfalls, *Spec. Pap.-Geol. Soc. Am.*, *398*, 55.

Wolfe, J. A., C. E. Forest, and P. Molnar (1998), Paleobotanical evidence of Eocene and Oligocene paleoaltitudes in midlatitude western North America, *Geol. Soc. Am. Bull.*, *110*(5), 664–678, doi:10.1130/0016-7606(1998)110<0664:PEOEAO>2.3.CO;2.

Woodcock, N. H. (1977), Specification of Fabric Shapes Using an Eigenvalue Method, *Geol. Soc. Am. Bull.*, *88*(9), 1231–1236, doi:10.1130/0016-7606(1977)88<1231:SOFSUA>2.0.CO;2.

Wood, R. (2013), Transient Hillslope Response to an Incision Wave Sweeping up a Watershed: A Case Study from the Salmon River, *Masters Theses*.

Wu, T.-F., C.-J. Lin, and R. C. Weng (2004), Probability Estimates for Multi-class Classification by Pairwise Coupling, *J Mach Learn Res*, *5*, 975–1005.

Yamaguchi, Y., A. B. Kahle, H. Tsu, T. Kawakami, and M. Pniel (1998), Overview of Advanced Spaceborne Thermal Emission and Reflection Radiometer (ASTER), *Ieee Trans. Geosci. Remote Sens.*, *36*(4), 1062–1071, doi:10.1109/36.700991.

Yanai, R. D., J. J. Battles, A. D. Richardson, C. A. Blodgett, D. M. Wood, and E. B. Rastetter (2010), Estimating Uncertainty in Ecosystem Budget Calculations, *Ecosystems*, *13*(2), 239–248, doi:10.1007/s10021-010-9315-8.

Yang, X., G. Tang, C. Xiao, and F. Deng (2007), Terrain revised model for air temperature in mountainous area based on DEMs, *J. Geogr. Sci.*, *17*(4), 399–408, doi:10.1007/s11442-007-0399-9.

Yoo, K., and S. M. Mudd (2008), Toward process-based modeling of geochemical soil formation across diverse landforms: A new mathematical framework, *Geoderma*, *146*(1-2), 248–260.

Yoo, K., R. Amundson, A. M. Heimsath, and W. E. Dietrich (2005), Process-based model linking pocket gopher (Thomomys bottae) activity to sediment transport and soil thickness, *Geology*, *33*(11), 917–920, doi:10.1130/G21831.1.

Yoo, K., R. Amundson, A. M. Heimsath, W. E. Dietrich, and G. H. Brimhall (2007), Integration of geochemical mass balance with sediment transport to calculate rates of soil chemical weathering and transport on hillslopes, *J. Geophys. Res.- Ser.-*, *112*(F2), 2013.

Yoo, K., B. Weinman, S. M. Mudd, M. Hurst, M. Attal, and K. Maher (2011), Evolution of hillslope soils: The geomorphic theater and the geochemical play, *Appl. Geochem.*, *26*, S149–S153.

Zachos, J., M. Pagani, L. Sloan, E. Thomas, and K. Billups (2001), Trends, rhythms, and aberrations in global climate 65 Ma to present, *Science*, *292*(5517), 686–693, doi:10.1126/science.1059412.

Zhao, F., Q. Guo, and M. Kelly (2012), Allometric equation choice impacts lidar-based forest biomass estimates: A case study from the Sierra National Forest, CA, *Agric. For. Meteorol.*, *165*, 64–72, doi:10.1016/j.agrformet.2012.05.019.

Zwieniecki, M. A., and M. Newton (1995), Roots growing in rock fissures: Their morphological adaptation, *Plant Soil*, *172*(2), 181–187, doi:10.1007/BF00011320.